IRCCS, Integrated Research Consortium on Chemical Sciences

統合物質創製化学研究推進機構

平成29年度 事業報告書

IRCCS, Integrated Research Consortium on Chemical Sciences

統合物質創製化学研究推進機構

平成29年度 事業報告書

目　次

1

統合物質創製化学研究推進機構について

1-1

本機構の背景

１−１．本機構の背景

革新的な機能性物質の発見と創造が、科学と科学技術に飛躍的な発展をもたらしてきた。その根幹を担ってきたのが、原子・分子レベルで物質を探求し、創造しつづけてきた「ものづくり」の化学、すなわち物質創製化学である。豊かな物質に彩られた現代社会の恒常的発展を維持し、我が国の科学技術立国としての地位を揺るぎないものとするためにも、次世代の飛躍を約束する新たな機能性物質群を創造していかねばならない。特に、緊迫するエネルギー・環境問題の解決や最先端バイオ・情報技術の進展を図り、科学技術全般の国際的競争力を高めるためにも、革新的な機能性物質群の創造と、それらの合理合成法の開拓に向けた新学術基盤の構築が急務である。化学者に課せられた任務は極めて重い。

次世代の機能性物質創製の鍵を握るのが、物質を構成する元素、分子、分子集合体という階層性の理解と制御であると考えられている。元素により特徴づけられる多種類の原子が結合を作ることにより分子が形成され、さらに分子が集積することにより分子集合体へと組織化され、それぞれの階層に特有の性質や機能がある。生体物質の構造に例えると、個々の原子の特性を基礎とし（元素）、その機能を発揮する最小単位となるタンパク質や核酸が構成され（分子）、これらがさらに集積してウイルスや細胞内組織であるミトコンドリア（分子集合体）となる。高度に機能化された革新的な物質を創製するためには、全ての階層における構成単位を創製する術を学び、その機能を解明しなければならない。

本事業に参画する京都大学・名古屋大学・九州大学・北海道大学の４研究組織は、それぞれ「元素」「分子」「集合体」「触媒」をキーワードとした強力な中核的国際研究拠点として認知されている。本事業の前身となる「統合物質創製化学推進事業 − 先導的合成の新学術基盤構築と次世代中核研究者の育成（H22〜27 年度）」においては、４研究組織のそれぞれがストロング・ポイントをもつ各物質階層を中心に、個別に蓄積されてきた物質合成における知識と知恵を融合・深化させるとともに、物質合成概念の統合にも取り組んだ。すなわち、古典的な化学反応を利用した「化学的物質合成」ともに、高温超伝導体や発光材料、半導体などの開発に利用されてきた「物理的物質合成」や、生命体が穏和な条件下に日常的に行っている精巧かつ高効率な「生命物質合成」にも学ぶことによって、持続型経済社会を実現する、環境に調和した新たな「物質創製概念」の創出を実践した。「物質階層の統合」と「物質合成概念の統合」を合

言葉として、各研究機関の知識と経験を融合・深化させて新たな物質創製化学を遂行した結果、天然窒素還元酵素における機能中心構造の全合成、カーボンナノチューブ構造の化学合成、低環境負荷の鉄触媒による液晶材料の合成、強誘電性と強磁性が共存するマルチフェロイック物質の開発など、革新的な研究成果が生まれた。さらに、若手研究者に自由闊達な研究環境と、大学の垣根を越えた共同研究や情報交換の機会を与えたことによって、物質創製化学の未来を切り開く力量ある次世代中核研究者の育成を実現した。本事業は、この 4 大学間連携事業をさらに組織化・システム化した「新機構」を設立し、社会のニーズに応える「統合物質創製化学」を推進する。

1-2

本機構の目的

１－２．本機構の目的

新物質創製は、化学結合の形成のための新しい方法論や、機能の発現のための物質構築論などを探求する極めて基礎的な基盤学術である一方、その成果は、新触媒や新材料開発はもちろん、イノベーション創成を通じてエネルギー・資源から環境・創薬に至る極めて広い範囲に適用される。ここでは、基礎と応用が直結し（縦糸）、また化学を中心として物理から生命科学までの多くの研究分野の協力が必須である（横糸）。すなわち、物質と情報そして人が集結することが何より重要な分野と言えよう。しかしながら、我が国の物質創製研究は極めて高い国際競争力をもつにもかかわらず、新物質創製を総合的かつ戦略的に進める機関・組織は、残念ながら我が国には存在しない。基礎と応用を結ぶ縦糸と多様な分野を結ぶ横糸を組み合せ、近年長足の進歩を遂げたナノ計測や計算化学を取り込んだ統合的な研究組織の構築が急務である。その一方で、現在のひっ迫した財政の下では、多くの面積とポストを必要とする新研究所設立のような事業は現実的ではない。物質創製の学術を継承・発展させ、迫りくる環境問題などの重点課題を解決し、また新産業創出を成すためには、産官学連携や国際

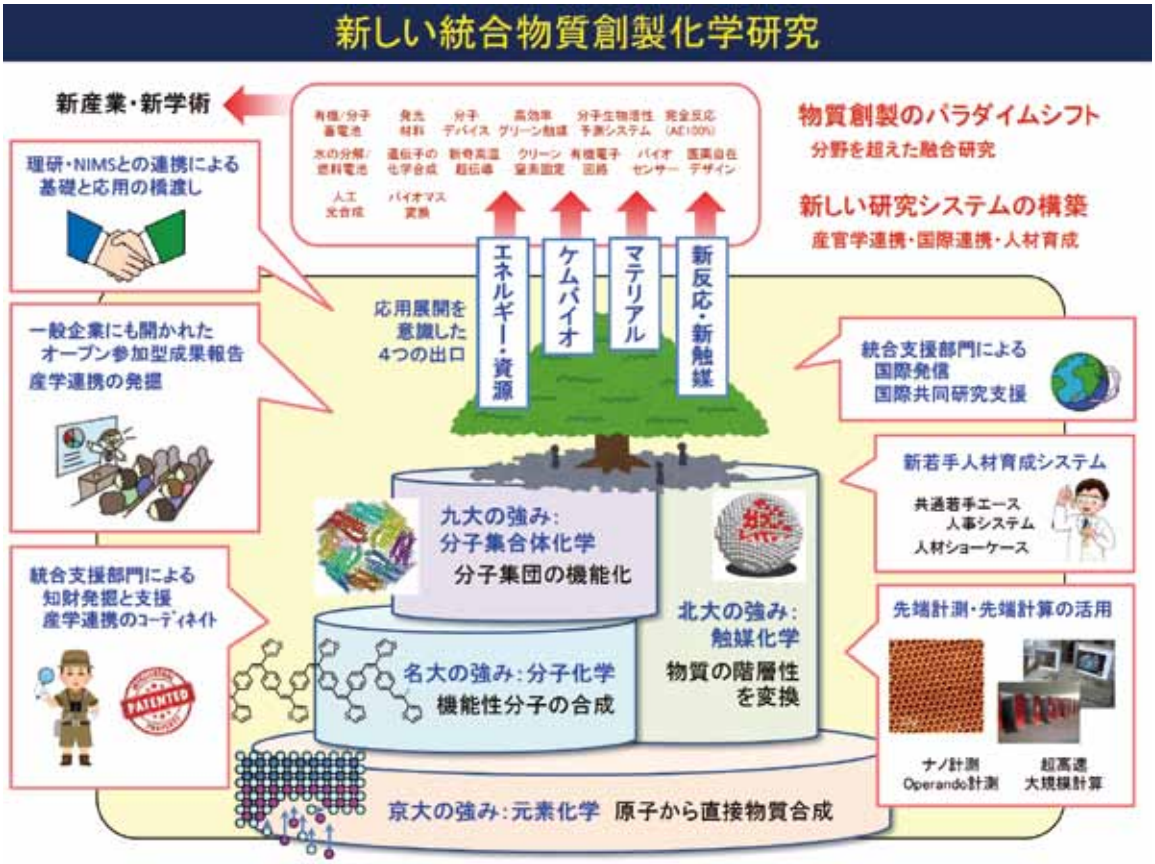

図１

連携を前面に出し、責任あるマネージメント体制を持ちながらも、最小限の面積とポストの獲得で遂行できる、大学間連携を基盤とした「統合物質創製化学研究推進機構」は、必要かつタイムリーな事業である。

図１に統合物質創製化学研究推進機構の概念図を示す。本機構事業に参画する名古屋大学・京都大学・九州大学・北海道大学の４研究組織は、「分子」、「元素」、「集合体」、「触媒」の化学研究において、それぞれに特色ある強力な中核的国際研究拠点として認知されているが、以下に示すそれぞれのストロング・ポイントを活かしながら、物質の階層構造を縦断する研究連携を実現する。

名古屋大学：無機化学から有機化学にわたる分子性物質の合成と機能の発現、さらには不斉反応を含む分子触媒の開発研究において卓越した成果をあげてきた。最近では、生物無機化学やナノ炭素科学分野においても世界をリードする。

京都大学：元素の特性の解明と、それに基づく機能創出の化学において先導的な研究成果をあげている。機能性元素科学という新しい研究パラダイムを提唱し、分子性物質から凝縮系物質に至る様々な革新的新物質群の出現を促してきた。

九州大学：複雑な分子集合体・集積体を構築する新概念を提出し、多くの機能性集積体の合成研究を通してナノサイエンス・テクノロジー研究に先鞭をつけた。最近では、核酸ナノマシンやナノハイブリッド材料の創出などで顕著な成果を挙げる。

北海道大学：触媒化学において世界を先導する中核的研究拠点である。触媒元素・分子のナノ・ミクロ集積・集合化学の研究を推進し、資源高度利用触媒、環境触媒、バイオ利用触媒、燃料電池・電極触媒、光触媒などで多くの成果を挙げる。

さらに本研究推進機構では、基礎研究を中心とする一方、「新反応・新触媒」、「マテリアル」、「エネルギー・資源」、「ケムバイオ」という、応用展開を意識した４つの出口を設定して基礎と応用を直結させる。その上で、産官学連携や国際連携を組織的に取り込み、新しい研究システムや研究支援体制、人材育成システムを取り入れた、社会に開かれた新組織である。物質創製における我が国の研究の厚みを継承し、新学術・新産業の創出と後継人材の育成を両立させながら、持続可能な社会の発展を導く。

1-3

本機構の組織

１－３．本機構の組織

本機構事業では、１－２で説明した機構研究の概念を実現するため、全く新しい大学間連携のフレームワークを構築する。一般論だが、これまでの大学間ネットワーク事業が抱える問題点としは、

① 高い大学間の壁
② 出口設定が難しく、研究目標を立てにくい
③ 平等主義によるガバナンス不足
④ 縦割り（大学別）の研究支援と人材育成支援
⑤ 外部意見が反映されにくい
⑥ 連携のメリットがネットワーク内に閉じる

などが挙げられる（図２(a)）。最大の問題点は⑥で、連携のメリットが社会発信されず、また社会の要請による事業という意識も希薄であった。ネットワーク形成のような大学強化事業は、社会からの認知によってはじめて達成されるもので、本研究推進機構事業においては、成果、情報、人材がネットワークの外側に輩出される外部発信型の連携を目指している。研究推進機構の組織図を図３に示すが、以下、運営体制、統括研究部門、研究支援部門についてその概要を説明する。

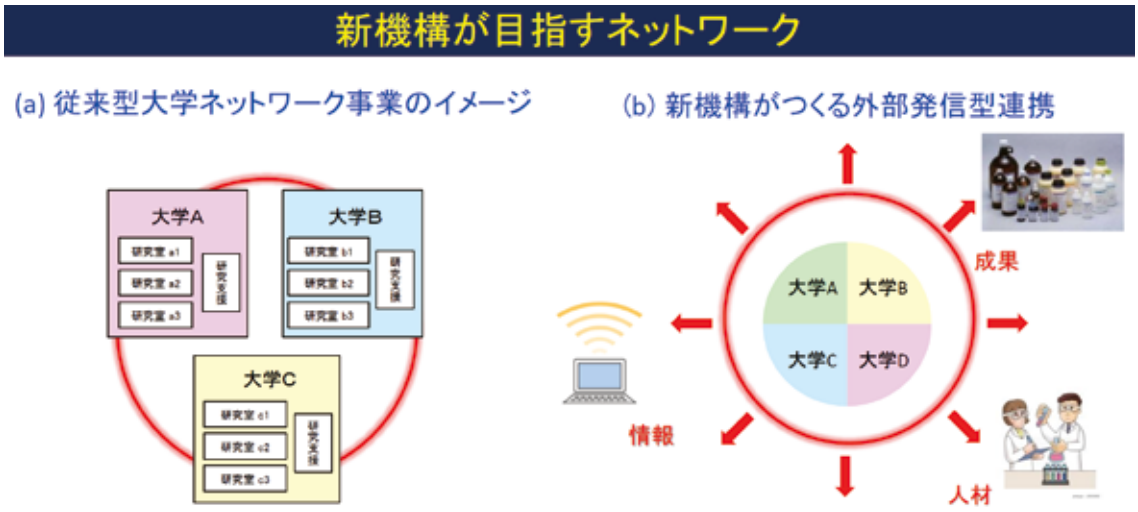

図２

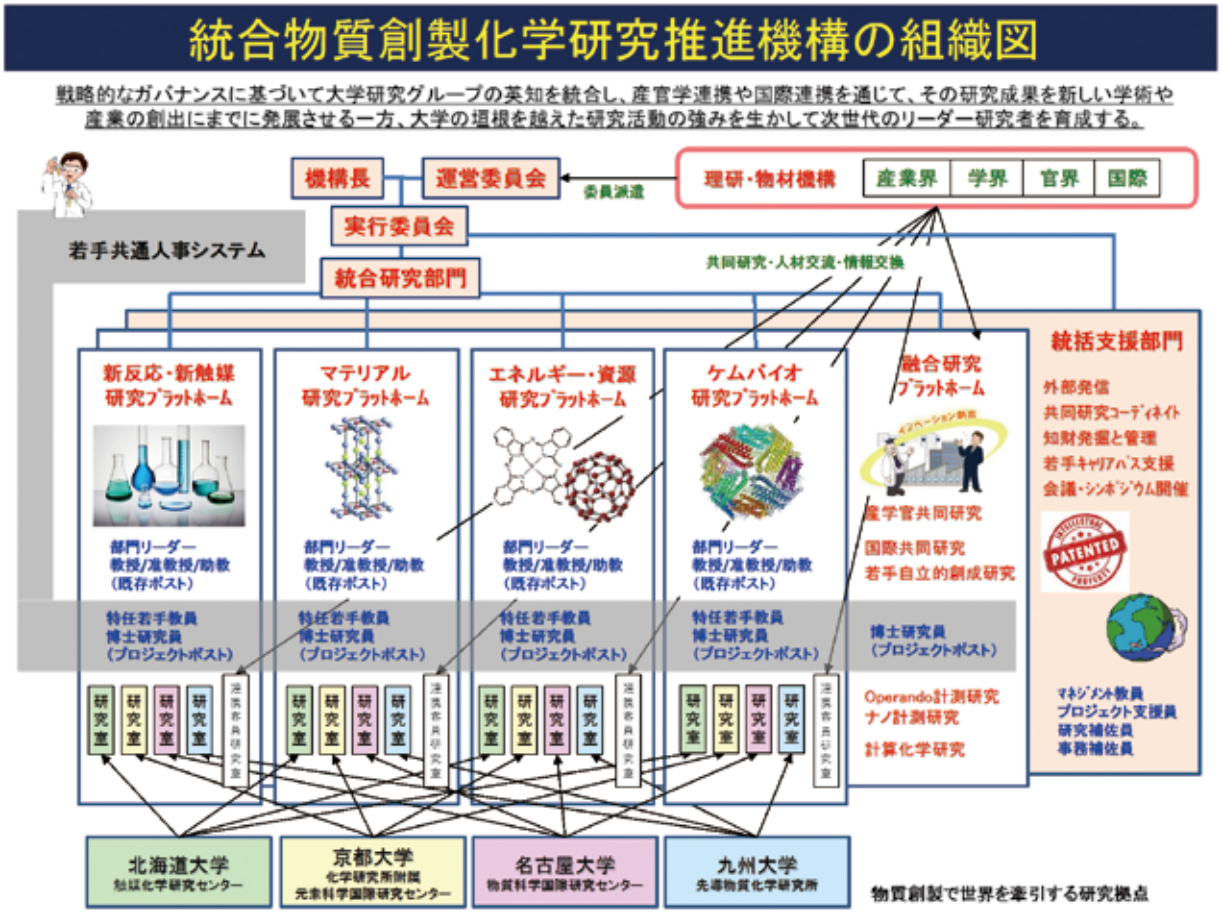

運営体制

本事業推進に全責任を負う機構長を置く。機構長は、国内の学識経験者（4～6 名）や理化学研究所などの連携機関から派遣された委員、本事業の実行委員から構成される運営委員会を組織する。運営委員会は、連携事業計画の策定と成果の取纏めを行う。運営委員会で制定された事業計画は、研究統括部門の研究プラットホーム・リーダーから構成される実行委員会によって遂行される。

統合研究部門

機構長および運営委員会のリーダーシップの下、応用という研究の出口を意識した統合研究部門（新反応・新触媒、マテリアル、エネルギー・資源、ケムバイオの４研究プラットホーム）を設置する。各プラットホームには、連携大学から１研究室ずつ選抜した４研究室と、産官学・海外から招聘した連携客員研究室を設置して共同研究を実施する。各プラットホームにおける研究内容は以下の通りである。

新反応・新触媒研究：連携４大学の固体触媒（北大）、分子触媒（名大）、元素触媒（京大）、分子集合体触媒（九大）の研究チームの共同研究によって、ゼロエミッション・カップリング反応の開発など、必要なものを必要なだけグリーンにつくりだす化学を発展させ、炭素ナノ材料や医薬品の革新的合成に展開する。

マテリアル研究：炭素材料、ナノ粒子、有機物、無機固体、金属錯体、高分子に至る物質群の開発は、機構４大学が世界を先導している分野である。その研究は多岐にわたるが、例えば４大学が開発する新規光機能性分子を超分子化することによって、既存の細胞イメージングから、分子イメージングや更には機能イメージングへと発展させる。

エネルギー・資源研究：エネルギー・資源問題は化学が取り組むべき緊急課題である。金属ナノ粒子・界面の機能化（北大、名大）や革新的ナノカーボン材料開発（名大）を通じて、新しい燃料電池や太陽電池を開発する（北大、京大、九大）。X 線吸収スペクトル計測（北大、名大）などによって反応機構を押さえながら、ユビキタス元素が生み出すグリーンエネルギーを創製する。

ケムバイオ研究：人工酵素を実現するための基本設計の確立は、生命科学における主題の一つである。生体分子合成（九大）とナノクラスター導入技術（京大）、ミューテーション技術（名大）を組み合わせ、計算シミュレーション（九大）を道しるべとしながら、機能をつくりこんだ人工酵素の合成にまで発展させる。

各研究プラットホームの構成は以下の通りである。

プラットホーム名	リーダー	コア研究室メンバー
新反応・新触媒	中野環（北大）	唯美津木・伊丹健一郎（名大）、中村正治（京大）、永島英夫・國信洋一郎（九大
マテリアル	島川祐一（京大）	清水研一（北大）、山口茂弘（名大）、高原淳・友岡克彦（九大）
エネルギー・資源	阿波賀邦夫（名大）	福岡淳（北大）、小澤文幸・村田靖次郎（京大）、佐藤治（九大）
ケムバイオ	吉澤一成（九大）	長谷川淳也（北大）、阿部洋（名大）、二木史朗（京大）

各プラットホームにグループリーダーを置き、各分野の連携研究の推進に責任をもつ。さらに、各プラットホームでは若手研究者を特任助教や博士研究員として雇用する。

これらの若手研究は、共通若手エース人事システムにより採用される。若手研究者の登竜門として機構を位置づけ、切磋琢磨による人材育成によって外部のパーマネント・ポジションに送り出す。

本機構内に限定せず、統合的な共同研究を促進するため、**融合創発研究**を実施する。共同研究提案を行い、運営委員会の審査を経て採択課題を決定し、実施する。また、年度末に研究成果について報告書を作成し、運営委員のレビューを受けるものとする。概ね毎年 10 件程度を実施する。

統括支援部門

名古屋大学物質科学国際研究センター内に設置し、センターに付設の化学測定機器室を用いて本事業の研究を支援するとともに、国際シンポジウム等の開催に必要な外国人研究者招聘に関わる事務手続き、本事業の研究成果の取纏め、ポスターの作成、ホームページの管理などの広報活動を担当する。具体的には、以下の支援を行う。

① **外部発信・国際発信**：機構の研究成果を、HP や種々のメディアなどを通じて国際的に広報する。
② **共同研究コーディネート**：機構研究全体を見渡して、新しい共同研究を萌芽させる。
③ **知財発掘と管理**：機構研究全体を見渡して、知財獲得を支援する。
④ **若手キャリアパス支援**：求職情報を若手に流布し、キャリアパスセミナーを実施する。
⑤ **会議・シンポジウム開催支援**：オープン参加型シンポなどを広報、支援する。

1-4

本機構の特徴

１－４．本機構の特長

社会に開かれた新機構は、以下の５つの特長を持つ。

① **戦略的なガバナンスに基づく融合研究**：機構長のリーダーシップの下、応用という研究の出口を意識した統合研究部門（新反応・新触媒、マテリアル、エネルギー・資源、ケムバイオの４研究プラットホーム）を設置し、各プラットホームには、連携大学から１研究室ずつ選抜した４研究室と、産官学・海外から招聘した連携客員研究室を設置して共同研究を実施する。更に融合研究部門を設置し、産官学や国際連携の場とする。大学間の壁を乗り越え、かつ開かれた研究組織を構築する。

② **イノベーション創出とグローバル化**（図４）：研究部門を横断的に支援するため統括支援部門を設置し、マネージメント教員、プロジェクト支援員などを配置する。共同研究コーディネート、知財獲得、国際発信、若手人材育成などを、大学間の壁を取り払って行う。理化学研究所などを連携機関として加え、イノベーション創出などを活性化する。

③ **外部発信型連携**：新しい産官学連携と国際連携のパラダイムを構築する。オープン参加型の成果報告会などを開催することによって、研究成果・研究情報・人材を、産業界、官界、学界、海外に対して外向きに発信・輩出する。

④ **共通若手エース人事システム**（図５）：大学院生から若手研究者まで、各階層のニーズに合わせた人材育成を行う。特任助教や研

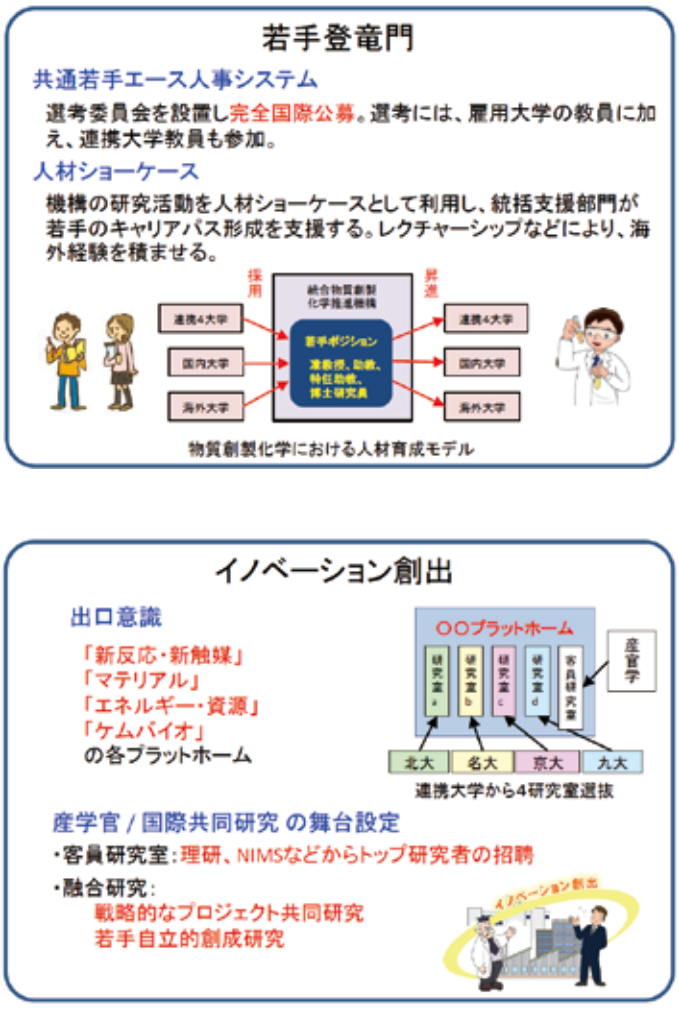

図４

究員の人事ついては、共通若手エース人事システムを採用する。すなわち、連携大学共通の選考委員会を設置して人選する。機構の研究活動を人材ショーケースとして利用して若手のキャリアパス形成を支援すると共に、レクチャーシップ派遣や招聘により国際的人脈形成を促す。若手研究者の登竜門として機構を位置づけ、切磋琢磨による人材育成によって外部のパーマネント・ポジションに送り出すことにより、物質創製分野における新たな人材育成モデルを実現する。

⑤ **ナノ計測と計算化学の支援**：ナノ計測と計算化学の支援の下、合理的な物質創製研究を展開する。

以上、基礎研究を重視しながらも、応用という研究の出口を意識した４テーマに各大学から１研究室を送り込む形で統合研究部門を形成することによって、互いの研究の強みを補完する研究体制を敷く。ガバナンスを効かした機構運営によって招聘される、理化学研究所などからの客員研究室の存在は、産官学との結びつきを強化すると共に、機構組織の流動性を高めるだろう。この上で、大学の壁を越えた統括支援部門による効率的な知財発掘や国際発信によって、新機構のビジビリティは必然的に高まる。このように、社会を意識した機構の研究活動は、院生や若手研究者の人材ショーケースとして作用し、前述した共通若手エース人事システムは人材の流動性を必然的に生み出す。

1-5

事業計画

１－５．事業計画

本事業のロードマップを図６に示す。

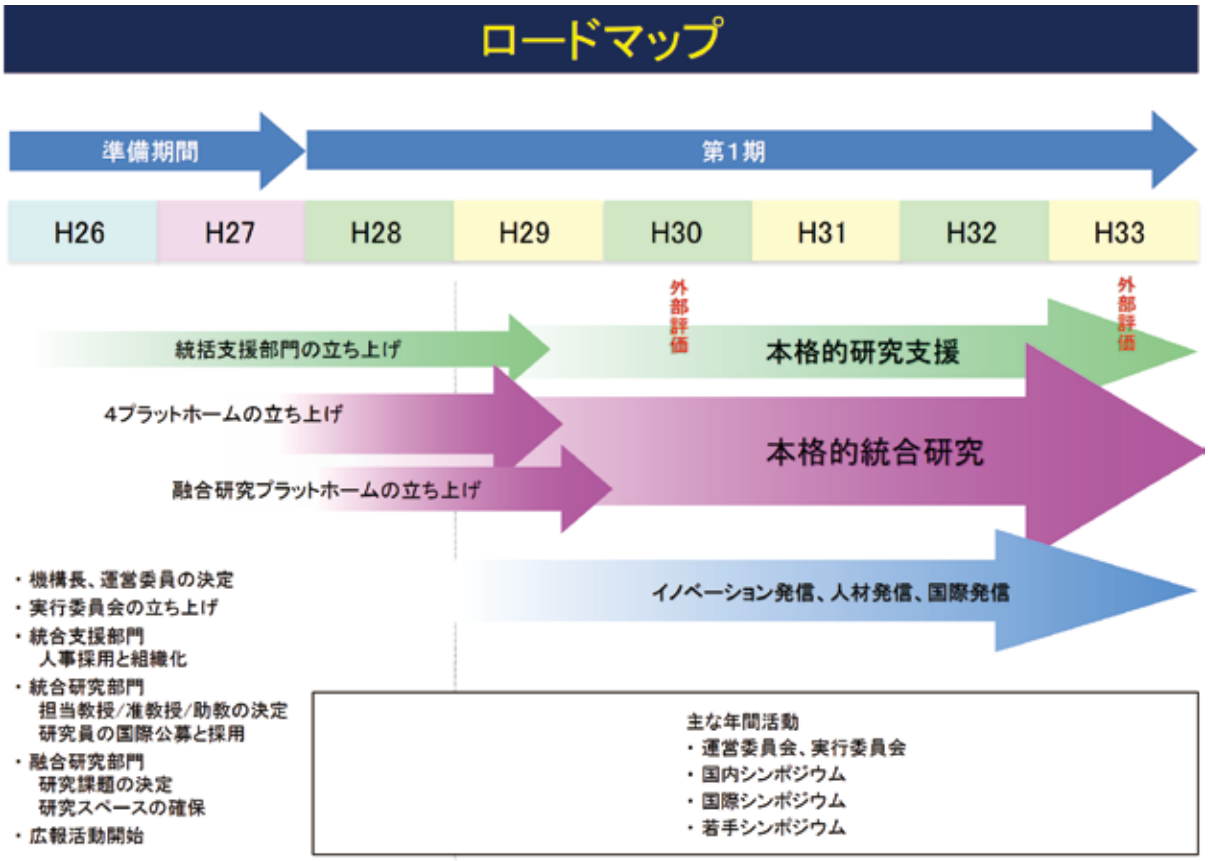

図６

1-6

本機構の期待される成果と波及効果

１－６．本事業の期待される成果と波及効果

１）本事業がめざす物質階層の統合と物質合成概念の統合により、総合的な物質観に基づく多彩な物質創製法が創出される。それらは、生体機能、電子機能、光機能、触媒機能などの有用機能をもつ機能性物質群を創造するための新学術基盤の構築へと展開される。

２）革新的な機能性物質群の創製は、材料科学分野に革新をもたらす。これまでの物質合成では、ナノテクノロジーで多用される熱力学支配による自己組織化が指導原理として用いられてきた。これに対して、本事業では、準安定物質の合成法の開拓により、自己組織化を超えた新規機能性物質群の創製法が開発されるものと期待される。これにより、高圧合成と薄膜技術の融合による非平衡物質群の創製、人工超格子をもつ特異な高次構造体の合成、光磁気特性を示す新規錯体や有機発光素子の開発、酵素反応の解明と生命機能の理解に資する人工酵素の合成などが達成され、最先端のバイオ・情報技術へと応用・展開される。

３）縦糸（基礎と応用）と横糸（多様な分野）が結ばれ、産官学及び国際的に開かれた物質創製化学研究が実施され、物質創製化学の新しい学術基盤が構築される。その結果、環境に優しい新触媒開拓、新規機能電子物質に基づく骨太イノベーション、更には新医薬品や生体活性物質開発が成される。これらは持続可能な文明社会の構築に大きく貢献する。

４）高度な研究機能をもつ国際研究拠点の有機的連携により、多くの若手研究者に広範な学問領域を統合した卓越した研究環境を提供することができる。このような環境は、幅広い知識と複眼的思考力を備えた中核研究者の養成に必要不可欠な要件である。本事業では、若手研究者を統合研究フェローとして処遇し、自由で創造的な研究環境を提供する。これにより、物質創製化学の将来を担う中核研究者を多数育成できるものと期待される。また、国際研究拠点の連携は、我が国の学術的先進性と国際競争力を確保するためにも重要であり、多くの若者に、海外の一流研究者と切磋琢磨する機会を提供し、国際的な研究者として成長するためのインセンティブを与える。

５）本申請が提案する新機構のスキームの有効性は、物質創製化学分野にだけ限定されない。このスキームにより、参加大学の強みを生かして我が国の学術を結集できるほか、大学間連携のメリットが産官学連携や国際連携を通じて外向きに発信されることにより、社会からの支持も得られる。この効果は、新国立研究所の設立にも匹敵す

る。このような外向きリンクの大学間連携事業のパイロットプログラムとして、他分野への波及効果やインパクトも大きい。

６）事業計画終了後は、新物質創製を総合的かつ戦略的に進める研究システムという枠組みは残しながらも、統括研究部門における研究テーマや参加研究室を全面的に見直し、また現在の連携 4 大学以外からの参加を促してオールジャパン体制をつくり、更に進んだ物質創製最先端研究を進める。

2

メンバー

2-1

コア研究室メンバー、連携研究室メンバー、リサーチフェロー

● 機構長

巽 和行

名古屋大学物質科学国際研究センター 特任教授

● 北海道大学

新反応・新触媒研究プラットホーム　メンバー一覧

＜コア・連携研究室＞

朝倉清高　教授（基礎研究系・触媒表面研究部門）

長谷川淳也　教授（基礎研究系・触媒理論研究部門）

福岡　淳　教授（基礎研究系・物質変換研究部門）

清水研一　教授（基礎研究系・触媒材料研究部門）

大谷文章　教授（基礎研究系・光触媒科学研究部門）

高橋　保　教授（基礎研究系・分子触媒研究部門）

中野　環　教授（基礎研究系・高分子機能科学研究部門）

西田まゆみ　教授（実用化推進系・研究開発部門）

＜リサーチフェロー＞ …平成 30 年 3 月末現在

SIDDIKI, S. M. A. Hakim 特任助教（基礎研究系・触媒材料研究部門）

YANG, Shubin 研究員（基礎研究系・光触媒科学研究部門）

LUO, Qian 研究員（基礎研究系・分子触媒研究部門）

● 名古屋大学

エネルギー・資源研究プラットホーム　メンバー一覧

＜コア・連携研究室＞

阿波賀邦夫 教授（物性化学）
山口茂弘 教授（機能有機化学）
伊丹健一郎 教授（有機化学）
唯美津木 教授（無機化学）
阿部洋 教授（生物有機化学）
野依良治 特別教授・斎藤進 教授（分子触媒化学）
田中健太郎 教授（分子組織化学）
菱川明栄 教授（光物理化学）
篠原久典 教授（物理化学）
渡辺芳人 教授（生物無機化学）

＜リサーチフェロー＞ …平成 30 年 3 月末現在

西川剛（機能有機化学）
澤口加奈（無機化学）
Wu Yang（物性化学）
辻厳一郎（生物有機化学）
Sawant Dinesh Nanaji（有機合成化学）
Li Yuanming（有機化学）
Dattatraya B. Bagal（有機合成化学）
阿部奈保子（生物有機化学）

● 京都大学

マテリアル研究プラットホーム　メンバー一覧

＜コア・連携研究室＞

中村 正治 教授（有機分子変換化学）
島川 祐一 教授（先端無機固体化学）
小澤 文幸 教授（錯体触媒変換化学）
金光 義彦 教授（光ナノ量子物性化学）
村田 靖次郎 教授（構造有機化学）
二木 史朗 教授（生体機能設計化学）
時任 宣博　教授（有機元素化学）

＜リサーチフェロー＞

GELDSETZER, Jan 特定研究員（有機分子変換化学）
後藤 真人 研究員（先端無機固体化学）
阿波連 知子 研究員（光ナノ量子物性科学）
GUO, Jing-Dong 研究員（有機元素化学）

● 九州大学

ケムバイオ研究プラットホーム　メンバー一覧

＜コア・連携研究室＞

吉澤　一成　教授（反応・物性理論分野・先導物質化学研究所）
佐藤　治　教授（分子物質化学分野・先導物質化学研究所）
國信　洋一郎　教授（機能分子化学分野・先導物質化学研究所）
友岡　克彦　教授（集積分子機能分野・先導物質化学研究所）
永島　英夫　教授（クラスター分子化学分野・先導物質化学研究所）
高原　淳　教授（複合分子システム分野・先導物質化学研究所）

＜リサーチフェロー＞ …平成 30 年 3 月末現在

SHENGQUN, Su　特任助教（分子物質化学分野・先導物質化学研究所）
河崎　悠也　特任助教（集積分子機能分野・先導物質化学研究所）

2-2

外部評価委員

● 外部評価委員

岩村 秀
　東京大学 名誉教授

岩澤康裕
　電気通信大学 燃料電池イノベーション研究センター長 特任教授

上村大輔
　神奈川大学 特別招聘教授

江崎信芳
　放送大学京都学習センター 所長

大峰 巌
　分子科学研究所 名誉教授

新海征治
　九州大学高等研究院 特別主幹教授

玉尾皓平
　理化学研究所グローバル研究 クラスタ長

3

平成29年度事業報告

3-1

第１回 統合物質若手の会

統合物質創製化学研究推進機構 (IRCCS)
第一回　若手の会

開催日：平成 29 (2017) 年 7 月 28 日(金) ～29 日(土)
会場：「サンパーク犬山」
主催：統合物質創製化学研究推進機構

プログラム

平成 29 年 7 月 28 日(金)
14:00–14:30 参加登録
14:30–14:36 開会の挨拶　阿波賀邦夫（Kunio AWAGA, 名古屋大学　教授）
趣旨説明　中寛史（Hiroshi NAKA, 名古屋大学　野依研助教）

研究発表
座長　小林広和（Hirokazu KOBAYASHI, 北海道大学）
14:36–14:48 田原淳士（Atsushi TAHARA, 九州大学　永島研助教）
「ジシラメタラサイクル骨格を有する 8 族遷移金属錯体を用いたアルケンの水素化に関する理論研究」

14:48–15:00 竹内勝彦（Katsuhiko TAKEUCHI, 京都大学　小澤研助教）
「平面四角形構造を有する白金(0)錯体 」

15:00–15:12 張中岳（Zhongyue ZHANG, 名古屋大学　阿波賀研助教）
「レドックス活性金属有機構造体: 新しいメカニズムを有するリチウム電池の正極材料」

15:12–15:24 鳥屋尾隆（Takashi TOYAO, 北海道大学　清水研助教）
「固体触媒によるカルボン酸誘導体の選択的水素化」

15:24–15:45 休憩

招待講演
座長　大町遼（Haruka OMACHI, 名古屋大学　篠原研助教）
15:45–16:30 原野幸治（Koji HARANO, 東京大学総括プロジェクト機構「革新分子技術」総括寄付講座　特任准教授）
「原子分解能電子顕微鏡で分子が動く，集まる，反応する様子をとらえる」

16:30–16:36 小休憩

研究発表
座長　金川慎治（Shinji KANEGAWA, 九州大学　佐藤研助教）
16:36–16:48 高島舞（Mai TAKASHIMA, 北海道大学　大谷研助教）
「タングステン酸ビスマス光触媒粒子による有機物分解反応における多電子移動機構の解明」

16:48–17:00 鄭知恩（Jieun JUNG, 名古屋大学　野依研助教）
「コバルト触媒を用いた水を電子源、酸素分子を酸素源とするベンゼンからフェノールへの光酸化反応」

17:00–17:12 辻雄太（Yuta TSUJI, 九州大学　吉澤研助教）
「結晶構造予測法による新規電子化物の材料探索」

17:12–17:24 河野健一（Kenichi KAWANO, 京都大学　二木研助教）
「曲率誘導性を有する両親媒性ヘリックスペプチドによるオクタアルギニンの膜透過促進」

17:24–17:45 小休憩

招待講演
座長　中寛史（Hiroshi NAKA, 名古屋大学　野依研助教）
17:45–18:30　北将樹（Masaki KITA, 名古屋大学大学院生命農学研究科　教授）
「タンパク質間相互作用を誘導する天然物の新展開」

18:30–19:00 写真撮影後にチェックイン

19:00–20:00 夕食

20:00–22:00 研究交流会（参加者自己紹介）

平成 29 年 7 月 29 日(土)
討論会
座長　中寛史，大町遼
09:00–09:30　　討論　話題 1　“Important Research Areas in the Coming 25 Years”
09:30–09:45　　発表および議論

09:45–10:15　　討論　話題 2　“Solutions Using IRCCS Frameworks”
10:15–10:30　　発表および議論

10:30–11:00 休憩

研究発表
座長　愛場雄一郎（Yuichiro AIBA, 名古屋大学　渡辺研助教）
11:00–11:12 木村康明（Yasuaki KIMURA, 名古屋大学　阿部研助教）
「求電子ホスホロチオエステルによる核酸の化学的連結反応」

11:12–11:24 栗海軍（Haijun LI, 北海道大学　高橋研博士研究員）
「ジルコナシクロペンタジエン及びハフナシクロペンタジエンの環拡大反応に関する研究」

11:24–11:36 河崎悠也（Yuuya KAWASAKI, 九州大学　友岡研特任助教）
「クリック反応素子DACNの機能化と反応」

座長　竹内勝彦（Katsuhiko TAKEUCHI, 京都大学　小澤研助教）
11:36–11:48 菅大介（Daisuke KAN, 京都大学　島川研准教授）
「原子レベル構造制御による遷移金属酸化物の機能開発」

11:48–12:00 大城宗一郎（Soichiro OGI, 名古屋大学　山口研助教）
「精密超分子重合を実現する非平衡系のデザイン」

12:00–12:30 閉会の挨拶　國信洋一郎（Yoichiro KUNINOBU, 九州大学　教授）
総括　中寛史（名古屋大学）
解散

Asst.Prof. Naka, Nagoya

Asst. Prof. Omachi, Nagoya

Prof. Awaga, Observer

Invited lecture, Dr. Harano, The University of Tokyo

Invited lecture, Prof. Hara, Nagoya

Asst. Prof. Zhang, Nagoya

Asst. Prof. Toyao, Hokkaido

Asst. Prof. Takashima, Hokkaido

Dinner

Mixer

Self-introduction

Self-introduction

Self-introduction

Meeting

Breakfast

Round-table discussion

Round-table discussion

Round-table discussion

Round-table discussion

Asst. Prof. Kawano, Kyoto

Assoc. Prof. Kan, Kyoto

Prof. Kuninobu, Observer

Group photo

Inuyama castle

3-2

第３回 統合物質国内シンポジウム

統合物質創製化学研究推進機構　第 3 回国内シンポジウム

「物質創製化学の新潮流」
平成 29 年 10 月 30 日（月）～31 日（火）
（京都大学化学研究所 共同研究棟 1 階 大セミナー室）

10 月 30 日（月）

13:00~13:10　開会の辞

13:10~13:40　研究報告　京都大学　中村 正治　教授
「化学資源を活用する有機合成化学の開拓」（新反応・新触媒研究プラットフォーム）

13:40~14:10　研究報告　北海道大学　安田 友洋　准教授
「Supported Ionic Liquid Phase を用いた逆シフト反応」（新反応・新触媒研究プラットフォーム）

14:10~14:40　研究報告　九州大学　佐藤 治　教授
「電子移動による原子価異性物質の分極制御」（エネルギー・資源研究プラットフォーム）

14:40~15:00　休憩

15:00~15:30　研究報告　名古屋大学　大町 遼　助教
「半導体性単層カーボンナノチューブの高効率分離法の開発と薄膜トランジスタへの応用」（エネルギー・資源研究プラットフォーム）

15:30~16:00　招待講演　岡山大学　仁科 勇太　准教授
「カーボンナノシート製造法の確立と用途開拓　－触媒に着目してー」

16:00~16:40　ショートプレゼンテーション　各大学 3 名（1 人 3 分）

16:40~18:00　ポスターセッション

18:00~19:30　交流・フリーディスカッション

10 月 31 日（火）

10:00~10:30　研究報告　北海道大学　長谷川 淳也　教授
「系間交差の計算化学」（ケムバイオ研究プラットフォーム）

10:30~11:00　研究報告　九州大学　塩田 淑仁　准教授
「量子化学を用いた触媒研究：メタン活性化の反応機構を中心に」（ケムバイオ研究プラットフォーム）

11:00~11:30　招待講演　分子科学研究所　椴山 儀恵　准教授
「ハロゲン結合とペルフルオロアリールで拓く合成化学」

11:30~13:00　昼食

13:00~13:30　招待講演　京都大学エネルギー理工学研究所　中田 栄司　准教授
「DNA ナノ構造体上に酵素を配置した分子コンビナート」

13:30~14:00　研究報告　名古屋大学　斎藤 進　教授
「遷移金属触媒を用いる再生可能資源の水素化と脱水素化」（マテリアル研究プラットフォーム）

14:00~14:30　研究報告　京都大学　水畑 吉行　准教授
「重いフェニルアニオンの化学」（マテリアル研究プラットフォーム）

14:30~14:40　閉会の辞

ポスターセッション

＊太字はショートプレゼンテーションの発表者

P01　Synthesis of weakly acidic carbon catalyst by Diels-Alder addition of maleic anhydride on activated carbon.
○Lina Mahardiani, Abhijit Shrotri, Atsushi Fukuoka【北大】

P02　[Fe_4] and [Fe_6] Hydride Clusters Supported by Phosphines: Synthesis and Application to the Catalytic Silylation of N_2.
○Yasuhiro Ohki, Ryoichi Araake, Mizuki Tada, Yoichi Sakai【名大】

P03　ビス（フェロセニル）ゲルミレンの合成と性質
○鈴木裕子、笹森貴裕、時任宣博【京大】

P04　吸着水の接着界面に及ぼす影響に関する理論的考察
村田裕幸、田中宏昌、○吉澤一成【九大】

P05　Synthesis of cubane-type [Mo_3S_4Fe] clusters supported by cyclopentadienyl ligands and their application in the N_2 activation.
○Ryota Hara, Mami Kachi, Keisuke Uchida, Mizuki Tada, Yoichi Sakai, Yasuhiro Ohki【名大】

P06　1.3-ジゲルマ-2-シラアレンの合成とその構造
○菅原知紘、笹森貴裕、時任宣博【京大】

P07　Low temperature oxidation of trace Ethylene with a hydrophobic SBA-15 supported Pt catalyst.
○Shazia Satter Sharmin, Kiyotaka Nakajima, Atsushi Fukuoka【北大】

P08　Photocatalytic Oxidation of Benzene to Phenol Using Dioxygen and Water.
○Jieun Jung, Ji Won Han, Yong-Min Lee, Wonwoo Nam, Shunichi Fukuzumi【名大】

P09　ゲルマおよびスタンナベンゼニルアニオンの合成と構造
○藤森詩織、水畑吉行、時任宣博【京大】

P10　二核銅酸素錯体を用いたメタン酸化反応触媒の理論的設計
○堀優太、宮西真由子、塩田淑仁、小寺政人、吉澤一成【九大】

P11　Development of Highly Active Ruthenium Catalysts for Hydrogenation of Carboxylic Acids.
○Shota Yoshioka, Masayuki Naruto, Ke Wen, Susumu Saito【名大】

P12　アルミニウム-鉄錯体の合成と性質
柳澤達也、○水畑吉行、時任宣博【京大】

P13　Synthesis of Helical Polyurethanes from (R)-1,10-Bi(2-naphthol) and Diisocyanates.
○Heshuang Dai, Yue Wang, Tamaki Nakano【北大】

P14　Trifluoroacetic Acid–Water Mixture for Rapid Conversion of Esters to Carboxylic Acids.
○Tomomi Banno, Hiroyuki Okabe, Ryoji Noyori, Hiroshi Naka【名大】

P15　Modification of Lipid Packing State by Amphipathic Peptides with Curvature Inducibility.
Tomo Murayama, **○Kenichi Kawano**, Shiroh Futaki【京大】

P16　フレークボール形状タングステン酸ビスマス光触媒微粒子における多電子移動機構の解明
○高島舞、堀晴菜、大谷文章【北大】

P17　ジインドロカルバゾールとサルフェンからなるジャイアントマクロサイクルを用いた分子認識
○坂田卓也、河野慎一郎、田中健太郎【名大】

P18　溶血ペプチドを改変したエンドソーム不安定化ペプチドの開発と抗体の細胞内送達
○秋柴美沙穂、武内敏秀、川口祥正、坂本健太郎、二木史朗【京大】

P19　ホウ素化 2-フェニルピリジン類の固相相転移とその機構解明
○吉越裕介、須崎裕司、小坂田耕太郎、國信洋一郎【九大】

P20　超分子型ポルフィリン・フタロシアニン窒素架橋鉄二核錯体による触媒的メタン酸化反応
○森田健太郎、山田泰之、三原のぞみ、高谷光、北河康隆、井川和宣、友岡克彦、田中健太郎【名大】

P21　Engineering of sequence-specific RNA binding proteins based on PUF proteins.
○Kouki Shinoda, Miki Imanishi, Shiroh Futaki【京大】

P22　Antimicrobial mechanism of bi-metal modified titania photocatalyst: enhanced activity by interaction between gold and silver.
○Maya Endo, Zhishun Wei, Bunsho Ohtani, Ewa Kowalska【北大】

P23　熱ショックタンパク質阻害性環状ペプチドとMoS_2ナノシートによる効率的がん細胞光熱療法
○有安真也、Jing Mu, Xiao Zhang, Ying Huang, Edwin Kok Lee Yeow, Hua Zhang, Bengang Xing【名大】

P24　イミダゾール縮環ベンゾチアジアゾール骨格を用いた近赤外吸収色素の開発
○岡崎修平、村田理尚、若宮淳志、村田靖次郎【京大】

P25　Theoretical Study on Rhodium-Catalyzed Hydrosilylation of C=C and C=O Double Bonds.
○趙黎明【北大】

P26　P450BM3 の新規再構成手法の開発およびマンガン錯体の導入による反応性の改変
○大村慧太、愛場雄一郎、荘司長三、渡辺芳人【名大】

P27　π拡張型キノリノール配位子を用いた金属錯体の合成と性質
○塚尾昌浩、村田理尚、若宮淳志、村田靖次郎【京大】

P28　TTFs-SCO ハイブリット分子結晶の合成と物性
○金川慎治、福本佳弘、佐藤治【九大】

P29　緑膿菌のヘム輸送蛋白質複合体 (PhuUV-PhuT) に関する研究
○榊原えりか、荘司長三、渡辺芳人【名大】

P30　ペプチドデンドロンチオラート修飾金クラスターの光触媒機能
○上野亮、磯﨑勝弘、石橋幸典、高谷光、中村正治【京大】

P31　酸化セリウム触媒を用いた二酸化炭素とメタノールからのジメチルカーボネート合成に関する理論的研究
○杉山利行【北大】

P32　ゲスト包接伝導性化合物の伝導機構に関する理論研究
○林拓、土方優【名大】

P33　鉄触媒鈴木-宮浦カップリング反応によるα-アリールプロピオン酸類の不斉合成
○奥園智絵美、岩本貴寛、アダク ラクスミカンタ、神将吉、中村正治【京大】

P34　第一原理計算による酸化セリウム触媒の機能解析
○中山哲【北大】

P35　RISM with DMRG-CASPT2 for calculating near infrared dyes.
○Ryosuke Shimizu, Takeshi Yanai, Yuki Kurashige, Daisuke Yokogawa【名大】

P36　パラジウム触媒による高選択的直接的アリール化重合：1,2-ジチエニルエテン含有 DA ポリマーの合成
○脇岡正幸、森田葉月、市原暢子、小澤文幸【京大】

P37　Tuning orbital angular momentum by a dynamic bond in a cobalt (II) complex.
○Shengqun Su, Osamu Sato【九大】

P38　フェムト秒レーザーフィラメントによる気相炭化水素/Ar フロー系における会合反応過程の観測
○橋ヶ谷かすみ、澤木美里、松田晃孝、菱川明栄【名大】

P39　Pd ナノクラスター触媒の構造とカーバイド形成
○朝倉清高【北大】

P40　EUV 励起による Xe 多電子ダイナミクスの時間分解光電子計測
○河辺佳喬、橋ヶ谷かすみ、伏谷瑞穂、松田晃孝、彦坂泰正、菱川明栄【名大】

P41　平面四角形白金(0)錯体の構造と物性に及ぼす補助配位子の効果
○竹内勝彦、田口廣臣、谷川一平、松尾司、田中宏昌、吉澤一成、小澤文幸【京大】

P42　クリック反応素子 DACN を用いた分子連結法の開発
○河崎悠也、青山慎、柏木健、井川和宣、友岡克彦【九大】

P43　可視光触媒を用いた脱炭酸型 sp3 炭素アミノ化反応の開発
○榊原陽太、伊藤江里、村上慧、伊丹健一郎【名大】

P44　パラジウム触媒による高選択的直接的アリール化重合：2,2'-ビチオフェン含有 DA ポリマーの合成
○山下菜摘、脇岡正幸、森裕樹、西原康師、小澤文幸【京大】

P45　酸素プラズマ処理により調製した TiO2(110)担持金ナノ粒子サイズの特異な担持量依存性
高草木達、関聡史、木工淳、三輪寛子、○朝倉清高【北大】

P46　光架橋反応を用いた共有結合性有機ナノチューブの新規合成法
○戸谷充寿、前田果歩、伊藤英人、伊丹健一郎【名大】

P47　光電流ビート分光によるハロゲン化鉛ペロブスカイト太陽電池の光電流生成機構の研究
○田原弘量、若宮淳志、金光義彦【京大】

P48　8 族遷移金属錯体を用いた他置換アルケンの水素化に関する理論研究
○田原淳士、砂田祐輔、田中宏昌、塩田淑仁、吉澤一成、永島英夫【九大】

P49　Controlled fabrication of graphene liquid cells for real-time TEM imaging of liquids.
◯**Yoshimasa Michiya**, Yutaka Ohno, Hisanori Shinohara, Ryo Kitaura【名大】

P50　ハロゲン化鉛ペロブスカイトナノ粒子における光励起ダイナミクス
○湯本郷【京大】

P51　メタン活性化触媒 In/SiO2 の XAFS 解析
○永松伸一、西川祐太、萩原仁志、井波雄太、山中一郎、朝倉清高【北大】

P52　Concise Synthesis of MoS_2 Nanoribbon using Inner Space of Carbon Nanotubes.
◯Motoki Aizaki, Haruka Omachi, Hisanori Shinohara【名大】

P53　Sn ハライドペロブスカイトに対する $SnCl_2$ 添加の効果
○阿波連知子【京大】

P54　担持 Pt 触媒による 2 級アルコールとアミノアルコールからの 2,5-二置換ピロールの合成
○清水研一、A.S. Touchy, 鳥屋尾隆、S.M.A. Hakim Siddiki【北大】

P55　CNT-Template Synthesis of Graphene Nanoribbon and Extraction by Chemical Oxidation.
◯Yuka Oka, Haruka Omachi, Hisanori Shinohara【名大】

P56　Excitonic properties in $CH_3NH_3Pb\mathit{X}_3$ (X = I and Br) single crystals.
○Le Phuong Quang【京大】

P57　イノラートを用いたトリプチセンのワンポット合成とその変換
○岩田隆幸、吉永達郎、藤原匠、深見拓人、新藤充【九大】

P58　Development of Anti-cancer Agents based on Synthetic Lethality by LATS Mutation.
○Nguyen Hong Nhung, 木村康明、村上優子、阿部洋【名大】

P59　1 光子および 2 光子発光励起分光を用いた $CH_3NH_3Pb\mathit{X}_3$ (X = I, Br, Cl)単結晶のバンド端近傍での光学特性の研究
○山田琢允【京大】

P60　Photo-induced b-Elimination Leading to a Vinyl Monomer.
Hassan Nageh, Liming Zhao, Akira Nakayama, Jun-ya Hasegawa, Yue Wang, ○Tamaki Nakano【北大】

P61　ロタキサン構造形成による新規アンチセンス法の開発
○富田貴志、阿部奈保子、木村康明、阿部洋【名大】

P62　ハロゲン化金属ペロブスカイト太陽電池における光キャリア再結合および輸送機構
○半田岳人【京大】

P63　Photo-transformation and Polymerization of (R)-1,10-Bi(2-naphthol).
○Yue Wang, Zhaoming Zhang, Tamaki Nakano【北大】

P64　抗ウイルス活性を指向した 2'-β-チオ核酸の開発
○片倉秀雄、木村康明、阿部洋【名大】

P65　単一 $FAPbBr_3$ ナノ粒子の発光ダイナミクス
○鎗田直樹【京大】

P66　熱転移による高次構造変化と光アクチュエータ能のスイッチング
○五島健太、谷文都【九大】

P67　ゲスト分子挿入によるＭＯＦの物性変化
○山本祥平、張中岳、阿波賀邦夫【名大】

P68　$CsPb(Br_{1-x}I_x)_3$ ナノ粒子におけるバイエキシトンとトリオンのダイナミクス
○中原聡志【京大】

P69　配位子変換に基づく水熱合成 ZnO ナノワイヤの成長促進メカニズム及び分子識別エレクトロニクスへの展開
○長島一樹、酒井大樹、井上暉英、中村千枝、Yong He, 金井真樹、Gouzhu Zhang, 高橋綱己、竹田精治、柳田剛【九大】

P70　シラジチエノローダミンの合成および近赤外蛍光特性
○木村奈央【名大】

P71　幾何学的フラストレート格子をもつ 3*d* 遷移金属化合物の構造と磁性
○後藤真人、齊藤高志、島川祐一【京大】

P72　拡張型ゲルマペリサイクリンの合成および物性
○谷本裕樹、森淳太、藤原太郎、垣内喜代三【奈良先端大】

P73　硫黄を含む中員環縮環チオフェンによる π 電子系の分子配向制御
○早川雅大、深澤愛子、戸田雄佑、山口茂弘【名大】

P74　ミスト CVD 法によるスズ酸化物透明導電性エピタキシャル薄膜の作製
○丹羽泰之、菅大介、島川祐一【京大】

P75　交差シクロファン型ドナーのイオンラジカル塩における電子物性
○殿内大輝、松下未知雄、阿波賀邦夫、菅原正【名大】

Opening, Prof. Tokito

Chair, Prof. Yamaguchi

Prof. Nakamura, Kyoto

Assoc. Prof. Yasuda, Hokkaido

Prof. Sato, Kyushu

Asst. Prof. Omachi, Nagoya

Invited lectuer, Assoc. Prof. Nishina, Okayama

Short presentation

Short presentation

Short presentation

Short presentation

Short presentation

Short presentation

Short presentation

Short presentation

Short presentation

Short presentation

Short presentation

Short presentation

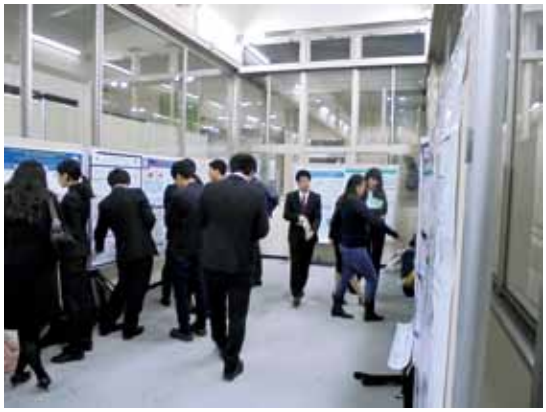

Poster session

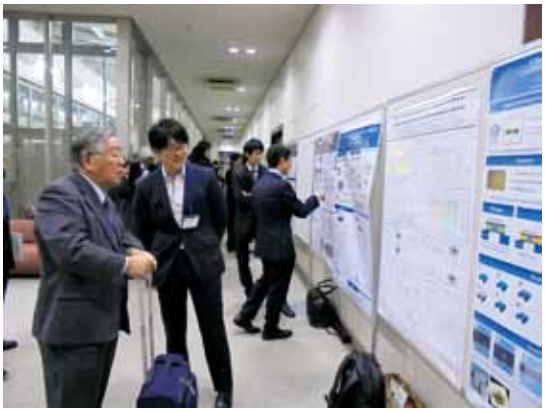

Poster session

Participants

Discussion

Director of IRCCS, Prof. Tatsumi

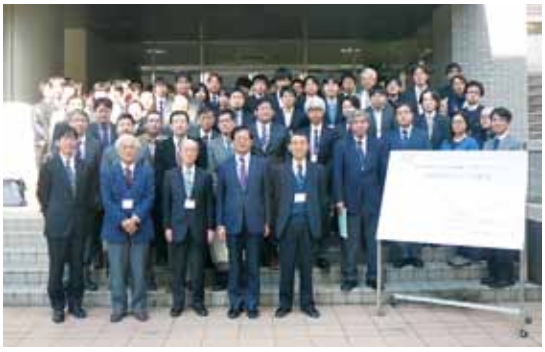

Group photo

3-3

第１回 統合物質国際シンポジウム

IRCCS-JST CREST Joint Symposium

"Chemical sciences facing difficult challenges"

Jan. 24th-26th, 2018

Chikushi Campus, Kyushu University, Fukuoka, Japan

IRCCS The 1st International Symposium
Jan. 24th-25th

The 2nd Base Metal Catalysis Symposium
Jan. 25th-26th

Invited Lecturers

IRCCS Session

Prof. Ren-Gen Xiong
Southeast University, P. R. China

Prof. Jonathan Clayden
University of Bristol, UK

IRCCS / Base Metal Joint Session

Prof. Rinaldo Poli
CNRS, Laboratoire de Chimie de Coordination, France

Prof. Eiichi Nakamura
The University of Tokyo, Japan

Base Metal Session

Prof. Paul J. Chirik
Princeton University, USA

Prof. Karl Kirchner
Vienna University of Technology, Austria

Prof. Hairong Guan
University of Cincinnati, USA

Prof. Audrey Moores
McGill University, Canada

Prof. Ning Jiao
Peking University, P. R. China

Prof. Shaozhong Ge
National University of Singapore, Singapore

Prof. Nobuaki Kambe
Osaka University, Japan

Prof. Takashi Ohshima
Kyushu University, Japan

Contribution from IRCCS members

Prof. Ken-ichi Shimizu
Hokkaido University, Japan

Dr. Zhiyi Song
Hokkaido University, Japan

Prof. Kentaro Tanaka
Nagoya University, Japan

Dr. Soichiro Ogi
Nagoya University, Japan

Prof. Shiroh Futaki
Kyoto University, Japan

Dr. Takahiro Iwamoto
Kyoto University, Japan

Prof. Katsuhiko Tomooka
Kyushu University, Japan

Dr. Tomoyasu Hirai
Kyushu University, Japan

IRCCS JST CREST KYUSHU UNIVERSITY IMCE

Supported by

Integrated Research Consortium on Chemical Sciences (IRCCS)
Japan Science and Technology Agency (JST)
Institute for Materials Chemistry and Engineering, Kyushu University
Research and Education Center for Advanced Energy Materials, Devices, and Systems, Kyushu University
Research and Education Center of Carbon Resources, Kyushu University

Contact

IRCCS The 1st International Symposium
Kazunari Yoshizawa
E-mail: kazunari@ms.ifoc.kyushu-u.ac.jp
Phone: +81-92-802-2529

Secretary office
E-mail: irccs-crest@cm.kyushu-u.ac.jp
Phone&Fax: +81-92-583-7839

The 2nd Base Metal Catalysis Symposium
Hideo Nagashima
E-mail: nagasima@cm.kyushu-u.ac.jp
Phone: +81-92-583-7819

http://jointproject-cscri.rcms.nagoya-u.ac.jp/
http://irccs-crest.cm.kyushu-u.ac.jp/

IRCCS-JST CREST Joint Symposium

"Chemical sciences facing difficult challenges"

[Part I] Jan. 24th-25th, IRCCS The 1st International Symposium
[Part II] Jan. 25th-26th, The 2nd Base Metal Catalysis Symposium

Chikushi Hall, Chikushi Campus, Kyushu University, Fukuoka, Japan

January 24th (Wed.)

12:00–13:00 Registration

13:00–13:10 Opening Remarks

(Chair: Osamu Sato, Kyushu University)

13:10–13:50 [IL-1] **Ren-Gen Xiong** (*Southeast University, P. R. China*)
"Ceramic-like Molecular Ferroelectrics"

13:50–14:10 [YR-1] **Tomoyasu Hirai** (*Kyushu University, Japan*)
"Synthesis and Characterization of Novel Polymer Brush with Well-controlled Stereoregularity"

(Chair: Tamaki Nakano, Hokkaido University)

14:10–14:30 [YR-2] **Soichiro Ogi** (*Nagoya University, Japan*)
"Seed-initiated Supramolecular Polymerization of π-Conjugated Molecules"

14:30–15:00 [SR-1] **Shiroh Futaki** (*Kyoto University, Japan*)
"Cytosolic Antibody Delivery by Lipid-sensitive Endosomolytic Peptide"

15:00–15:20 Break

(Chair: Kazunari Yoshizawa, Kyushu University)

15:20–15:50 [SR-2] **Kentaro Tanaka** (*Nagoya University, Japan*)
"Molecular Architectures towards Soft Materials and Switching Molecular Systems"

15:50–16:10 [YR-3] **Zhiyi Song** (*Hokkaido University, Japan*)
"Lithiation of Palladated Dihydropentacene: New Route for Introduction of Substituents from Both of Electrophiles and Nucleophiles to Pentacene"

(Chair: Shigehiro Yamaguchi, Nagoya University)

16:10–16:30 [YR-4] **Takahiro Iwamoto** (*Kyoto University, Japan*)
"Iron-Catalyzed *anti*-Selective Carbosilylation of Internal Alkynes"

16:30–17:00 [SR-3] **Katsuhiko Tomooka** (*Kyushu University, Japan*)
"Chemistry of Medium-sized Unsaturated Heterocycles"

17:00–18:30 Poster Session 1 (P-001 ~ P-091)

18:40–20:10 Banquet

January 25th (Thu.)

(Chair: Yuichi Shimakawa, Kyoto University)

09:20–09:50 [SR-4] **Ken-ichi Shimizu** (*Hokkaido University, Japan*)
"Cooperative Heterogeneous Catalysis for Selective Transformations of Carboxylic Acid Derivatives, CO_2 and Hydrocarbons"

09:50–10:10 Short Talk 1
[ST-1] **Hajime Hojo** (*Kyushu University, Japan*)
[ST-2] **Hiroshi Yoshida** (*Kumamoto University, Japan*)

(Chair: Yasuhiro Uozumi, Institute for Molecular Science)

10:10–10:50 [IL-2] **Audrey Moores** (*McGill University, Canada*)
"Sustainable Nanoparticles and Surface Plasmon Resonance enhanced Hydrogenation Catalysis"

10:50–11:10 Break

(Chair: Satoshi Hata, Kyushu University)

11:10–11:30 [IL-3] **Mitsuhiro Murayama** (*Virginia Tech, USA*)
"Dynamic Observation on the Propagation of a Nanoscale Crack in an Industrial

Aluminum Alloy: an Application of in-situ Electron Tomography System to an Engineering Material"

(Chair: Jun-ichiro Hayashi, Kyushu University)

11:30–12:30 [PL-1] **Eiichi Nakamura** (*The University of Tokyo, Japan*)
"Atomic Resolution Electron Microscopy for Organic Chemists"

12:30–13:30 Lunch Break

(Chair: Katsuhiko Tomooka, Kyushu University)

13:30–14:10 [IL-4] **Jonathan Clayden** (*University of Bristol, UK*)
"Naturally Inspired Solutions in Synthesis: Reactivity, Relays and Receptors"

(Chair: Hisashi Shimakoshi, Kyushu University)

14:10–14:50 Short Talk 2
[ST-3] **Yoichi M. A. Yamada** (*RIKEN, Japan*)
[ST-4] **Ryoichi Kuwano** (*Kyushu University, Japan*)

(Chair: Hiroshi Furuno, Kyushu University)

14:10–14:50 Short Talk 3
[ST-5] **Masaya Sawamura** (*Hokkaido University, Japan*)
[ST-6] **Masanari Kimura** (*Nagasaki University, Japan*)

(Chair: Mitsuru Shindo, Kyushu University)

14:50–15:30 [IL-5] **Takashi Ohshima** (*Kyushu University, Japan*)
"Direct Catalytic Asymmetric Addition of Various Nucleophiles to *N*-Unprotected Ketimines"

15:30–15:50 Break

(Chair: Toru Oishi, Kyushu University)

15:50–16:30 [IL-6] **Ning Jiao** (*Peking University, P. R. China*)
"Base Metal Catalyzed Oxygenation and Nitrogenation Reactions"

(Chair: Seiji Shirakawa, Nagasaki University)

16:30–17:00 Short Talk 4
[ST-7] **Hikaru Takaya** (*Kyoto University, Japan*)
[ST-8] **Yasuhiro Arikawa** (*Nagasaki University, Japan*)

[ST-9] **Yoshihito Shiota** (*Kyushu University, Japan*)

(Chair: Takashi Ohshima, Kyushu University)

17:00–17:40 [IL-7] **Rinaldo Poli** (*CNRS, Laboratoire de Chimie de Coordination, France*)
"Copper and Iron-catalyzed Processes Involving Radicals"

17:40–19:10 Poster Session 2 (P-070 ~ P-140)

January 26th (Fri.)

(Chair: Ryoichi Kuwano, Kyushu University)

09:20–10:00 [IL-8] **Hairong Guan** (*University of Cincinnati, USA*)
"Iron- and Cobalt-Catalyzed Hydrogenation of Esters and Nitriles"

(Chair: Yusuke Sunada, The University of Tokyo)

10:00–10:30 Short Talk 5
[ST-10] **Kouki Matsubara** (*Fukuoka University, Japan*)
[ST-11] **Hisashi Shimakoshi** (*Kyushu University, Japan*)
[ST-12] **Sachie Arae** (*Kumamoto University, Japan*)

10:30–10:50 Break

(Chair: Takashi Nishikata, Yamaguchi University)

10:50–11:10 Short Talk 6
[ST-13] **Yoshiaki Nakao** (*Kyoto University, Japan*)
[ST-14] **Naohiko Yoshikai** (*Nanyang Technological University, Singapore*)

(Chair: Hideo Nagashima, Kyushu University)

11:10–12:10 [PL-2] **Paul J. Chirik** (*Princeton University, USA*)
"New Opportunities in Synthesis with Iron and Cobalt Catalysts"

12:10–13:40 Lunch Break & Poster Session 3 (P-070 ~ P-140)

(Chair: Yoshiaki Nakao, Kyoto University)

13:40–14:20 [IL-9] **Karl Kirchner** (*Vienna University of Technology, Austria*)
"New Chemistry Based on Non-Precious Metal Pincer Complexes"

(Chair: Naohiko Yoshikai, Nanyang Technological University)

14:20–15:00 [IL-10] **Shaozhong Ge** (*National University of Singapore, Singapore*)
"Cobalt-Catalyzed Hydrofunctionalization of Unsaturated Hydrocarbonds"

15:00–15:20 Break

(Chair: Shigeki Sasaki, Kyushu University)

15:20–16:00 [IL-11] **Nobuaki Kambe** (*Osaka University, Japan*)
"Cross- and Multicomponent-Coupling Reactions Catalyzed by Base Metals"

16:00–16:10 Closing Remarks

IRCCS, The 1st International Symposium

Prof. Nagashima, Organiser

Prof. Sato, Kyushu

Discussion

Prof. Shimakawa, Kyoto

Asst. Prof. Hirai, Kyushu

Asst. Prof. Ogi, Nagoya

Prof. Futaki, Kyoto

Chair, Prof. Nakano, Hokkaido

Chair, Prof. Yoshizawa, Kyushu

Prof. Tanaka, Nagoya

Chair, Prof. Yamaguchi

Prof. Tomooka, Kyushu

Poster session

Poster session

Director of IRCCS, Prof. Tatsumi

Committee member, Prof. Iwamura

Banquet

Comittee member, Prof. Tamao

Regio and Chemoselective Conversions Controlled by Specific Atomic Arrangement of Ordered Alloys

Masayoshi, Miyazaki,[1] Shinya Furukawa,[2] Takayuki Komatsu[1]

1 Department of Chemistry, Tokyo Institute of Technology, Tokyo, Japan, 2 Institute for Catalysis, Hokkaido University, Hokkaido, Japan,

Introduction

Selective Catalysis governed by specific surface atomic arrangement of ordered alloys

(1) ***Seteroselective*** alkene isomerization (Z to E) by H_2

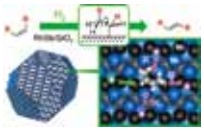

One-dimentionally aligned Rh allows one-atom hydrogenation for isomerization

ChemCatChem, **2015**, *7*, 3472.

Combined with Pd_3Pb alkyne semihydrogenation catalyst

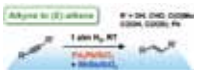

Selective one-pot synthesis of (*E*)-alkenes from alkynes with 1 atm H_2 at 25˚C.

ACS Catal., **2016**, *6*, 2121.

(2) ***Chemoselective*** nitroarene hydrogenation

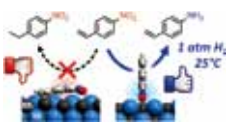

Concave Rh and convex In sites can recognize end-on adsorption of nitroarenes and allows its hydrogenation.

Chem. Sci., **2016**, *7*, 4476.

The aim of this study

Discovery of the 3rd example of this unique surface chemistry:
(3) ***Regioselective*** hydrogenation system using ordered alloys

Target reaction

Hydrogenation of asymmetric diene to monoene

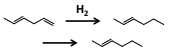

No heterogeneous catalyst has been achieved this type of reaction with high yields.

Conclusion

- Regio and chemoselective hydrogenation of dienes to monoenes can be achieved using RhBi/SiO_2 with high yield.
- The combination of one-dimensionally aligned Rh allays and steric hindrance of large Bi atoms allows preferential adsorption of terminal C=C moiety.

M. Miyazaki, S. Furukawa,* T. Komatsu,* *J. Am. Chem. Soc.*, **2017**, *139*, 18231.

Catalyst survey

Hydrogenation of 1,4-hexadiene over various catalysts

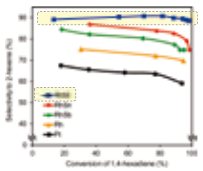

Reaction condition
catalyst: 50 mg (Rh 3 wt%)
Substrate: 0.5 mmol
solvent: AcOEt 5 ml
H_2 pressure: 1 atm
temperature: 70°C
conversion: @0.5 h
selectivity: @95% conv.

RhBi/SiO_2 gave 2-hexane with 90% yield.

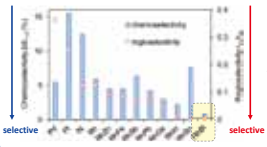

RhBi showed the best regio and chemo selectivities (lowest ΔS_{1+2} and r_{1h}/r_{2h} values)

Chemoselectivity: ΔS_{1+2} decrease in alkenes selectivity during the reaction

Regioselectivity: r_{1h}/r_{2h} relative formation rate of 1-hexene to that of 2-hexene

Substrate scope of RhBi/SiO_2

Table 1. Hydrogenation of various dienes using RhBi/SiO_2

Entry	substrate	product	time / h	conv. (%)	sel. (%)	
1			5.5	95	90	intra
2			20	99	88	intra
3			6	85	89	intra
4			9	90	95	intra
5			18	97	80	intra
6			10	83 9	90 10	inter

Reaction condition: catalyst: 10 mg, substrate: 0.2 mmol, temp.: 25˚C, solvent: THF 5 mL

The corresponding inner alkenes were obtained with high yields for not only **intramolecular** but also **intermolecular** fashions.

Characterization

TEM & STEM images of RhBi/SiO_2

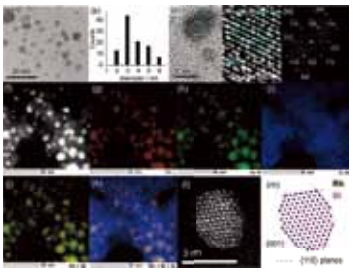

Small nanoparticles (ca. 3 nm) of single crystals of intermetallic RhBi were formed.

FT-IR spectra of adsorbed CO

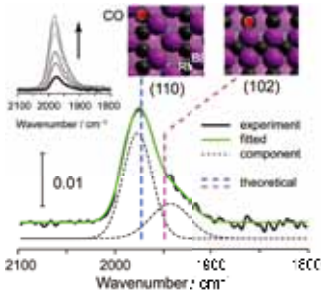

Theoretical values (by DFT) of the vibratonal frequencies of CO on RhBi(110) and (102) agreed finely with the experimental values, supporting the exposure of these planes.

XRD patterns of RhM/SiO_2

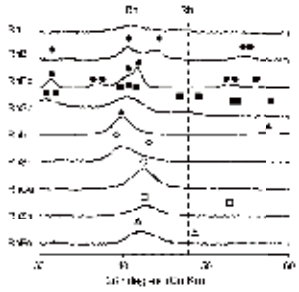

The desired ordered alloy phases were successfully formed with high phase-purity.

Kinetic studies

Reaction orders

$$r = k P_{H_2}^{1.0} [\text{diene}]^{-0.4}$$

Based on the following kinetic model, this result indicates that **the rate-determining step is a surface reaction** (H diffusion or attack).

Kinetic model based on a Langmuir-Hinshelwood-type mechanism

Considering a Langmuir-Hinshelwood type mechanism for the diene hydrogenation, the reaction steps are described as follows:

$H_2 + \sigma \rightleftarrows 2\,H\cdot\sigma$: H_2 adsorption
$S + \sigma \rightleftarrows S\cdot\sigma$: diene adsorption
$2\,H\cdot\sigma + S\cdot\sigma \rightleftarrows P\cdot\sigma + \sigma$: surface reaction
$P\cdot\sigma \rightleftarrows P + \sigma$: alkene desorption

where, S, P, and σ are reactant diene, product alkene, and adsorption site, respectively.

Assuming that the surface reaction is the rate determining step, the overall reaction rate can be expressed as follows:

$$r = k\theta_H^2\theta_S$$

Besides, other steps can be regarded to be in equilibrium. Therefore, the equilibrium constants are defined as follows:

$$K_1 = \theta_H^2/P_{H_2}(1-\theta)$$
$$K_2 = \theta_S/[S](1-\theta)$$
$$K_4 = [P](1-\theta)/\theta_P$$

where, k, θ_S, and $(1-\theta)$ are the rate constant of surface reaction, coverage of X, and percentage of vacant site: $1-(\theta_H+\theta_S+\theta_P)$, respectively. Here, the coverages are expressed as follows using the corresponding sticking probabilities, k_S:

$$\theta_H = 2K_{H_2}P_{H_2}(1-\theta)$$
$$\theta_S = k_S[S](1-\theta)$$
$$\theta_P = k_P[P](1-\theta)$$
$$1-\theta = \frac{1}{1+2K_4P_{H_2}+K_4[S]+K_4[P]}$$

Based on these, the overall reaction rate can be descried as follows:

$$r = \frac{kK_1K_2P_{H_2}[S]}{(1+2K_4P_{H_2}+K_4[S]+K_4[P])^2}$$

When adsorption of H_2 and diene are very weak and strong, respectively ($K_{H_2}P_{H_2} \ll 1$, $K_4[S] > 1$) and assuming low diene conversions ([P]~0), this equation is approximated simply as follows:

$$r = \frac{kK_1K_2P_{H_2}[S]}{(1+K_4[S])^2}$$

This equation indicates the first-order dependence of r on P_{H_2} and that the reaction order of [S] ranges from −1 to 1. Considering $K_4[S] > 1$, the reaction order of [S] inclines to the negative side. This strongly agrees with the experimental reaction orders (1.0 and −0.4 for P_{H_2} and [P], respectively), supporting the validity of this kinetic model.

A first-order dependence of H_2 pressure on reaction rates generally suggests the following situations, (1) diffusion (or dissolving) limiting, (2) adsorption limiting, and (3) surface reaction limiting. However, the negative order of reactant diene and the low KIE value observed for D_2 excludes (1) and (2), respectively. Therefore we conclude that the surface reaction is rate-limiting.

DFT Calculations

Crystal structure of RhBi

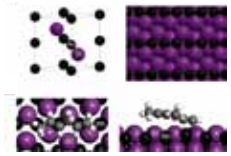

RhBi(110) plane

Optimized structure of adsorbed 1,4-hexadiene

Transition state structure

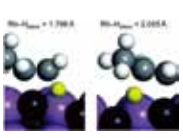

Rh-H distance at TS
terminal C=C < inner C=C

Energy diagram of 1,4-hexadiene hydrogenation

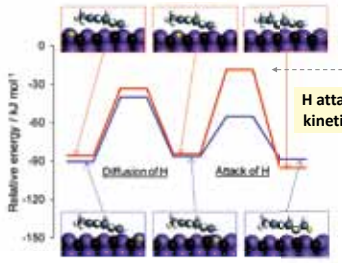

H attack to inner C=C

H attack to inner C=C is kinetically unfavorable

H attack to terminal C=C

Regioelectivity vs. atomic radius of M

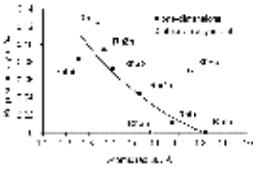

- The larger the second atom is, the higher the regioselectivity is.
- More clear relationship was observed among RhM with one-dimentionally aligned Rh.

The regioselectivity relies on the bulkiness of M and one-dimentional alignment of Rh atoms.

Machine Learning Prediction of Adsorption Energies on Metal Alloys for Effective Utilization of Methane

Takashi Toyao,[a,b] Satoru Takakusagi,[a] Ichigaku Takigawa,[c] Ken-ichi Shimizu,[a,b]

[a] *Institute for Catalysis, Hokkaido university, N-21, W-10, Sapporo 001-0021, Japan*
[b] *Elements Strategy Initiative for Catalysts and Batteries, Kyoto University, 615-8520, Kyoto, Japan*
[c] *Graduate School of Information Science and Technology, Hokkaido University, N-14, W-9, Sapporo 060-0814, Japan*

Introduction

Previous study

Machine-learning prediction of the d-band center for metals and bimetals

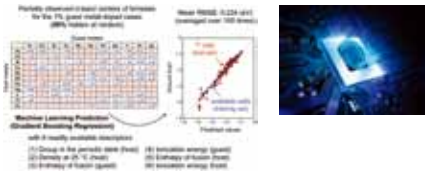

Takigawa, K. Shimizu, K. Tsuda, S. Takakusagi, RSC Advances, 2016, 6, 52587
Highlighted in Chemistry World

Brønsted-Evans-Polanyi relation

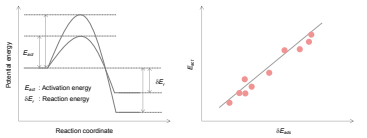

Linear relationship between activation energy and dissociative chemisorption energy

Utilization of CH_4

Partial oxidation reaction

$CH_4 \rightarrow CH_3OH$

Coupling reaction

$CH_4 \rightarrow C_2H_4,\ C_2H_6,\ C_6H_6$

The key is how to produce CH_3 species and prevent successive formation of CH_2 species

H. Schwarz, Angew. Chem. Int. Ed. 2011, 50, 10096
X. Bao et al., Science, 2014, 344, 616

This study

We have predicted adsorption energies of CH_4 related species (CH_3, CH_2, CH, C, and H) on the Cu-based alloys toward efficient utilization of CH_4.

The process employed to discover new materials for specific applications typically utilizes screening of large compound libraries. In this approach, the performance of a compound is correlated to the properties of elements referred to as descriptors. In the effort described below, we developed a simple and eiicient machine learning (ML) model for predicting adsorption energies of CH_4 related species, namely CH_3, CH_2, CH, C, and H on the Cu-based alloys. The developed ML model predicted the DFT-calculated adsorption energies with 12 descriptors, which are readily available values for the selected elements. The predictive accuracy of 4 regression methods (ordinary linear regression by least squares (OLR), random forest regression (RFR), gradient boosting regression (GBR), and extra tree regression (ETR)) with diirerent numbers of descriptors and different test-set/training-set ratios were quantitatively evaluated using statistical cross validations. Among 4 types of regression methods, we have found that ETR gave the best performance in predicting the adsorption energies with the average root mean squared errors (RMSE) below 0.3 eV. Strikingly, despite its simplicity and low computational cost, this model predicts well the adsorption energies on a range of Cu-based alloy models (46 in total number) as calculated by using DFT. In addition, we show the ML prediction for the differences in the adsorption energies of CH_3 and CH_2 on the same surface. This would be of great importance especially when designing the selective catalytic reaction processes to suppress the undesired over reactions. The accuracy and simplicity of the developed system suggest that adsorption energies can be readily predicted without time-consuming DFT calculations, and eventually, this would allow us to predict the catalytic performances of the solid catalysts.

Methods and results

Computational methods for DFT calculations

- ✓ Vienna ab initio simulation package (VASP)
- ✓ Perdew–Burke–Ernzerhof (PBE) generalized gradient functional
- ✓ Cutoff energy = 400 eV
- ✓ 3 × 3 surface unit cell with 4 atomic layers
- ✓ 1 surface- and centered-atom-exchanged Cu(111)
- ✓ 15 Å vacuum height
- ✓ The bottom 2 layers were fixed at the corresponding bulk positions

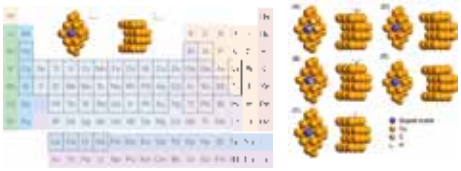

DFT-calculated adsorption energies of CH_3, CH_2, CH, C, and H

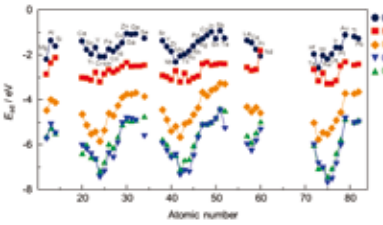

Machine learning methods

- ◆ Ordinary linear regression by least squares (OLR): Linear model
- ◆ Random forest regression (RFR): Non-linear model
- ◆ Gradient boosting regression (GBR): Non-linear model
- ◆ Extra trees regression (ETR): Non-linear model

Correlation of descriptors

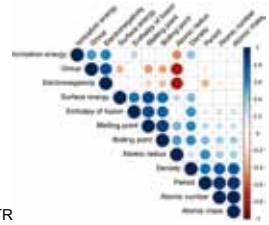

Screening of predictive ML methods using adsorption energies of CH_3

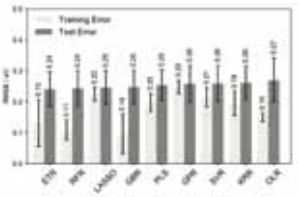

Evaluation of descriptor importance for ETR

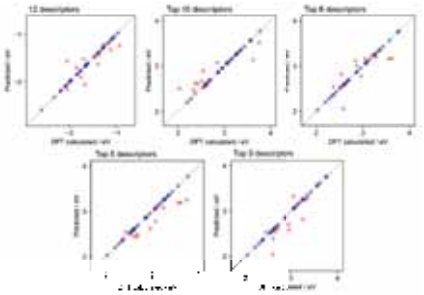

The robust ML prediction performance remained constant even when using even only 3 descriptors. The top 3 descriptors of the doped metal include its group in the periodic table, surface energy, and melting point.

Prediction of adsorption energies of CH_3 with 4 ML methods

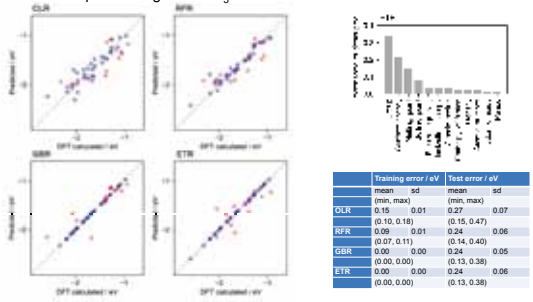

	Training error / eV		Test error / eV	
	mean (min, max)	sd	mean (min, max)	sd
OLR	0.15 (0.10, 0.18)	0.01	0.27 (0.15, 0.47)	0.07
RFR	0.09 (0.07, 0.11)	0.01	0.24 (0.14, 0.40)	0.06
GBR	0.00 (0.00, 0.00)	0.00	0.24 (0.13, 0.38)	0.05
ETR	0.00 (0.00, 0.00)	0.00	0.24 (0.13, 0.38)	0.06

The three nonlinear methods (RFR, GBR, and ETR) showed better prediction performance than the OLR method. The three methods gave almost the same predicting accuracy. ETR and RFR are known to be less hyperparameter sensitive than GBR, and thus we can avoid demanding hyperparameter tuning. Moreover, the training time for ETR is considerably smaller than RFR and GBR because ETR is based on random-splitting trees. We therefore concluded that the ETR model is the best choice for prediction of the adsorption energies explored in this study.

Prediction of values of E_{CH3}-E_{CH2} for CH_4 utilization

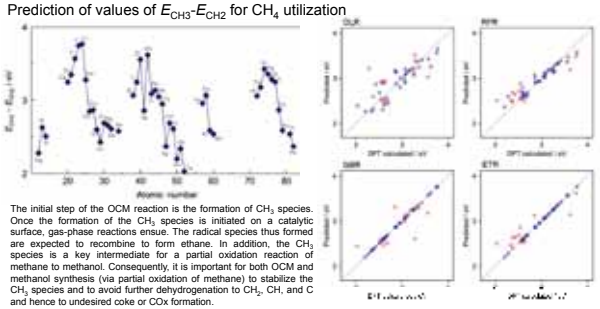

The initial step of the OCM reaction is the formation of CH_3 species. Once the formation of the CH_3 species is initiated on a catalytic surface, gas-phase reactions ensue. The radical species thus formed are expected to recombine to form ethane. In addition, the CH_3 species is a key intermediate for a partial oxidation reaction of methane to methanol. Consequently, it is important for both OCM and methanol synthesis (via partial oxidation of methane) to stabilize the CH_3 species and to avoid further dehydrogenation to CH_2, CH, and C and hence to undesired coke or COx formation.

For the catalysts design, therefore, creating surfaces on which the CH_3 species adsorbs more strongly than does the CH_2 species is crucial. For this reason we compared the adsorption energies of CH_3 and CH_2 on the Cu-based alloy surfaces. The difference in the adsorption energies of CH_3 and CH_2, obtained by subtraction of the adsorption energies of CH_3 from those of CH_2 (E_{CH3}-E_{CH2}) are presented above. If our hypothesis is correct, elements that show small E_{CH3}-E_{CH2} values (e.g., Te, Sn, and Mg) are the best-suited doping metals. On the contrary, elements that show large E_{CH3}-E_{CH2} values (e.g., Cr, V, and Mo) could generate Cu surfaces that induce the undesired reactions of methane.

Prediction of adsorption energies of CH_2, CH, C, and H

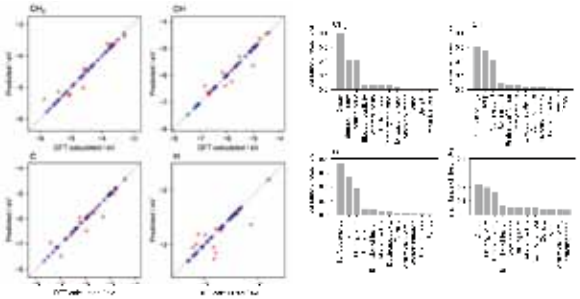

Conclusions

- ✓ DFT-calculated adsorption energies of CH_3, CH_2, CH, C, and H on Cu-based alloys (46 in total number for each adsorbate) were predicted by machine learning methods by using 12 descriptors, which are readily available values for the selected elements
- ✓ Among 4 types of regression methods (ordinary linear regression by least squares (OLR), random forest regression (RFR), gradient boosting regression (GBR), and extra tree regression (ETR)), ETR gave the best performance in predicting the adsorption energies with the average root mean squared errors (RMSE) below 0.3 eV.
- ✓ ML prediction for the differences in the adsorption energies of CH_3 and CH_2 on the same surface was also presented for practical use to design the selective catalytic reaction processes to suppress the undesired over reactions.

Proof of multielectron transfer processes in heterogeneous photocatalysis

Mai Takashima,[1,2] Haruna Hori,[2] Shugo Takeuchi[2], Mai Takase[3] and Bunsho Ohtani[1,2]
[1]Institute for Catalysis and [2]Graduate School of Environmental Science, Hokkaido University,
[3]Graduate School of Engineering, Muroran Institute of Technology

commercial titania

- 4 kinds of commercial titania
  - small anatase; Ishihara Sangyo ST-01 (4 nm): SA
  - small rutile; Tayca MT-150A (13 nm): SR
  - large anatase; Fluka (170 nm): LA
  - large rutile; Showa Denko Ceramics ST-G2 (360 nm):LR
- photocatalytic activity tests
  O_2 system; $2H_2O + 4h^+ \rightarrow 4H^+ + O_2$ with IO^{3-} or Fe^{3+}

flake ball-shaped bismuth tungstate

- hydrothermal synthesis
  - Bismuth Nitrate(Bi(NO3)3:5.0 mmol)
  - Sodium Tungstate (Na_2WO_4:2.75 mmol)
    - ✓ hydrothermal synthesis (433 K, 20 h)
    - ✓ calcination (773 K for 3 h in air)
    - ✓ wet milling (a planetary ball mill, 500 rpm for 6 h)
- photocatalytic activity tests
  CO_2 system; $CH_3COOH + 2O_2 \rightarrow 2CO_2 + 2H_2O$

light intensity dependency

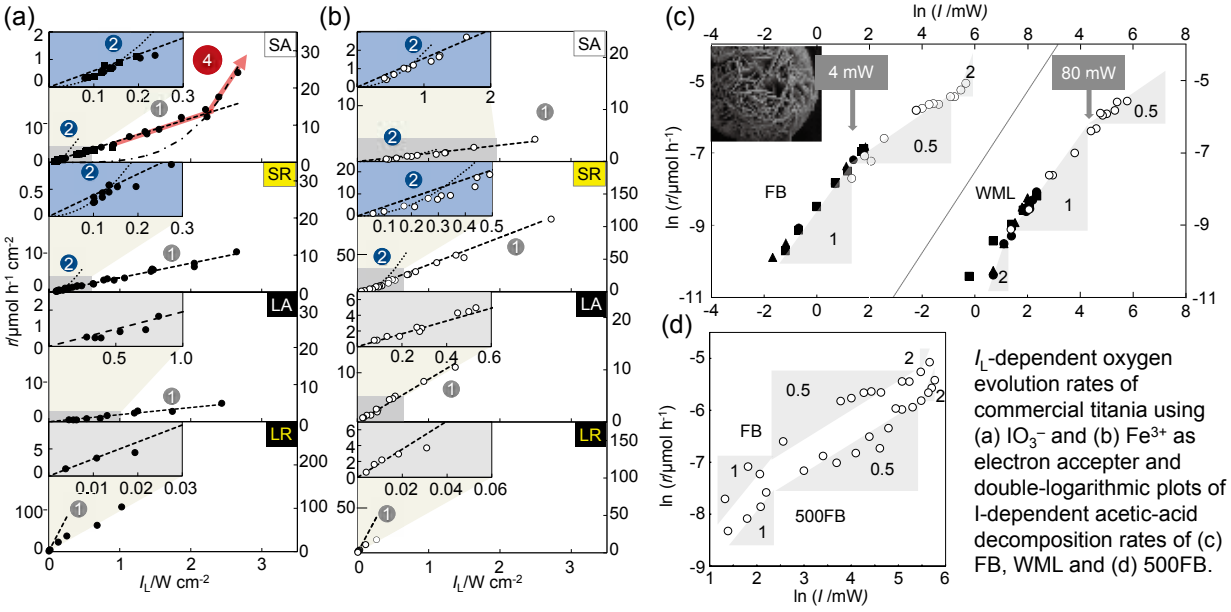

I_L-dependent oxygen evolution rates of commercial titania using (a) IO_3^- and (b) Fe^{3+} as electron accepter and double-logarithmic plots of I-dependent acetic-acid decomposition rates of (c) FB, WML and (d) 500FB.

kinetic model

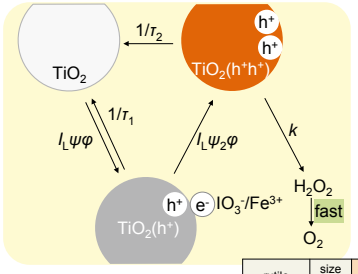

I_L : light intensity
ψ : photoabsorption efficiency
ψ_2 : photoabsorption efficiency <$TiO_2(h^+)$>
φ : quantum efficiency of e^- capture
k : rate constants

(reaction step)	(rate)	(description)
<BWO> + $h\nu$ → < BWO(1e)>	$I\psi_0\Phi$	first excitation
< BWO(1e)> + $h\nu$ → < BWO(2e)>	$I\psi_1\Phi$ [BWO(1e)]	second excitation
<BWO(1e)> → <BWO>	k_d [BWO(1e)]	deactivation
< BWO(2e)> + RH → <BWO> + R• k_r	[BWO(2e)][RH]	radical formation
R• + O_2 → RO_2•	k_i [R•][O_2]	initiation
RO_2 • + RH → RO_2H + R•	k_p [RO_2•][RH]	propagation
$2RO_2$• → RO_4R	k_t [RO_2•]^2	termination

$$r = \frac{I^2\psi_0\psi_1\Phi^2}{k_d + I\psi_1\Phi} + k_p[RH]\left(\frac{\psi_0\psi_1\Phi^{2\,0.5}}{k_t}\right)\left(\frac{I^2}{k_d + I\psi_1\Phi}\right)^{0.5}$$

direct hole reaction

radical chain reaction with peroxy radical as a chain carrier

BWO> : photocatalyst, RH : substrate
I : light intensity
ψ_0 : photoabsorption efficiency of <BWO>
ψ_1 : photoabsorption efficiency <BWO(1e)>
Φ : quantum efficiency of e-h+ production
k : rate constants

$$r = \frac{k\, I_L^{\,2}\psi\psi_2\varphi^2}{(1/\tau_1)\,(k + 1/\tau_2 + (k + 1/\tau_2)\, I_L\, \psi_2\varphi)}$$

at lower I, $r = I_L^{\,2}\psi\psi_2\varphi^2\tau_1$
at higher I, $r = I_L\,\psi\varphi$

$I_{thr} = 1/\psi_2\varphi\tau_1$

IO_3^-	rutile	size /nm	acceptor	(φ)	I_{thr}/mW	($\psi'\varphi'\tau$)
	SR	13	IO_3^-	1	80	1
	SR	13	Fe^{3+}	13	190	0.4

rutile	size /nm	(φ)	I_{thr}/mW	($\psi'\varphi'\tau$)
SR	13	1	80	1
SR calcined at 973 K	69	10	20	4.0
LR	350	22	< 1	> 80

at lower I → $I\psi_1\Phi << k_d$
$r = I^2\psi_0\psi_1\Phi^2k_d^{-1} + k_3[RH](I^2\psi_0\psi_1\Phi^2k_d^{-1}k_t^{-1})^{0.5} \rightarrow (\alpha/k_d^{0.5})\, I$

at higher I → $I\psi_1\Phi >> k_d$
$r = I\psi_0\Phi + k_p[RH](I\psi_0\Phi k_t^{-1})^{0.5} \rightarrow (\alpha/(\psi_1\varphi)^{0.5})\, I^{0.5}$

$I_{thr} = k_d(\psi_1\Phi)^{-1}$

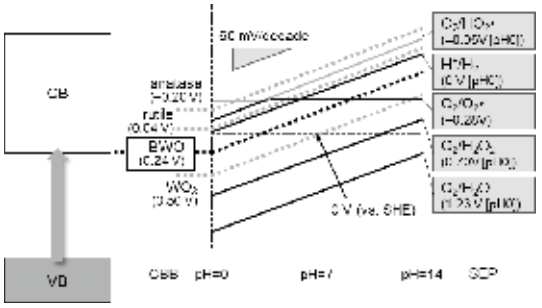

Conclusion

Light-intensity dependences of rates for photocatalytic water oxidation and oxygen reduction were studied using commercial titania and laboratory-made bismuth tungstate powders under high-intensity 365-nm UV-LED photoirradiation and processes of multielectron (mainly two-electron) transfer reaction were supported based on kinetic models.

[1] S. Takeuchi, M. Takashima, M. Takase and B. Ohtani, *Chem. Lett.*, accepted
[2] H. Hori, M. Takashima, M. Takase and B. Ohtani, *Catal. Today*, in press (10.1016/j.cattod.2018.01.001)

Multielectron Oxygen Reduction on Copper(I) oxide-Loaded Titanium-oxide Photocatalysts in Decomposition of Organic Compounds

Peng Wang and Bunsho Ohtani

Institute for Catalysis, Hokkaido University, Sapporo 001-0021, Japan
Email: wang.p@cat.hokudai.ac.jp

Introduction

ADVANTAGES:
- Low cost
- High chemical stability
- Photocatalytic reactions

TiO_2

DISADVANTAGES:
- Large band gap (3.0-3.2 eV)
- Ultraviolet light absorption (3-5 %)
- Absence of specific reaction site to accumulate excited electrons (rutile)

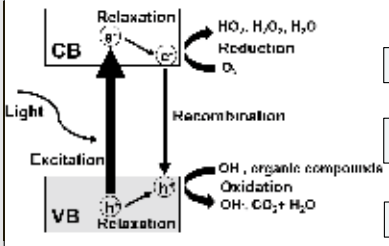

Fig. 1 Mechanism of titania in photocatalytic reactions.

Research Objectives

Photoabsorption ✚ **Photocatalytic activity** ✚ **Role of FCPs**

Experimental

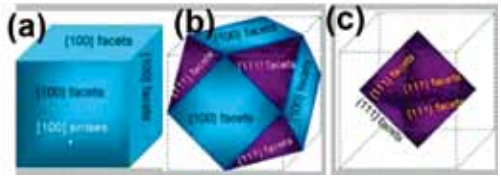

Fig. 2 3-D geometry models of faceted copper(I) oxide polyhedrons. (a) cube; (b) cuboctahedron; (c) octahedron.

Faceted Cu_2O particles (FCPs)
- Cubes (c): six {100} facets
- Cuboctahedrons (co): eight {111} and six {100} facets
- Octahedrons (o): eight {111} facets

Room temperature: r-c, r-co and r-o.

FCPs-loaded titania: c-S, co-S, o-S, r-c-S, r-co-S and r-o-S.

Results and Discussions

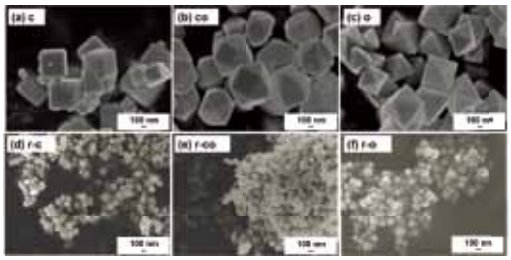

Fig. 3 SEM images of faceted Cu_2O particles (FCPs).
- Cube → Cuboctahedron → Octahedron
- Low temperature: small particle size

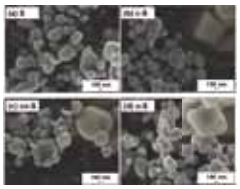

Fig. 4 SEM images of titania and FCPs-loaded titania.

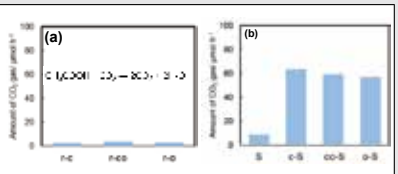

Fig. 5 (a) Photocatalytic activity of FCPs in CO_2 system; (b) Photocatalytic activity of titania and FCPs-loaded titania in CO_2 system.

- Loading amount: 2 wt%
- Good interaction
- XRD, UV-vis, EDS: copper(I) oxide (data not shown)

Photocatalytic activity:
- r-c, r-co and r-o: low activity
- FCPs-loaded titania > titania
- c-S > co-S > o-S > S

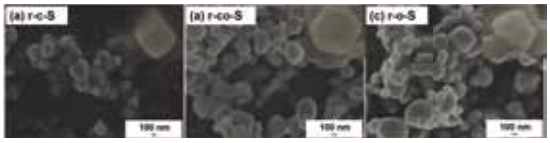

Fig. 6 SEM images of titania (STG2) and FCPs-loaded titania.

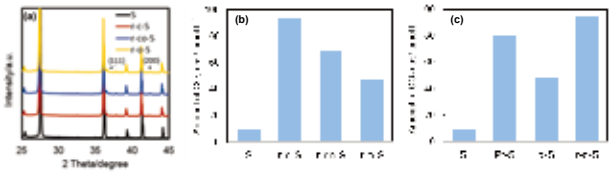

Fig. 7 (a) XRD patterns of titania (STG2) and FCPs-loaded titania; (b) Photocatalytic activity of titania and FCPs-loaded titania in CO_2 system; (c) Photocatalytic activity of titania, Pt-loaded titania, copper(I) oxide-loaded titania(denoted as b-S, mixed by mortar) and FCPs-loaded titania in CO_2 system.

Photocatalytic activity:
- r-c-S > r-co-S > r-o-S > S, {100} facet is the most active facet
- r-c-S > b-S, better interaction by in-situ one-pot wet chemical synthesis
- r-c-S > Pt-S, suppress electron/hole recombination
- Multielectron oxygen reduction (two or four)

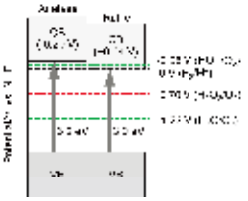

Fig. 8 Schematic diagram of possible oxygen reduction reactions of titania.

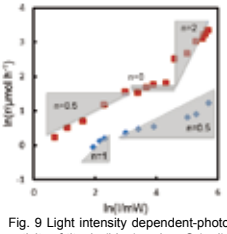

Fig. 9 Light intensity dependent-photocatalytic activity of titania (blue) and r-c-S (red).

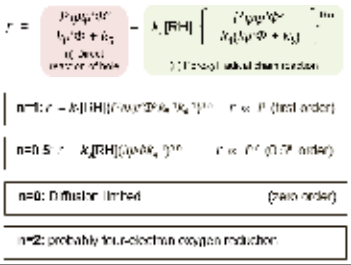

Two-electron oxygen reduction

<PC> + $h\nu \rightarrow$ <PC> (e^-)	$I\psi\Phi$
<PC> (e^-) + $h\nu \rightarrow$ <PC>*	$I\psi'\Phi$
<PC>* + RH → <PC> + R ·	k_1
R · + $O_2 \rightarrow RO_2$ ·	k_2
RO_2 · + RH → RO_2H + R ·	k_3
$2RO_2$ · → RO_4R	k_4
<PC> (e^-) → <PC>	k_5

<PC> : photocatalyst
I : light intensity
Φ : quantum efficiency
k : rate constant
RH : reactive substrate
Ψ : absorption efficiency (<PC>)
Ψ' : absorption efficiency (<PC> (e^-))

Acknowledgements and References

The author (pw) acknowledges the financial support from JSPS Postdoctoral Fellowship Program for Overseas Researchers.

(1) Abe R.; Takami H.; Murakami N.; Ohtani B. J. Am. Chem. Soc. 2008, 130, 7780
(2) Zhang, D.; Zhang, H.; Guo; L. Zheng, K.; Han X.; Zhang Z. J. Mater. Chem. 2009, 29, 5220-5225

Crystalline characteristics and photocatalytic activity of decahedral-shaped anatase titania particles

Kenta Kobayashi,[1] Mai Takashima,[1,2] Mai Takase[3] and Bunsho Ohtani[1,2]
[1]*Graduate School of Environmental Science and* [2]*Institute for Catalysis, Hokkaido University,*
[3]*Graduate School of Engineering, Muroran Institute of Technology*

■Decahedral anatase titania particles (DAP)

(001)
high surface energy
(101)
thermodynamically stable

high-level photocatalytic activity

crystalline phase transition
anatase (metastable state) ⇨ rutile (stable state)

phase transition occurred from (001) facet showing lower stability

Chem. Mater, **26**, 1014 (2014)

effect of particles fusion on
- transition behavior
- photocatalytic activity

■Effect of fusion on DAP properties

sample	*SSA* /$m^2\ g^{-1}$	crystalline size/nm	anatase (%)	rutile (%)	non crystal (%)	activity (CO_2)	activity (H_2)	phase transition temperature/K	transition rate/K^{-1}	*NCP*
nf-DAP	14.3	73.8	86.39	2.45	11.16	115	264	1205	-1.09	1.32
f-DAP	13.7	55.7	86.72	7.40	5.88	97	187	1150	-0.734	4.19
reference	97.5	11.7	78.28	6.65	15.07	(100)	(100)	990	-0.721	-

degree of fusion

number of composition particles (*NCP*) = number of particles / number of group

anatase-rutile phase transition

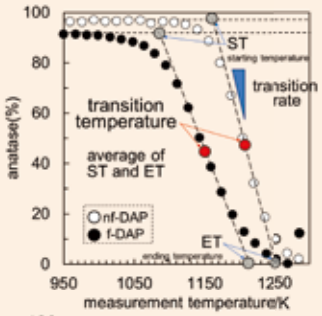

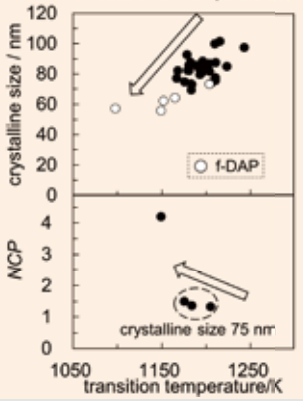

f-DAP show small crystalline size

higher *NCP*, lower phase transition temperature

progression of phase transition easily by grain boundary

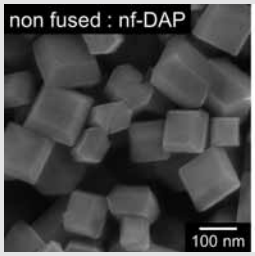

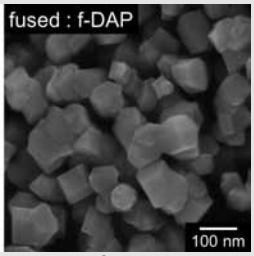

distance from tube to foil 7.5 cm 5.5 cm

fusion caused by lattice defects or impurity

grain boundary leading to crystalline defects and high interface energy

photocatalytic activity

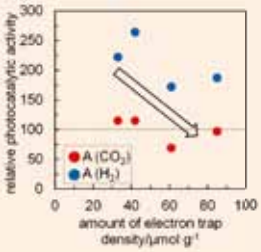

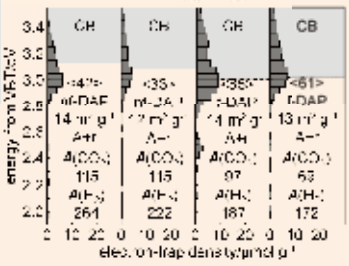

high amount of electron trap density derived grain boundary

effect of particles fusion decreasing phase transition temperature and photocatalytic activity

future plan
- Investigation of energy-resolved distribution of electron traps

■Experimental

DAP preparation by gas-phase reaction

$TiCl_4 + O_2 \rightarrow TiO_2 + 2Cl_2$

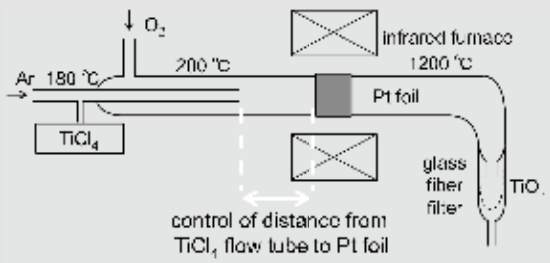

Photocatalytic activity test

$CH_3COOH+2O_2 \rightarrow 2CO_2+2H_2O$
$CH_3OH \rightarrow H_2+HCHO$

photocatalytic activity evaluated with rate of production liberation

light source: mercury lamp (λ>290 nm)
reference photocatalyst: FP-6 (Showa Denko Ceramics)

Temperature programed XRD measurement

Temperature condition		XRD measurement condition	
increasing rate	2 K min^{-1}	scanning rate	10° min^{-1}
measurement rate	573-1523 K	scanning range	10-90°

X-ray diffraction analysis on thermal anatase-rutile transformation of titania particles

Bob John,[1] Mai Takashima[1,2] and Bunsho Ohtani1[1,2]

(Graduate School of Environmental Science,[1] Institute for Catalysis,[2] Hokkaido University)

Anatase-rutile transition (ART)

<Purpose>
what governs anatase-rutile (ART) transition

metastable form

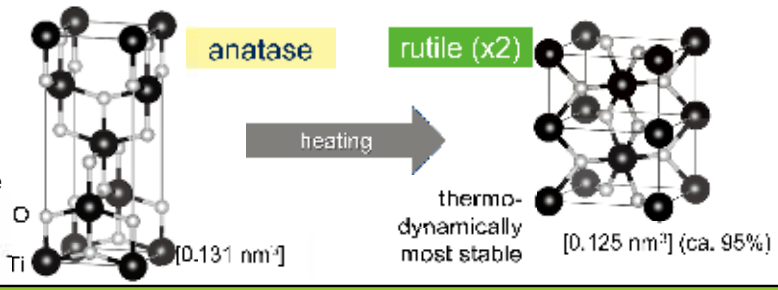

ART
- important in material science
- kinetically controlled
- unknown mechanism
- different behaviour depending on the physical/structural properties

Analysis of ART by temperature-programmed XRD

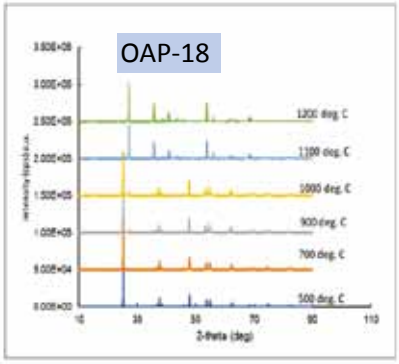

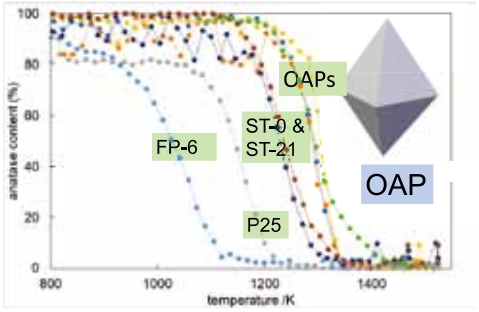

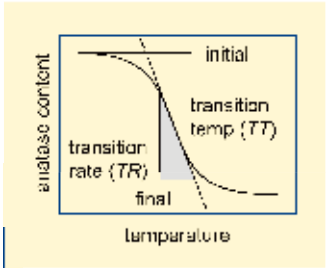

- 2θ: 10-90°
- rate: 2 K min^{-1}
- scan rate: 10 K min^{-1}
- temperature: 573 -1523 K

- OAP: octahedral anatase particles
- hydrothermally (HT) synthesized
- 6, 9, 12 & 18: HT times (hrs)

sample	anatase (%)	rutile (%)	non crystal (NC) (%)	specific surface area/m^2 g^{-1}	anatase-crystallite size/nm	transition temp. (TT)/K	transition rate (TR)/K^{-1}
FP-6	83	8	9	104		918	0.76
P-25	82	15	3	58		1048	0.74
ST-01	80	0	20	344		1235	0.90
ST-21	87	0	13	67		1237	0.82
OAP-6	78	0	22	59	21	1234	0.86
OAP-9	81	0	18	49	23	1264	1.13
OAP-12	83	0	17	41	23	1250	1.24
OAP-18	85	0	15	40	23	1303	1.58

Crystallite size analysis

crystallite size = Scherrer equation
- 2θ =25.2 for anatase {101} plane
- 2θ = 27.2 for rutile {110} plane

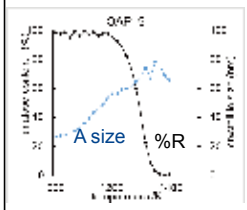

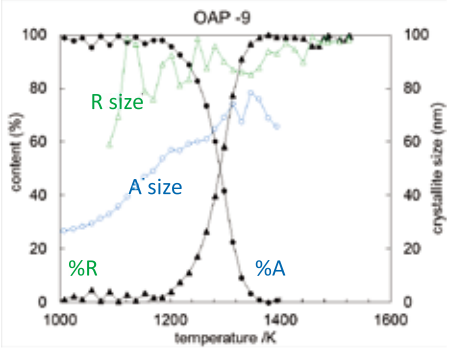

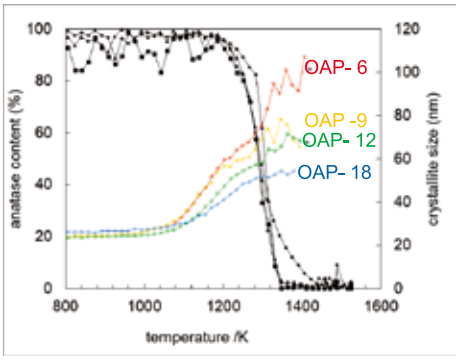

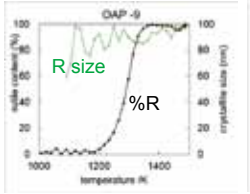

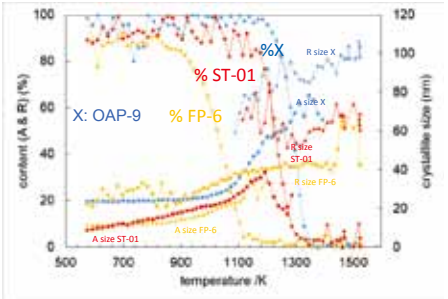

Conclusion

- ART was successfully studied by programmed XRD method.
- OAP has higher thermal stability
- crystallite size of anatase increase with temperature
- ART process: amorphous-anatase→rutile
  (smaller anatase→rutile
  larger anatase→ rutile)

Excited-state Aggregate Formation of A Near-infrared Dye

Yue Wang[a], Rong Wang[b], Tamaki Nakano[a]*

*[a]Institute for Catalysis (ICAT), Graduate School of Chemical Sciences and Engineering, and Integrated Research Consortium on Chemical Sciences (IRCCS), Hokkaido University, Japan *E-mail: tamaki.nakano@cat.hokudai.ac.jp*
[b]On leave from College of Chemistry and Molecular Engineering, Peking University, China

Abstract: Dyes that emit light in the near infra-red (NIR) region are important in medicinal and physiological fields because they can be applied for diagnosis and imaging of tissues due to the fact that water and hemoglobin do not seriously interfere through scattering and absorbance in the range of around 700-900 nm. 3,3'-Diethylthiatricarbocyanine iodide (DTCI) is a representative example among such dyes and has been studied from various view points. In this work, we investigated excited-state properties of DTCI in solution and found that DTCI forms at least two distinctive excited-state aggregates whose structures and contents vary depending on concentration and solvent. Such a phenomenon has been reported only for a system on the surface of gold but is unprecedented in a homogeneous system including solution.

1 Introduction

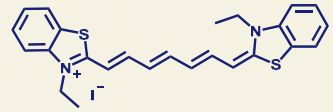

3,3'-Diethylthiatricarbocyanine Iodide (**DTCI**)

- Intense near-infrared absorption and emission
- High fluorescence quantum yield
  - -- Optical biological probe
  - -- Fluorescence imaging

2 Photophysical Properties

Emission and Excitation Spectra of DTCI in EtOH and in H_2O

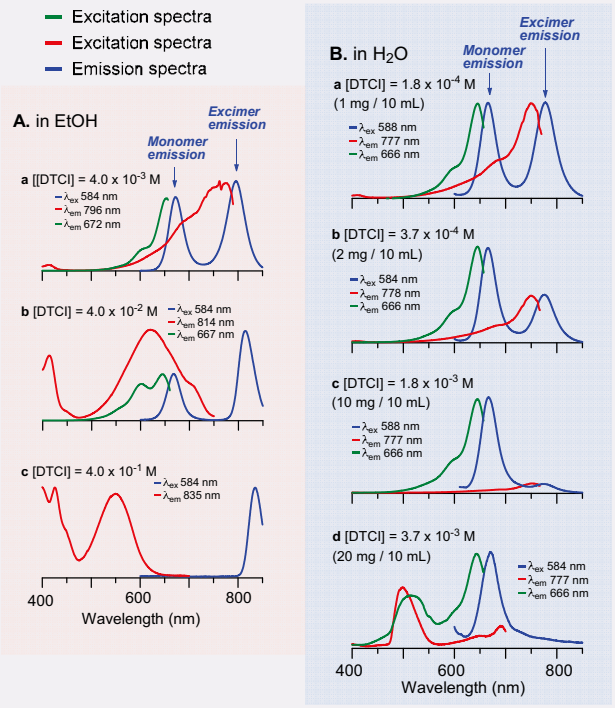

Fig. 1. Emission (blue) and excitation (green and red) spectra of DTCI in EtOH (A) and in H_2O (B) at different concentrations.

Emission and Excitation Spectra of DTCI in MeOH and in DMSO

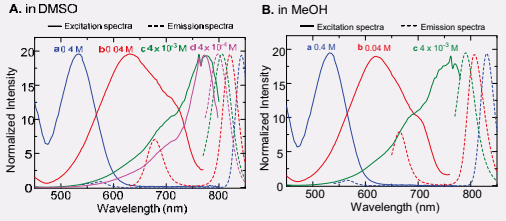

Fig. 2. Emission and excitation spectra of DTCI in DMSO (A) and in MeOH (B) at different concentrations.

Absorbance Spectra of DTCI in EtOH and in H_2O

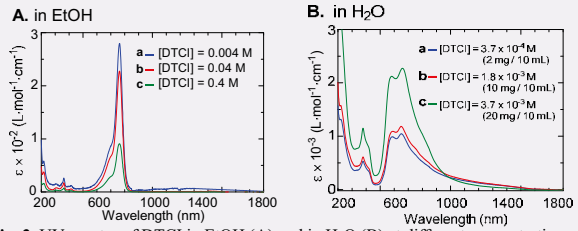

Fig. 3. UV spectra of DTCI in EtOH (A) and in H_2O (B) at different concentrations.

Aggregation of DTCI

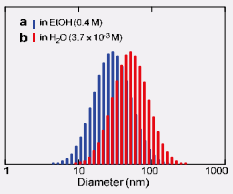

Fig. 4. Intensity-weighted Gaussian distribution of particle size of DTCI obtained through dynamic light scattering in EtOH (a) and in H_2O (b).

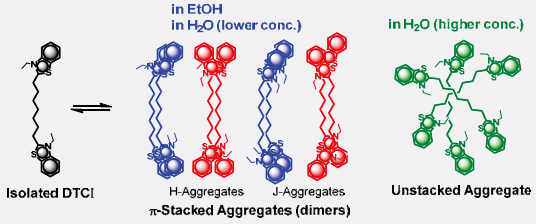

Fig. 5. Proposed basic aggregate structures of DTCI.

3 Conclusions

- DTCI shows monomer (600-700 nm) and excimer (750-850 nm) emissions.
- DTCI is proposed to form ***π-stacked aggregates*** in EtOH at all concentrations and also in H_2O at lower concentrations and ***unstacked aggregates*** in H_2O at higher concentrations.
- In EtOH, ***π-stacked aggregates*** with various structures with different excitation energies are responsible for the excimer emission. In H_2O at lower concentrations, ***π-stacked aggregates*** with rather uniform structure are responsible for the excimer emission. In both cases, the monomer emission may arise from ***isolated DTCI***.
- In H_2O at higher concentrations, ***unstacked aggregates*** as well as ***isolated DTCI*** may contribute to both monomer and excimer emissions.

4 Future Plans

- Studies on photophysical properties of DTCI in the presence of chiral molecules are under way to maximize the function of DTCI through chirality effects in bio imaging applications.

Synthesis and Properties of Antioxidant Polymers

Shunta Asada, Yue Wang, and Tamaki Nakano*

Institute for Catalysis (ICAT), Graduate School of Chemical Sciences and Engineering, and Integrated Research Consortium on Chemical Sciences (IRCCS), Hokkaido University, N 21, W 10, Kita-ku, Sapporo 001-0021, Japan
**tamaki.nakano@cat.hokudai.ac.jp*

Abstract: 4-Vinyldiphenylamine (VDPA) was prepared and polymerized under free-radical and cationic conditions to lead vinyl polymers as antioxidant materials. The polymers were suggested to possess partially branched structure which may have been created through chain-transfer to the amino group of the monomer or a unit in polymer chain. The polymers reacted with 1,1-diphenylpicrylhyrazyl (DPPH) as a free-radical oxidant model at high efficiency, and the efficiency was higher for the polymers than that of diphenyamine (DPA). It is intriguing that a polymer exhibited a higher reactivity compared with a corresponding small molecule.

Introduction

Natural antioxidants (flavonoids)

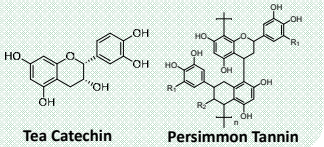

Artificial antioxidants

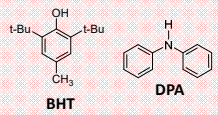

Example of antioxidant polymer

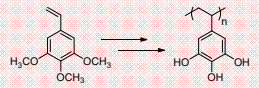

K. Zhan, H. Ejima, N. Yoshie, *ACS Sustain. Chem. Eng.* **2016**, *4*, 3857–3863

Radical-trapping mechanism

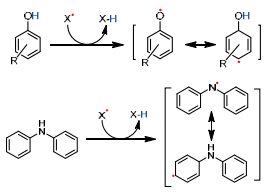

Monomer and Polymer Synthesis

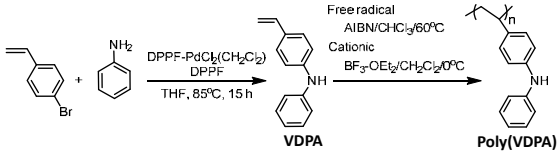

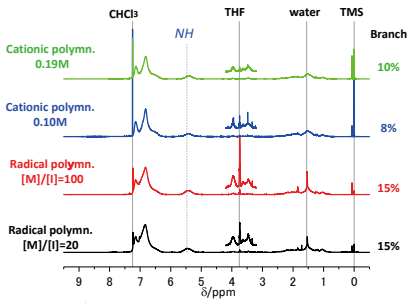

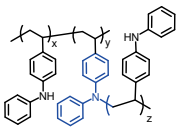

Partially branched structure

Figure 1. ^{1}H NMR spectra of poly(VDPA)s prepared under different conditions. [400 MHz, r.t., $CDCl_3$]

Table 1.Free-radical polymerization with AIBN for 24h[a]

Entry	Solvent	Temp. (°C)	[VDPA] (M)	[AIBN] (M)	[VDPA]/[AIBN]	Conv.[b] (%)	MeOH-insol. part[c] Yield (%)	M_n[d]	M_w/M_n[d]
1			1.00	0.200	5	>99	3	3,370	3.73
2	$CHCl_3$	60	1.00	0.050	20	>99	16	4,100	3.17
3			1.00	0.010	100	>98	46	8,820	2.27
4	Toluene	60	1.00	0.010	100	18	—	—	—
5	Acetone	60	1.00	0.010	100	19	—	—	—

[a]$CHCl_3$ 1.0 mL, Toluene 1.0 mL, Acetone 1.0 mL. [b]Determined by ^{1}H NMR spectra from the intensity ratio of remaining VDPA =CH_2 and aromatic singals. [c]Reprecipitated in MeOH and collected with a centrifuge. [d]Estimated by SEC (vs polystyrene).

Table 2.Cationic polymerization with BF_3-$O(C_2H_5)_2$ in CH_2Cl_2 at 0°C for 1.5h[a]

Entry	[VDPA] (M)	[BF_3-$O(C_2H_5)_2$] (M)	[VDPA]/[BF_3-$O(C_2H_5)_2$]	Conv.[b] (%)	MeOH-insol. part[c] Yield (%)	M_n[d]	M_w/M_n[d]
1	0.195	0.010	21	>99	37	12,390	3.44
2	0.100	0.010	20	>99	40	6,690	2.00

[a]Entry1 CH_2Cl_2 5.12 mL Entry2:CH_2Cl_2 25.7 mL. [b]Determined by ^{1}H NMR spectra from the intensity ratio of remaining VDPA =CH_2 and aromatic singals. [c]Reprecipitated in MeOH and collected with a centrifuge. [d]Estimated by SEC (vs polystyrene).

Antioxidant Properties

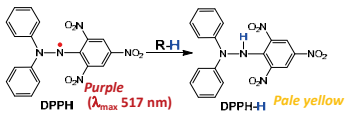

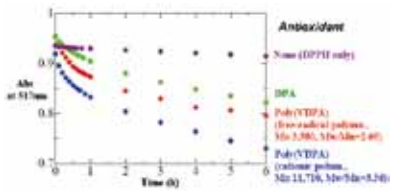

Figure 2. Absorbance at 517 nm-vs.-reaction time plots.
Conditions: [DPPH] = 789μM, [poly(VDPA) (cationic polymn., Mn 11,710)] =202μM, [poly(VDPA) (radical polymn., Mn 4,430)] =201μM, [DPA] = 199μM, cell path = 1 mm.

A. DPPH + poly(VDPA)(cationic polymn.)

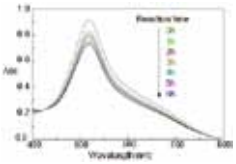

B. DPPH + DPA

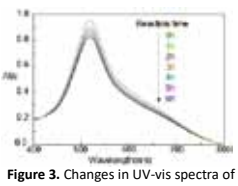

Figure 3. Changes in UV-vis spectra of a THF solution of DPPH on addition of poly(VDPA) (cationic polymn., Mn 11,710) (A) and DPA (B).
Conditions: [DPPH] = 789 μM, [Cationic poly(VDPA)] = 202 μM, [DPA] = 199 μM, cell path = 1 mm.

Partially π-Stacked Conformation

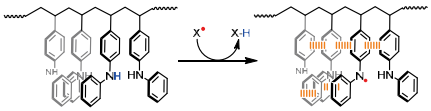

Stabilization of radical by a π-stacked conformation

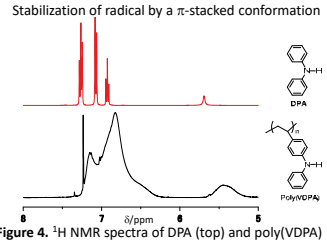

Figure 4. ^{1}H NMR spectra of DPA (top) and poly(VDPA) (bottom). [400 MHz, r.t., $CDCl_3$, TMS].

Conclusions

- ✓ Poly(VDPA) was prepared as a novel antioxidant, polymeric material.
- ✓ Poly(VDPA) efficiently reacted with DPPH as an oxidant model where stabilization of radical species through a partially π-stacked conformation may have a role.

Future plans

- ✓ Studies on effects of molar mass and stereo structure of poly(VDPA) on antioxidant properties.
- ✓ Synthesis and properties of VDPA-styrene copolymers and VDPA-containing polymer gels.
- ✓ ESR studies on radical stabilization effects of poly(VDPA).

Polyurethanes as Macromolecular Ligands for Catalytic Reactions

Akihiro Kimura,[1] Haruka Hayama,[1] Jun-ya Hasegawa,[1,2] Hassan Nageh,[1] Yue Wang,[1,2] Naofumi Naga,[3] Mayumi Nishida,[1,2] and Tamaki Nakano[1,2*]

[1]*Institute for Catalysis (ICAT) and Graduate School of Chemical Sciences and Engineering, Hokkaido University, N 21, W 10, Kita-ku, Sapporo 001-0021, Japan;* [2]*Integrated Research Consortium on Chemical Sciences (IRCCS);*
[3]*Graduate School of Science and Engineering, Shibaura Institute of Technology, 3-7-5 Toyosu, Koto-ku Tokyo 135-0061, Japan*
E-mail: tamaki.nakano@cat.hokudai.ac.jp

Abstract: Ir(I)-catalyzed direct borylation of aromatic compounds[1] was conducted in the presence of polyurethanes prepared by polycondensation of 4,4'-bis(hydroxylmethyl)-2,2'-bipyridyl with 1,6-diisocyanatohexane, 1,4-diisocyanatobenzene, 1,4-diisocyanato-3-methylbenzene, and bis(4-isocyanatophenyl)methane. The polymer prepared from 1,6-diisocyanatohexane showed best activities under most conditions. The borylation reaction systems with the polymers were biphasic where the top and bottom layers contained the product and the polymer-based catalysts, respectively. Due to the phase separation, the product isolation and catalyst recycle were readily performed through simple decantation.

1) T. Ishiyama, J. Takagi, K. Ishida, N. Miyaura, N. R. Anastasi, J. F. Hartwig, *J. Am. Chem. Soc.* **2002**, *124*, 390-391.

Polymerization

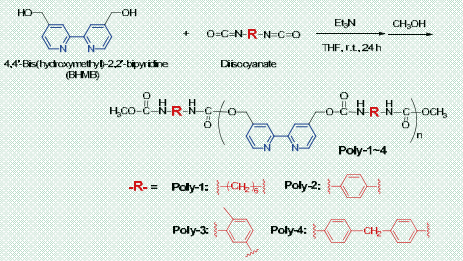

Table 1. Polycondensation between BHMB and diisocyanate[a]

Run	Product	[Diisocyanate]/[BHMB]	Conv.[b] of BHMB (%)	Yield (%)	DP[c]	M_n[d]
1	**Poly-1**	1.1	75	89[e]	11	4600
2	**Poly-2**	1.2	82	69[f]	29	11000
3	**Poly-3**	1.3	>99	97	8	3400
4	**Poly-4**	1.2	86	65[g]	2	1400

[a]Time 24 h, THF 2 mL, Et_3N 0.11 mL, BHMB 0.25–0.50 mmol, temp. 23 °C. [b]Determined by ^{1}H NMR spectra base on the intensity ratio of remaining BHMB -CH_2- and main-chain -CH_2- singals. [c]Estimated by ^{1}H NMR spectra based on the intensity ratio of terminal -OCH_3 and main-chain -CH_2- signals. [d]Calculated from DP. [e]Containing 6% BHMB. [f]Containing 12% BHMB. [g]Containing 8% BHMB.

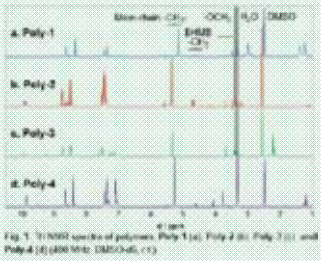

Catalytic reaction: Direct borylation

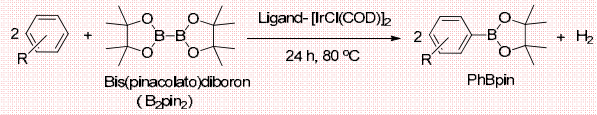

Benzene

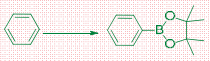

Table 2. Direct borylation of benzene[a]

Run	Ligand	Reaction for 4 h: Yield (%)[b]	Reaction for 4 h: TON	Reaction for 24 h: Yield (%)[b]	Reaction for 24 h: TON
1	bpy	98	66	95	64
2	BHMB	89	59	88	58
3	**Poly-1**	81	54	78	52
4	**Poly-2**	1	1	47	31
5	**Poly-3**	1	1	70	46
6	**Poly-4**	0	0	61	40

[a]Benzene 5.3 mL, 1/2[IrCl(COD)]$_2$ 5.56 mM (3 mol% of B_2pin_2), B_2pin_2 185 mM, nonane (internal standard) 100 mM, time 24 h, temp. 80 °C. [b]Estimated by GC mass spectroscopy using nonane as internal standard.

Anisole

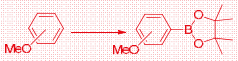

Table 3. Direct borylation of anisole[a]

Run	Ligand	Yield[b] (%)	TON	Isomer (%)[b]: *o*-	*m*-	*p*-
1	bpy	83	55	1	63	36
2	BHMB	78	52	2	70	29
3	**Poly-1**	1	1	24	41	35
4	**Poly-2**	8	5	2	78	20
5	**Poly-3**	6	4	2	76	21
6	**Poly-4**	15	10	2	80	18

[a]Time 24 h, anisole 6.50 mL, 1/2[IrCl(COD)]$_2$ 4.62 mM (3 mol% of B_2pin_2), B_2pin_2 154 mM, nonane 81.7 mM, temp. 80 °C. [b]Estimated by GC mass spectroscopy using nonane as internal standard.

Table 4. Effect of reaction time in anisole borylation[a]

Run	Ligand	Time (h)	Yield[b] (%)	TON	Isomer (%)[b]: *o*-	*m*-	*p*-
1	bpy	0.2	0.1	0.05	37	44	18
2	bpy	0.3	37	25	1	66	33
3	bpy	24	83	55	1	63	36
4	**Poly-1**	24	1	1	24	41	35
5	**Poly-1**[c]	24	50	11	3	72	25

[a]Anisole 6.50 mL, 1/2[IrCl(COD)]$_2$ 4.62 mM (3 mol% of B_2pin_2), B_2pin_2 154 mM, nonane 81.7 mM, temp. 80 °C. [b]Estimated by GC mass spectrometry using nonane as internal standard. [c]1/2[IrCl(COD)]$_2$ 13.66 mM (9 mol% of B_2pin_2)

Formation of polymer complex

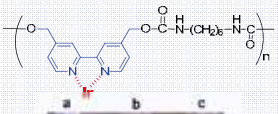

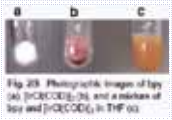

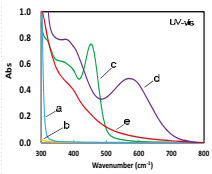

Fig. 2C. UV spectra of ligands, Ir species, and ligand-Ir mixtures in THF: bpy (a), Poly-1(b), 1/2[IrCl(COD)]$_2$ (c), bpy-1/2[IrCl(COD)]$_2$ (d), poly-1-1/2[IrCl(COD)]$_2$ (e). ([bpy] = [polymer (residue)] =5.56 mM in a and b; [Ir] = 5.56 mM in c, [bpy] = [polymer (residue)] = [Ir] = 5.56 mM in d and e, cell path = 1 mm). Samples for b and e were heterogeneous.

Catalyst recycle

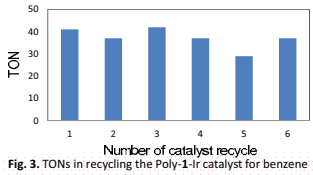

Fig. 3. TONs in recycling the Poly-**1**-Ir catalyst for benzene borylation conducted under the conditions of run 3 in Table 2 for 24 h.

Fig. 4. Photographic images of reaction systems with anisole with **poly-4** (run 6 in Table 5) (a) and with **BHMB** (run 2 in Table 5).

Inter-chain H-bonding

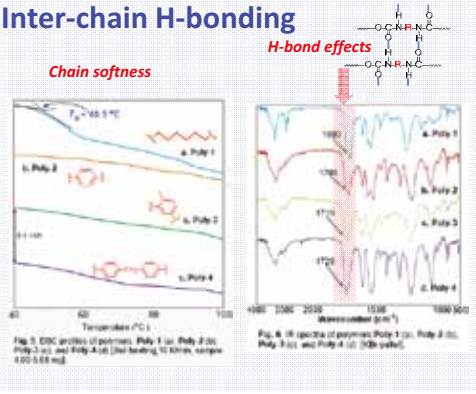

Polymer morphology

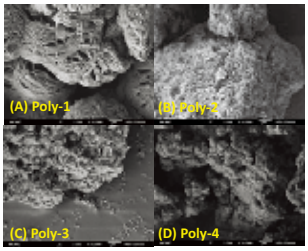

Fig. 7. SEM images of Poly-1 (A), Poly-2 (B), Poly-3 (C), and Poly-4 (D). [magnification × 10,000]

Conclusions:

1) **Poly-1** performed better than the other three polymers; the fact that this polymer has a Tg lower than that of the catalytic reaction and higher tendency of H-bond formation may be resposible for the performance.

2) The *o*-Isomer was preferentially generated in the reaction with anisole in the early stages of reaction.

3) The reaction systems involving the polymer catalysts are biphasic where product isolation and catalyst recovery were conducted through simple decantation or centrifuge.

4) Catalyst recycle was confirmed for the poly-1-Ir system with benzene as substrate.

Synthesis and Structure of Chiral Polyelectrolytes for Gene Delivery

Nino Zavradashvili,[1,2] Yue Wang,[1] Ramaz Katsarava,[2] Tamaki Nakano[1,*]

[1]*Institute for Catalysis (ICAT) and Integrated Research Consortium on Chemical Sciences (IRCCS), Hokkaido University, N 21, W 10, Kita-ku, Sapporo 001-0021, Japan*

[2]*Institute of Chemistry and Molecular Engineering, Agricultural University of Georgia, Kakha Bendukidze University Campus, 240 David Aghmashenebeli Alley, Tbilisi 0159, Georgia*

**tamaki.nakano@cat.hokudai.ac.jp*

Abstract: Gene delivery, a technique to introduce foreign DNA into a cell, can be performed using an artificial vector material including synthetic polyelectrolytes. In this work, we studied the structures and basic properties of polyelectrolytes consisting of arginine- and spermine-based monomeric units in a salt form with *p*-toluenesulfonic acid as candidates of a novel synthetic gene vector. The polymers were found to form chiral complex with methyl orange whose structure was investigated by circular dichroism (CD) and ultra violet (UV) spectroscopic analyses.

Monomer Synthesis

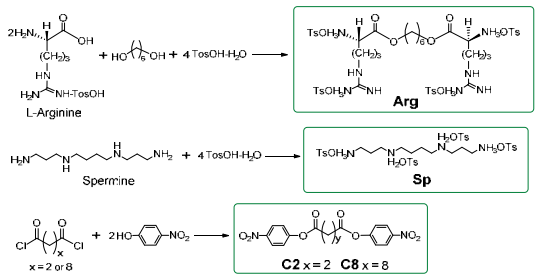

Scheme 1. Synthesis of monomers.

NMR Analysis

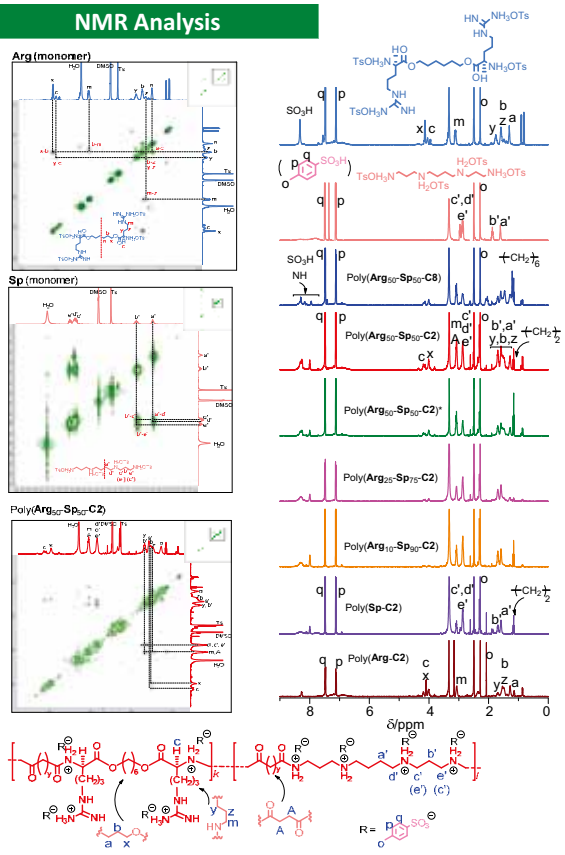

Fig. 1. 2D H-H COSY (lef) and 1D $_1$H NMR spectra of monomers and polymers (400 MHz, DMSO-d_6, r.t.).

Conclusions

The novel, chiral polyelectrolytes were successfully prepared and found to form chiral complex with methyl orange possibly through ionic interaction or (partial) anion exchange.

Polymerization

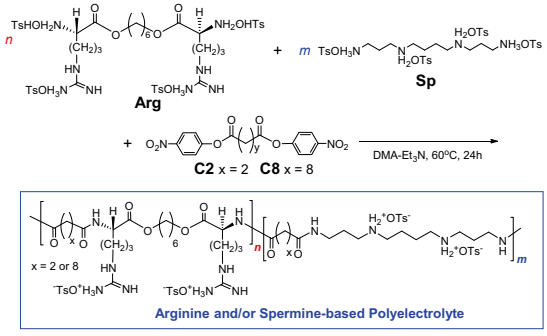

*Poly(**Arg**$_{50}$-**Sp**$_{50}$-**C2**) was reacted with a small amount of 1,6-diisocyanatohexane leading to poly(**Arg**$_{50}$-**Sp**$_{50}$-**C2**) *.*

Scheme 2. Synthesis of polyelectrolytes.

Polymer-Methyl Orange Complexation

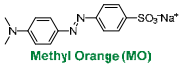

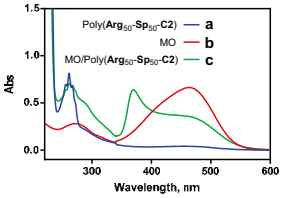

Fig. 2. Absorbance spectra of poly(**Arg**$_{50}$-**Sp**$_{50}$-**C2**) (0.01 M) (a), MO (0.0003 M) (b), and a mixture of the polymer and MO ([unit]/[MO] = 1/1) (c) in H_2O (1-mm cell).

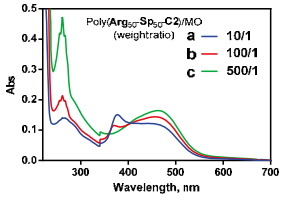

Fig. 3. Absorbance spectra of mixtures of poly(**Arg**$_{50}$-**Sp**$_{20}$-**C2**) and MO where [MO] = 0.01 g/L at [polymer]/[MO] = 10/1 (a), 100/1 (b), and 500/1 (c) (weight ratio) in H_2O (1-mm cell).

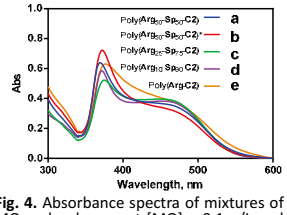

Fig. 4. Absorbance spectra of mixtures of MO and polymers at [MO] = 0.1 g/L and [polymer] = 1.0 g/L in H_2O (1-mm cell).

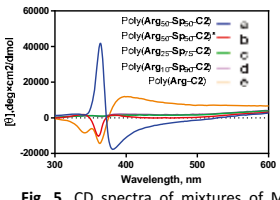

Fig. 5. CD spectra of mixtures of MO and polymers at [MO] = 0.1 g/L and [polymer] = 1.0 g/L in H_2O (1-mm cell).

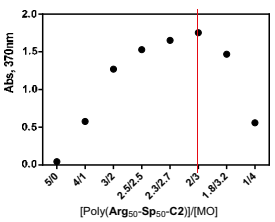

Fig. 6. Job's plot for mixtures of poly(**Arg**$_{50}$-**Sp**$_{50}$-**C2**) and MO at [**Arg** and **Sp** units] + [MO] = 0.0016 M in H_2O (1-mm cell).

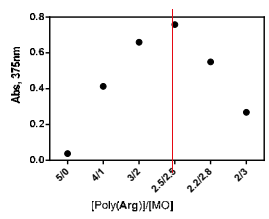

Fig. 7. Job's plot for mixtures of poly(**Arg-C2**) and MO at [**Arg** unit] + [MO] = 0.0016 M in H_2O (1-mm cell).

Control of Surface Inhomogeneity and its Catalytic Properties.

Huang Hua and Kiyotaka Asakura[1)]
Institute for Catalysis, Hokkaido University, Sapporo 001-0021, Japan
askr@cat.hokudai.ac.jp

High-performance catalysts are often composed of two or more active phases, which are believed to interact with each other at the mesoscopic scale structure. Unlike conventional powder catalysts flat surfaces is advantageous in that its surface structure can be precisely designed. We prepared precisely designed $Sb_2O_4/VSbO_4/Si$ catalysts containing Sb_2O_4 ribbons with finely controlled width and separation by electron lithography(1). We demonstrated that the acrolein generation rate on the catalysts was related to the width and separation of the Sb_2O_4 ribbons. This work shows the possibility to regulate catalysis by inhomogeneity of the surface structure at the mesoscopic level.

Introduction

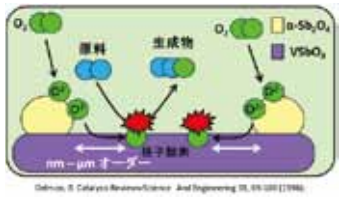

Remote Control Mechanism

Delmon, B.; Froment, G. F. Catal. Rev. 1996, 38, 69.

Motivation

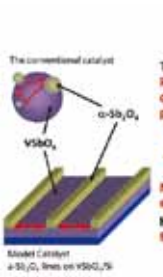

The conventional catalyst
Powder is
difficult to control size and
position is not confided.

Modelling

Model Catalyst is
easy to control size and position

How to fabricate?
Electron beam lithography

Experimental

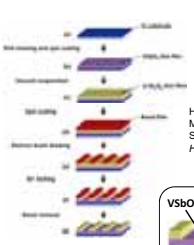

6 mm x 6 mm = 36 mm²

Haraguchi, Y., Wada, T., Ominami, Y., Matsudaira, N., Ariga, H., Takakusagi, S, Asakura, K. , *Hyomen Kagaku* **33**, 426-430 (2012).

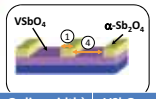

Sample	α-Sb_2O_4 linewidth` m,① /μm	$VSbO_4$ separation n,②/μm
1 μm	0.25	1
2 μm	0.5	2
4 μm	1	4
16 μm	4	16
32 μm	8	32

XRD

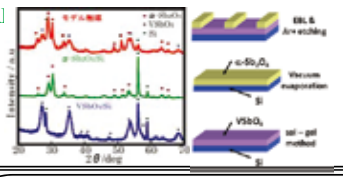

XPS

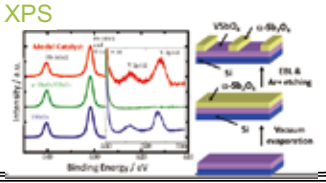

Reaction rate was related to the microstructure

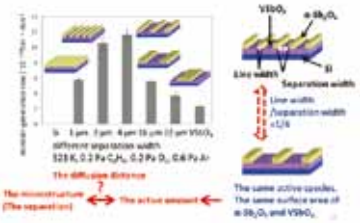

Reaction rate trend varied with the temperature

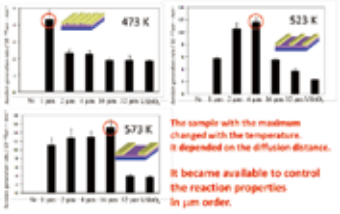

The sample with the maximum changed with the temperature. It depended on the diffusion distance.

It became available to control the reaction properties in μm order.

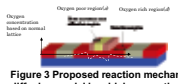

Figure 3 Proposed reaction mechanism based on the surface diffusion model in which separation is larger than the diffusion distance. The white lines represent proposed oxygen concentration.

$$r \propto a * d * N$$

$$N = \frac{CL}{m,n} = \frac{CL}{5m} \quad n=4m$$

$$r \propto a * d * N = a * d * \frac{CL}{5m} \quad 2a<m,\ 2d<n$$

$$r \propto \frac{m}{2} * d * N = d * \frac{CL}{10} \quad 2a>m$$

$$r \propto \frac{m}{2} * \frac{n}{2} * N = n * \frac{CL}{20} \quad 2d>n$$

In this work, we demonstrated the feasibility of controlling and tuning the reaction properties of α-$Sb_2O_4/VSbO_4/Si$ samples by adjusting the Sb_2O_4 ribbon width and separation on the mesoscopic scale. Lithography is an attractive method to fabricate catalysts with precisely designed mesoscopic structure and it will lead to a new catalyst preparation methods that involve computer-controlled design and manufacture.

This work has been supported by CREST-JST “Resolution Catalyst”.

Reference:Huang, H. H.; Wada, T.; Ariga, H.; Takakusagi, S.; Asakura, K.; Iwasawa, Y. *Chem. Phys.Lett.* ***2017, 683, 18.***

First-Principles Simulations of Catalytic Reactions at the Water/CeO_2(111) Interface: Hydration of 2-Cyanopyridine

Akira Nakayama[1,2*], Masazumi Tamura[2,3], Ken-ichi Shimizu[1], and Jun-ya Hasegawa[1]

[1]*Institute for Catalysis, Hokkaido University, Sapporo 001-0021, Japan*
[2]*JST PRESTO, 4-1-8 Honcho Kawaguchi, Saitama 332-0012, Japan*
[3]*Department of Applied Chemistry, Graduate School of Engineering, Tohoku University, Sendai 980-8579, Japan*

*e-mail: nakayama@cat.hokudai.ac.jp

Introduction

Catalysis of CeO_2-based Materials

Cerium(IV) Oxide (fluorite structure)

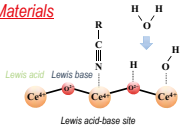

Lewis acid-base site

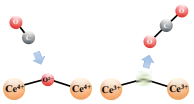

Mars-van Krevelen mechanism (redox mechanism)

CeO_2 has unique ..

- Redox properties
- Oxygen storage capacity
- Acid-base properties

Hydration of 2-cyanopyridine over metal-oxide catalysis

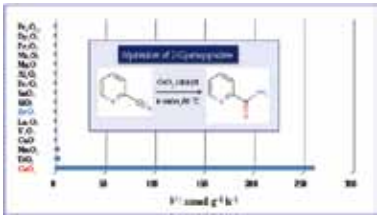

M. Tamura, H. Wakasugi, K. Shimizu, and A. Satsuma, Chem. Eur. J. **17**, 11428 (2011).

Substrate Specificity

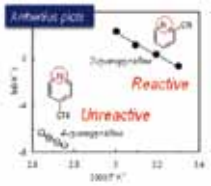

Proposed mechanism

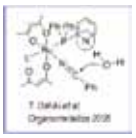

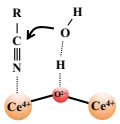

Unique adsorption structure of 2-cyanopyridine on CeO_2(111)

2-cyanopyridine | 4-cyanopyridine

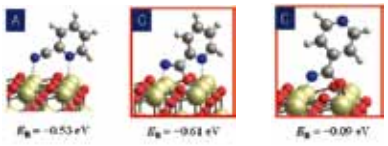

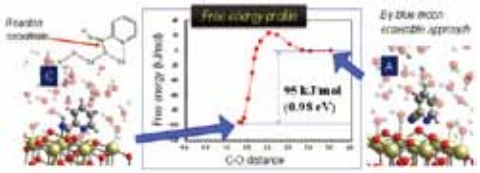

Free energy profiles

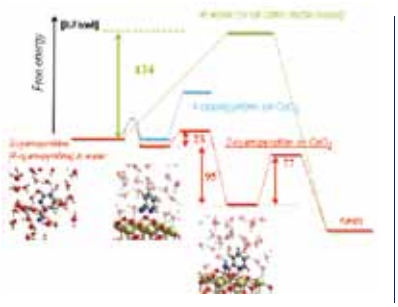

Computational details

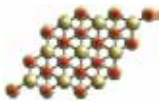

- DFT calculations
  - Periodic boundary DFT+U: (PBE functional, U = 7.0 eV)
  - DZVP (MOLOPT type basis set) and GTH pseudopotentials
  - Energy cutoff of 400 Ry for auxiliary plane wave expansion
  - Γ-point only in the k-point sampling
  - CP2K program package
- Simulation cell (CeO_2(111) surface)
  - p(3 × 3) and 3 O-Ce-O tri-layers (27 CeO_2 unit)
  - a = b = 11.56, c = 25.0 Å and α = β = 90, γ = 60 degrees
- MD simulations
  - NVT ensemble (T=330 K)
  - Time step of 1.0 fs (the mass of a hydrogen is replaced with that of deuterium)
  - Blue moon ensemble and metadynamics approach for free energy calculations

Results and Discussions

Adsorption structure of 2-cyanopyridine on CeO_2(111)

2-cyanopyridine (reactive) | 4-cyanopyridine (unreactive)

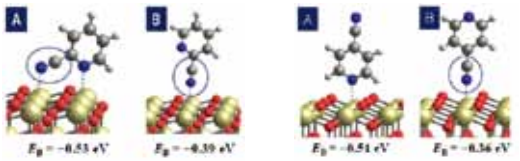

Free energy profile (metadynamics simulation)

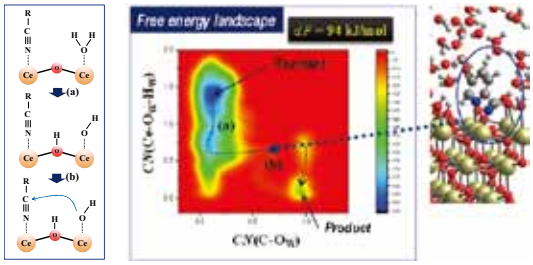

Lattice oxygen mechanism in hydration of 2-cyanopyridine

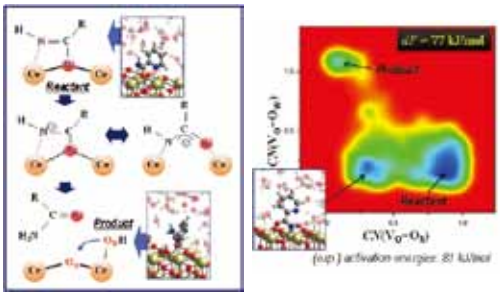

Water/ZrO_2 interface

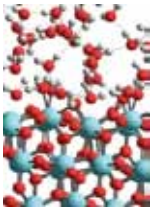

- Adsorption energy of water molecule: (molecularly or dissociative) ~ −1.0 eV
- Surface hydroxylation increases with water adsorption energy

Lewis acid site is not available for adsorption of nitriles

Self-assembled hybrid metal-oxide based catalysis

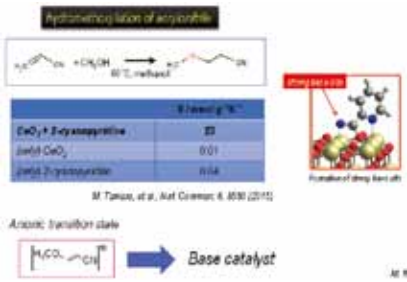

Catalytic reactions with hybrid catalysis

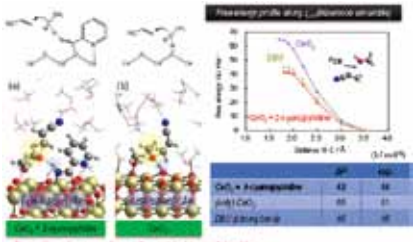

Y. Yamamura, R. Kishi, A. Nakayama, Y. Nakagawa, J. Hasegawa, and K. Tomishige, J. Am. Chem. Soc. **139**, 11857 (2017).

Theoretical Study on Rhodium-Catalyzed Hydrosilylation of C=C and C=O Double Bonds

Liming Zhao,[1] Naoki Nakatani,[2] Yusuke Sunada [3], Hideo Nagashima [3], Jun-ya Hasegawa[2]
[1]Graduate School of Chemical Science and Engineering, Hokkaido University
[2]Institute for Catalysis, Hokkaido University, Sapporo, Japan
[3]Institute for Materials Chemistry and Engineering, Kyushu University, Japan

Introduction

Hydrosilylation describes the reaction that unsaturated bond insertion into Si-H bond under a certain catalyst. It's an important way to produce organosilicon products. Using Rh as the catalyst, very mild reaction conditions can be achieved.

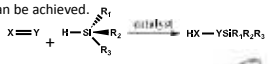

From an analogy to Rh-catalyzed hydrosilylation of alkenes,[1] it was assumed that the Rh-catalyzed hydrosilylation of carbonyl group occurs through modified Chalk-Harrod (MCH) mechanism, although there is no evidence. Our recent work that the Pt-catalyzed hydrosilylation of carbonyl group can occur via Chalk-Harrod (CH) mechanism with a bifunctional hydrosilane.[2] Thus it is worth to theoretically investigate which mechanism is taken place in such reactions.

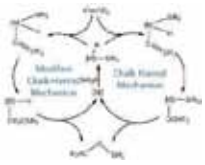

Method & Model

Catalyst:

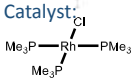

Hydrosilane:

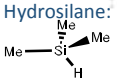

Unsaturated bonds:

Acetone / ethylene

Method: Density Functional Theory (ωB97XD functional)

Basis sets:

BS I

Rh	*Stuttgart/Dresden (611111/22111/411)+ECP*
Si C H	*6-31g**
P O Cl	*6-31+g**

BS II

Rh	*Stuttgart/Dresden (611111/22111/411)+ECP+f*
Si C H	*6-311g***
P O Cl	*6-311+g***

Existing Mechanisms — CH & mCH mechanism

Free energy profiles for acetone hydrosilylation in mCH cycle (upper) and CH cycle (bottom)

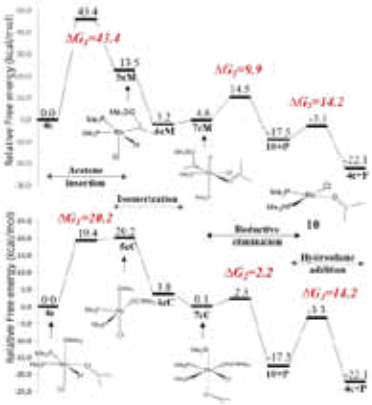

Important transition states:

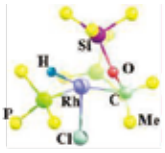

ts1

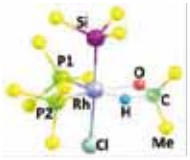

ts2

➢ For the Rh-catalyzed hydroilylation of acetone, much higher energy barrier in mCH mechanism (43.4 kcal/mol) makes it less possible to take place.
➢ The energy different between CH and mCH mechanism is well explained by the structures of transition states.

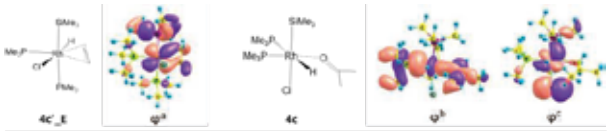

4c_E | 4c

➢ In Rh-catalyzed hydrosilylation of ethylene, mCH mechanism is most favorable mechanism for the backdonation interaction in precursor complex.

Newly proposed mechanisms

Alternative Chalk-Harrod (aCH) mechanism

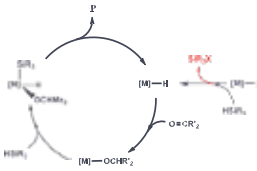

aCH mechanism

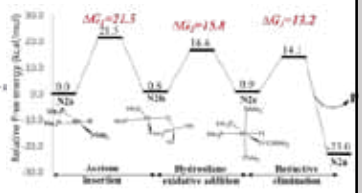

Free energy profile of acetone hydrosilylation in aCH cycle.

➢ In acetone case, the rate-determining step in aCH mechanism is acetone insertion into Rh-H bond taking 21.5 kcal/mol energy.
➢ In ethylene case, the rate-determining step is Si-C reductive elimination reaction with the energy barrier of 24.1 kcal/mol.
➢ CH and aCH mechanism have the same rate-determining step and similar energy barriers in both C=C and C=O double bond hydrosilylation. As the consequence, in other cases (such as using Pt as the catalyst) when CH mechanism is applicable, we should consider the possibility of aCH mechanism.

Double-hydride (DH) mechanism

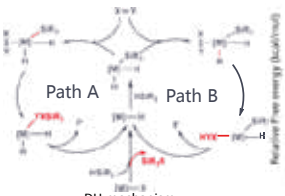

DH mechanism

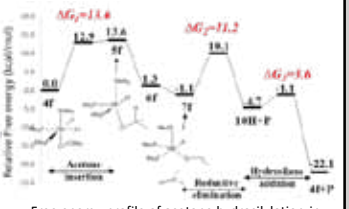

Free energy profile of acetone hydrosilylation in DH cycle.

➢ In acetone case, the rate-determining step in DH mechanism is also acetone insertion into Rh-H bond and the energy barrier is 13.6 kcal/mol. This value is much smaller than in other catalytic cycle, which makes it become the most possible mechanism in acetone hydrosilylation.
➢ In ethylene case, the rate-determining step is Si-C reductive elimination reaction with the energy barrier of 12.7 kcal/mol. This value is just 1.5 kcal/mol higher than the largest energy barrier in mCH cycle. Thus DH and mCH mechanism are two most favorable mechanisms in ethylene hydrosilylation.

More discussions

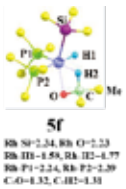

5f

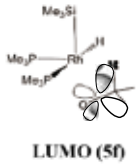

LUMO (5f)

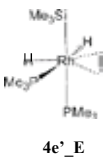

4e'_E

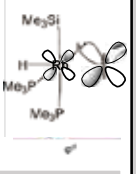

➢ Incompletely broken C=O double bond and agostic interaction make the energy barrier to be low in DH mechanism path A.
➢ π antibonding is found to have no interaction with Rh d orbital in the precursor complex 4e'_E before ethylene insertion into Rh-Si bond. Thus Path B takes much more energy than mCH mechanism and consequently being excluded.

Conclusions

➢ Two new mechanisms were proposed, alternative Chalk-Harrod mechanism and double hydride mechanism.
➢ For ethylene, mCH mechanism is the most favorable mechanism. At the same time, DH mechanism is competitive to the mCH mechanism.
➢ For acetone, DH mechanism is the most favorable mechanism.

[1] S. Sakaki, M. Sumimoto, M. Fukuhara, M. Sugimoto, H. Fujimoto and S. Matsuzaki, *Organometallics* **2002**, *21*, 3788-3802.
[2] N. Nakatani, J. Hasegawa, Y. Sunada, and H. Nagashima, *Dalton Trans.* **2015**, *44*, 19344-19356.

Reaction Mechanism of DMC Formation from CO_2 and Methanol over CeO_2 : A DFT Study

北海道大学 HOKKAIDO UNIVERSITY

○Toshiyuki Sugiyama, Akira Nakayama, and Jun-ya Hasegawa

Institute for Catalysis, Hokkaido University, Sapporo 001-0021, Japan

Institute for Catalysis CAT

Background

$$CO_2 + 2CH_3OH \xrightarrow{CeO_2} H_3CO(C=O)OCH_3 + H_2O$$

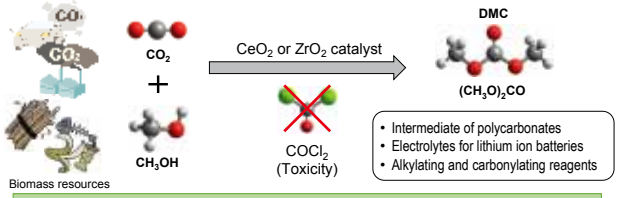

- Intermediate of polycarbonates
- Electrolytes for lithium ion batteries
- Alkylating and carbonylating reagents

A green and sustainable process to replace the conventional methods

CeO_2 catalyst

- Acid-base sites (Lewis acid-base pairs)
- Redox properties

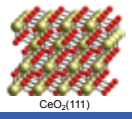

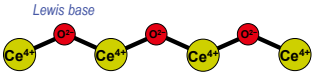

In this work

We investigate reaction mechanisms of DMC formation over CeO_2 and clarify the role of the acid-base sites.

Ref : Tomishige, K.; Sakaihori, T.; Ikeda, Y.; Fujimoto, K. *Catal. Letters* **1999**, *58*, 225–229.
Yoshida, Y.; Arai, Y.; Kado, S.; Kunimori, K.; Tomishige, K. *Catal. Today* **2006**, *115*, 95–101.

Computational details

Method : Periodic boundary DFT + U (PBE functional)

Unit cell : $p(4\times4)$ with 2 O-Ce-O tri-layers (32 CeO_2 units) 15.42 × 15.42 × 25.0 Å^3

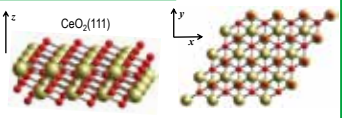

Adsorption structures of the reactants

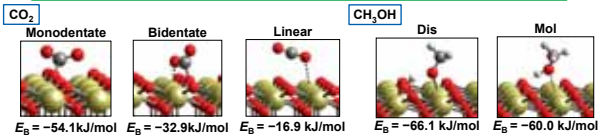

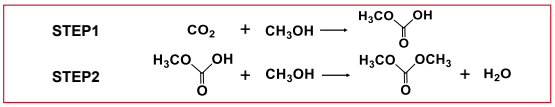

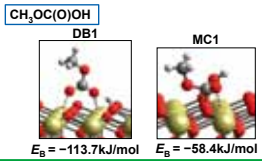

- Adsorption structures of CO_2
  - ◊ Surface carbonate species
    - Monodentate / Bidentate → MC1
  - ◊ Molecular adsorption
    - Linear → DB1
- Adsorption structures of CH_3OH
  - ◊ Dissociated adsorption
  - ◊ Molecular adsorption

→ Both structures exhibit similar E_B.

Analysis of reaction mechanism : Potential energy

Potential energy profile of Path A

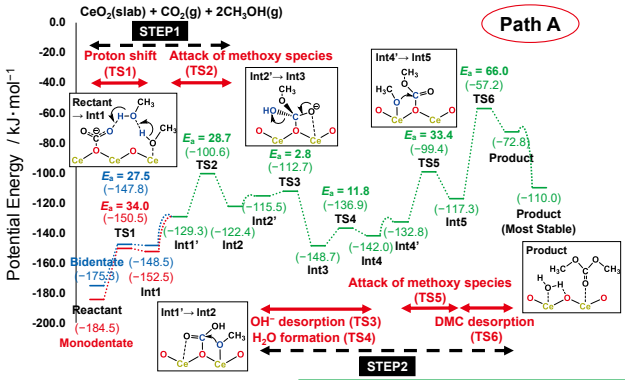

Potential energy profile of Path B

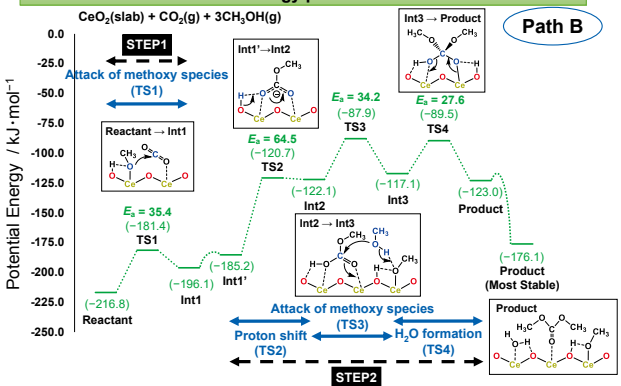

Analysis of reaction mechanism : Free energy

Problems of the calculations based on the potential energy profile

- Numerous local minima on the potential energy surface.
- Conformation change between substrate and solvent molecules.
- Thermal fluctuation of solvent molecules.

Free energy profile in solution at finite temperature was obtained by first principle MD simulation.

Blue moon ensemble approach

Integration of the mean force obtained by MD simulation leads to the free energy profile of a chemical reaction along a specified reaction coordinate.

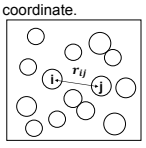

$$W(\xi) = \int_{\xi_0}^{\xi_1} \frac{\partial W}{\partial \xi} d\xi$$

$W(\xi)$: Free energy

$\frac{\partial W}{\partial \xi}$: Mean force

$$\xi = r_{ij} = \sqrt{(r_i - r_j)^2}$$

Method: DFT-based molecular dynamics (NVT ensemble, T=360K)
DFT: Periodic boundary DFT(PBE) + U
Unit cell: $p(3\times3)$ with 3 O-Ce-O tri-layers (27 CeO_2 units) 11.56 × 11.56 × 25.0 Å^3

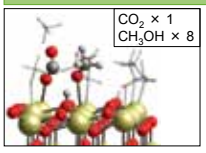

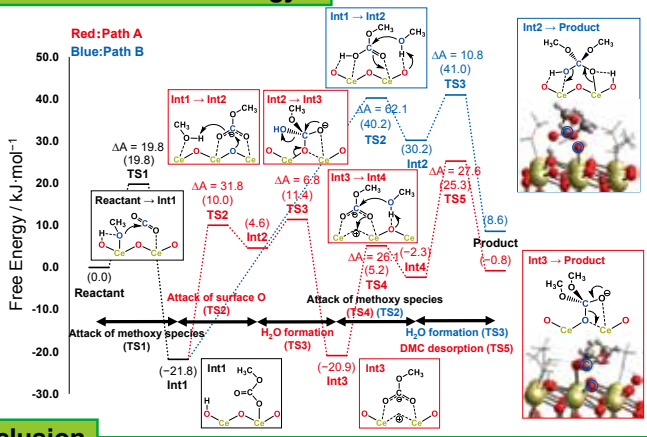

Conclusion

- The reaction mechanisms of DMC formation over CeO_2 were theoretically investigated.
- The role of the acid-base sites on CeO_2 was clarified.

Adsorption and Catalytic Hydrolysis of Cellulosic Molecules by Microporous Materials

Mizuho Yabushita,[1,2] Hirokazu Kobayashi,[1] Omar K. Farha,[3] Alexander Katz,[2] Atsushi Fukuoka[1]

[1]Institute for Catalysis, Hokkaido University, Japan (m.yabushita@cat.hokudai.ac.jp)
[2]Department of Chemical and Biomolecular Engineering, University of California, Berkeley, USA
[3]Department of Chemistry, Northwestern University, USA

Objectives

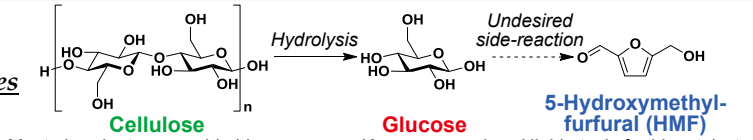

Cellulose — Most abundant, renewable biomass

Glucose — Key compound

5-Hydroxymethyl-furfural (HMF) — Highly-toxic for biocatalysts

- Highly active catalysts for cellulose hydrolysis are required.
- For 2nd-generation bioethanol production, by-products such as aromatics need to be devised.

Zeolite-Templated Carbon (ZTC)

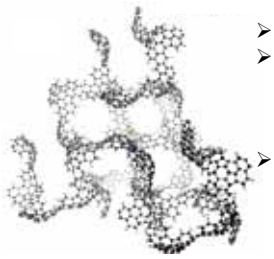

H. Nishihara *et al.*, *Carbon* **2009**, *47*, 1220.

- Consisted of warped-graphene
- High surface area (≥ 3000 $m^2\ g^{-1}$)
  → Suitable for organics adsorption

  P.-W. Chung *et al.*, *Langmuir* **2012**, *28*, 15222;
  M. Yabushita *et al.*, *ChemSucChem* **2014**, *7*, 1443.
- Micropororous structure (1.1 nm)
  → Ideal size for β-glucan guests
  → β-Glucan was taken in the pore within 2 min.

  M. Yabushita *et al.*, *ACS Catal.* **2015**, *5*, 6422.

H_2O_2 Treatment

Properties of parent and H_2O_2-treated ZTCs

Material	Acid site /mmol g^{-1}	$A_{micropore}$ /$m^2\ g^{-1}$	V_{pore} /$cm^3\ g^{-1}$
ZTC	1.05	3480	1.91
Z-H(5)	1.81	3700	1.90
Z-H(15)	2.10	3360	1.81
Z-H(30)	2.32	3400	1.82
Z-H(60)	2.48	3050	1.61

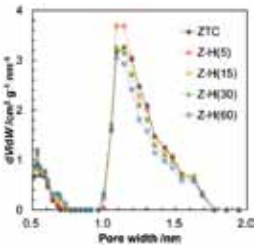

- Acid sites are successfully introduced by H_2O_2 treatment, with minimal change to microporous structure.

Adsorption and Hydrolysis of β-Glucans

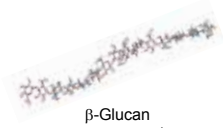

β-Glucan (3,600 g mol^{-1})

1. Adsorption
2 g L^{-1} β-glucan solution (40 mL), 20 mg ZTC, 277 K, 10 min

2. Hydrolysis
ca. 25 mg β-glucan/ZTC, 1 mL H_2O, 453 K, 3 h

Glucose

Adsorption uptake of β-glucans by ZTCs

Material	β-Glucan uptake /$mg_{Glc\text{-}unit}\ g^{-1}$
ZTC	306
Z-H(5)	390
Z-H(15)	315
Z-H(30)	328
Z-H(60)	315

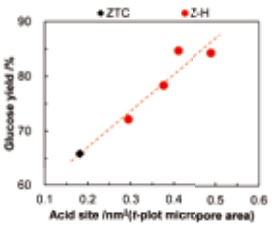

- All ZTC materials exhibit similar β-glucan uptake regardless of the H_2O_2-treatment.
- The catalytic hydrolysis activity of ZTC directly increases upon increasing acid-site density.

Metal–Organic Framework (MOF) NU-1000

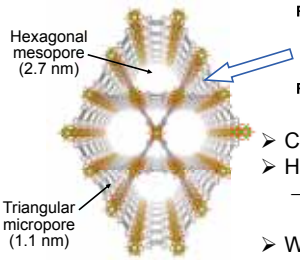

O. K. Farha *et al.*, *J. Am. Chem. Soc.* **2013**, *135*, 10294.

- Consisted of pyrene units
- High surface area (2320 $m^2\ g^{-1}$)
  → Suitable for organics adsorption
- Well-ordered micropororous structure (1.1 nm)

Biomass-Derived Toxins for Biocatalysts

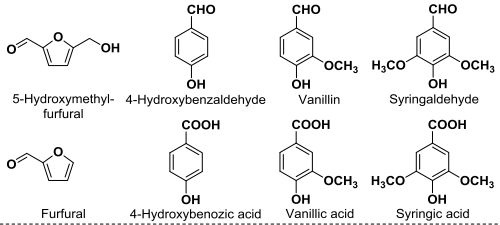

Competitive-Mode Adsorption

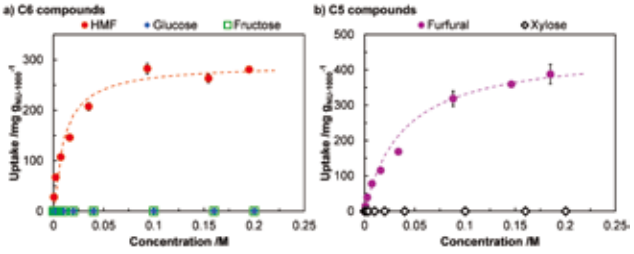

- NU-1000 discriminates furanics from monomeric sugars in their aqueous mixtures.

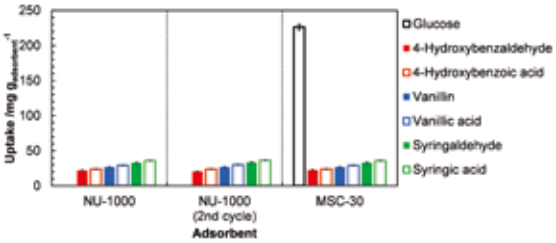

- Only NU-1000 can selectively remove aromatics from aqueous soluitons.

Conclusions

- H_2O_2-modified ZTCs, which have high acid-site density and surface area as well as ideally sized micropores, show good performance in both β-glucan adsorption and subsequent hydrolysis.

  M. Yabushita *et al.*, *ACS Sustainable Chem. Eng.* **2016**, *4*, 6844.
- NU-1000 adsorbs aromatic compounds from aqueous solutions containing glucose co-solute, with an outstanding degree of selectivity comparable to biomolecules.

  M. Yabushita *et al.*, *Chem. Commun.* **2016**, *52*, 7094; *Chem. Commn.* **2016**, *52*, 11791; *Langmuir* **2017**, *33*, 4129.

Stereoselective isomerization of eugenol to trans-isoeugenol catalyzed by Ni(0) phosphines: experimental and theoretical studies

Y. Permana,[1] **Arifin**,[2] L. Saputra,[1] N. Gustini,[1] S. Irle,[2] A. Patah,[1] M. A. Martoprawiro[1]

[1]*Chemistry Department, Faculty of Mathematics and Natural Sciences, Institut Teknologi Bandung, Bandung, Indonesia*
[2]*Institute of Transformative Bio-Molecules, Nagoya University, Nagoya, Japan*

I Conversion of natural products

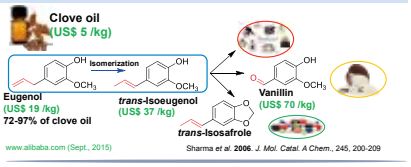

Catalysts:

(1) KOH : 150 °C, 10 h, Conv. 60%, excess base
Cerveny *et al.* **1987**. *React. Kinet. Catal. Lett.* 33, 471-476.

(2) NiAl-HT : 200 °C, 6 h, Conv. 77%, Select. 84%
Jinesh *et al.* **2010.** *Catal. Lett.* 134, 337-342.

(3) $RuCl_2(PPh_3)_3$: 78 °C, 3 h, Conv. 99%, Select. 96%
Sharma *et al.* **2010**. *J. Mol. Catal.* 245, 200-209.

High conversion and selectivity of trans- product can be achieved with the expensive ruthenium complex as the catalyst.

II Catalyst design

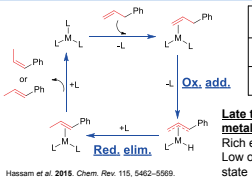

Fe	Co	**Ni**
Ru	**Rh**	**Pd**
Os	Ir	Pt

Late transition metal: Rich electron Low oxidation state

Ligands: Good *σ* donor (for example phospine ligand)

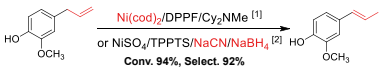

[1] Gogsig *et al.*, **2012**, *J. Am. Chem. Soc.*, 134, 443-452; [2] Kuntz *et al.*, **2007**, *Oil Gas Sci. Technol.*, 62, 781-785

Ni(0) is an important species for the oxidative addition step.

III This work

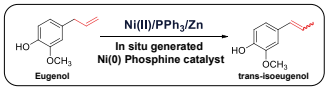

Computational details

Program package: Gaussian 09 version D.01

Method: PBE0-D3

Basis sets:
Ni: Stuttgart RSC 1997 with ECP
N, O, P: 6-31+G(d)
C in alkene and acetonitrile: 6-31G(d)
C in alkene and acetonitrile: 6-31G(d,p)
All other atoms: 6-31G

We evaluated the performance of catalysts and elucidate the reaction mechanisms.

IV Ni source effects

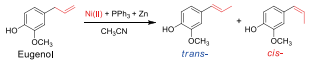

Entry	Ni(II) sources	Conv. (%)	*trans*-Select. (%)	TOF (h^{-1})
1[a]	$NiCl_2(PPh_3)_2$	8	91	7
2	$NiCl_2(PPh_3)_2$	99	97	96
3[b]	$NiCl_2(PPh_3)_2$	99	94	1,116
4	$NiCl_2·6H_2O$	99	97	96
5	$Ni(NO_3)_2·6H_2O$	99	95	94
6	$Ni(OAc)_2·4H_2O$	99	96	95
7	$2NiCO_3·3Ni(OH)_2·4H_2O$	11	92	10
8	$(NH_4)_2Ni(SO_4)_2·6H_2O$	8	92	7
9	Ni(salen)	9	92	8

Reaction conditions: 0.05 mmol of Ni(II), 5 mmol of eugenol, 0.5 mmol of Zn, 0.5 mmol of PPh_3, 3 mL of MeCN, 353 K, 1 h, N_2 atmosphere. [a]No addition of Zn or excess of PPh_3. [b]Substrate: 30 mmol of eugenol.

High activity can be achieve with $NiCl_2(PPh_3)$ as the precursor.

V Ligand effects

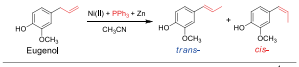

Entry	Ligands	Conv. (%)	*trans*- Select. (%)	TOF (h^{-1})
1	$P(OPh)_3$	3	92	3
2	PPh_3	99	97	96
3	$P(Ph\text{-}pOMe)_3$	99	96	95
4	$P(Ph\text{-}pMe)_3$	99	97	96
5	Phenantroline	5	92	5

Reaction conditions: 0.05 mmol $NiCl_2·6H_2O$, 5 mmol eugenol, 0.5 mmol ligands, 0.5 mmol Zn 3 mL of CH_3CN, 80 °C, 1 h, stirring at 400 rpm, 1 atm N_2.

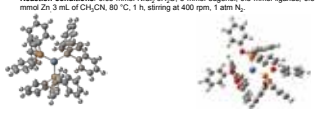

A strong sigma donative ligand may increase electron density at Ni(0).

VI Solvent effects (1)

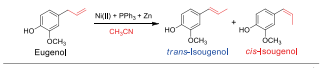

Entry	Solvents	Conv. (%)	*trans*- Select. (%)	TOF (h^{-1})
1	Solvent free	17	80	14
2	Methanol (50 °C)	25	92	23
3	DMSO	11	87	10
4	Pyridine	29	89	26
5	Nitromethane	9	91	8
6	DMF	29	89	26
7	THF (50 °C)	4	86	3
8	Acetone (50 °C)	28	94	26
9	THF (50 °C) + 100 µL Acetonitrile	70	87	10
10	Acetone (50 °C) + 100 µL Acetonitrile	96	89	26
11	Acetonitrile	99	97	96
12	4-Chlorobutyronitrile [a]	99	96	95
13	Acrylonitrile	99	95	94

Reaction conditions: 0.05 mmol $NiCl_2(PPh_3)_2$, 5 mmol eugenol, 0.5 mmol Zn, 0.5 mmol PPh_3, 3 mL solvent, 80 °C, 1 h, stirring at 400 rpm, 1 atm N_2. [a]Using 1 mL of 4-Chlorobutyronitrile.

MeCN is the best solvent to achieve the best catalytic activity.

VII Solvent effects (2)

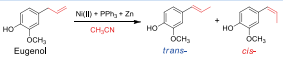

Entry	CH_3CN (mL)	mol CH_3CN:Ni(II)	Conv. (%)	*trans*- Select. (%)	TOF (h^{-1})
1	3.0	1,149	99	97	96
2	2.0	766	99	96	95
3	1.0	383	98	96	94
4	0.5	192	98	95	93
5	0.25	96	98	96	94
6	0.10	38	98	95	93
7	0.05	19	97	95	92
8	0.025	10	96	95	91
9	0.005	2	94	86	81
10	0.005 [a]	1	95	86	82
11	0	0	17	80	14

Reaction conditions: 0.05 mmol $NiCl_2(PPh_3)_2$, 5 mmol eugenol, 0.5 mmol Zn, 0.5 mmol PPh_3, 80 °C, 1 h, stirring at 400 rpm, 1 atm N_2. [a]Using 0.005 mL of 4-Chlorobutyronitrile besides acetonitrile.

A small amount of MeCN dramatically increased the catalytic activity.

VIII Time Profile of MeCN addition

Reaction conditions: 0.05 mmol of $NiCl_2(PPh_3)_2$, 30 mmol of eugenol, 0.5 mmol of Zn, 0.5 mmol of PPh_3, 3 mL of MeCN, 353 K, N_2 atmosphere.

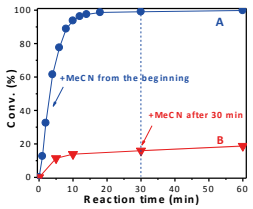

How does MeCN increase the catalytic activity?

VIII Proposed mechanism

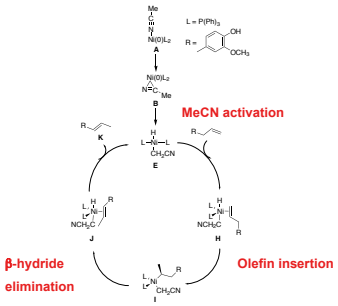

There are three important steps.

IX Free energy profiles

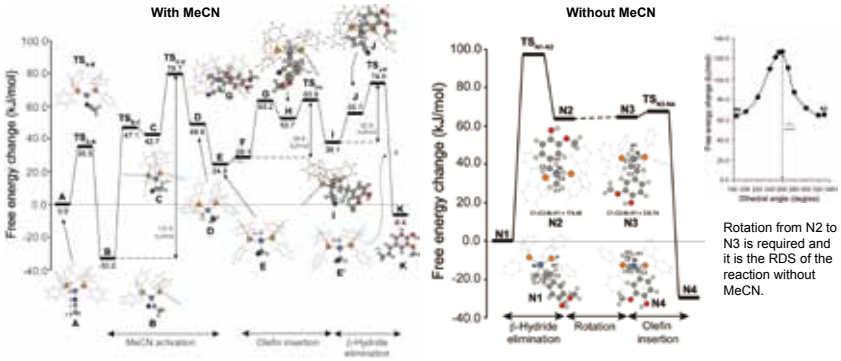

Rotation from N2 to N3 is required and it is the RDS of the reaction without MeCN.

Ni(0) can activate MeCN through the C-H activation reaction.

X Summary

- Trans-isomerization of eugenol with high conversion and selectivity is successfully catalyzed by simple Ni(0) complex.
- The importance of MeCN in the reaction mechanisms is clearly elucidated.

Acknowledgement

Financial support by:
Dispatching Young Researchers Abroad Program at the Graduate School of Science, Nagoya University, Japan

Theoretical Investigation on Photo-activation Process of Diaryl Pyrido Cyanine

A. Sarinastiti[1], Arifin[1], R. Shimizu[2], K. Suda[2], K. Uno[2], Y. Sato[1], D. Yokogawa[1,2]
[1]Institute of Transformative Bio-Molecules (WPI-ITbM), Japan
[2]Department of Chemistry, Graduate School of Science, Nagoya University, Nagoya, Japan

I Cyanine Properties to Applications

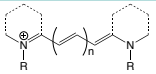

The most investigated family of synthetic pigments.

Example:
cyanine dyes as pH-responsive probes to detect cancer cells.

Hilderbrand, S. A. et al., *Bioconjugate Chem.*, **2008,** *19*, 1635.

Cyanine dyes have great potential applications.

II Chlorinated Cyanine

In general, however, cyanine dyes has a poor chemical and photochemical stability.

Chlorinated cyanine is one of intermediate molecules for further derivatization to improve water solubility, prevent aggregation, etc.

Ptaszek, M. et al., *Progress in Molecular Biology and Translational Science*, **2013,** *113*, 59.

How is the photo property of cyanine derivatives?

III Photo properties of cyanine derivatives

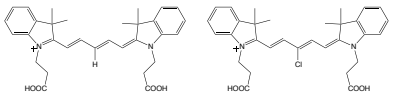

A B

Molecule	Molar Absorptivity ($M^{-1}cm^{-1}$)	Stokes Shift (nm)
A	60,700	22
B	32,200	18

Dost, T. L. et al., *Analytical Chemistry Insights*, **2017,** 12, 1.

The properties of cyanine dyes depend on its substituent.

IV Chlorinated Diaryl Pyrido Cyanine

Symmetrical cyanine with 4 double bonds for long wavelength absorption

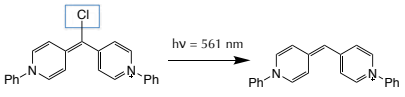

DCl DH

Uno, K. Doctoral Dissertation, Nagoya University, **2017**

How is the mechanism of substitution of chlorine atom by photo-activation of DCl in water?

V Computational Details

Ground state calculation : CAM-B3LYP/aug-cc-pVDZ

Excited state calculation : TD-CAM-B3LYP/aug-cc-pVDZ

Solvation Theory : RISM-SCF-SEDD

Solvent : Water
Temperature : 300 K

Program Package : GAMESS 2012 and Gaussian 16

VI Proposed Mechanism

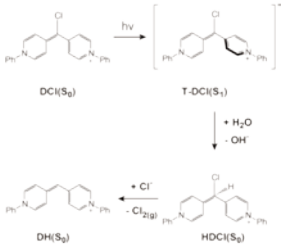

There are three steps: excitation process, insertion of proton, and Cl dissociation.

VII Energy Diagram

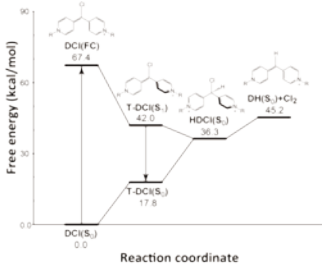

What is the important factor for Cl substitution process?

VIII Model Comparison

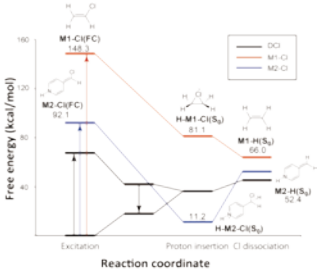

In DCl, low excitation energy and Cl-dissociation barrier are important for Cl substitution reaction.

VIII Excitation Process

Kohn-Sham Orbital

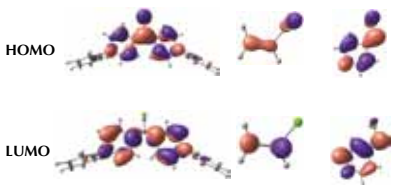

Delocalized HOMO ease the electron transfer during excitation.

IX Proton Insertion Process

DCl(S_0) **T-DCl(S_1)**

Table of charge changes

Atom	DCl (S_0)	T-DCl (S_1)
Cl	-0.05	0.10
C2	-0.09	-0.13

Proton insertion becomes easier because the charge of C2 is more negative, which increases nucleophilicity of C2.

XI Summary

- The mechanism of photo-activation of diaryl pyrido cyanine dyes has been studied.
- Delocalized HOMO is important to lowering excitation energy.
- The twisted state of DCl is important for proton insertion step.

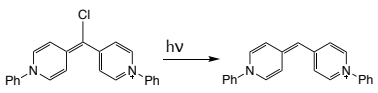

DCl DH

Acknowledgement

Financial support by
Grant-in-Aid for Young Scientist B (No.2473C015) and Scientific Research (C) (No. 15K05385)

名古屋大学
NAGOYA UNIVERSITY

Preparation, characterization, and catalytic performances of ceria-based mixed metal oxide catalysts

Satoshi Muratsugu,[1,2] Xiubing Huang,[3] Shoko Nagase,[1] Gen-ichi Yokota,[1] Satoru Ikemoto,[1] Hirosuke Matsui,[1] Mizuki Tada[1,3,4]

1 Department of Chemistry, Graduate School of Science, Nagoya University, Nagoya, Japan, 2 JST PRESTO
3 Research Center for Materials Science (RCMS), Nagoya University, Nagoya, Japan
4 Integrated Research Consortium on Chemical Sciences (IRCCS), Nagoya University, Nagoya, Japan

Introduction and Purpose

$CeO_2 \leftrightarrow CeO_{2-\delta} + \delta/2\ O_2$

- Ceria has been extensively studied as oxygen storage materials due to its easy conversion between CeO_2 and $CeO_{2-\delta}$.
- Introducing transition metals into ceria structures would lead to a higher oxygen storage capacity and lower oxygen removal temperature than pure CeO_2.

Mixed metal oxides with co-doped 1st and 2nd transition metals into CeO_2 framework:
(1) Synergetic effects among these species on oxygen storage performance;
(2) Improved oxygen storage capacity and lowered oxygen removal temperature;
(3) Insights into the deep understanding of oxygen transfer mechanism;
(4) Possible applications in selective oxidation of hydrocarbons at low temperatures.

Preparation and Structural Characterization of Mixed Metal Oxides

Preparation Scheme

Metal salts: M = Cr, Mn, Fe, Cu, M' = Ru, Rh; Ce/M/M' = 1-x-y/x/y (molar ratio)
→ Hydrothermal reaction: NaOHaq., in autoclave (100 °C, 24 h)
→ Washing
→ Calcination: Under Air (300 °C, 2 h)
→ $Ce_{1-x-y}M_xM'_yO_z$

XRD $Ce_{1-x-y}Cr_xRh_yO_z$

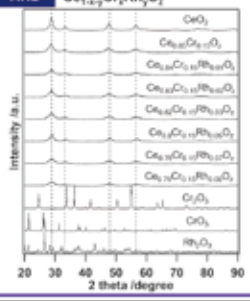

STEM-EDS $Ce_{0.8}Cr_{0.15}Rh_{0.05}O_z$

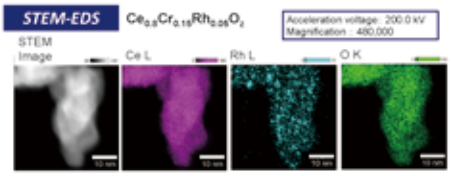

STEM-EELS $Ce_{0.8}Cr_{0.15}Rh_{0.05}O_z$

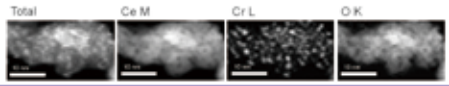

BET, ICP $Ce_{1-x-y}Cr_xRh_yO_z$

Sample	BET Surface areas /m² g⁻¹	ICP Composition of Ce/Cr/Rh
CeO_2	118	—
$Ce_{0.85}Cr_{0.15}O_z$	106	0.853 / 0.146 / 0.000420
$Ce_{0.84}Cr_{0.15}Rh_{0.01}O_z$	99.5	0.842 / 0.148 / 0.0103
$Ce_{0.83}Cr_{0.15}Rh_{0.02}O_z$	106	0.832 / 0.148 / 0.0198
$Ce_{0.82}Cr_{0.15}Rh_{0.03}O_z$	98.5	0.823 / 0.147 / 0.0299
$Ce_{0.8}Cr_{0.15}Rh_{0.05}O_z$	97.7	0.798 / 0.152 / 0.0502
$Ce_{0.78}Cr_{0.15}Rh_{0.07}O_z$	99.9	0.787 / 0.148 / 0.0658
$Ce_{0.75}Cr_{0.15}Rh_{0.09}O_z$	95.1	0.767 / 0.148 / 0.0857

Bulk structures of mixed oxides were observed to be similar to the fluorite structure of ceria. For $Ce_{0.8}Cr_{0.15}Rh_{0.05}O_z$, additional metals were found to be dispersed into ceria.

Redox Performances of Mixed Metal Oxides

H_2 TPR $Ce_{1-x-y}Cr_xRh_yO_z$

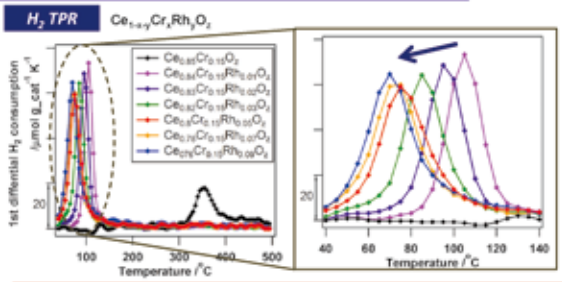

- Low temperature redox behavior was observed on $Ce_{0.8}Cr_{0.15}Rh_{0.05}O_z$ compared with CeO_2 and mixed metal oxides with only one metal (Cr or Rh).
- Reversible Cr (IV) ⇔ Cr (III) oxidation state change was responsible for this redox behavior.
- The amount of hydrogen consumption at H_2-TPR (1.78 mmol/g_cat) was comparable to that of Cr oxidation state change (1.41 mmol/g_cat).

H_2 TPR –Oxidation cycle

Fresh sample : Fresh
→ 1st cycle H_2-TPR: H_2, 5 °C/min. : Red.
→ Oxidation in O_2 @300 °C, 1 h : Oxi.
→ 2nd cycle H_2-TPR: H_2, 5 °C/min.
→ ...

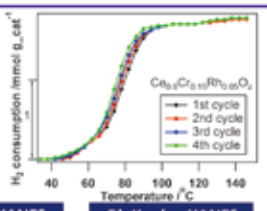

Ce L_{III}-edge XANES

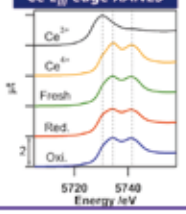

Cr K-edge XANES

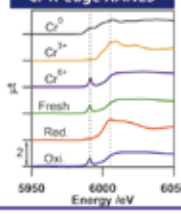

Rh K-edge XANES

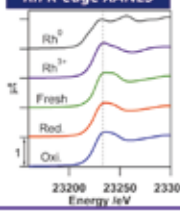

Catalytic Performances of Mixed Metal Oxides

Selective oxidation of alcohols

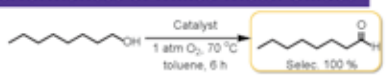

Entry	Catalyst	Yield[a] (Aldehyde) %	TOF[b] /h⁻¹
1	(Blank)	0	0
2	$Ce_{0.8}Cr_{0.15}Rh_{0.05}O_z$	6.8	7.5
3	CeO_2	0.8	0.2
4	$Ce_{0.85}Cr_{0.15}O_z$	5.0	5.2
5	$Ce_{0.95}Rh_{0.05}O_z$	1.3	0.7
6	Recycled (Filtration)	0.8	—
7	Recycled (Drying)	2.9	—
8	Recycled (Calcination, 300 °C)	7.1	—

[a]Yield % = (amount of octanal/ double amount of IS) × 100 %.
[b]TOF /h⁻¹ indicates the slope of yield within the reaction time of 30 min or 1 h.
Reaction condition: Rh/Cr/1-octanol/IS = 1/3/100/50, 1-octanol 0.42 mol/L in toluene.
Dodecane was used as internal standard (IS).

Cr K-edge XANES

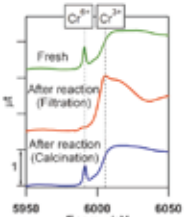

Ammoxidation of alcohols

Entry	Catalyst	Conversion[a] %	Yield[b] (Nitrile) %
1	(Blank)	0	0
2	CeO_2	71	2
3	$Ce_{0.8}Cr_{0.15}Rh_{0.05}O_z$	58	2
4	$Ce_{0.8}Mn_{0.15}Rh_{0.05}O_z$	74	28
5	$Ce_{0.8}Mn_{0.15}Ru_{0.05}O_z$	87	50
6	$Ce_{0.8}Fe_{0.15}Rh_{0.05}O_z$	39	1
7	$Ce_{0.8}Fe_{0.15}Ru_{0.05}O_z$	91	11
8	$Ce_{0.8}Cu_{0.15}Rh_{0.05}O_z$	71	66
9	$Ce_{0.8}Cu_{0.15}Ru_{0.05}O_z$	79	73

[a] Conversion % == (initial mole of reactant - residual mole of reactant)/initial mole of reactant × 100 %.[b] Yield % = (mole of benzonitrile)/initial mole of reactant × 100 %.
Reaction condition: M/benzyl alcohol/NH_3 = 1/100/200, Benzyl alcohol 1.33 mol/L in toluene, 1.0 MPa of O_2, 24 h. Dodecane was used as internal standard (M/dodecane = 1/100) after the reaction.

Conclusions

(1) Ceria-based mixed oxides $Ce_{1-x-y}M_xM'_yO_z$ were prepared by co-doping of first- and second- period transition metals (1st : M = Cr, Mn, Fe, Cu, 2nd : M' = Ru, Rh) to ceria to achieve high redox activity at low temperatures. Bulk structures of mixed oxides were observed to be similar to the fluorite structure of ceria. For $Ce_{0.8}Cr_{0.15}Rh_{0.05}O_z$, additional metals were found to be dispersed into ceria.
(2) The reduction temperature was decreased on $Ce_{1-x-y}M_xM'_yO_z$. Repetitive oxidation/reduction were observed, suggesting reversible redox behavior.
(3) The prepared mixed oxides were catalytically active for selective alcohol oxidation, even at room temperature for $Ce_{0.8}Cr_{0.15}Rh_{0.05}O_z$. Ammoxidation of alcohol to corresponiding nitrile was selectively proceeded on $Ce_{0.8}Cu_{0.15}Ru_{0.05}O_z$.

Perparation, characterization, and catalytic performances of Pt nanocluster – polymer – carbon nanotube composites

Dept. of Chemistry[1], RCMS[2] and IRCCS[3], Nagoya University

○Kentaro ICHIHASHI[1], Shota MIYAMOTO[1], Kana SAKAMOTO[1], Satoshi MURATSUGU[1], Mizuki TADA[1, 2, 3]

Introduction and Purpose

Anodic reaction of fuel cells:

$O_2 + 4H^+ + 4e^- \xrightarrow{Pt/C} 2H_2O$ Oxygen reduction reaction (ORR)

Pt/C: Carbon-supported platinum catalyst

Issues on Pt/C catalysts

- **Large particle size distribution** (> 3 nm)
  Since there are few active sites, ORR activity and electromotive force decrease.
- **Aggregation of Pt nanocluster**
  The active sites are further reduced, resulting in a large degradation of Pt/C.

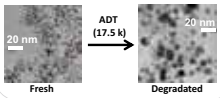

Nanoclusters Isolated on Support Surfaces

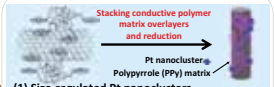

(1) Size-regulated Pt nanoclusters
(2) Stability enhancement as catalyst
(3) Low Pt loading (< 4 wt%)

Langmuir, **2017**, *33*, 10271.

Purpose

Preparation of size regulated and highly stable Pt nanoclusters with high Pt loading

Catalyst Design

Strategy: Preparing Pt nanoclusters and polymer matrix in one step by co-polymerization

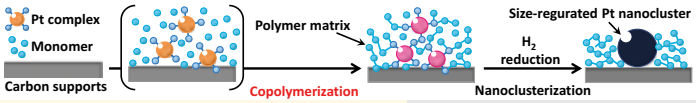

Pt_4-Pyrrole complex

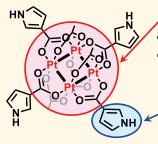

Pt_4 core cluster

- In-plane acetate ligand is replaceable.
- Polymerization unit can be introduced.

Yamaguchi, T. et al *Chem. Eur. J.* **2001**, *7*, 5409.
Tanaka, S. et al *Inorg. Chem.* **2011**, *50*, 11384.

Pyrrole unit

- Co-polymerize with pyrrole monomer

Carbon support

Multi-walled carbon nanotube (MWCNT)

- High conductivity and electrochemical resistance
- Large specific surface area

Polymer matrix

Polypyrrole (PPy)

- Co-polymerize with Pt_4-Pyrrole complex
- Electrically conductive

Synthesize of Pt_4-Pyrrole

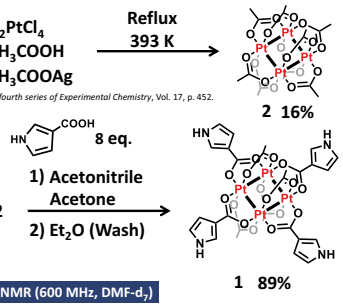

The fourth series of Experimental Chemistry, Vol. 17, p. 452.

^{1}H NMR (600 MHz, DMF-d_7)

δ = 11.4 (s, 4H), 7.66 (dd, 4H), 6.92 (dd, 4H), 6.72 (dd, 4H), 2.02 (s, 12H)

^{13}C NMR (150 MHz, DMF-d_7)

δ = 194.2, 180.1, 124.8, 119.5, 116.7, 110.2, 21.1

Elemental Analysis

Calcd. for $C_{28}H_{28}N_4O_6Pt_4 \cdot C_3H_6O$: C: 24.6, H: 2.26, N: 3.70
Found : C: 25.1, H: 2.44, N: 3.39

ESI-TOF MS

m/z 1479.05 $[M+Na]^+$ (Calcd. for $C_{28}H_{28}N_4O_6Pt_4Na$)

Catalyst Preparation and Characterization

MWCNT

1) SDS[1] aq.
2) Pyrrole, 8.8 mmol
3) 1/MeCN, 23 mmol
4) APS[2], 0.27 mmol
5) Stir 24 h, 274.5 K
6) H_2O, MeOH (Wash)

[1]:SDS = Sodium dodecyl sulfate
[2]:APS = Ammonium peroxisulfate

TEM

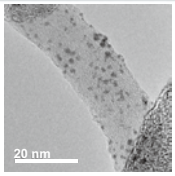

B

1) Δ 573 K, 2 h Evacuated
2) H_2, 40 kPa 573 K, 1 h

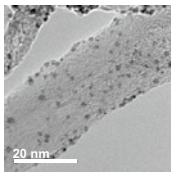

A

	B	A
BET	174 $m^2 g^{-1}$	161 $m^2 g^{-1}$	163 $m^2 g^{-1}$
XRF	12.6 wt%	12.6 wt%

Particle Size Distribution

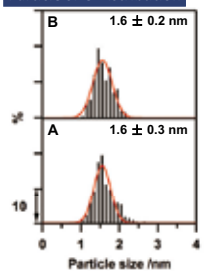

Pt L_{III}-edge XANES

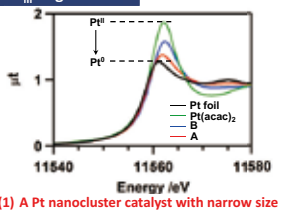

TGA 1st Differential

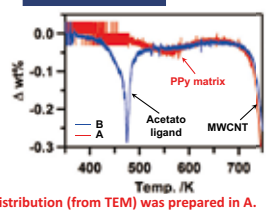

(1) A Pt nanocluster catalyst with narrow size distribution (from TEM) was prepared in A.
(2) Sufficient amounts of Pt loading (12.6 wt%) on A was confirmed by XRF.
(3) Pt species in A was reduced to almost zero valence from Pt L_{III}-edge XANES.
(4) The presence of PPy was confirmed by TGA.

ORR Activity and Durability of the Prepared Pt Catalyst

Rotating disk electrode (RDE) method

Measuring system of RDE method

Measurement Conditions

Set up of measuring system
WE: GC-RDE, CE: Pt plate, RE: RHE
Electrolyte: 0.1 M $HClO_4$ aq., 293K

Preparation of working electrode
- Suspension of catalyst was dropped on RDE.
- Nafion soln. (5 μL) was then dropped on RDE.
- Pt surface density (D_{Pt}): 8.8 μg_{-Pt} cm^{-2}

Measurement Procedure

Evaluation of catalytic active site

↓ Electrocatalytic surface area (ECSA)
Calculated by H_2 desorption peak area (S_H) in cyclic voltammogram.

Evaluation of ORR activity

↓ Mass specific activity (MSA)
Measured by ORR polarization curve (Rotating speed: 400, 900, 1600, 2500 rpm).

Accelerated durability test (ADT)

↓ Conducted by Square wave potential cycles (3 s, 0.6 V_{RHE}−3 s, 1.0 V_{RHE}, 6000 cycles).

Evaluation of catalytic durability

Evaluated by decrease ratio of MSA after the ADT from that of before the ADT.

Cyclic Voltammograms and Electrochemical Surface Area (ECSA)

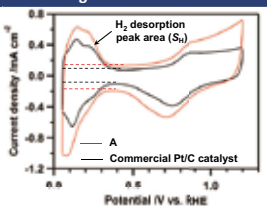

$$\text{ECSA } (m^2 g^{-1}) = \frac{S_H\ (C\ V\ s^{-1}\ m^{-2})}{2.10\ (C\ m^{-2}) \times \nu\ (V\ s^{-1}) \times D_{-Pt}\ (g_{-Pt}\ m^{-2})}$$

Analysis Conditions
Electrolyte: 0.1 M N_2-satulated $HClO_4$ aq., 293K
Scanning rate (ν): 50 mV s^{-1}

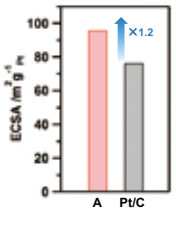

ORR Polarization Curves at 1600 rpm and Mass Specific Activity (MSA)

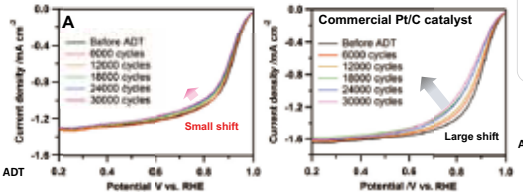

Koutecky-Levich equation:
$j^{-1} = j_k^{-1} + j_L^{-1} = j_k^{-1} + (B\omega^{1/2})^{-1}$
j: measured current density
j_k: kinetic current density
j_L: diffusion-limiting current density
B: Levich constant, ω: angular velocity

$MSA = j_k / D_{-Pt}$

Analysis Conditions
Electrolyte:
0.1 M O_2-satulated $HClO_4$ aq., 293K
Scanning rate: 10 mV s^{-1}

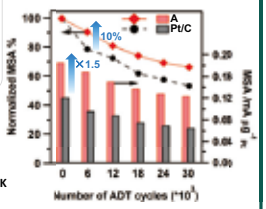

(1) A exhibited 1.2 times larger ECSA value than commercial Pt/C catalyst, which suggests that A has more ORR active site per Pt weight than commercial Pt/C.
(2) The initial mass specific activity (MSA) of A was 1.5 times larger than that of commercial Pt/C catalyst, and the durability of A on the accelerated durability test (ADT) was improved by about 10%.

Conclusions

- We succeeded in synthesizing the new Pt_4 complex (1) with pyrrole unit by the ligand exchange reaction of in-plane acetate ligands.
- A high loading Pt^0 nanocluster catalyst (A) with narrow size distribution was successfully prepared by the copolymerization method of 1 and pyrrole on MWCNT.
- The mass specific activity for ORR and catalyst durability on A was improved compared to a commercial Pt/C catalyst.

Non-Equilibrium Supramolecular Polymerization of Fluorescent Dye in Aqueous Media

([1]Grad. Sch. Sci., Nagoya Univ.; [2]WPI-ITBM, Nagoya Univ.) ○Natsumi Fukaya[1], Soichiro Ogi[1] and Shigehiro Yamaguchi[1,2]

1. Introduction

Fibril formation in living system

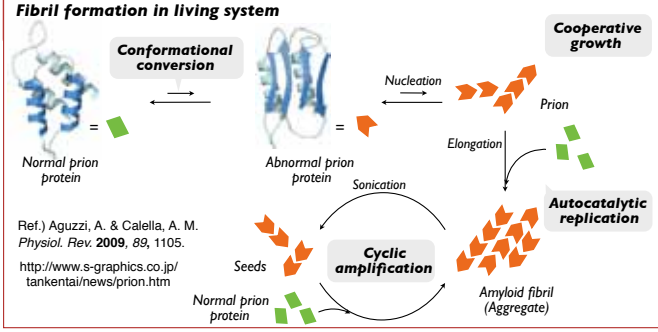

Ref.) Aguzzi, A. & Calella, A. M. *Physiol. Rev.* **2009**, *89*, 1105.

http://www.s-graphics.co.jp/tankentai/news/prion.htm

Biomimetic supramolecular polymerization in solvents of low polarity

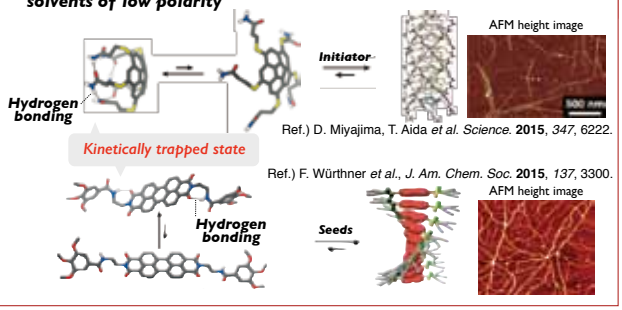

Ref.) D. Miyajima, T. Aida *et al. Science.* **2015**, *347*, 6222.

Ref.) F. Würthner *et al., J. Am. Chem. Soc.* **2015**, *137*, 3300.

2. Molecular design in this work

Design of kinetically trapped state in water

Diketopyrrolopyrrole
Highly fluorescent molecule
Planar π-system
π−π stacking interaction

Amide group
Intra- and intermolecular hydrogen-bonding

Triethylene glycohol group
High solubility to water

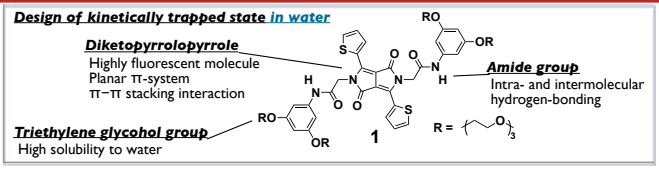

Working hypothesis

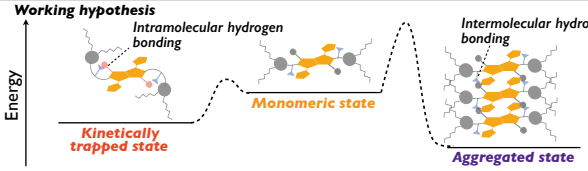

Optimized structure

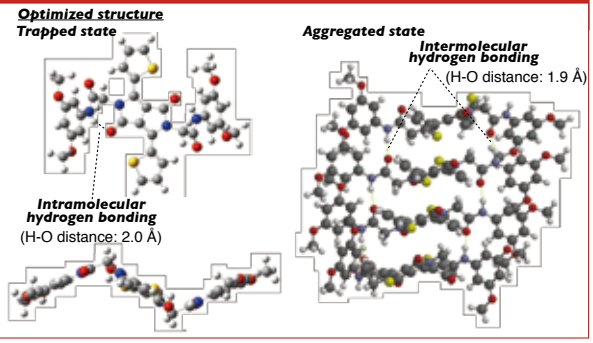

3. Temperature-dependent self-assembly

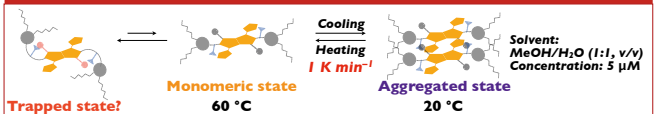

UV-vis absorption spectral change upon heating

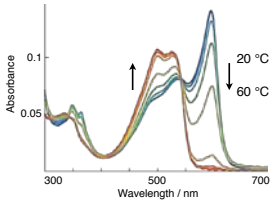

Absorbance change at 601 nm

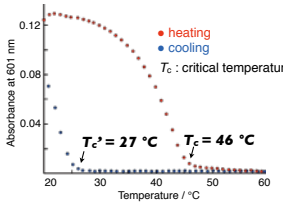

A thermal hysteresis with T_c' (27 °C) from T_c (46 °C) was observed in a cycle of formation and disassembly of J-aggregates.

4. Time-dependent self-assembly

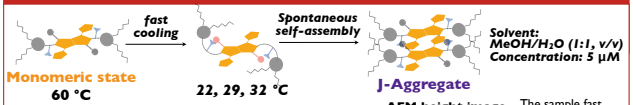

Absorbance change at 601 nm

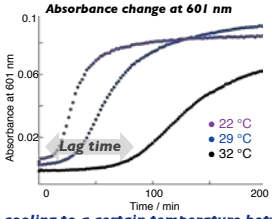

AFM height image
3.5 μm × 3.5 μm

The sample fast cooled to 30 °C

A fast cooling to a certain temperature between T_c' and T_c resulted in a spontaneous formation of J-aggregate with a lag time, where monomers are kinetically trapped.

5. Effect of H-bonding on trapping and assembly

Effect of H-bonding on trapping ***^{1}H MNR spectrum in THF-d_8/D_2O = 1:1 (v/v)***

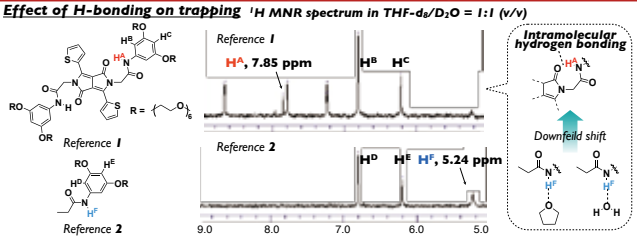

Effect of H-bonding on assembly ***UV-vis absorption spectrum in MeOH/H_2O = 1:1 (v/v) at 20 °C***

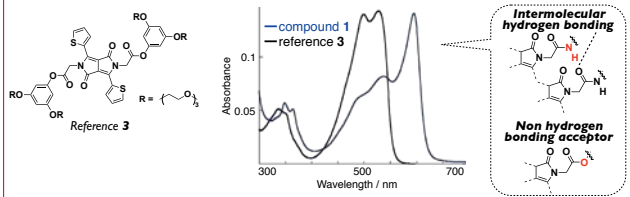

The amide hydrogens are hydrogen-bonded intramolecularly in the monomeric state and intermolecularly in the aggregated state.

6. Seeded polymerization

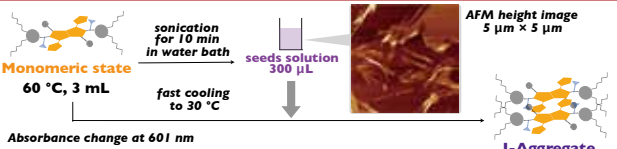

Absorbance change at 601 nm

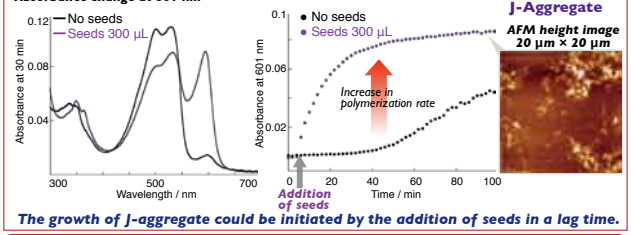

The growth of J-aggregate could be initiated by the addition of seeds in a lag time.

7. Summary

- ***J-aggregate formation of amphiphilic DPP in solvent of high polarity***
- ***Thermal hysteresis in a cycle of the assembly and disassembly***
- ***Monomers trapped kinetically between T_c and T_c'***
- ***Seeded polymerization of J-aggregate nanorods***

Rapid Access to Fused Aromatics by Palladium-catalyzed Annulative Dimerization of Aryl (Pseudo)halides

Taito Hiraga,[1] Yoshito Koga,[1] Yutaro Saito,[1] Kei Murakami[1, 3] and Kenichiro Itami[1, 2, 3]
[1]Graduate School of Science, Nagoya University, Chikusa, Nagoya 464-8602, Japan.
[2]JST, ERATO, Itami Molecular Nanocarbon Project, Nagoya University
[3]Institute of Transformative Bio-Molecules (WPI-ITbM), Nagoya University

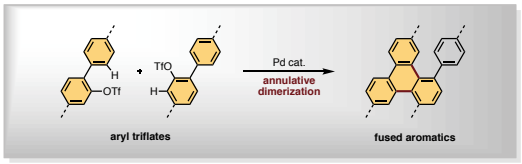

Herein, we develop a one-step palladium-catalyzed annulative dimerization of aryl triflates. This reaction allows the synthesis of various π-conjugated molecules from *o*-hydroxybiphenyl-based starting materials, which can be easily prepared by hydrogenation of dibenzofuran derivatives.

Discussion

Concept

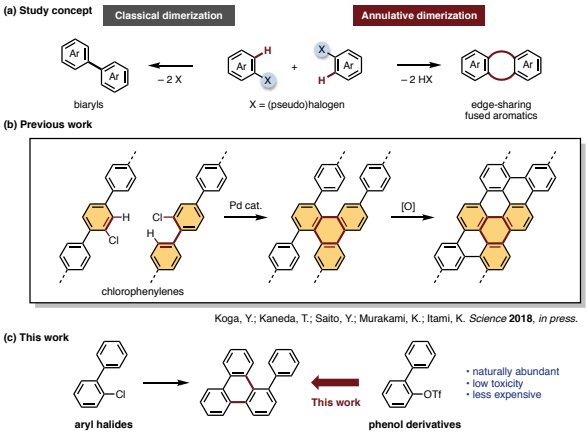

Condition Screening

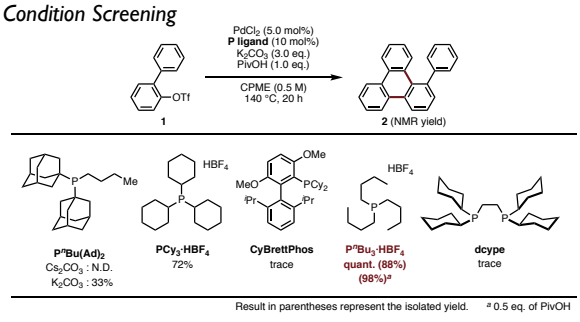

Result in parentheses represent the isolated yield. [a] 0.5 eq. of PivOH

Substrate Scope

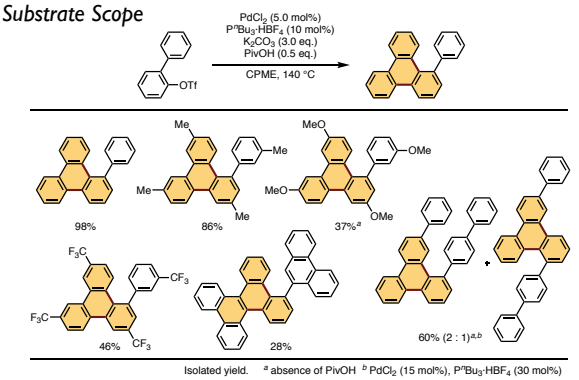

Isolated yield. [a] absence of PivOH [b] $PdCl_2$ (15 mol%), P^nBu_3·HBF_4 (30 mol%)

Possible Mechanism

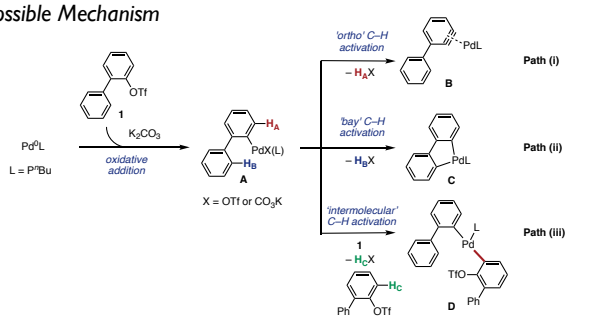

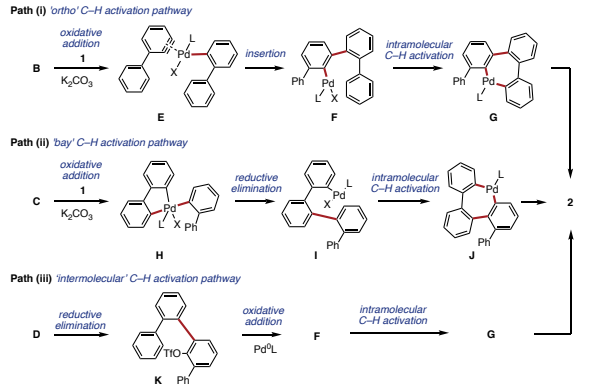

Application

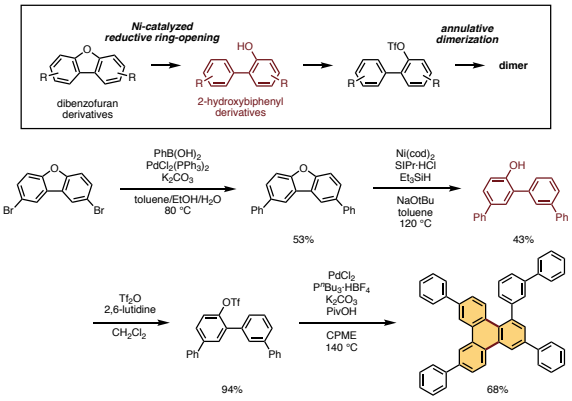

Rapid N-Alkylation of Amines by Alcohols Using a Copper–Gold Photocatalyst

○ Lyu-Ming Wang[1], Yuna Morioka[1], Kellie Binder[2], Andrew E. H. Wheatley[2], Susumu Saito[1], and Hiroshi Naka[1]

[1]Graduate School of Science and Research Center for Materials Science, Nagoya University
[2]Department of Chemistry, University of Cambridge

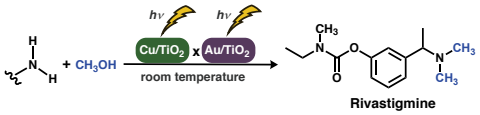

Abstract: Late-stage functionalization of amino groups in complex organic compounds is one of the most important key technologies in modern organic synthesis towards bio-active molecules and pharmaceuticals. We report here the first late-stage N-alkylation of pharmaceutically relevant amines with alcohols at ambient temperature. The mixed photocatalytic system enabled the rapid N-alkylation of pharmaceutically relevant molecules, the selective mono- and di-alkylation of primary amines, and the non-symmetrical dialkylation of primary amines to hetero-substituted tertiary amines.

Introduction

N-Alkylamines in Pharmaceuticals

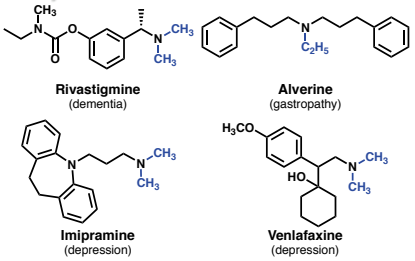

N-Alkylation of Amines with Alcohols

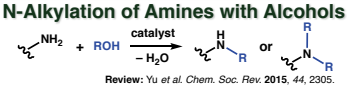

Review: Yu *et al. Chem. Soc. Rev.* **2015**, *44*, 2305.

homogeneous catalysts
transition metal complexes (e.g. Ru, Ir, Fe, Co, Mn)
– broad substrate scope
– high temperature requested (typically > 80 °C)

heterogeneous catalysts
e.g. Metal(OH)$_x$/Al$_2$O$_3$, Metal/Al$_2$O$_3$, Metal/TiO$_2$, *et al.*
– selectivity/recyclable catalyst
– harsh reaction conditions (typically > 110 °C) or high pressure (5 atm)

photocatalysts
Pt/TiO$_2$ (Ohtani, Kagiya, 1986), Pd/TiO$_2$ (Shiraishi, 2013; Shi, 2015)
Au/TiO$_2$ (Sá, 2013), Ag/TiO$_2$ (Saito, 2015), Cu-Mo/TiO$_2$ (Shi, 2015)

– limited scope of both simple amines and simple alcohols
– large excess (> 140 equiv) of alcohols
– long reaction time (> 4 h for completion of 0.2-mmol scale)

This Work

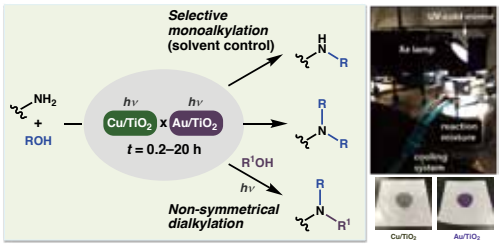

▶ Applicable to pharmaceutical synthesis (up to 1 g)

Results and Discussion

1. Optimization Study for Rapid Reaction

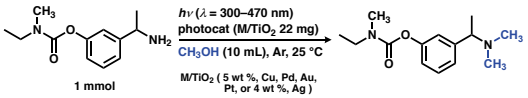

1. Au/TiO$_2$ showed highest Conv. in 1 h

M	Au	>	Pt	>	Pd	>	Cu	>	Ag
Conv.	93%		75%		74%		60%		54%

major intermediate

2. Cu/TiO$_2$ gave highest yield in 7 h

M	Cu	>	Pd	>	Ag	>	Au	>	Pt	>	none
Yield	92%		65%		68%		5%		1%		<1%

major side product

3. mixed Cu/TiO$_2$ & Au/TiO$_2$ showed best result in increasing reaction rate in 2 h

Cu + M	Cu + Au	>	Cu + Pt	>	Cu + Pd	>	Cu + Ag	>	Cu (double)	>	Cu	>	Cu + Au
Yield	70%		59%		50%		42%		40%		21%		< 1% (dark)

91% (4 h) isolated yield Cu + Au

2. Synergistic Effect in Cu–Au Mixed Photocatalytic System

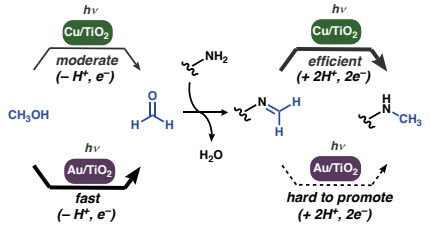

3. Rapid Synthesis of (*rac*)-Rivastigmine

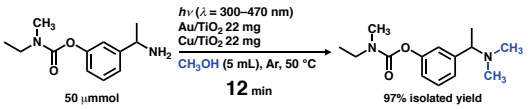

4. Substrate Scope

(a) Dialkylation of Amines

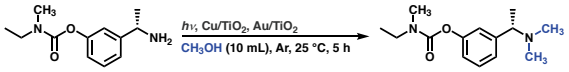

neat conditions (alcohols 10 mL), 1 mmol

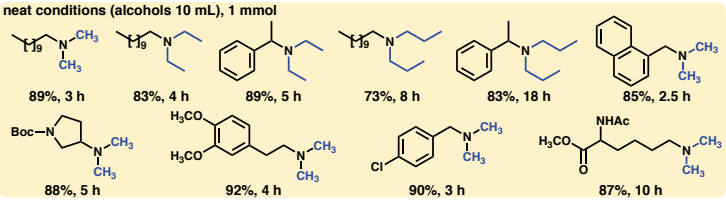

(b) Monoalkylation of Amines by Solvent Control

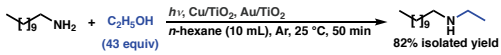

in *n*-hexane (10 mL), 0.2 mmol scale

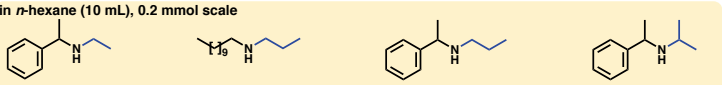

in CPME (10 mL), 1 mmol scale

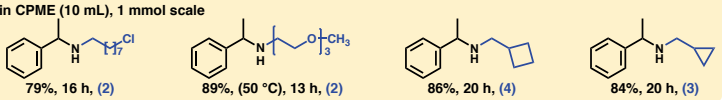

(c) Non-Symmetrical Dialkylation

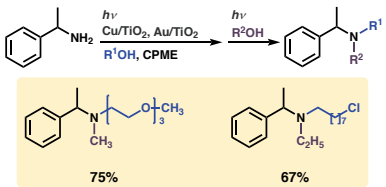

(d) Catalyst recycling

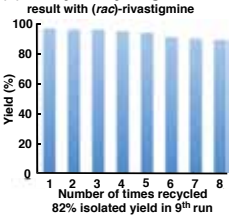

5. Synthesis of Bioactive Compounds

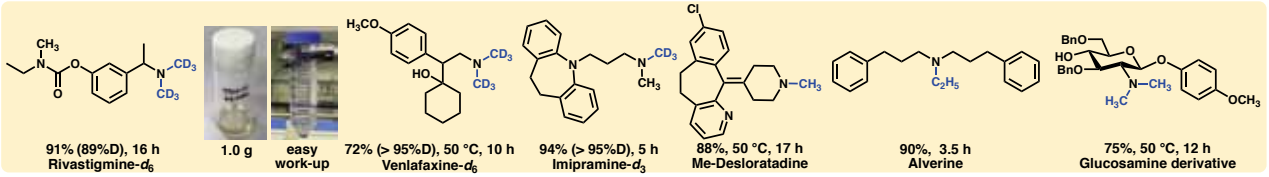

Development of TiO_2 and Ni Complex Hybrid Catalyst for Photocatalytic Aminocarbonylation with Formamides

Shogo Mori,[1] Takahiro Aoki,[1] Susumu Saito*[1,2]
[1]Graduate School of Science, [2]Research Center for Materials Science, Nagoya University

Abstract

We developed a novel catalytic system using heterogeneous TiO_2 photocatalyst and homogeneous Ni catalyst[1] for aminocarbonylation. Cross coupling between electrophilic carbons was realized without inorganic reductant in this hybrid catalyst system. As far as we know, this is the first example of aminocarbonylation with formamides at allylic position.

(1) Sciano, J. C. *et al. ACS Catal.* **2017**, *7*, 2171.

1. Introduction

Aminocarbonylation

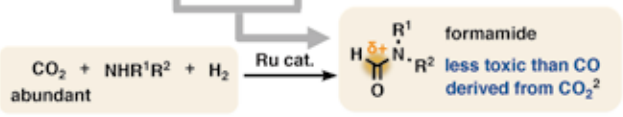

(2) Noyori, R. *et al. J. Am. Chem. Soc.* **1994**, *116*, 8851.

Umpolung using photocatalyst

2. Previous Reports

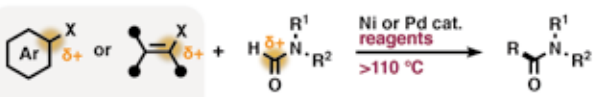

cat. and reagents

$Pd(OAc)_2$ / Xantphos[3a] or $Pd_2(dba)_3$[3b]	$Pd(OAc)_2$ / dppf[3d]	$Ni(OAc)_2 \cdot 4H_2O$[3e]
$POCl_3$ (2 equiv.)	(0.8 equiv.)	NaOMe (4 equiv.)
$PdCl_2$[3c] WCl_6 (2 equiv.)		

stoichiometric amount of waste

(3) (a) Bhanage, B. M. *et al. J. Org. Chem.* **2011**, *76*, 5489. (b) Nozaki, K.; Hiyama, T. *et al. Org. Lett.* **2002**, *4*, 2849. (c) Iranpoor, N.; Firouzabadi, H. *et al. RSC Adv.* **2014**, *4*, 43178. (d) Iranpoor, N.; Panahi, F. *et al. Eur. J. Org. Chem.* **2016**, 1781. (e) Lee, S. *et al. J. Org. Chem.* **2009**, *74*, 9358.

3. Our Hybrid Catalyst System

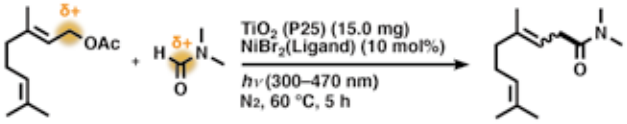

0.25 mmol 1.5 mL 91%

- ✓ Umpolung without stoichiometric amount of waste
- ✓ The first aminocarbonylation with formamides at allylic position

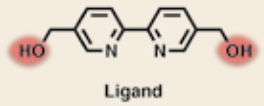

OH group is known for interaction with surface of TiO_2

ligand screening

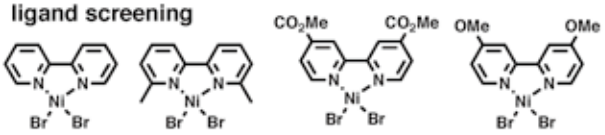

80% 1% 73% 35%

4. Substrate Scope

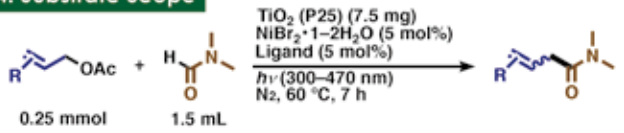

0.25 mmol 1.5 mL

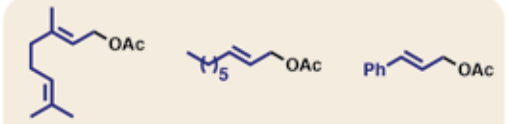

82% 73% 52%

Investigation is ongoing.

5. Carbamoyl Radical as Intermediate

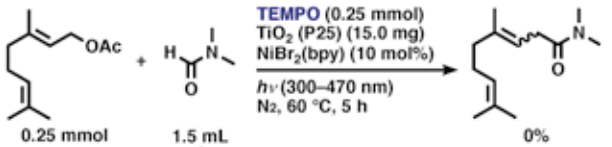

0.25 mmol 1.5 mL 0%

81%[4]

(4) compound data is consistent with the following reference; Zhang, X.-G. *et al. J. Org. Chem.* **2014**, *79*, 9907.

0%

6. Functional Group Tolerance

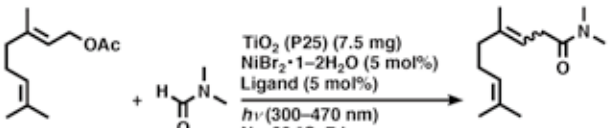

0.25 mmol Olefin 0.25 mmol 1.5 mL at least 63% Olefin recovery

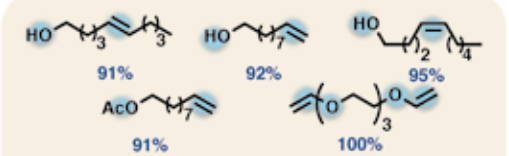

91% 92% 95% 91% 100%

Aliphatic olefins, electron rich olefins alcohol, ester, ether were tolerated.

Catalytic Oxidation of Small Gaseous Alkanes by P450BM3 with Decoy Molecules

Shinya Ariyasu,[1,2] Zhiqi Cong,[1,2] Osami Shoji,[1,2] Yuichiro Aiba,[1,2] Chie Kasai,[1,2] Hiroki Onoda,[1] Kazuto Suzuki,[1] Hiroshi Sugimoto,[2,3] Yoshitsugu Shiro,[3] Takashi Kamachi,[2,4] Kazunari Yoshizawa,[2,4] Yoshihito Watanabe,[5]

[1]*Department of Chemistry, Graduate School of Science, Nagoya University.* [2]*JST-CREST.* [3]*RIKEN SPring-8 Center, Harima Institute.* [4]*Institute for Materials Chemistry and Engineering, Kyushu University.* [5]*Research Center for Materials Science, Nagoya University.*

1. About Methane-Oxidation

Methane is main component of natural gas and is used for starting molecule of various organic compounds.

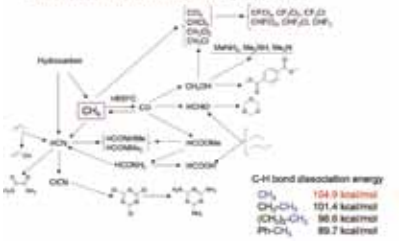

2. Methane-Oxidizing Enzymes

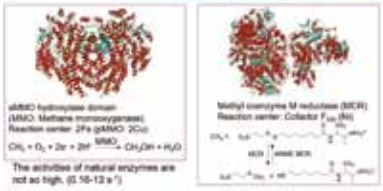

The activities of natural enzymes are not so high. (0.18-12 s^{-1})

3. Hydroxylation of Long Fatty Acids by P450BM3

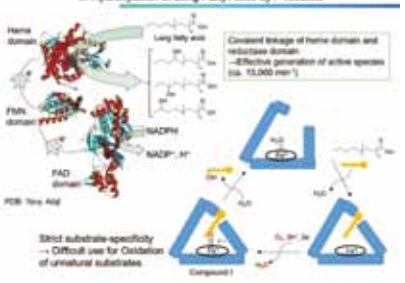

4. Oxidation of Small-sized Alkanes by P450BM3 with Decoy Molecules

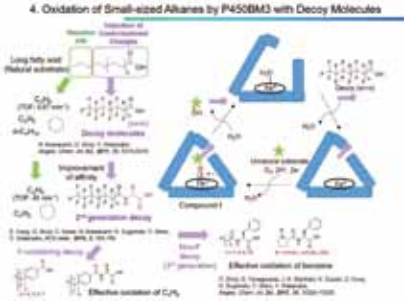

For Methane-Oxidation by P450BM3 with Decoy

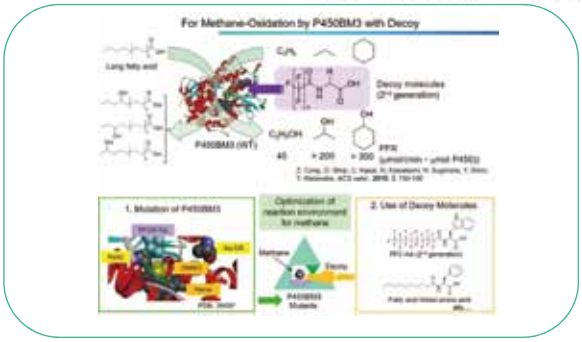

6. Experimental Procedure

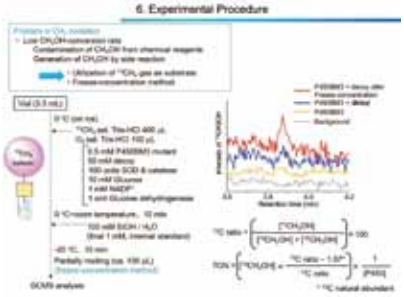

7. Screening of P450BM3 Mutants

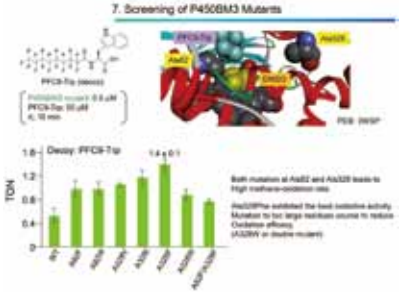

Both mutation at Ala82 and Ala328 leads to high methane-oxidation rate.

Ala328Phe exhibited the best oxidative activity. Mutation to two large residues seems to reduce Oxidative efficiency. (A328W or double mutant)

8. Screening of Perfluoroacyl Amino Acid-Type Decoys

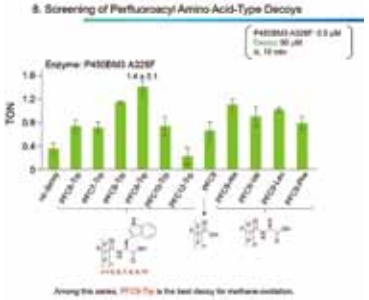

Among this series, PFC9-Trp is the best decoy for methane-oxidation.

9. X-ray Crystal Structure Analysis of P450BM3 A328F with PFC9-Trp

Crystallization condition

In the obtained crystal structure, PFC9-Trp was not observed.

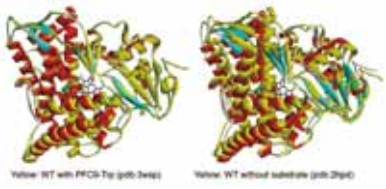

The obtained crystal structure is almost same to that of WT with PFC9-Trp, suggesting that PFC9-Trp induces conformational change of A328F variant.

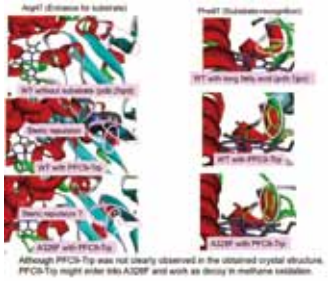

Although PFC9-Trp was not clearly observed in the obtained crystal structure, PFC9-Trp might enter into A328F and work as decoy in methane oxidation.

10. Development of High-pressure Reactor

High pressure of CH_4 gas is promising way to increase CH_4 concentration in reaction mixture. However, it is difficult to achieve >1 MPa (ca. 10 atm) due to law-restriction.

GL Science High Pressure Reactor (Installed at IIYS) (Submission of patent: 1045)

11. $^{13}CH_4$ Oxidation under High Pressure

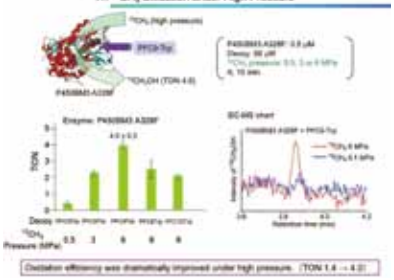

Oxidation efficiency was dramatically improved under high pressure. TON 1.4 → 4.0

12. Conclusion

- We achieved catalytic methane-oxidation by using P450BM3 mutants with decoy molecules.
- X-ray crystallography suggested that PFC9-Trp might work as decoy in P450BM3 A328F mutants during methane-oxidation.
- The catalytic activity of methane-oxidation was dramatically improved under high pressure of methane induced by a new-type high-pressure reactor.

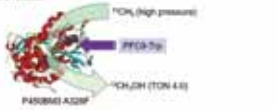

New Insight into dsDNA Invasion by NLS-PNAs

○Gerardo Urbina[1], Yuichiro Aiba[1], Osami Shoji[1], Yoshihito Watanabe[2]

[1]Department of Chemistry, Graduate School of Science, Nagoya University
[2]Research Center for Material Science, Nagoya University

Introduction

Peptide Nucleic Acid (PNA)

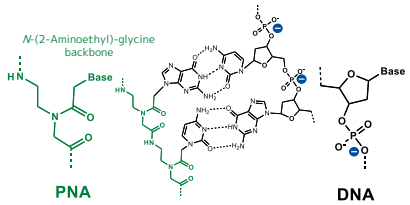

PNA possesses an **electrostatically neutral** backbone.
No repulsion between PNA and the phosphate groups of DNA.

PNA/DNA duplex is more stable than double-stranded DNA

Double-Duplex Invasion

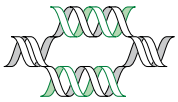

Two PNA strands can **"invade"** dsDNA

Since **it can recognize dsDNA directly and sequence-specifically**, PNA is a good candidate as a tool in molecular biology and in the development of nucleic acid medicines.

However...

dsDNA becomes stable under high salt concentrations, resulting in a low invasion efficiency.

⇒ **A more stable invasion complex is necessary.**

Improving Invasion Efficiency:
NLS-conjugated PNA (NLS-PNA)

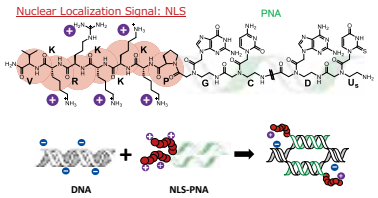

Electrostatic interaction between NLS and DNA
➔ **Higher invasion efficiency**

Aiba, et al. *Chem. Eur. J.* 21: 4021–4026.

Objectives

Development of an NLS-PNA that shows **high invasion efficiency under physiological conditions** (high salt concentration) by studying:

① The effect of **the location of the NLS** (C- or N-terminus) on invasion efficiency.

② The dependence of invasion efficiency on **salt concentration**. [NaCl]

③ The effect of a change in **the NLS composition.**

In order to...

Optimize the NLS modification for *in vivo* and *in cell* applications of PNA invasion

Methods

A **10-mer PNA, shorter than those used in previous works**, was used.

```
(5′)...ATCATCAGTAACC...(3′)
       ||||||||||
       c-GUDGUCDUUG-n
       n-CDUCDGUDDC-c
       ||||||||||
(3′)...TAGTAGTCATTGGG...(5′)
```

A **130 bp DNA** from the pBR322 plasmid was used as a **target.**

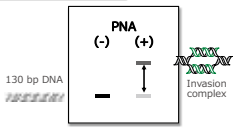

Invasion efficiency was evaluated by a **shift in electrophoretic mobility**

Results and Discussion

Relation between invasion efficiency and salt concentration for U-PNA

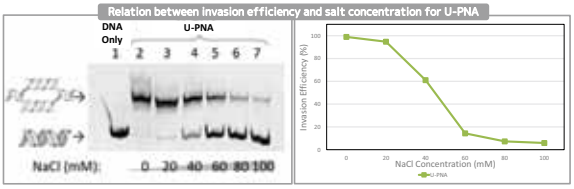

U-PNA shows a high invasion efficiency at first, but a **marked decrease is observed at higher salt concentrations**

This is **not enough** for *in vivo* applications!

Invasion Conditions:

[DNA] = 50 nM
[PNAs] = 75 nM (1.5 eq.)
[HEPES(pH 7.0)] = 5 mM
50°C for 1 h

PNAs used in this research:

U-PNA (unmodified PNA)
c-KK-GUDGUCDUUG-K-n
n-K-CDUCDGUDDC-KK-c

C-10PNA (C-terminal NLS)
c-VKRKKKP-GUDGUCDUUG-K-n
n-K-CDUCDGUDDC-PKKKRKV-c

N-10PNA (N-terminal NLS)
c-KK-GUDGUCDUUG-VKRKKKP-n
n-PKKKRKV-CDUCDGUDDC-KK-c

C-lys-10PNA (Arg → Lys)
c-VKKKKKP-GUDGUCDUUG-K-n
n-K-CDUCDGUDDC-PKKKKKV-c

Synthesized by solid phase peptide synthesis.

① The N-terminal NLS modification is detrimental for invasion efficiency

Comparison between N-PNA, U-PNA, C-Lys-PNA

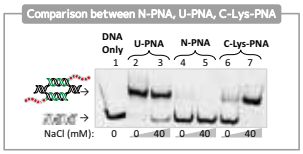

N-PNA showed a low invasion efficiency especially at high salt concentration

② C-PNA shows a high invasion efficiency even at high salt concentration

Invasion Efficiency Trends

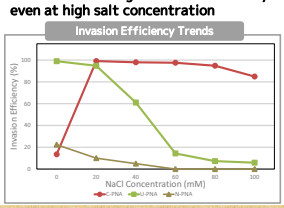

C-PNA shows a **high invasion efficiency at salt concentrations above 20 mM**

③ The composition of the NLS affects both efficiency and specificity

C-PNA and C-Lys-PNA comparison (with NaCl)

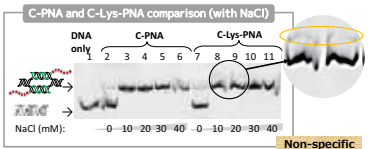

Non-specific invasion

C-PNA and C-Lys-PNA comparison (w/o NaCl)

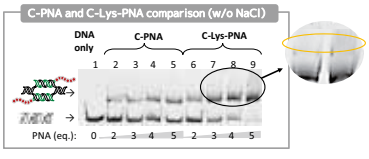

In the case of C-Lys-PNA, **non-specific bands** appeared when the invasion efficiency was high

Conclusions

- NLS-PNAs can invade dsDNA **even under high salt concentrations.**
- The effect of the NLS modification varies dramatically depending on which side of the PNA is modified. In particular, **a C-terminal modification was extremely beneficial.**
- The decrease in invasion efficiency with higher salt concentrations was **less marked for C-PNA.**
- In order to obtain a higher invasion efficiency, just a positive charge is not enough: The efficiency and specificity **vary depending on the amino acid composition** of the NLS.

⇒ **With the optimal composition, an even higher invasion might be obtained. Using such NLS-PNAs, a broader range of PNA applications is possible.**

Improvement of Catalytic Activity of Self-sufficient Cytochrome P450 by Enzymatic Ligation

NAGOYA UNIVERSITY

○Keita Omura[1], Shinya Ariyasu[1], Yuichiro Aiba[1], Osami Shoji[1,2], Hiroshi Sugimoto[2,3], Yoshitsugu Shiro[4], Yoshihito Watanabe[1]

([1]Nagoya Univ., [2]JST-CREST, [3]RIKEN SPring-8, [4]Univ. of Hyogo)

CHEMISTRY Nagoya University

Introduction

- P450BM3 (BM3) from *Bacillus megaterium*
  - ✓ Hydroxylation of fatty acids (→ C-H activation)
  - ✓ Self-sufficient cytochrome P450 fused with its redox partner
  - ✓ Very high catalytic activity among P450s (16400 min^{-1}, arachidonic acid)

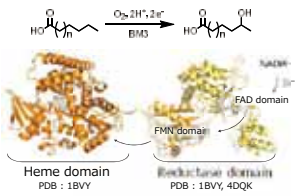

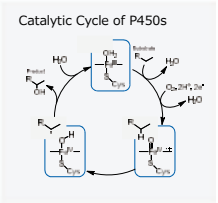

- Decoy system
  - ✓ Altering the substrate specificity by using natural substrate analog
  - ✓ Enabling hydroxylation of various small organic substrates, which is not usually recognized as substrate (benzene, cyclohexane, propane, etc.)
    - O. Shoji. *et al. Angew. Chem. Int. Ed.* **52**, 6606-6610 (2013), Z. Cong. *et al. ACS Catalysis*, **5**, 150–156 (2015).

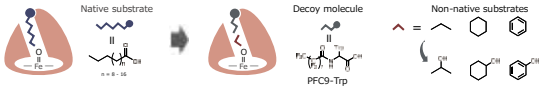

Aim

- Development of metal-substituted BM3 to catalyze difficult reactions
  - ✓ Improvement of catalytic activity of hemoprotein by substitution of central metal (Fe ⟶ Mn, Co,..)
  - ✓ Oxidation of substrates which are difficult to be oxidized like methane (CH_4 ⟶ CH_3OH)

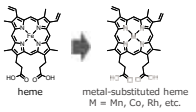

Problem

- No reports for heme substitution of full-length BM3
  - ✓ Structural complexity prevents BM3 from being reconstituted in its full-length form. BM3 : 120 kDa (e.g. myoglobin : 18 kDa)
  - ✓ BM3 is denatured by conventional reconstitution method using acid/organic solvent.
  - ✓ The heme domain (not full-length BM3) can be reconstituted with an artificial metal complex (but catalytic activity is lost).

- Kawakami, N. *et al. ChemBioChem* **13,** 2045–7 (2012).

➢ New method for reconstitution was required

Strategy

- Ligating heme-substituted heme domain with reductase domain

➢ SortaseA

- ✓ A type of transpeptidase
- ✓ Isolated from *Staphylococcus aureus*
- ✓ Sortase A recognizes the specific peptide sequence and catalyzes formation of new peptide bond

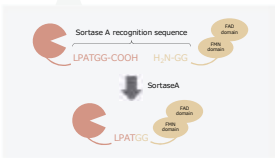

Result 1 | Effect of ligation by Sortase A

- Reconstitution of full-length Fe-BM3
  - ✓ We investigated the effect of ligation between the reductase domain and the heme domain containing heme as cofactor
  - ✓ Catalytic activity was measured by pNCA assay (UV absorbance at 410 nm)

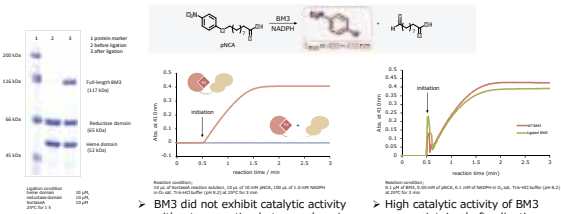

➢ BM3 did not exhibit catalytic activity without connection between domains

➢ High catalytic activity of BM3 was maintained after ligation

Result 2 | Preparation of Mn-BM3

- Introduction of Mn-protoporphyrin IX (Mn-PPIX) into heme domain
  - ✓ Apo heme domain was expressed in Fe-limiting culture.
  - ✓ Mn-PPIX was introduced into heme pocket.
  - ✓ Incorporation of Mn-PPIX was confirmed by UV-vis spectra, ICP-OES, and X-ray crystallography.

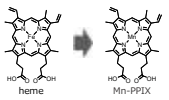

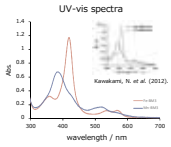

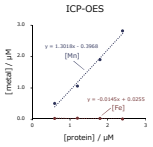

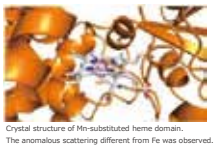

Crystal structure of Mn-substituted heme domain.
The anomalous scattering different from Fe was observed.

- Reconstitution of Mn-substituted full-length BM3
  - ✓ Ligation was confirmed by SDS-PAGE.
  - ✓ Catalytic activity of Mn-BM3 was confirmed by pNCA assay.

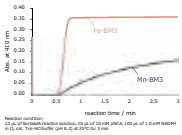

➢ Full-length BM3 containing Mn-PPIX (Mn-BM3) was successfully reconstituted.
➢ Mn-BM3 exhibited catalytic activity for pNCA

Result 3 | Catalytic properties of Mn-BM3

- Propane oxidation

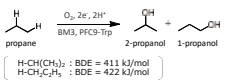

H-CH(CH3)2 : BDE = 411 kJ/mol
H-CH2C2H5 : BDE = 422 kJ/mol

- ✓ Selectivity for 1-propanol was improved.
- ✓ In contrast, TOF decreased.

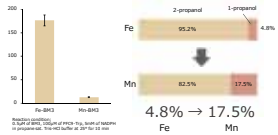

- Methane oxidation

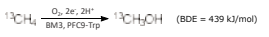

methane oxidation is challenging because of;

- ✓ extremely high C-H bond dissociation energy
- ✓ low solubility in water

High pressure reactor was developed
(methane gas pressure : 0.1 MPa → 10 MPa)

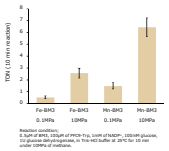

➢ TOF for methane was improved

Conclusion

- ☐ It was found that this reconstitution method was useful for preparing the BM3 containing artificial metal complexes.
  Therefore, this method have potential for expanding the reaction scope of BM3.
- ☐ Mn-BM3 exhibited catalytic activity for C-H hydroxylation.

Design of Whole-cell Biocatalyst for Aromatic Hydroxylation Utilizing P450BM3 and Decoy Molecules

Masayuki Karasawa,[1] Sota Yanagisawa,[1] Osami Shoji,[1,2] Yoshihito Watanabe,[3]

[1] Dept. of Chem., Grad. Sch. of Sci., Nagoya Univ., [2] CREST, Japan Science and Technology Agency, [3] Research Center for Materials Science, Nagoya Univ.

CHEMISTRY Nagoya University

Introduction

Cytochrome P450BM3 (P450BM3)

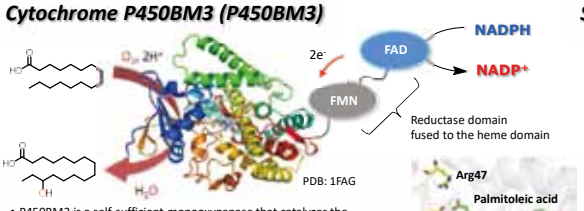

- P450BM3 is a self-sufficient monooxygenase that catalyzes the hydroxylation of long-chain fatty acids at the sub-terminus.
- P450BM3 possesses one of the highest catalytic activities among P450s.
- P450BM3 shows the high substrate specificity that imposes the limitation on the practicality of the enzyme.

Substrate Misrecognition System

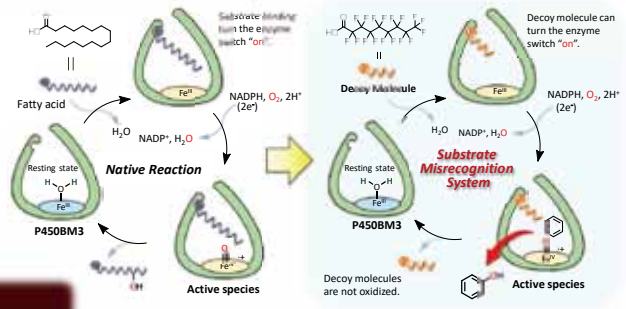

✓ Inert dummy substrates are misrecognized by P450BM3 and thus control the catalytic activities of the enzyme.

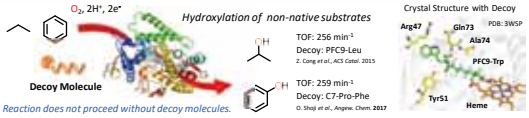

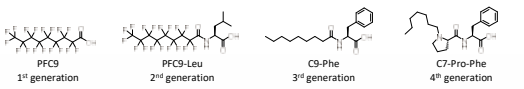

Substrate misrecognition system is a promising platform for the hydroxylation of small organic molecules.

Research Aim

Developing the Whole-cell Biocatalyst using Substrate Misrecognition System

✓ *Hydroxylation by P450BM3 is supported with the intracellular production of NADPH cofactor via glucose metabolism.*

NADPH: 20,000,000 yen/mol
Glucose: 20 yen/mol

✓ *This unique reaction system would be a potential green alternative for current high energy-consuming process to produce phenol.*

Can decoy molecules function as a activator of the intracellular enzyme?

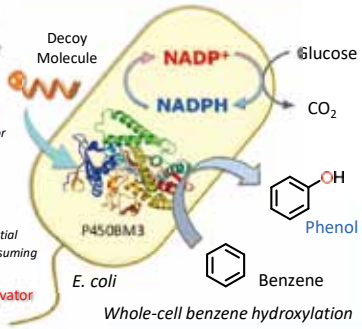

Summary

- Decoy molecules permeates into the cell and thus activates P450BM3 expressed in the cell.
- Efficient whole-cell biocatalyst for aromatic hydroxylation has been developed.

Results and Discussion

■ Experimental Procedure

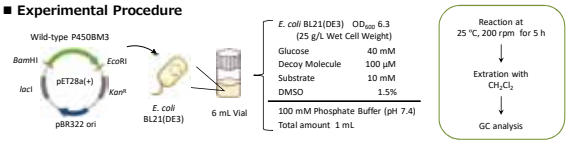

◆Whole-cell Benzene Hydroxylation

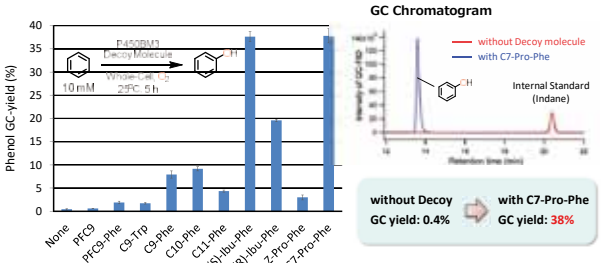

GC Chromatogram

without Decoy GC yield: 0.4% ⇨ **with C7-Pro-Phe** GC yield: 38%

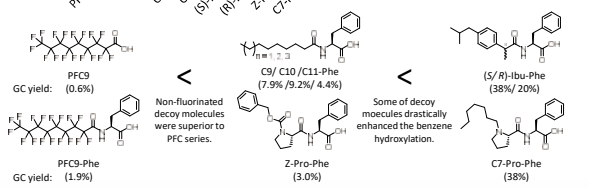

- We presume that decoy molecules are selectively taken into a microbial cell depending upon the structures, affecting the effective concentration of decoy molecules present in the cell.

✓ *We demonstrated that decoy molecules can permeate into the cell and thus activate intracellular P450BM3.*

✓ *We succeeded in developing the efficient whole-cell biocatalyst for benzene hydroxylation, reaching a phenol yield of 38%.*

■ Concentration Dependence

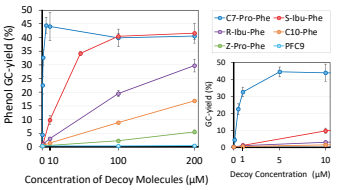

■ Time Course Experiment

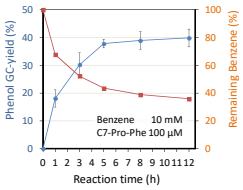

■ Fluorescence Microscopy after Reaction

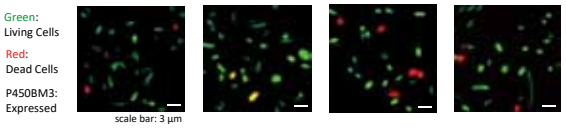

- Time course experiment revealed that the reaction rate of the whole-cell biotransformation of benzene is relatively high, reaching a phenol yield of 18% after 1 h reaction.
- C7-Pro-Phe activate intracellular P450BM3 even at a low concentration of 0.5 μM.
- C7-Pro-Phe has not shown serious toxicity towards *E. coli,* even though it is taken into the cell.

◆Hydroxylation of Mono-substituted Benzenes

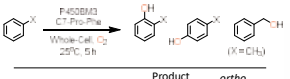

Substrate (10 mM)	Product GC-yield (%)	*ortho* Selectivity (%)
Toluene (Ph-CH_3)	26	97
Anisole (Ph-OCH_3)	63	90
Fluorobenzene (Ph-F)	25	64
Chlorobenzene (Ph-Cl)	13	89

In the presence of 25 mM α-cyclodextrin as a solubilizer

GC Chromatogram (Anisole)

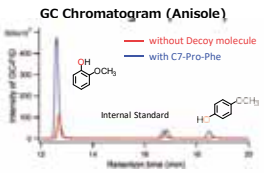

Without Decoy Molecule GC yield: 15% ⇨ With C7-Pro-Phe GC yield: 63%

✓ *The ortho position of Mono-substituted benzenes was selectively hydroxylated by P450BM3.*

Studies on the Heme Uptake Proteins (PhuUV-T) from *Pseudomonas aeruginosa*

○ Erika Sakakibara [1] · Yuma Shisaka [1] · Osami Shoji [1] · Hiroshi Sugimoto [2] · Yoshihito Watanabe [3]

[1] *Department of Chemistry, Graduate School of Science, Nagoya University;*
[2] *RIKEN SPring-8 Center;* [3] *Research Center for Materials Science, Nagoya University*

Introduction

◆ *Pseudomonas aeruginosa*

- Opportunistic bacteria
- Appearance of multi-drug resistant *P. aeruginosa* is a critical issue
- Iron is necessary for the survival

◆ Heme acquisition

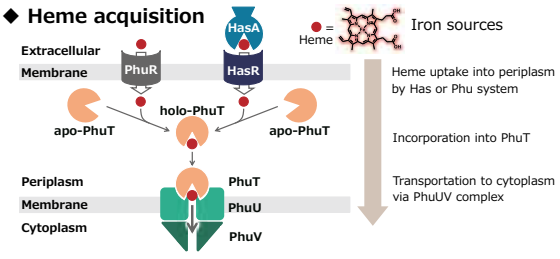

PhuUV complex is the sole passage of heme from periplasm to cytoplasm

◆ Previous study on heme transporter

The crystal structure of a heme transporter ortholog (BhuUV-T complex) has been reported

Unfortunately, the mechanism of heme transport has **not been elucidated**

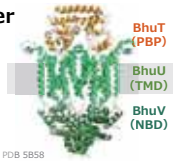

Y. Naoe, *et al.*, *Nat. Commun.* **2016**, *7*, 13411 PDB 5B58

Strategy & Aim

◆ Crystal structure of PhuT

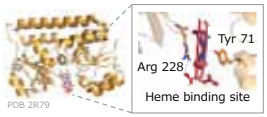

The heme binding site is exposed to the outside of PhuT

This suggests that the heme in PhuT can be replaced with a synthetic metal complex

◆ Analysis of the interaction between PhuT and PhuUV

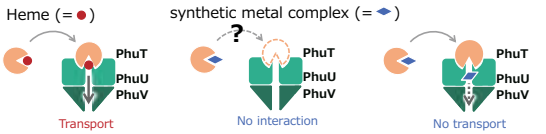

Collection of further information about the heme-transport mechanism using PhuT containing synthetic metal complexes

Summary

- We developed a reconstruction method of PhuT and succeeded in introducing synthetic metal complexes
- The structure of Mesoheme-PhuT was determined by X-ray crystal structure analysis
- We constructed the expression system of PhuV using *E. coli*

Orange : Holo-PhuT
Cyan : Mesoheme-PhuT

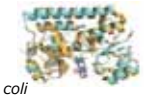

Experiment & Result

◆ Preparation of apo-PhuT

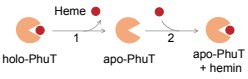

1. After the removal of heme, apo-PhuT was obtained by dialysis
2. Heme was added to the solution of apo-PhuT

UV-Vis spectroscopy

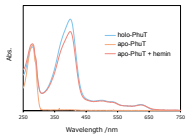

ESI-TOF MS

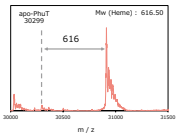

CD spectroscopy

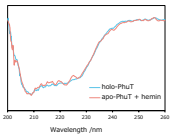

Heme was successfully incorporated into the prepared apo-PhuT

◆ Introduction of synthetic metal complex

Method

Addition of complex to apo-PhuT

Dialysis of the mixture to remove DMSO

Purification by anion exchange column

Column chart

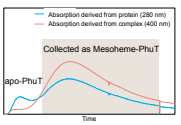

Heme diOMe | Mesoheme | Fe Pc | Fe TPP

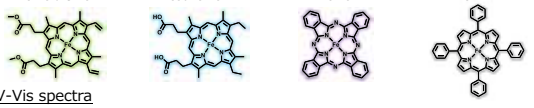

UV-Vis spectra

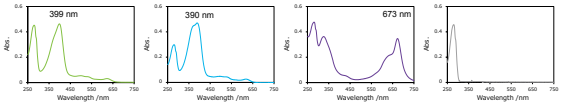

ESI-TOF MS

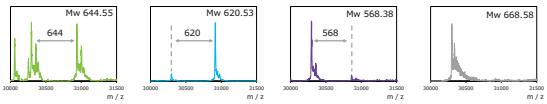

We succeeded in the introduction of synthetic metal complexes

◆ Crystal structure analysis

Orange : Holo-PhuT (PDB : 2R79)
Cyan : Mesoheme-PhuT

Mesoheme-PhuT

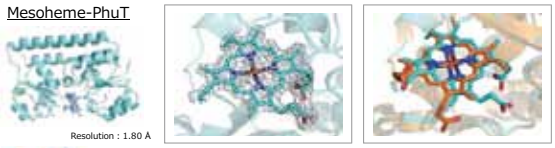

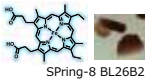

SPring-8 BL26B2

The angle of mesoheme was different from that of heme

The difference of the angle may have an effect on heme transport

We succeeded in the crystal structure analysis of Mesoheme-PhuT

◆ PhuUV Expression

Plasmid design

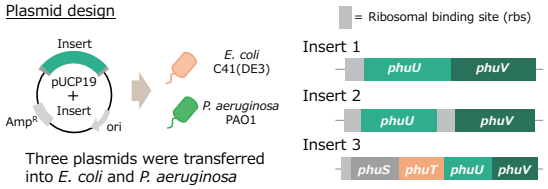

Three plasmids were transferred into *E. coli* and *P. aeruginosa*

In *E. coli*

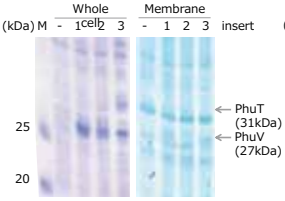

In *P. aeruginosa*

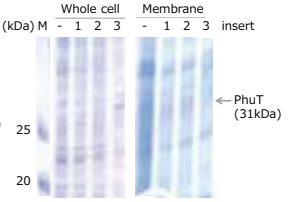

The expression of PhuV was observed using *E. coli* as the host cell

In the future, we will perform immunoblotting assay to specifically detect PhuU

Covalent Organic Frameworks for Electrochemical Energy Storage

NAGOYA UNIVERSITY

Yang WU, Zhongyue ZHANG, and Kunio AWAGA*

Department of Chemistry & Integrated Research Consortium on Chemical Sciences (IRCCS), Nagoya University

Covalent Organic Frameworks (COFs)

A class of porous crystalline polymers with periodic structures

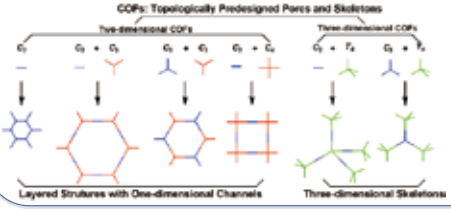

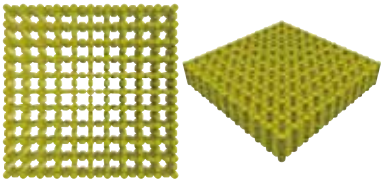

- Large Surface Area: Thousands m^2/g
- Designed Pore Size: Micropore (< 2 nm) Mesopore (> 2 nm)
- Lightweight Elements: C, H, B, O, N
- Strong Covalent Bonds

I. Covalent Organic Framework-*graft*-polysulfide (COF-*graft*-PS)

Synthesis

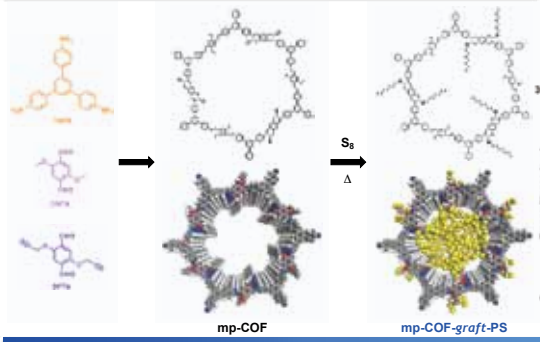

Characterization

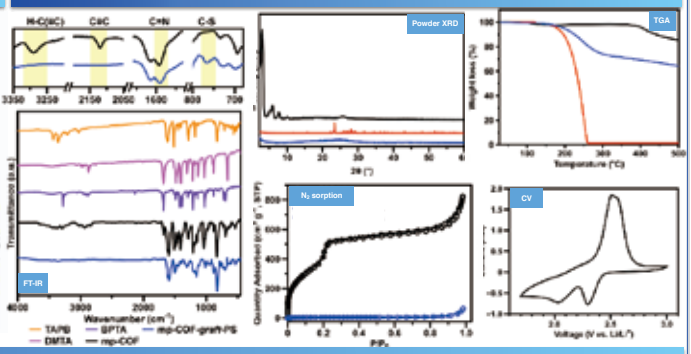

Battery tests

1 Separator 2 Gasket
3 Cathode (70 wt% COF-*graft*-PS, 20 wt% carbon black and 10 wt% PVDF)
4 Positive pole (cell can)
5 Anode (Lithium) 6 Negative pole

Electrolyte: 1 M LiTFSI in DOL/DME(1:1, v/v) with 0.2 M of $LiNO_3$

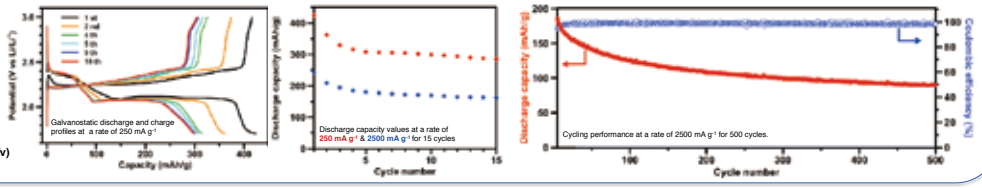

II. Poly(3,4-ethylenedioxythiophene)@Covalent Organic Framework (PEDOT@COF)

Strategy

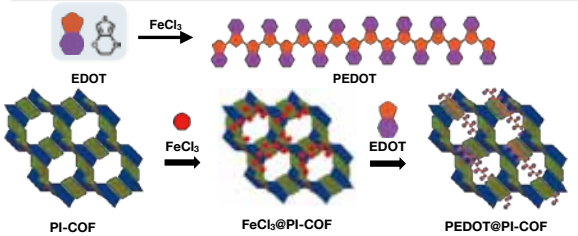

Electrochemical redox reaction

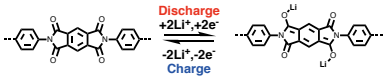

Synthesis

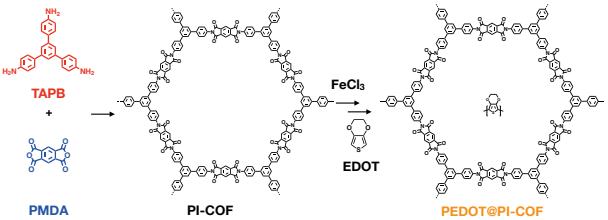

Characterization

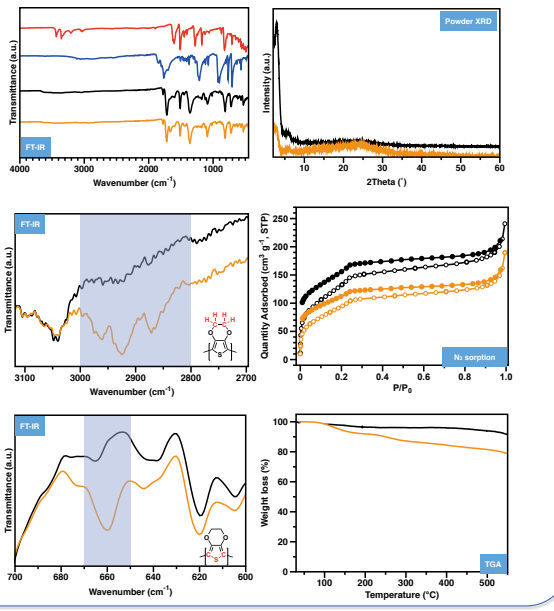

Impurity doping to molecule-based honeycomb lattices of organic radicals

○[1]Ryo Ushiroguchi, [1]Yoshiaki Shuku, [2]Byeong-Kwan An, [3]Ji Eon Kwon, [3]Soo Young Park, [1]Kunio Awaga
([1]Department of Chemistry, Nagoya Univ. [2]Department of Chemistry, The Catholic University of Korea, [3]Department of Materials Science and Engineering, Seoul National University)

Introduction

Carbon allotropes

Graphene sp^2 2D conductor

Diamond sp^3 3D insulator

K_4 Carbon sp^2 3D Metallic (calculation) M. Itoh, *Phys. Rev. Lett.*, 2009, **102**, 055703.

Our interest
Band structure, Magnetic property ...

Previous work

K_4 lattice by Rb_3NDI - Δ

replace

sp^2 Carbon

Radical anion of NDI - Δ

Crystal structure

K_4 was successfully obtained by replacing sp^2 carbon with NDI - Δ

A. Mizuno, Y. Shuku, R. Suizu, M.M. Matsushita, M. Tsuchiizu, D. Reta Maneru, F. Illas, V. Robert, K. Awaga, *J. Am. Chem. Soc.* 2015, **137**, 7612-7616

A. Mizuno, Y. Shuku, M.M. Matsushita, M. Tsuchiizu, Y Hara, N. Wada, Y. Shimizu, K. Awaga, *Phys. Rev. Lett.* 2017, **119**, 057201

Electrochemistry of TTQ

TTQ (Trypticene **T**ri**q**uinone)

- Electron acceptor
- Air-stable radical

p-benzoquinone (p-BQ)

π-π interaction between radicals induce dimerization

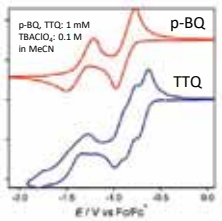

This work

replace

sp^2 Carbon

- Hard to doping by atom substitution
- Chemical modification is not available

TTQ

- Substitution available
- Variable functional group

Crystallize

doping

Impurity molecular

TDQ (Trypticene **D**i**q**uinone)

TMQ (Trypticene **M**ono**q**uinone)

Objective

① Construction of honeycomb structure by organic radical molecular

② Find property change by doping impurity molecular

Crystal structure?
Magnetic property?

Sample preparation

Electrochemical method

Pt wire

MeCN

$RbClO_4$

Quinones

- TTQ
- TTQ : TDQ = 1:1 (TDQ 50% fed)
- TTQ : TMQ = 1:1 (TMQ 50% fed)

Result and discussion

Crystal structure of anion radical salt

Honeycomb structure

Layered structure

1D pore

Ideal honeycomb structure with 1D pore
Even though impurity was doped, honeycomb structure was retained.
Impurity molecules were disordered in crystal.

Band calculation

Rb_3TTQ

Similar

Graphene

TTQ
Hexagonal, *P6/m*(#175)
$a = b = 11.6406(19)$, $c = 8.6575(14)$ Å
$V = 1016.0(3)$ Å^3
R_1 ($I > 2\sigma(I)$) = 0.0249, wR_2 (all) = 0.0621, GOF = 1.119
Residual electron density in pore was removed by SQUEEZE
$T = 123$ K

TDQ 50% fed
Hexagonal, *P6/m*(#175)
$a = b = 11.6708(6)$, $c = 8.7595(6)$ Å
$V = 1033.26(10)$ Å^3
R_1 ($I > 2\sigma(I)$) = 0.1161, wR_2 (all) = 0.3136, GOF = 1.168
Residual electron density in pore was removed by SQUEEZE
$T = 123$ K

TMQ 50% fed
Hexagonal, *P6/m*(#175)
$a = b = 11.65100$, $c = 8.67300$ Å
$V = 1019.59188$ Å^3
R_1 ($I > 2\sigma(I)$) = 0.0656, wR_2 (all) = 0.1745, GOF = 1.227
Residual electron density in pore was removed by SQUEEZE
$T = 123$ K

- Occupancy of quinone moiety

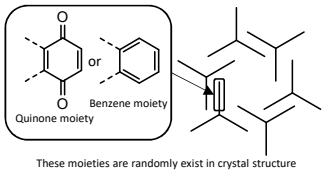

These moieties are randomly exist in crystal structure

Occupancy	TTQ(reference)	TDQ 50% fed	TMQ 50% fed
Quinone	0.98	0.82	0.88
Benzene	0.02	**0.18**	**0.12**

Occupancy of benzene increased
→ Impurities molecular seem to be introduced

- Extension along c axis

	c axis(Å)	Extension
Rb3TTQ	8.6575(14)	0%
TDQ 50%fed	8.7595(6)	**1.178%**
TMQ 50%fed	8.67300	0.179%

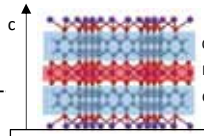

Inter layer force: Rb-O bond
Impurity doping → Rb-O bond decrease
→ c axis extension

High temperature EPR measurement

From curie's law
Intensity ∝ 1/T

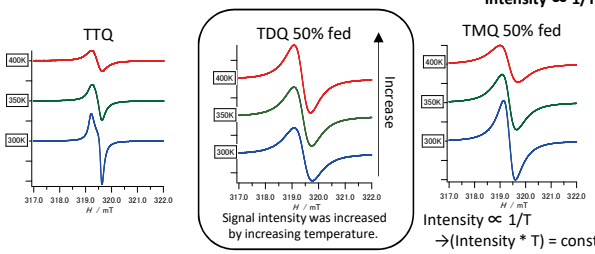

Signal intensity was increased by increasing temperature.

Intensity ∝ 1/T
→(Intensity * T) = const.

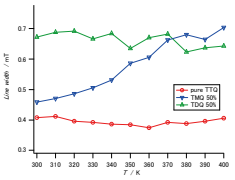

Line width change
→ spin environment change

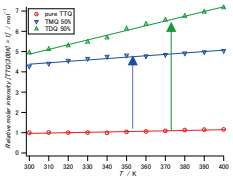

Molar (EPR intensity * T) increased
→Number of isolated spin increased
→Thermal activation

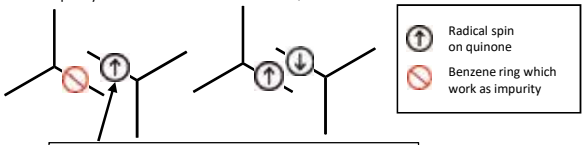

1. Isolated spin generated by addition of impurity
2. Weak interaction make thermal activation easier

Conclusion

- Honeycomb lattice by TTQ and impurity molecules were prepared by electrochemical method.
- Occupancy change of quinone and benzene moiety in mixed crystal was observed
- Extension of c axis around 1% was observed in crystal structure of TDQ 50% fed.
- Thermal excitation phenomena was observed at doped crystals.
- Determination of actual ratio of TTQ and TDQ or TMQ was failed. → Future work

Three-dimensional photoelectron momentum imaging of D_2 in circularly polarized intense laser fields

○T. Nakamura[1], M. Yamamoto[1], M. Fushitani[1], A. Hishikawa[1, 2]

[1]*Department of Chemistry, Nagoya University,* [2]*Reserch Center of Materials Science, Nagoya University*

Introduction

Chemical reaction ; Frontier orbital (FO) theory

"*frontier* electron plays a decisive role in chemical reaction" Fukui *et al., J. Chem. Phys.* **20**, 722 (1952)

Nitration of naphthalene

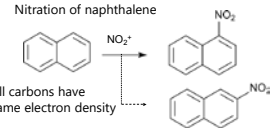

All carbons have same electron density

This selectivity can't be explained by electronic theory

Highest occupied molecular orbital (HOMO)
More large electron density: NO_2^+ attacks C1 site

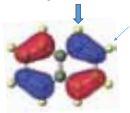

Imaging of molecular orbitals by tunneling ionization

Intense laser fields ~10^{14} W/cm^2 **Tunneling Ionization** refers to the shape of molecular orbital (MO)

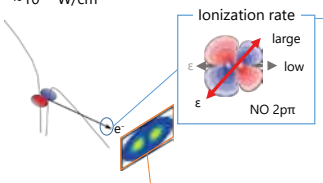

Fragmented ion

Ground state Alnaser *et al., Phys. Rev. Lett.* **93**, 163002 (2004).

Excited state Endo *et al., Phys. Rev. Lett.* **116**, 163002 (2016).

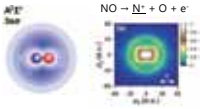

Photoelectron transverse momentum distribution (TMD)

Photoelectron image normal to pol. axis
two dimensional MO information

MFPAD: integral over TMD

HOMO Staudte *et al., Phys Rev. Lett.* **102**, 033004 (2009).

HOMO-1 Akagi *et al., Science* **325**, 1364 (2009).

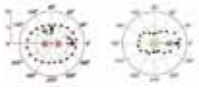

- Probing 3D shape of MO by measuring TMD
- ➢ More direct understanding of chemical reaction

This work

Probing electron dynamics by measuring 4π str photoelectron momentum

- **Construction of electron-ion three dimensional momentum imaging system**
- **Performance test with D_2 in intense circularly polarized UV laser fields**

Circularly polarized intense laser fields
Avoiding recollision process→conservation of initial information
Convenient rotation sweep of laser electric fields

Experiment

Electron-ion three dimensional momentum imaging system

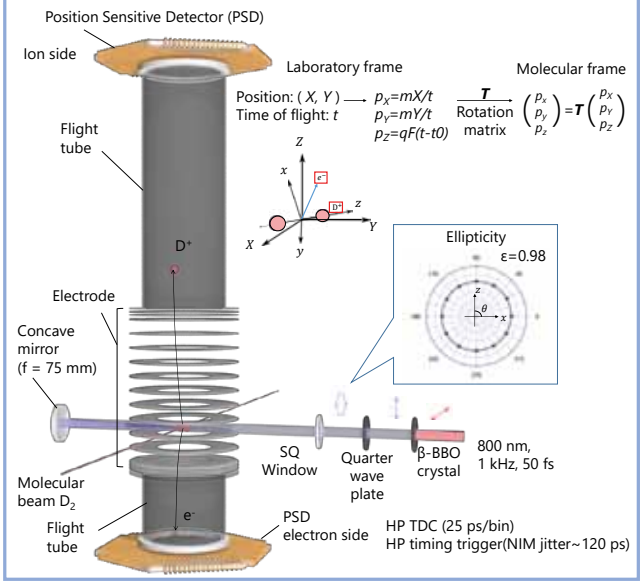

Results and Discussion

Molecular frame three-dimensional photoelectron momentum images

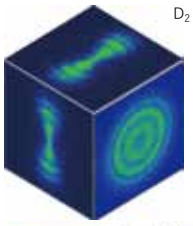

$D_2 \rightarrow D^+ + D + e^-$

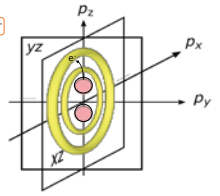

Concentric torus-like distributions

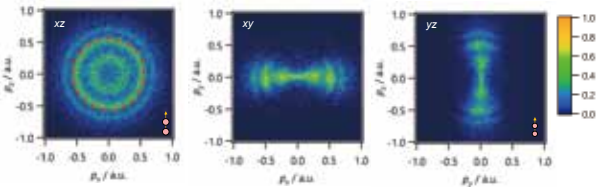

Red dashed line :p_0= 0.56 a.u.

Three-dimensional photoelectron imaging !

Molecular frame photoelectron angular distribution

Electron momentum spectrum

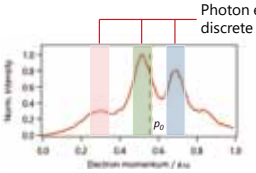

Photon energy discrete peaks → Above threshold ionization

Non-perturbative response
cf. $\Gamma^{(n)}=\sigma^{(n)}I^n$

$p_0=F/\omega$=0.56 a.u. for tunneling model
(position and velocity =0 at tunneling)

MFPAD

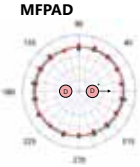

Circular distribution
UV laser fields
multiphoton regime
↕
Elliptical distribution
NIR laser fields
tunneling regime
Staudte *et al.*, PRL **102**, 033004 (2009).

Transverse momentum spectrum

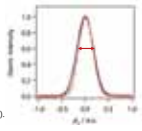

σ=0.217(2) a.u.
WFAT tunneling theory
$p(\boldsymbol{p}_\perp) \propto \exp(-\kappa p_\perp^2/F)$
$\rightarrow \sigma = 0.235$ a.u.
$\kappa=\sqrt{2I_0}$
F: laser electric fields
Tolstikhin *et al.*, PRA **84**, 053423 (2011).

Electron-ion coincidence imaging

(1)$D_2 \rightarrow D_2^+ + e^-$ (2)$D_2 \rightarrow D^+ + D + e^-$ (3)$D_2 \rightarrow D^+ + D^+ + 2e^-$

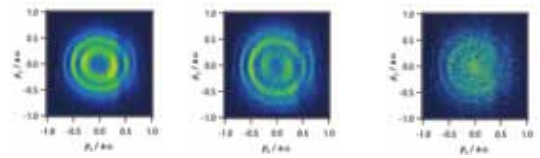

Ion momentum image

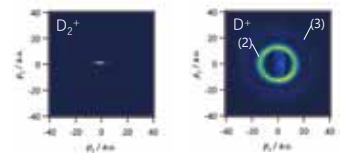

Kinetic energy release spectrum

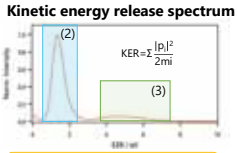

Labeling photoelectron

Summary

- ✓ Construction of three-dimensional momentum imaging system
- ✓ Observation of molecular frame photoelectron tori

D_2 —401 nm, 70 fs, 2.6×10^{14} W/cm^2, circ. pol.→
(1) $D_2^+ + e^-$ (Parent ion)
(2) $D^+ + D + e^-$ (Dissociative ionization)
(3) $D^+ + D^+ + 2e^-$ (Coulomb explosion)

Outlook：molecular orbital imaging

Synthesis of Cyclopropane Nucleoside Analogues

○Daichi Fushihara[1], Satoshi Shuto[2], Hiroshi Abe[1]

[1]Department of Chemistry, Nagoya University, Nagoya 464-8602, Japan
[2]Faculty of Pharmaceutical Sciences, Hokkaido University, Sapporo 060-0812, Japan

Nucleoside Analogues for Anti-virus Drug

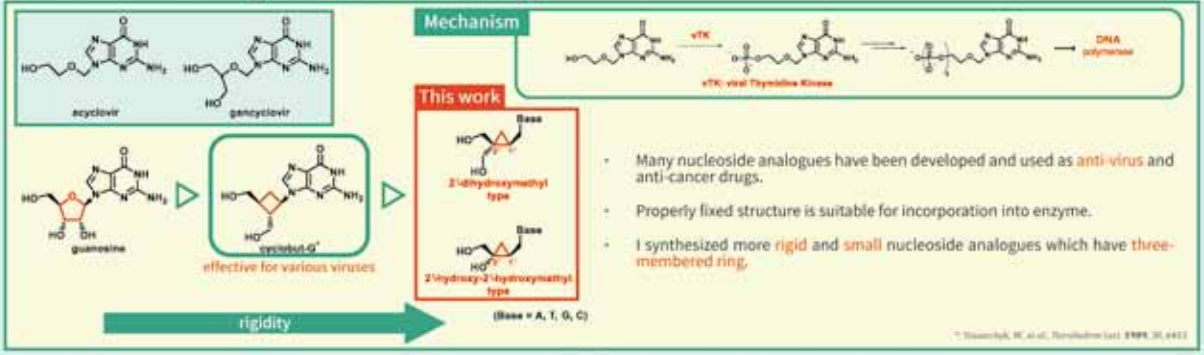

- Many nucleoside analogues have been developed and used as anti-virus and anti-cancer drugs.
- Properly fixed structure is suitable for incorporation into enzyme.
- I synthesized more rigid and small nucleoside analogues which have three-membered ring.

Conformer calculation

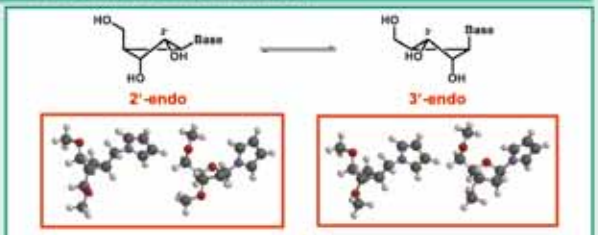

A nucleoside has two types of conformation (2'- and 3'-endo). Quantum chemical calculation (DFT/B3LYP/6-31G) showed that each of the designed compounds is fixed to a different conformation.

2'-Dihydroxymethyl Type

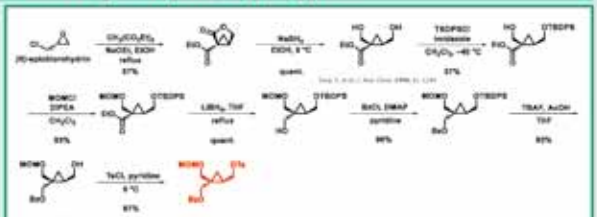

Selective introduction of adenine

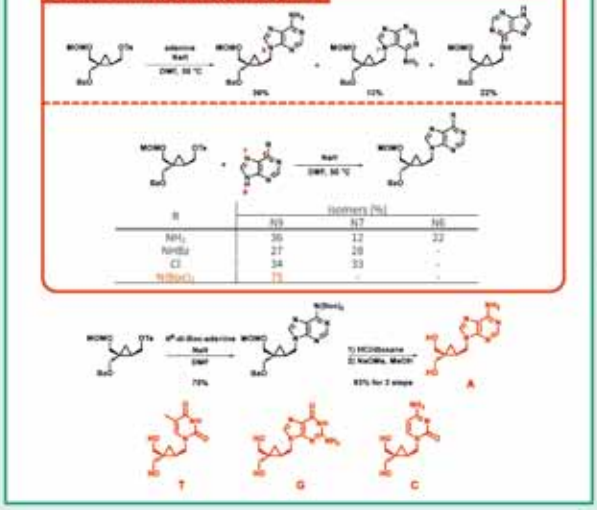

R	isomers (%) N9	N7	N6
NH_2	36	12	22
NHBu	27	28	-
Cl	34	33	-
$N(Boc)_2$	73	-	-

2'-Hydroxy-2'-hydroxymethyl Type

Dehomologation

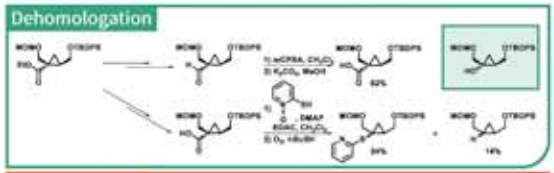

Dihydroxylation

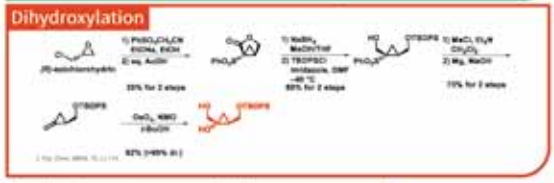

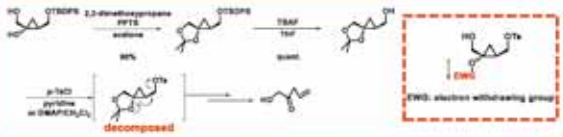

Stabilization of active intermediate

Summary

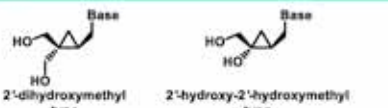

Anti-virus activity of these compounds is currently under investigation.

Development of Phosphorofluoridate Groups for Medicinal Chemistry

○Wataru Tanabe, Haruka Fujikawa, Yasuaki Kimura, Hiroshi Abe
Department of Chemistry, Graduate School of Science, Nagoya University

名古屋大学 NAGOYA UNIVERSITY

Introduction

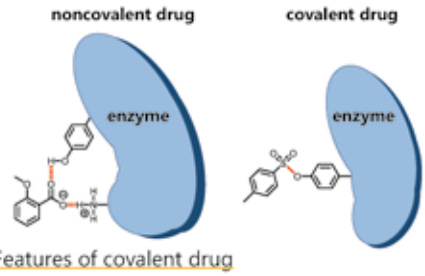

Features of covalent drug

- High potency ・Low dose ・Longer effect
- Side effects

Features of phosphorofluoridate

- Stable in the water
- Reactivity can be adjusted

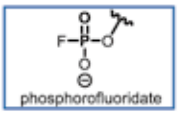

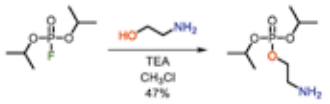

Features of Phosphodiesterfluoridate

- Not react with amino group
- Reacts with hydroxy groups

Can. J. Chem., **1966**, *45*, 495

Design

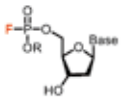

A nucleoside analog in which fluorine has been introduced into the phosphate moiety was designed.

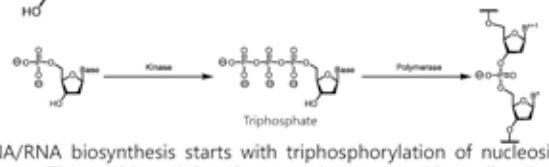

DNA/RNA biosynthesis starts with triphosphorylation of nucleosides by kinases. The resulting triphosphates are incorporated into oligo DNA/RNA by polymerases.

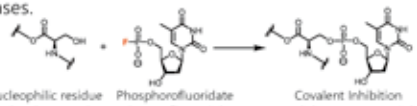

We expected that phosphorofluoridate would react with nucleophilic residues around the active pocket of the kinases.

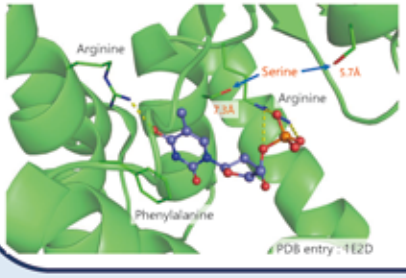

We confirmed that there are several nucleophilic residues around the active site of human TMP kinase and expected that the designed analogue would be effective as a covalent drug for kinases.

Experimental Results

1. Benzoyl Form Synthesis

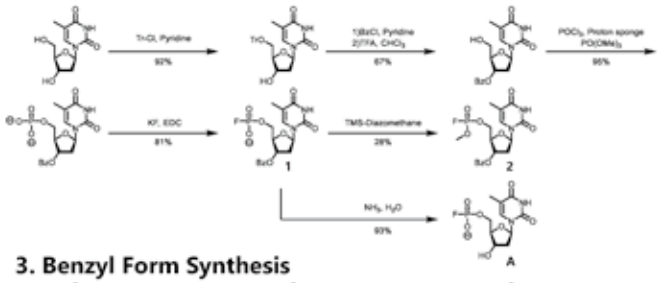

3. Benzyl Form Synthesis

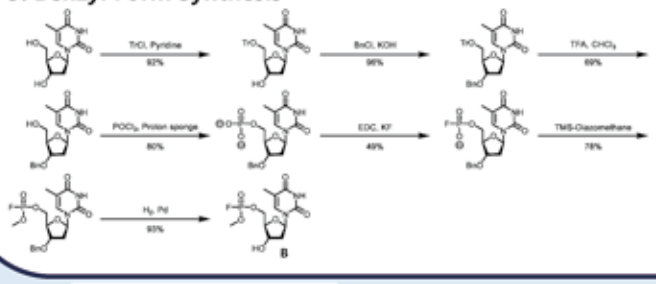

2. Reactivity of Phosphorofluoridate

Before measuring the activity to organisms, the tendency of chemical reactivity of phosphorofluoridate was investigated. The method was examined by dissolving compound **1** and **2** in methanol.

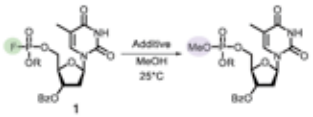

Entry	R	Additive	Time (h)	Yield (%)
1	K	none	72	0
2	H	none	5	25
3	H	CsF (1.5 eq)	72	4
4	H	HF･Py (1 eq)	72	9
5	H	BF_3･ Et_2O (1 eq)	5	47
6	Me	none	5	66
7	Me	BF_3･ Et_2O (1 eq)	5	76

It was found that the methyl form had higher reactivity.

Conclusion & Prospect

- Thymidine derivatives having a phosphorofluoridate group was synthesized.
- As a result of examining the reactivity of the compounds **1** and **2**, it was found that the reactivity of the methyl compound was higher.

- We are currently measuring anti-virus activity of compounds **A** and **B**.
- We will also examine the triphosphate form and the other nucleotide analogs different in nucleobases to identify the active compound.

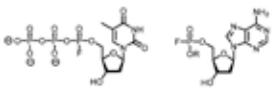

Synthesis and Evaluation of Covalent GST Inhibitors with Improved Cell Permeability

Haruka Fujikawa[1,2], Yuko Shishido[1,3], Yasuaki Kimura[1], Fumiaki Tomoike[1], Yuko Murakami-Tonami[4], Masahiro Aoki[2,5], Hiroshi Abe[1]

[1] Nagoya University, [2] Nagoya City University, [3] Hokkaido University, [4] Juntendo University , [5] Aichi Cancer Center

1. Introduction

GST : Glutathione *S*-transferase

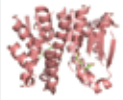

- Catalyze the conjugation of glutathione (GSH) to a wide variety of hydrophobic and electrophilic compounds in phase-II metabolism.
- Involved in detoxification of xenobiotics (Fig.1) and suppression of apoptosis, causing drug resistance and cell proliferation in cancer cells.

→GST inhibition is a promising approach to cancer.

- Since existing GST inhibitors are competitive inhibitors, high concentrations are required to obtain sufficient inhibitory activity.
- We have developed a covalent inhibitor GS-ESF which is expected to have potent inhibitory activity. (Fig. 2)
- A sulfonyl fluoride group was introduced as a reactive functional group for tyrosine, which is an active residue of GST, at the cysteine residue end of GSH.
- However, GS-ESF had poor cell membrane permeability. Therefore, in order to increase cell membrane permeability, covalent inhibitors based on small molecules were developed.

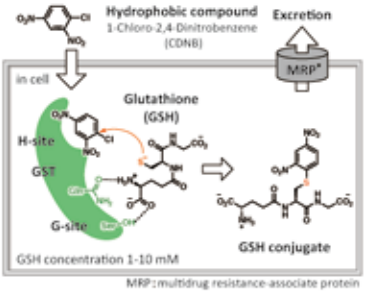

Fig. 1 Detoxification mechanism

Fig. 2
Novel GST inhibitor

Ref.) Chem. Commun., 2017, 53, 11138.

2. Inhibitor design

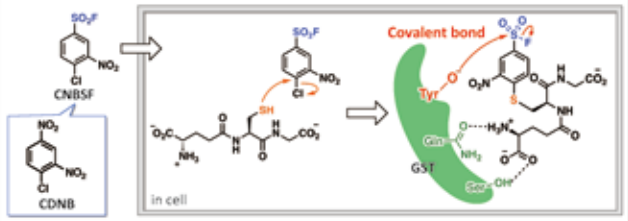

- We developed a covalent inhibitor based on CDNB.
- CNBSF reacts with GSH ***in cell*** to become GSH conjugate and occupys G-site. The sulfonyl fluoride group and tyrosine would form a covalent bond and inhibit GST activity.

3. Result of CDNB Derivative

IC_{50} assay

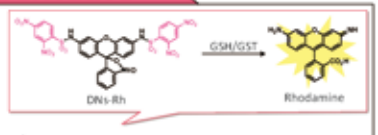

Inhibitor GST, GSH → Pre-incubation 37 °C → DNs-Rh → Fluorescence measurement Ex 490 nm, Em 520 nm

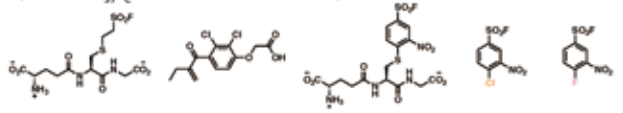

GS-ESF	Ethacrynic acid (EA)	GS-NBSF	CNBSF	FNBSF
IC_{50}= 12 μM	4.2 μM	68 μM	82 μM	98 μM

Reversibility assay

Inhibitor GST, GSH → Pre-incubation 37 °C, 2 h

- Non wash: Fluorescence measurement
- Washout: amicon ultra-0.5, 10K (Ultrafiltration) & washed x3 with phosphate buffer → Fluorescence measurement

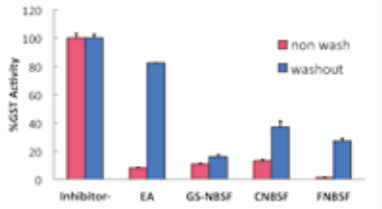

Intracellular GST inhibitory activity

Cell turbid solution → Inhibitor, Pre-incubation 37 °C, 15 min → DNs-Rh, Pre-incubation 37 °C, 1 h → FACS-Aria

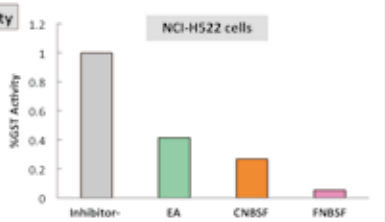

- The IC_{50} of the CDNB derivative was higher than that of EA and GS-ESF ***in vitro***. However, their GST inhibitory activity greatly exceeded that of ethacrynic acid in cell.
- Both CNBSF and FNBSF were suggested to be irreversible inhibitors.

4. Result of CNBSF Derivative

- Derivatized CNBSF for further improvement of GST inhibitory activity.

IC_{50} assay

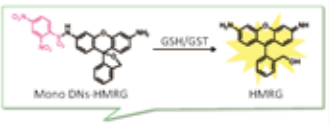

Inhibitor GST, GSH → Pre-incubation 37°C → Mono DNs-HMRG → Fluorescence measurement Ex 490 nm, Em 520 nm

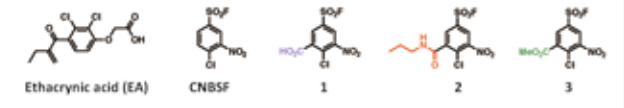

Ethacrynic acid (EA)	CNBSF	1	2	3
IC_{50}= 2.5 μM	132 μM	123 μM	25 μM	43 μM

Reversibility assay

Inhibitor GST, GSH → Pre-incubation 37°C, 1h

- Non wash: Fluorescence measurement
- Washout: amicon ultra-0.5, 10K (Ultrafiltration) & washed x3 with phosphate buffer → Fluorescence measurement

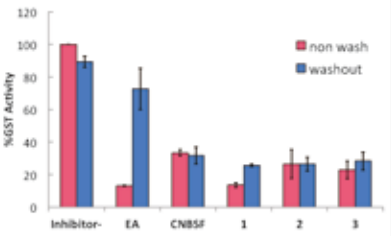

Cytocidal activity

Cell → Inhibitor, 37 °C, 24 h → MTT assay

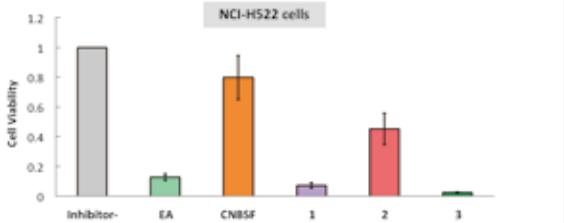

- The IC_{50} of compounds 2, 3 significantly exceeded that of CNBSF ***in vitro***. It was also suggested that they were irreversible inhibitors.
- The cytocidal activity of compounds 1, 3 in cancer cells exceeded that of EA.

5. Conclusion

- We have developed small molecule based covalent inhibitor. Since the membrane permeability was improved, the inhibitory activity in cells was improved.
- The cytocidal activity of the CNBSF derivative exceeded that of EA. And it was suggested that all compounds were irreversible inhibitors.

Synthesis of Doped Reduced Graphene Oxide and application to batteries

Tsukasa Inoue, Haruka Omachi[1], Hirofumi Yoshikawa[2], Ryo Kitaura[1], Yusuke Nakanishi[1] and Hisanori Shinohara[1]

[1]Department of Chemistry and Institute for Advanced Research, Nagoya University, Nagoya, 464-8602, Japan
[2]School of Science and technology, Kwansei Gakuin University, Sanda, 669-1337, Japan

Background

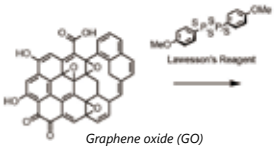

Liu et al., **J. Mater. Chem. C**, (2013)

Lawesson's Reagent can reduce GO and dope hetero atoms into graphene from GO

✓Graphene is for coordination material

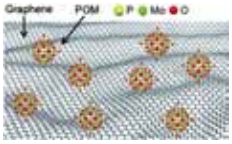

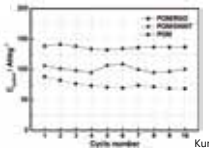

Kume et al., **J. Mater. Chem. A.** (2014)

Polyoxometalate(POM) and graphene (reduced graphene oxide ; rGO) performs as energy storage

✓Graphene is battery active material

My work

- Measuring performance of POM/Doped GO hybrid material
- Determine how to synthesize the best Doped GO for an energy storage

Experience

doped GO synthesis

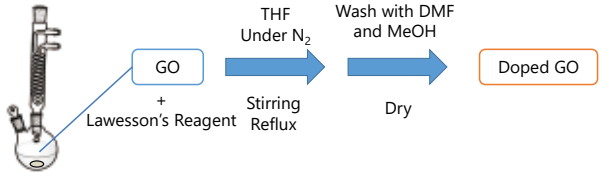

POM/GO nanohybrid materials preparation

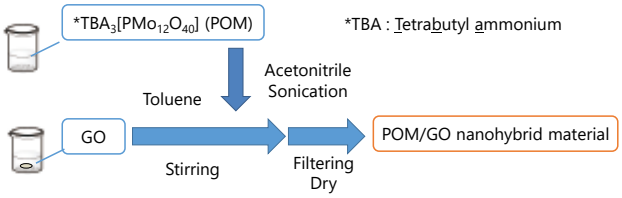

GO analysis

X-ray photoelectron spectroscopy

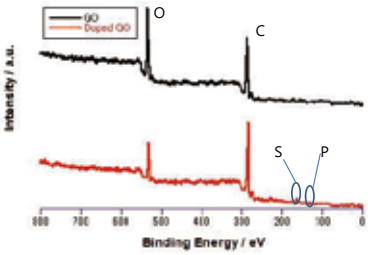

	Atomic conc. / %			
	C	O	P	S
GO	74	26		
Doped GO	79	16	2	3

✓ GO was reduced
✓ Sulfur and phosphorus doped GO was synthesized

Nanohybrid Material observation

TEM image

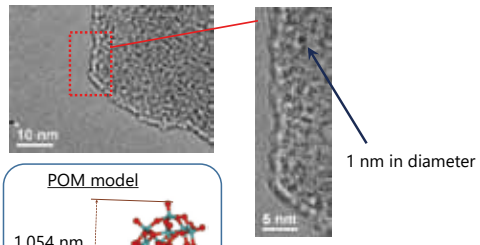

POM model

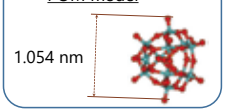

EDX analysis

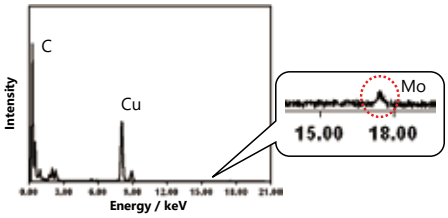

✓ POM molecules were on the surface of doped GO

Cycle performance measurement

Initial capacity

POM	260
rGO	66
Doped GO	60

(mAhg^{-1})

Battery coin cell preparation

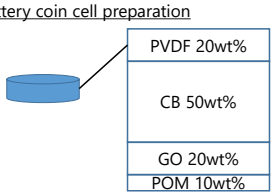

Comparison of Doped GO and rGO

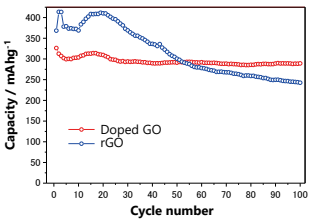

	Doped GO/POM	rGO/POM
Initial capacity	326	368
After 100 cycle	289	242

(mAhg^{-1})

✓ Stable battery capacity was gained by S and P doped GO/POM nanohybrid material

Future plan

➢Optimize battery performance by how synthesize Doped GO another way

Semiconducting Carbon Nanotubes Extraction by Aqueous-Two Phase (ATP) System and Thin-Film-Transistor Application

Kazuki Ueno[1], Haruka Omachi[1,2], Tomohiko Komuro[1], Jun Hirotani[3], Yutaka Ohno[3,4], and Hisanori Shinohara[1,5]

[1] Graduate School of Science, [2] Research Center for Materials Science, [3] Graduate School of Engineering, [4] Institute of Materials and Systems for Sustainability, and [5] Institute for Advanced Research, Nagoya University, Nagoya Japan

E-mail: omachi@chem.nagoya-u.ac.jp, noris@nagoya-u.jp

Background

Single-Wall Carbon Nanotubes (SWCNTs)

✓ Durable and flexible ✓ High carrier mobility

Promising materials for electric devices

Metallic(m-) and Semiconducting(s-) due to chirality

s-SWCNT thin film transistor (s-SWCNT TFT)

Require separation from m-SWCNT

Conventional Method :

Gel Filtration[1]

Density Gradient Ultracentrifugation[2]

[1] T. Tanaka *et al.*, *Appl. Phys. Express*, 2, 125002 (2009).
[2] M. S. Arnold *et al.*, *Nature. Nanotech.*, 1, 60 (2006).

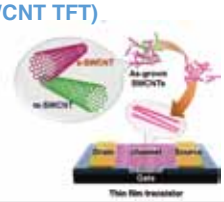

Aqueous-Two Phase (ATP) System

Method

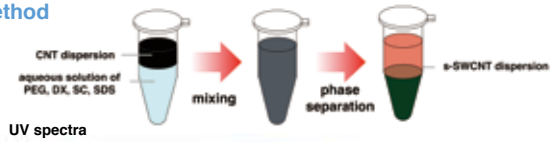

UV spectra

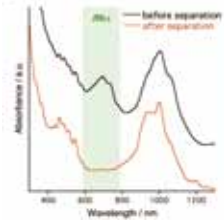

✓ High purity

High reproducibility

✓ Easy to scale up

Large scale extraction

✓ Fast process

Accomplish within 30 min

Separated s-SWCNT thin film

AFM image

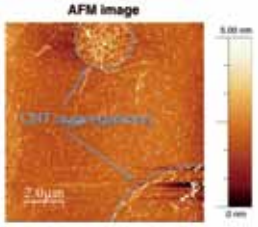

Crown ether type complex

Z.-Z. Huang *et al.*, *J. Org. Chem.*, 67, 3095 (2016).

Polymer-Surfactant Interaction

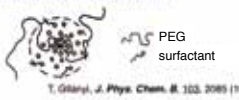

T. Gilányi, *J. Phys. Chem. B*, 103, 2085 (1999).

TFT performance with separated s-SWCNT

Transfer characteristics

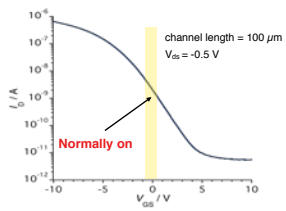

XPS spectra

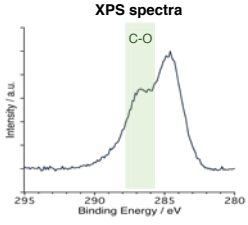

High performance, but normally-on state due to p-type doping by PEG

TFT performance will be improved by elimination of PEG

PEG removal treatment

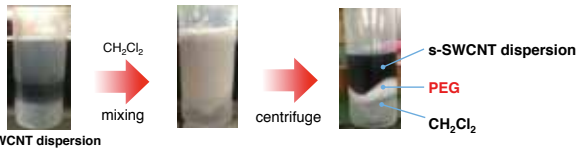

^{1}HNMR spectra (CD_3CN)

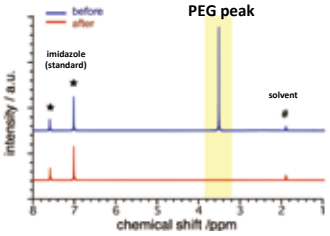

PEG-CH_2Cl_2 interaction

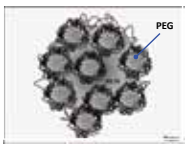

Form emulsion → Rapid precipitation

A. M. Fréon *et al.*, ***Eur. J. Pharm. Biopharm.***, 73, 66-73 (2009).

>99% of PEG was removed

TFT fabrication

Fabrication Steps

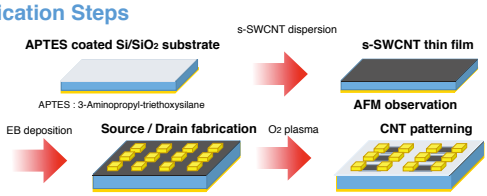

s-SWCNT thin film

AFM image

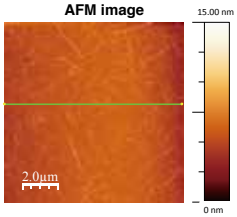

Height profile

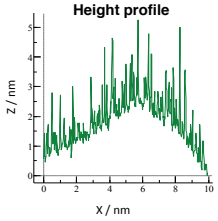

Uniform 1–2 thin layer film

TFT characterization

Transfer characteristics

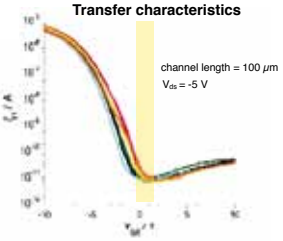

Output characteristics

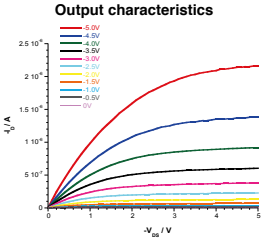

High on/off ratio >10^5 with normally-off state

Summary

High purity s-SWCNT was obtained by ATP system

Rapid and efficient removal of PEG was demonstrated

High performance with normally-off state was achieved

Reduction of "Heavy Benzenes"

Yoshiyuki Mizuhata, Shiori Fujimori, Shingo Tsuji, and Norihiro Tokitoh*
Institute for Chemical Research, Kyoto University, Gokasho, Uji, Kyoto 611-0011, Japan
mizu@boc.kuicr.kyoto-u.ac.jp

Introduction

Germabenzenes

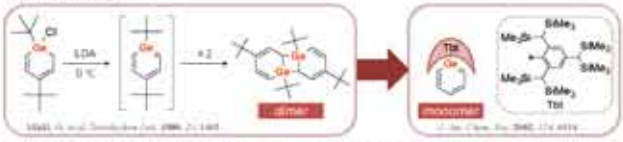

A kinetic stabilization by a bulky aryl group, Tbt, has been recognized to be efficient to stabilize germabenzene.

This Work

Mizuhata, Y., Fujimori, S., Sasamori, T., & Tokitoh, N.
"Germabenzenylpotassium: A Germanium Analogue of a Phenyl Anion"
Angewandte Chemie International Edition, 56(16), 4588–4593 (2017).
https://doi.org/10.1002/anie.201700801

Germabenzenylpotassium

Synthesis

yellow crystals, m.p. 315°C (dec.)
Anal. Calcd for $C_{24}H_{39}GeK$: C, 66.41; H, 9.05.
Found: C, 66.56; H, 9.75.

Supported by
-structural features -NMR electronic spectra- theoretical calculations

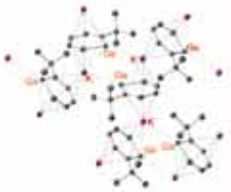

Thermal ellipsoid plot (50% probability)
Hydrogen atoms were omitted for clarity.

Selected Bond Lengths (Å), Angles (deg), and Sums of the Interior Angles (deg)

About germabenzenylpotassium ...

Complexation

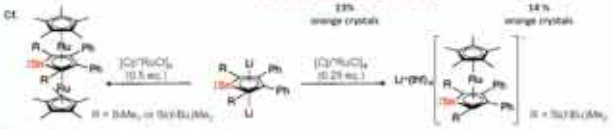

Structures

Ruthenium-substituted Germabenzene

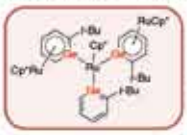

Thermal ellipsoid plot (50% probability)
Hydrogen atoms were omitted for clarity.

Selected Bond Lengths (Å), Angles (deg), and Sums of the Interior Angles (deg)

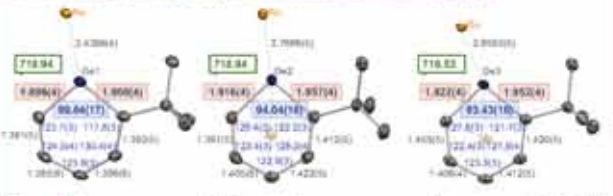

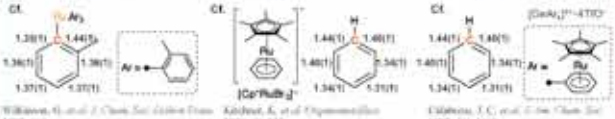

Complex A

Thermal ellipsoid plot (50% probability)
Hydrogen atoms were omitted for clarity.

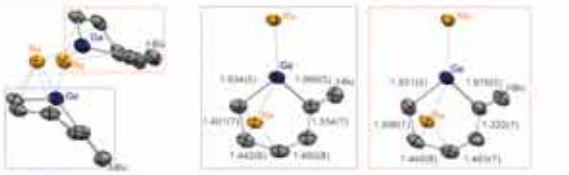

Germabenzenyllithium and sodium

Synthesis

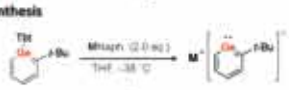

	yield	solubility
M = Na	66%	insoluble in hexane
M = Li	Not identified	soluble in hexane

Selected Bond Lengths (Å), Angles (deg), and Sums of the Interior Angles (deg)

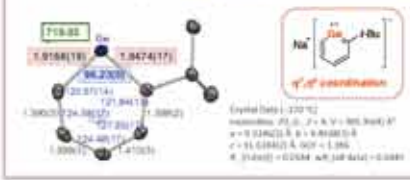

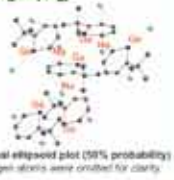

Thermal ellipsoid plot (50% probability)
Hydrogen atoms were omitted for clarity.

Reactivity of Germabenzenylpotasium

Summary

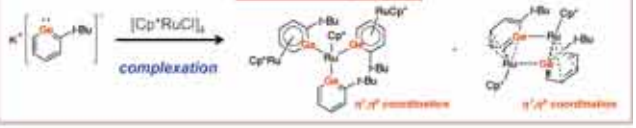

Acknowledgements

This work was supported by Grant-in-Aid for Scientific Research on Innovative Areas (No. 24109012), Scientific Research (S) (No. 26220802), Scientific Research (C) (No. 24550048), from the Ministry of Education, Culture, Sport, Science and Technology of Japan. S. T. thanks Research Fellowships of the Japan Society for the Promotion of Science for Young Scientists.

Synthesis and Properties of Endohedral C_{70} Co-Encapsulating HF and H_2O Molecules

Rui Zhang, Michihisa Murata, Atsushi Wakamiya, Yasujiro Murata

Institute for Chemical Research, Kyoto University, Uji, Kyoto 611-0011

Introduction

Inner Space of C_{60} and C_{70}

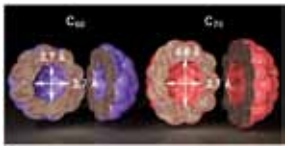

Doubly Encapsulating Fullerene C_{70}

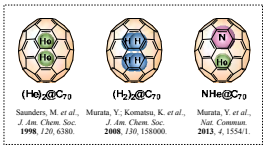

Previous Work

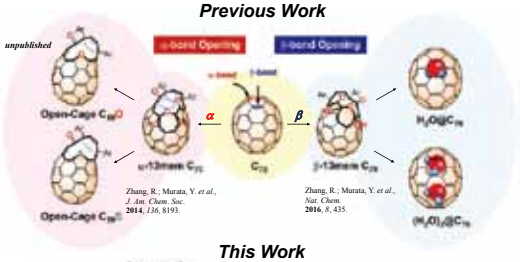

Synthesis of Endohedralfullerene ~Molecular Surgery Methods~

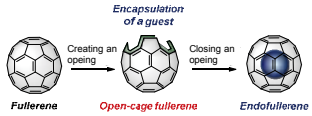

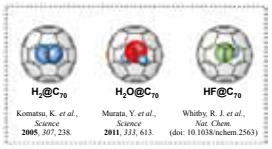

This Work

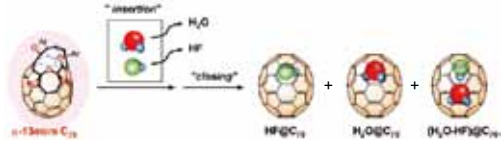

Results and Discussion

HF & H_2O Insertion

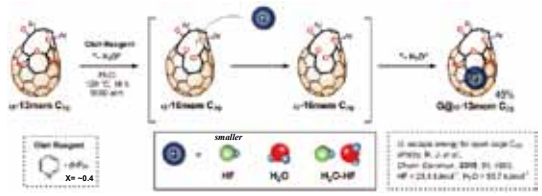

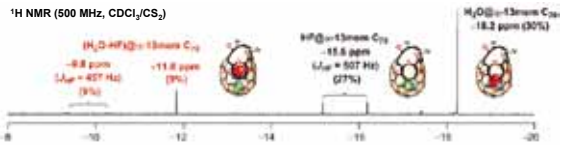

Insertion Mechanism of HF & H_2O (Push-and-Pull Strategy)

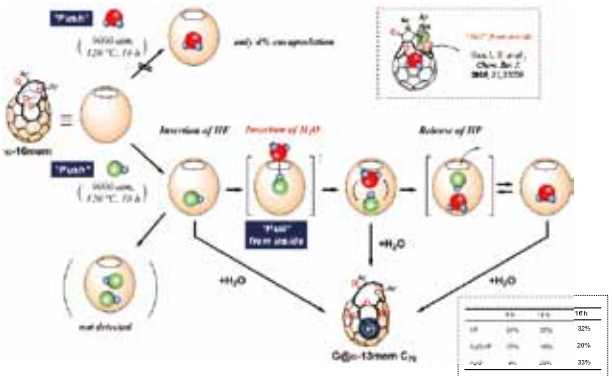

Restoration of an Opening

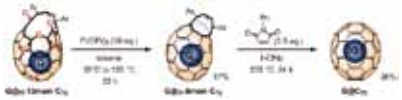

Estimated ratio[a]	Encapsulation ratio[a]	Estimated ratio[b]
Empty C_{70} : 34%	Empty C_{70} : 31%	Empty C_{70} : 43%
HF@C_{70} : 32%	HF@C_{70} : 34%	HF@C_{70} } 51% (mixture)
H_2O@C_{70} : 25%	H_2O@C_{70} : 27%	H_2O@C_{70} }
(H_2O-HF)@C_{70} : 9%	(H_2O-HF)@C_{70} : 8%	(H_2O-HF)@C_{70} : 6%

a) estimated by ^{1}H NMR. b) estimated by HPLC.

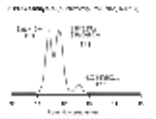

Almost no escape !

X-Ray Structure of (H_2O-HF)@C_{70}

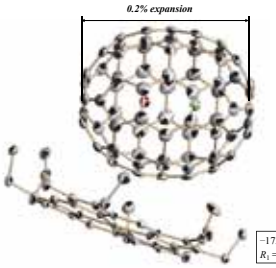

Encapsulated H_2O-HF Complex (X-ray)

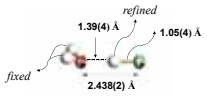

Free H_2O-HF Complex (calculated)

MP2/6-311++G(3df, 3pd)

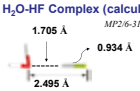

−173 °C, Triclinic, *P-1*
$R_1 = 0.0370$, $wR_2 = 0.1015$

NMR Measurements of HF@C_{70} & H_2O@C_{70} & (H_2O-HF)@C_{70}

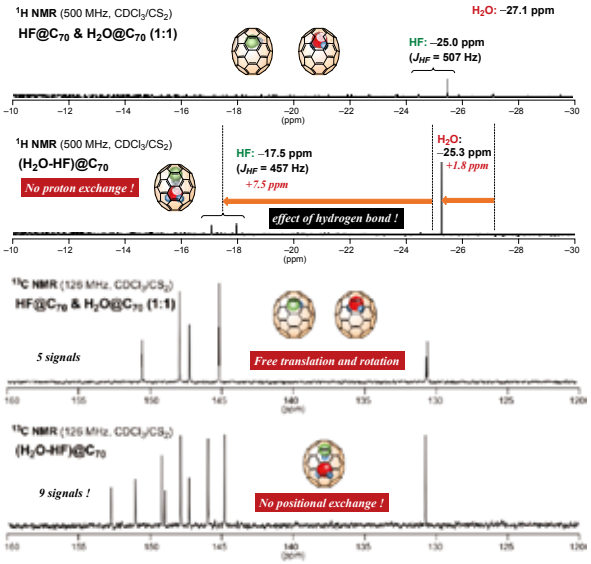

Summary

1. Push-and-Pull strategy resulted in the formation of (H_2O-HF)@C_{70} in high yield.
2. HF@C_{70} and H_2O@C_{70} were also obtained.
3. Single hydrogen bond is formed between HF and H_2O in the C_{70} cage without proton transfer even at 140 °C.
4. The position of encapsulated H_2O-HF complex is fixed in the C_{70}.

Fabrication of Sn-Based Perovskite Solar Cells Using Solvent-Coordinated SnX_2 Complexes as Key Precursors

([1]Institute for Chemical Research, Kyoto University, [2]Department of Applied Chemistry, Graduate School of Engineering, Osaka University)

○Masashi Ozaki,[1] Jiewei Liu,[1] Yukie Katsuki,[1] Taketo Handa,[1] Ryosuke Nishikubo,[2] Shinya Yakumaru,[1] Yoshifumi Hashikawa,[1] Yasujiro Murata,[1] Takashi Saito,[1] Yuichi Shimakawa,[1] Yoshihiko Kanemitsu,[1] Akinori Saeki,[2] Atsushi Wakamiya[1,*]

Introduction

❖ Pb-Based Perovskite Solar Cells (Pb-PSCs)

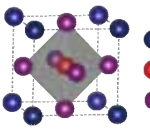

$CH_3NH_3PbI_3$ ($MAPbI_3$)

- ✓ Wide range absorption
- ✓ Solution processability
- ✓ High efficiency (~22.7%)
- × High toxicity

T. Miyasaka. et al., *J. Am. Chem. Soc.* **2009**, *131*, 6050.
M. Grätzel, N. G. Park, et al., *Sci. Rep.* **2012**, *2*, 591.
H. J. Snaith, et al. *Science* **2012**, *338*, 643.
E. K. Kim, J. H. Noh, S. I. Seok, et al. *Science* **2017**, *356*, 1376.

❖ Sn-Based Perovskite Solar Cells (Sn-PSCs)

82 **Pb** Lead → **$MAPbI_3$**

replace

50 **Sn** Tin → **$MASnI_3$**

- ✓ Environmentally friendly
- × Low efficiency (~9.0%)
- × Low stability ($Sn^{2+} \rightarrow Sn^{4+}$)

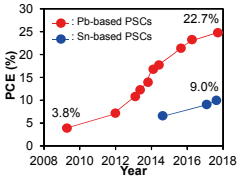

H. J. Snaith, et al., *Energy Environ. Sci.* **2014**, *7*, 3061.
M. A. Loi et al., *Adv. Energy Mater.* **2017**, 1702019.

❖ Purification of SnI_2

commercially available SnI_2 (99.9%, trace metals basis) → sublimed SnI_2

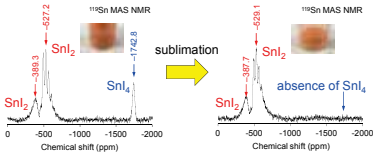

M. Ozaki, Y. Murata, A. Wakamiya, et al., *ACS Omega* **2017**, *2*, 7016.

❖ High PCE Sn-PSCs

8.1% PCE in inverted structure

Z. Liu and Z. Bian et al., *Adv. Sci.* **2017**, 1700204.

This work

- ❖ Further Purification of SnI_2 by Complexation
- ❖ Examination of Inherent Electronic Structures of $MASnI_3$ and $FASnI_3$
- ❖ Optimization of Fabrication Method for Sn-PSCs

Results and Discussion

❖ Isolation of $[SnX_2(S)_n]$ Complexes (S = DMF and DMSO)

Single-crystal X-ray Structures

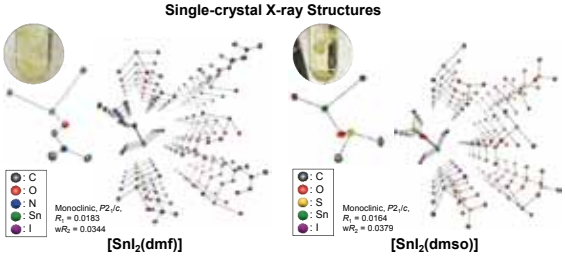

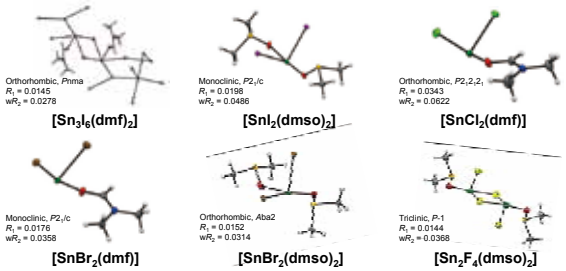

A series of $[SnX_2(S)_n]$ were developed as purified materials.

❖ Fabrication of $MASnI_3$ and $FASnI_3$ with $[SnI_2(dmf)]$

X-Ray Diffraction Patterns

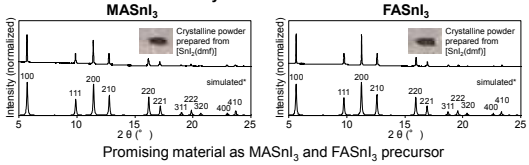

Promising material as $MASnI_3$ and $FASnI_3$ precursor

* M. G. Kanatzidis, et al., *Inorg. Chem.* **2013**, *52*, 9019.

❖ PYS, PL and Absorption Spectra of $MASnI_3$ and $FASnI_3$

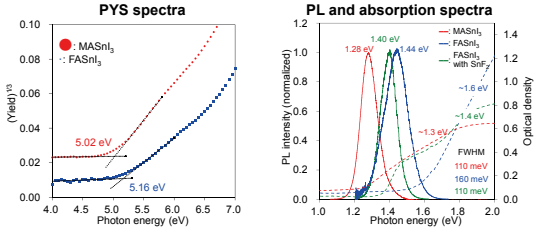

❖ Energy Level Diagram

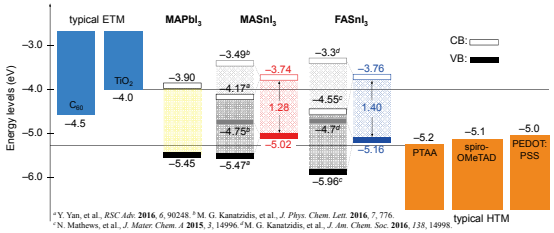

[a] Y. Yan, et al., *RSC Adv.* **2016**, *6*, 90248. [b] M. G. Kanatzidis, et al., *J. Phys. Chem. Lett.* **2016**, *7*, 776.
[c] N. Mathews, et al., *J. Mater. Chem. A* **2015**, *3*, 14996. [d] M. G. Kanatzidis, et al., *J. Am. Chem. Soc.* **2016**, *138*, 14998.

VBs of $MASnI_3$ and $FASnI_3$ are significantly higher than those of $MAPbI_3$ or typical HTM.

❖ Verification of the Reported Method

ref.) Z. Liu and Z. Bian et al., *Adv. Sci.* **2017**, 1700204.

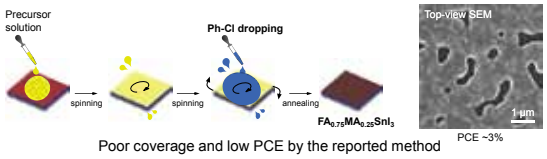

PCE ~3%

Poor coverage and low PCE by the reported method

❖ Impact of Ph-Cl Temperature

Top-View SEM Images

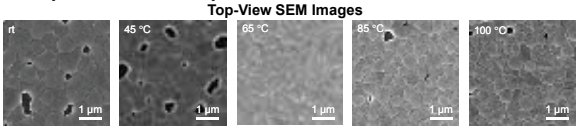

J–V Curves

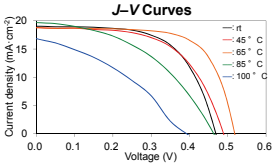

Photovoltaic Parameters

	J_{SC} (mA·cm^{-2})	V_{OC} (V)	FF	PCE (%)
rt	19.04	0.47	0.62	**5.50**
45 °C	18.80	0.49	0.59	**5.40**
65 °C	18.77	0.51	0.69	**6.62**
85 °C	19.68	0.46	0.45	**4.10**
100 °C	16.85	0.39	0.36	**2.35**

❖ Best Performance

J–V Curves

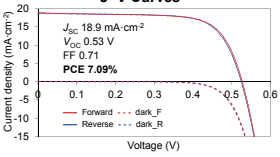

IQE, EQE, Reflectance Spectra

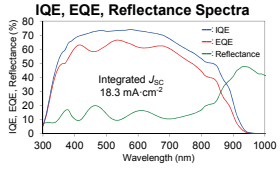

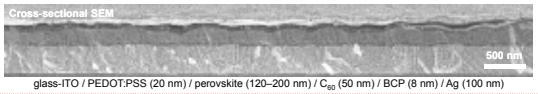

glass-ITO / PEDOT:PSS (20 nm) / perovskite (120–200 nm) / C_{60} (50 nm) / BCP (8 nm) / Ag (100 nm)

Summary

❖ Development of $[SnX_2(S)_n]$ Complexes as Purified Tin Halide Materials

❖ Improvement of Coverage with Hot Ph-Cl Dropping

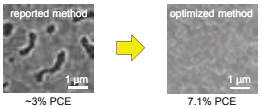

~3% PCE → 7.1% PCE

Acknowledgement

・SEM Images (Kyoto Univ.) by Prof. Toshiharu Teranishi, Prof. Masanori Sakamoto, Dr. Ryota Sato, and Dr. Tokuhisa Kawawaki

・Partially Supported by **ALCA**

Naphthalene Diimide-Based Electron-Transporting Layer for Planer Perovskite Solar Cells

(*Institute for Chemical Research, Kyoto Univ.*)
○Tomoya Nakamura, Nobutaka Shioya, Takafumi Shimoaka, Takeshi Hasegawa, Yasujiro Murata, Atsushi Wakamiya

Introduction

Molecular Orientation in Organic Electronics

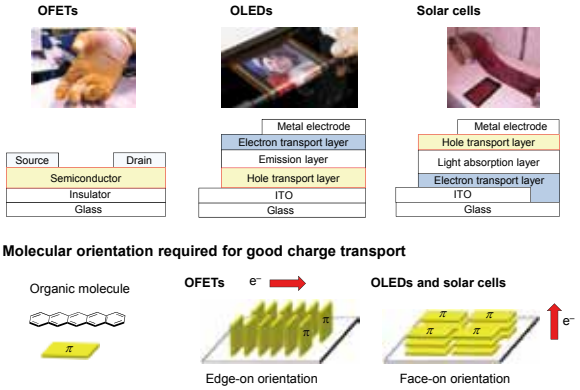

Electron Transport Layer for Perovskite Solar Cells

Previous work: TiOx as electron transport layer

× Need of sintering at high temperature (500 °C)
➔unsuitable for mass production and film application

ref. Wakamiya, A.; Saeki, A.; Scott, L. T. et al. *J. Am. Chem. Soc.* **2015**, *137*, 15656.

This work: Naphthalene diimide (NDI)-based electron transport layer

✓ High electron-accepting ability
✓ Transparency (absorption < 400 nm)

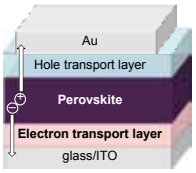

NDI-C6 (R = alkyl)

Edge-on orientation
In-plane mobility (OFET)
μ = 0.7 cm^2 V^{-1} s^{-1}

NDI-H (R = H)

Face-on orientation ??
Sheet-like structure:
Intermolecular N–H···O hydrogen bonds
Out-of-plane mobility (OLED & solar cells)

R = alkyl ➔ H

??

ref. Shukla, D. et al. *Chem. Mater.* **2008**, *20*, 7486–7491.

Results and Discussion

Molecular Orientation Analysis

p-Polarized multiple-angle incidence resolution spectrometry (pMAIRS)

NDI-C6 (R = alkyl) on Si

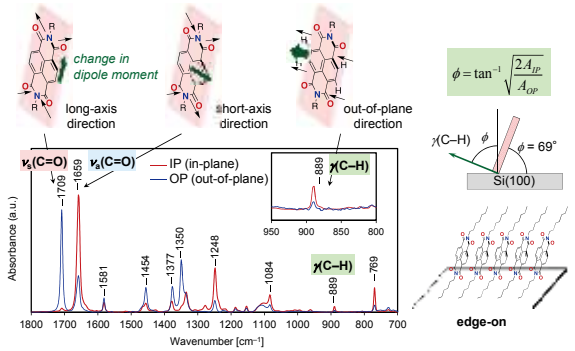

NDI-H (R = H) on Si

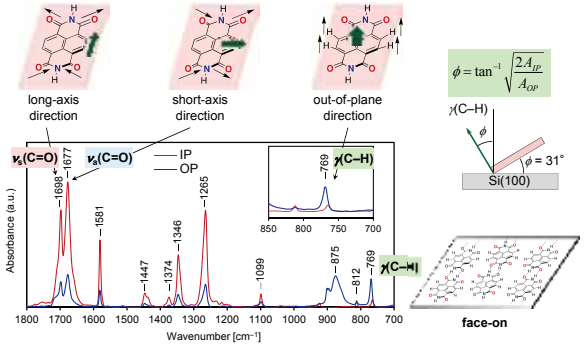

Two-dimensional grazing incidence X-ray diffraction (2D-GIXD)

Dr. T. Koganezawa (JASRI, Spring-8 BL19B2)

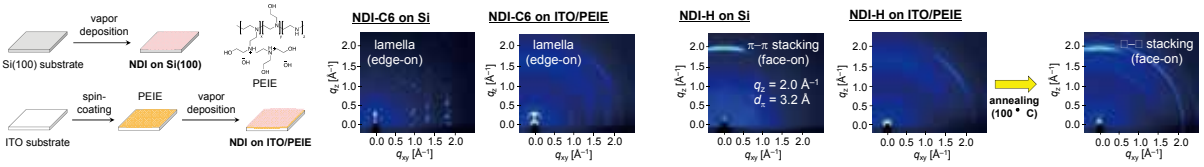

HOMO & LUMO Energy levels

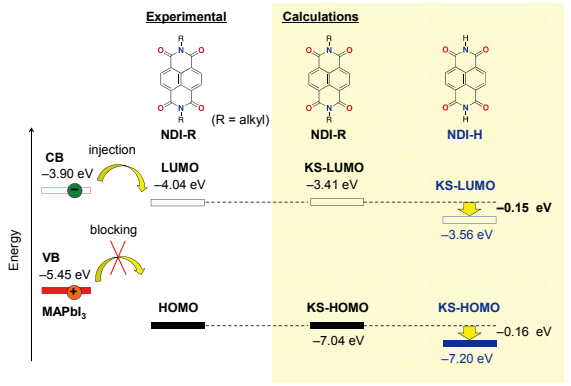

Applications to Perovskite Solar Cells

SEM image

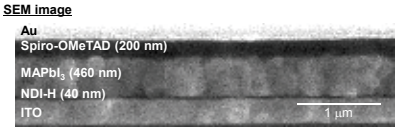

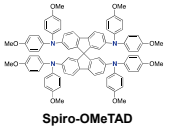

***J-V* characteristics**

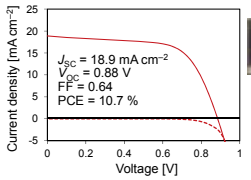

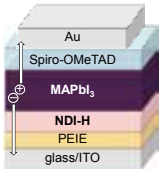

Acknowledgement

This work was partially supported by the Center of Innovation Program (COI) and Advanced Low Carbon Technology Research and Development Program (ALCA) from Japan Science and Technology Agency (JST).

Highly Selective Direct Arylation Polymerization of Bithiophene Derivatives

Masayuki Wakioka, Hazuki Morita, Natsumi Yamashita, Nobuko Ichihara, and Fumiyuki Ozawa

International Research Center for Elements Science, Institute for Chemical Research, Kyoto University, Uji, Kyoto 611-0011

1. Introduction

Synthetic Routes to DA Polymers

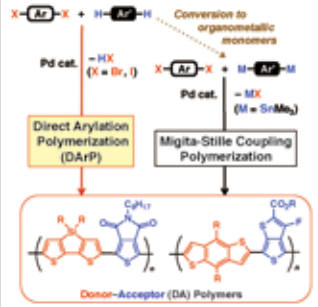

✔ *DArP realizes shortcut synthesis of DA polymers with reduced waste generation.*

Reviews on DArP: Ledux *et al.*, *Chem. Rev.* **2016**, *116*, 14225.

Problem of DArP: Insolubilization

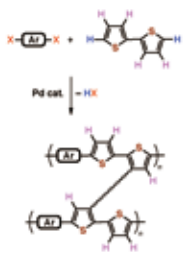

✔ *Direct arylation at undesirable C-H positions*

➡ *Branching & cross-linking*

➡ *Insoluble materials*

Kanbara *et al.*, *ACS Macro Lett.* **2012**, *1*, 67.

2. Previous Work

Highly Efficient Catalyst for DArP

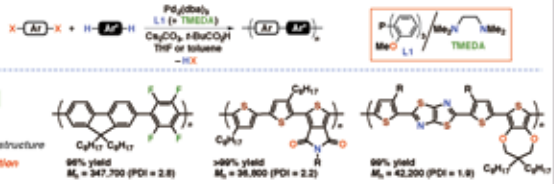

L1 only

✔ *High M_n*
✔ *Controlled structure*
✔ *Faster reaction*

96% yield, M_n = 347,700 (PDI = 2.8)

>99% yield, M_n = 86,800 (PDI = 2.2)

99% yield, M_n = 42,200 (PDI = 1.9)

L1 + TMEDA
Mixed-ligand catalyst

✔ *High M_n*
✔ *Controlled structure*
✔ *No insoluble material*
✔ *Slower reaction*

88% yield, M_n = 20,000 (PDI = 3.3)

>99% yield, M_n = 24,600 (PDI = 2.4)

reduction of C–X bonds → homocoupling → branching & cross-linking

(w/o TMEDA: homocoupling & insolubilization) *TMEDA prevents the reduction of C-X bonds*

Wakioka, Ozawa *et al.*, *Macromolecules* **2013**, *46*, 370; *Macromolecules* **2014**, *47*, 626; *Macromolecules* **2015**, *47*, 8382; *Macromolecules* **2015**, *48*, 2989; *Macromolecules* **2016**, *49*, 3310; *Macromolecules* **2017**, *50*, 927.

3. This Work

DArP of Dithienylethene and Bithiophene

✔ *Proper use of two catalytic systems*
✔ *High M_n & well-controlled structures*

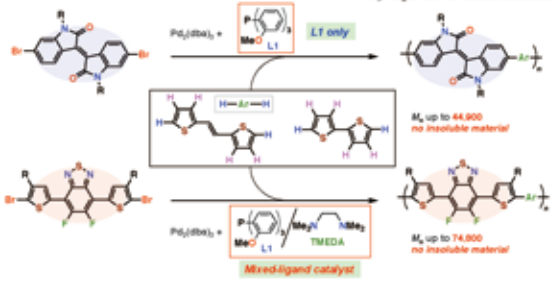

4. Effects of Dibromides

entry	M-H	time	insoluble materials[a]	yield[a]	M_n (PDI)[a]	homo coupling[d]	IID-Br end[d]	IID-H end[d]
1		24 h	0%	>99% [63%][c]	22,700 (4.3) [44,900 (2.2)][c]	0.8% ——	14% ——	11% ——
2		18 h	0%	>99%	21,400 (2.8)	——	——	——

[a] Isolated yield after Soxhlet extraction with acetone, hexane, and *o*-$C_6H_4Cl_2$. [b] GPC (PS†, 140 °C, *o*-$C_6H_4Cl_2$). [c] ^{1}H NMR (600 MHz, 130 °C, $C_6D_2Cl_4$). [d] Isolated yield after Soxhlet extraction with $CHCl_3$ and *o*-$C_6H_4Cl_2$.

reduction of C–Br bonds → homocoupling → branching cross-linking

✔ *The reduction of C–Br bonds hardly occurred.*

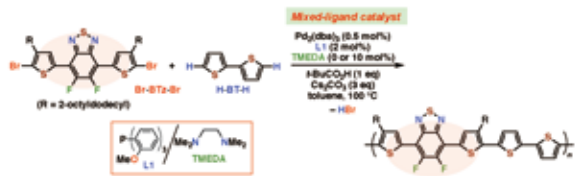

entry	time	coligands	insoluble materials[a]	yield[a]	M_n (PDI)[a]	homo coupling[d]	BTz-Br end[d]	BTz-H end[d]
1	24 h	——	31%	69%	52,200 (3.1)	1.5%	0%	63%
2	72 h	TMEDA	0%	>99% [99%][c]	50,500 (3.7) [74,800 (2.7)][c]	1.0% ——	14% ——	50% ——

[a] Isolated yield after Soxhlet extraction with acetone and PhCl. [b] GPC (PS†, 140 °C, *o*-$C_6H_4Cl_2$). [c] ^{1}H NMR (600 MHz, 130 °C, $C_6D_2Cl_4$). [d] Isolated yield after Soxhlet extraction with $CHCl_3$ and PhCl.

reduction of C–Br bonds → homocoupling → branching cross-linking

✔ *TMEDA prevents the reduction of C–Br bonds.*

5. Structural Analysis

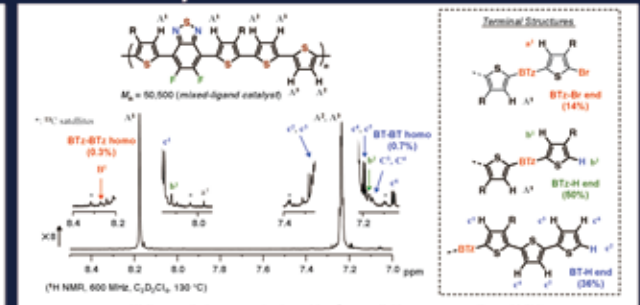

✔ *Well-controlled structure (no branching & cross-linking, cross-coupling = 99.0%)*

6. DArP vs. Migita-Stille Coupling Polymerization

Optical Properties

entry	Polymer	Polymerization	M_n [PDI]	λ_{max} (nm)[a]	E_g (eV)[a]	HOMO (eV)[a]	LUMO (eV)[a]
1	poly(IID-alt-DTE)	DArP	44,900 [2.2]	701	1.65	–5.53	–3.88
2[e]	poly(IID-alt-DTE)	Migita–Stille	86,800 [1.7]	703	1.64	–5.48	–3.84
3	poly(BTz-alt-BT)	DArP	74,800 [2.7]	695	1.66	–5.34	–3.68
4[e]	poly(BTz-alt-BT)	Migita–Stille	47,500 [ca. 2]	695	1.65	–5.34	–3.69

[a] in film. [b] $E_g = 1240/\lambda_{onset}$. [c] CV. [d] E_g – HOMO. [e] Yan, Gong *et al.*, *Adv. Mater.* **2017**, 1606217. [f] Liu *et al.*, *Nat. Commun.* **2014**, *5*, 5293.

BHJ OPV

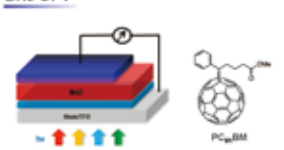

Glass/ITO/ZnO/BHJ/HTL-layer/Ag
BHJ: poly(BTz-alt-BT)/$PC_{61}BM$ = 1/1.5, spin-coated at 60 °C

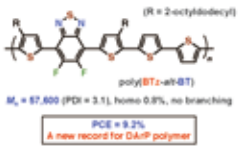

M_n = 57,600 (PDI = 3.1), homo 0.8%, no branching

PCE = 9.2%
A new record for DArP polymer

cf. Stille coupling polymer (M_n = 47,500)
PCE = 9.6%[a]

[a] Liu *et al.*, *Nat. Commun.* **2014**, *5*, 5293.

✔ *DArP affords the polymers which are comparable to Migita-Stille coupling products.*

Acknowledgement

We are grateful to Profs. Y. Murata and A. Wakamiya (ICR, Kyoto University) for analytical GPC assistance, and Dr. M. Furuya and Mr. M. Yabe (Mitsubishi Chemical Corp.) for evaluation of BHJ OPV. The NMR measurements (600 MHz spectrometers) were supported by the Joint Usage/Research Center (JURC) at ICR, Kyoto University.

Square Planar Complexes of Platinum(0)

Katsuhiko Takeuchi,[a] Hiro-omi Taguchi,[a] Ippei Tanigawa,[a] Shota Tsujimoto,[b] Tsukasa Matsuo,[b] Hiromasa Tanaka,[c] Kazunari Yoshizawa,[c] and Fumiyuki Ozawa[a]

[a]*International Research Center for Elements Science, Institute for Chemical Research, Kyoto University, Uji, Kyoto 611-0011, Japan*
[b]*Department of Applied Chemistry, Faculty of Science and Engineering, Kindai University, Higashi-Osaka, Osaka 577-8502, Japan*
[c]*Institute for Materials Chemistry and Engineering, Kyushu University, Nishi-ku, Fukuoka 819-0395, Japan*

1. Introduction

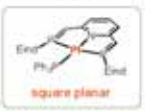

cf. M = Pd, Ni

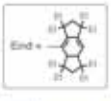

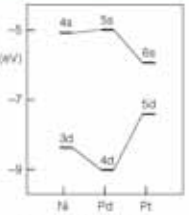

Calculated atomic orbitals energies of group 10 metals

L. L.; Schwarzenbach, G.; Ziegler, T. *Inorg. Chem.* **1995**, *34*, 3245.

- ✔ We found neutral square planar complexes of platinum(0).
- ⇒ Square planar geometry is very uncommon for formal d^{10} complexes.
- ✔ Strong s-d hybridization arising from relativistic effects produces this unique structure in conjunction with the PNP-pincer type phosphaalkene ligand with low-lying π* orbitals.
- ⇒ The s-d hybridization reduces the occupancy of $d_{(z^2)}$ orbital.
- ⇒ The coordination geometry reflects the shape and orientation of the partially unoccupied $d_{(x^2-y^2)}$ orbital.

Takeuchi, K.; Taguchi, H.; Tanigawa, I.; Tsujimoto, S.; Matsuo, T.; Tanaka, H.; Yoshizawa, K.; Ozawa, F. *Angew. Chem. Int. Ed.* **2016**, *55*, 15347.

2. Background

- ✔ Typically, formal d^{10} complexes adopt a tetrahedral geometry.
- ✔ Only a few examples have been reported for square planar complexes of formal d^{10} metals, all of which are anionic species with low-coordinate phosphorus ligands.

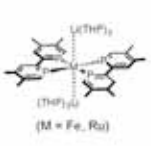

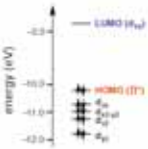

⇒ These complexes are actually six-coordinate complexes with Li^+ ions at the apical positions.

Le Floch, P. et al. *Angew. Chem. Int. Ed.* **2001**, *40*, 1251; *Chem. Commun.* **2003**, 1116; *New J. Chem.* **2001**, *25*, 839.

3. Synthesis of Complexes

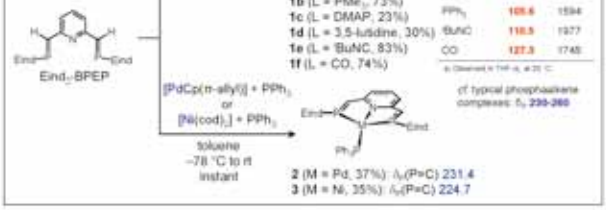

L	δ_P[a]	$^1J_{PC}$[a]
DMAP	96.8	1792
3,5-lutidine	98.2	1950
PMe$_3$	101.2	1883
PPh$_3$	105.6	1594
^{t}BuNC	110.5	1977
CO	127.3	1748

[a] Observed in THF-d_8 at 25 °C.

cf typical phosphaalkene complexes: δ_P 230-260

4. X-Ray Structures

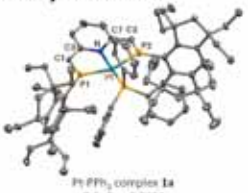

Pt-PPh$_3$ complex **1a**
$P\bar{1}$, R_1 = 0.0651
square planar [Σ(Pt) = 359°]

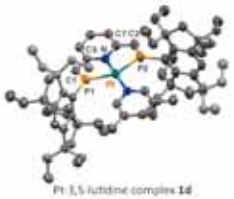

Pt-3,5-lutidine complex **1d**
$P\bar{1}$, R_1 = 0.0563
square planar [Σ(Pt) = 362°]

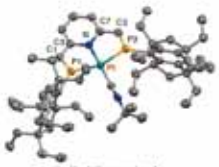

Pt-^{t}BuNC complex **1e**
$P\bar{1}$, R_1 = 0.0559
square planar [Σ(Pt) = 361°]

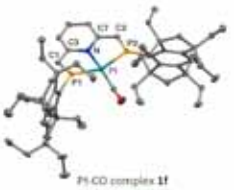

Pt-CO complex **1f**
$P2_1/c$, R_1 = 0.0377
square planar? [Σ(Pt) = 364°]

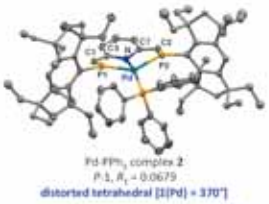

Pd-PPh$_3$ complex **2**
$P\bar{1}$, R_1 = 0.0679
distorted tetrahedral [Σ(Pd) = 370°]

Ni-PPh$_3$ complex **3**
$P\bar{1}$, R_1 = 0.0553
distorted tetrahedral [Σ(Ni) = 370°]

Selected Bond Lengths (Å) and Angles (°)

	Pt-PPh$_3$	Pt-3,5-lutidine	Pt-^{t}BuNC	Pt-CO	Pd-PPh$_3$	Ni-PPh$_3$
M–P1	2.301(2)	2.271(1)	2.2547(14)	2.2843(13)	2.349(1)	2.2552(9)
M–P2	2.325(2)	2.270(2)	2.2591(14)	2.2873(13)	2.341(2)	2.2594(9)
M–N	2.082(5)	2.045(5)	2.049(5)	2.050(4)	2.229(5)	2.056(2)
P1–C1	1.717(6)	1.707(5)	1.713(6)	1.707(5)	1.704(7)	1.706(3)
P2–C2	1.721(6)	1.713(7)	1.715(6)	1.716(5)	1.708(7)	1.713(3)
C1–C3	1.40(1)	1.396(7)	1.394(8)	1.416(7)	1.401(9)	1.427(3)
C2–C7	1.38(1)	1.400(8)	1.391(8)	1.388(7)	1.420(7)	1.414(4)
N–M–L	167.0(2)	174.3(2)	172.8(2)	169.14(18)	156.2(1)	154.97(6)
P1–M–P2	158.71(7)	155.80(5)	158.70(6)	153.53(5)	141.09(6)	148.26(3)
τ^4	0.10	0.21	0.20	0.27	0.44	0.40

5. DFT Calculations (Pt vs. Pd)

- Potential energy vs. ∠N-M-P3

model complexes
[M(PH$_3$)(H$_2$-BPEP)] (**M** = Pt, Pd)

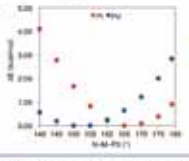

B3LYP/SDD <Pt, Pd>, 6-31G(d) <others>

- ✔ DFT calculations for simple models of **1a** (Pt) and **2** (Pd) indicate that the platinum complex prefers the planar geometry whereas the palladium complex prefers the distorted tetrahedral geometry in nature.

- Molecular Orbitals

energy: B3LYP-D3/SDD <Pt, Pd>, 6-31G(d) <others>, cpt: B3LYP-D3/LANL2DZ <Pt, Pd>, 3-21G(d) <others>

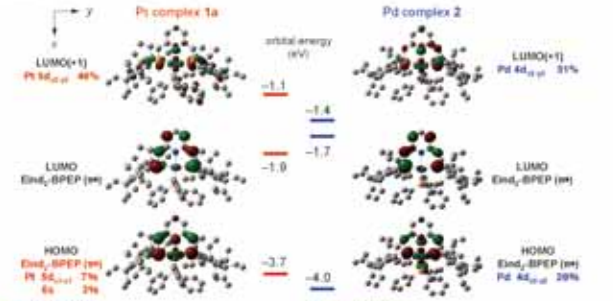

Common points
NBO charge: Pt (0.16), Pd (0.20)
⇒ Both complexes are M(0) species
Large contribution of π* orbital of Eind$_2$-BPEP in HOMO
The M to Eind$_2$-BPEP back-donation is insignificant.

Different points
Orbital occupancy of Pt complex: d 9.15, s 0.82
⇒ A large contribution of s-d hybridization to Pt due to **relativistic effect**
Orbital occupancy of Pd complex: d 9.37, s 0.39
⇒ A small contribution of s-d hybridization

6. Effect of Supporting Ligands

- Molecular Orbitals

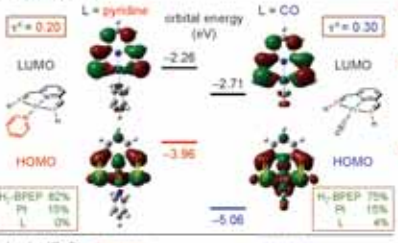

Bond order (P=C) decrease increase
δ_P(P=C) exp. 98.2 127.3

- ✔ X-ray structures of 3,5-lutidine and CO complexes were reproduced by DFT optimization of simple models.
- ✔ Supporting ligands L have almost no influence on the electron configuration of the Pt center, but lowers the planarity by π-accepting ability.
- ✔ π-Accepting CO ligand decreases occupancy of the BPEP ligand with the P=C antibonding character in HOMO.
- ☞ Bond order of the P=C double bond increases and the ^{31}P NMR signal shifts downfield.

- UV-Vis Spectra

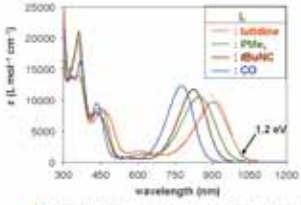

L	3,5-lutidine	PMe$_3$	^{t}BuNC	CO
λ_{max} (nm)	907	845	825	778
LUMO (eV)[a]	−1.88	−1.93	−2.00	−2.27
HOMO (eV)[a]	−3.64	−3.75	−3.84	−4.29

[a] B3LYP/SDD for Pt, 6-31G(d) for others

- ✔ Extremely small HOMO–LUMO gap ⇒ Absorption in near-infrared region
- ✔ As the π-accepting property of L increased, the longest wavelength absorption band tends to shift to short wavelength.
- ☞ HOMO energy level decreased due to π-back donation with L.

The Role of Chloride Additives on Tin Halide Perovskite Solar Cells and Thin Films

Tomoko Aharen, Taketo Handa, Atsushi Wakamiya and Yoshihiko Kanemitsu
Institute for Chemical Research, Kyoto University

Introduction

Lead (Pb) based perovskite solar cell
- Incredible performance over 22 % as polycrystalline thin film solar cell (https://energy.gov/eere/sunshot/downloads/research-cell-efficiency-records)
- High environmental impact is a major drawback

Tin (Sn) based perovskite solar cell as primary substitution
- Similar chemistry (same family with Pb)
- Instability of Sn(II) is a major drawback
- Additive required Usually

Group14

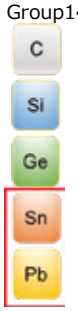

Key to make Sn-based solar cells workable to date
1 : Sn(II) excess and 2: some reducing condition
M. H. Kumar. et al, Adv. Mater., 26: 7122–7127 (2014), Tze-Bin Song et al, ACS Energy Lett., 2, 897–903 (2017)

So far, SnF_2 has been demonstrated as efficient additive but still gives some problems (agglomeration etc)

For crystal quality, Chloride (Cl^-) inclusion works for improvement on optical properties and crystallinity for Lead based solar cells Zhang, W. et al. Nature Commun. 6, 6142 (2015) : Tidhar, Y. et al.. J. Am. Chem. Soc. 136, 13249–13256 (2014),:Williams, S. T. et al.. ACS Nano 8, 10640–10654 (2014) :Moore, D. T. et al.. J. Am. Chem. Soc. 137, 2350–2358,(2015)
→ Could it be applicable for Sn analogues?

$SnCl_2$ also meets excess Sn and moderate reducing condition and offers combination with potential for improvement in crystal quality

Material Preparation and Characterization

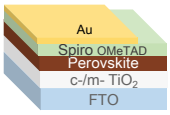

Device Architecture (standard cell)

1. Compact TiO_2
   spray pyrolysis on patterned FTO, $TiCl_4$ treatment and annealed at 500 C
2. Mesoporous TiO_2
   spincoating a diluted TiO_2 nanoparticle paste on c-TiO_2 and annealed
3. Perovskite ($FASnI_3$)
   spincoating 1M perovskite precursor solution ($SnCl_2$ additive included) and annealed
4. SpiroOMeTAD
   spin coating SpiroOMeTAD with additives in chlorobenzene
5. Au – Thermal evaporation

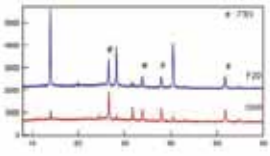

PXRD patterns for SnF_2 added (blue) and $SnCl_2$ added (red) $FASnI_3$ films are equivalent. No additional phases observed

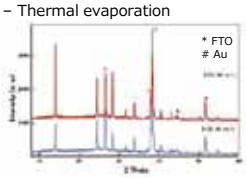

PXRD patterns for $SnCl_2$ 30 mol% added (blue) and $SnCl_2$ 50 mol% added (red) No additional phases observed

Optical Properties

PL energy for thin films with various $SnCl_2$ ratio

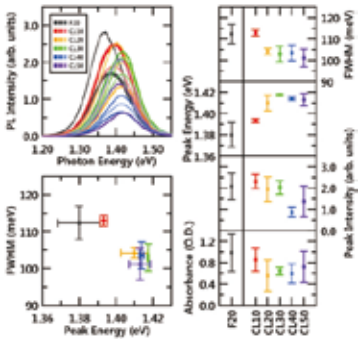

- Blue shift in PL energy for all $SnCl_2$ additions → Slight Cl inclusion contribution(?)
- Particularly, samples more than 20 mol % $SnCl_2$ added show greater blue shifts and the devices based on such composition are workable

PL lifetime for thin films with various $SnCl_2$ ratio

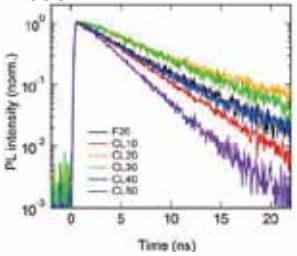

Sample	Lifetime (ns)
F20	5.0
Cl10	4.0
Cl20	6.6
Cl30	6.2
Cl40	4.5
Cl50	3.0

Longer lifetime than SnF_2 additive

Device Performance and characterization

Device performance with DMSO precursor solution

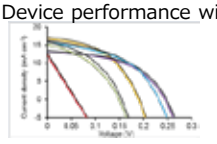

	Jsc (mA cm-2)	Voc (V)	FF	PCE
Cl10	12.89	0.06	0.14	0.1
Cl20	17.20	0.19	0.44	1.4
Cl30	15.91	0.15	0.42	1.0
Cl40	16.45	0.23	0.45	1.6
Cl50	13.33	0.25	0.49	1.7

V_{oc} increases as Cl addition increases

Device performance with DMF/DMSO precursor solution
-fabricated with toluene dripping

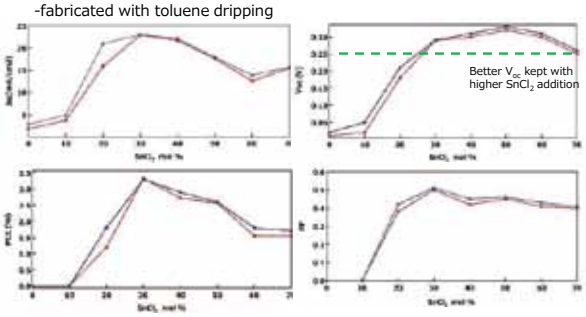

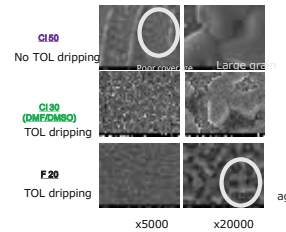

agglomeration

Surface SEM images
- No severe agglomeration observed for Cl addition (surface SEM). Surface coverage partially improved by changing solvent mixture(!?)
- Larger grain size obtained (reducing boundary area) for Cl additions

Summary

$SnCl_2$ also works as effective additive and the trend was found in V_{oc} vs $SnCl_2$ ratio. Optical measurements show longer lifetime with $SnCl_2$, supporting potential for comparable performance to SnF_2 additive version. Diminishing the trading off between J_{sc} and V_{oc} observed in device performance seems working by solvent engineering.

Acknowledgement

CREST and IRCCS for funding
Shimakawa Lab for access to XRD facility, Teranishi Lab and Matsuda Lab for access to SEM

Synthesis and structural analysis of Ag-Bi-I for solar cells

Anucha Koedtruad, Takashi Saito, Atsushi Wakamiya, and Yuichi Shimakawa
Institute for Chemical Research, Kyoto University, Uji, Kyoto 611-0011, Japan

Introduction

Solar cells

Main components:
1) Solar absorber layers
2) Hole transport layers (HTL)
3) Electron transport layers (ETL)

Working principle:
Photons captured by absorber materials activate electrons in valence bands to conduction bands producing electrons and holes. The charges then are separated: Electrons are injected into and transported through the ETL layer to an electrode, while positive charge holes move to the HTL layer and a counter electrode.

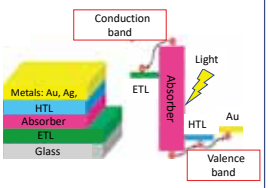

A solar cell device and a working principle

The key properties of solar absorbers:
suitable band gap (1.1 - 1.55 eV), strong solar absorption, high charge carrier mobilities, close band alignment with HTL and ETL, high stability and non-toxicity

Ag-Bi-I

Ag-Bi-I compounds were reported to be used as solar absorbers. The compounds are stable and non-toxicity.
- $AgBiI_4$ ($Ag_{0.5}Bi_{0.5}I_2$) and $AgBi_2I_7$ ($Ag_{0.29}Bi_{0.57}I_2$) with defect spinel structures
- Ag_2BiI_5 ($Ag_{0.8}Bi_{0.4}I_2$) and Ag_3BiI_6 ($AgBi_{0.33}I_2$) with $CdCl_2$-type structures

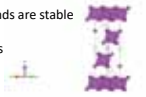
$CdCl_2$-type structure

Problems at the current stage:
- It was difficult to obtain single phase samples.
- Actual chemical compositions for the compounds were not revealed.
- Detailed crystal structures were not clarified.

Aims of the research

- Synthesis of single phase of Ag-Bi-I compounds
- Analysis the chemical compositions and crystal structures
- Evaluation of physical and chemical properties

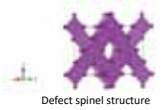
Defect spinel structure

Reference: *Chem.Commun.* **2017**, *53*, 20 – 44.

Experiments

Synthesis by solid state reaction

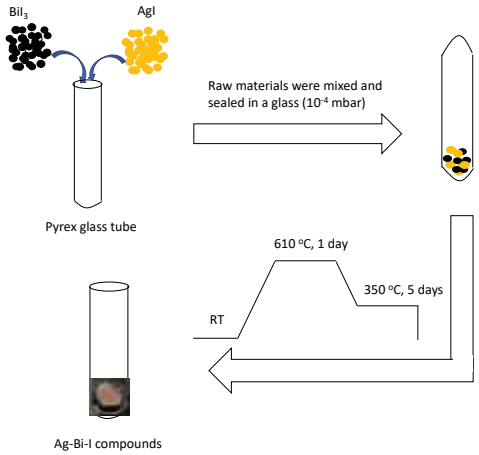

Materials characterization

- Phase identification by XRD
- Structure analysis with synchrotron XRD data
- Measurement of Valence band energy levels by photoelectron spectroscopy
- Measurement of band gap by UV-Vis spectroscopy

Results and discussion

Synchrotron X-ray diffraction and structural refinement

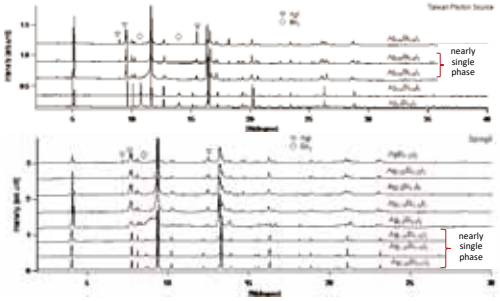

Synchrotron X-ray diffraction spectra of $Ag_xBi_yI_2$ (x = 0.20 – 1.00 , y = 0.33 – 0.60)

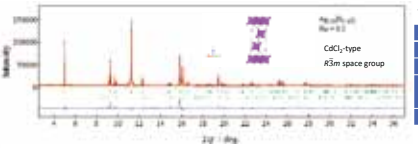

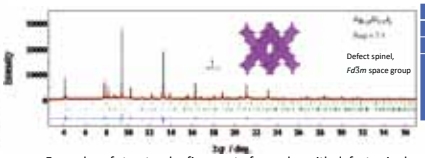

Examples of structural refinement of samples with defect spinel and $CdCl_2$-type structures

The structure analysis with synchrotron X-ray diffraction data revealed two distinct phases: the defect spinel structure with the $Fd\bar{3}m$ space group and the $CdCl_2$-type structure with the $R\bar{3}m$ space group.

Atom	Site
Bi	3a (0 0 0)
Ag1	3a (0 0 0)
I	6c (0 0 z)
	z = 0.24762
Ag2	3b (0 0 1/2)

$CdCl_2$-type structure, $R\bar{3}m$ space group
Nearly single phase compositions : $Ag_xBi_yI_2$ (x = 0.56 – 0.65, y = 0.45 – 0.48)
Impurity phase : AgI

Atom	Site
Bi	16c (0 0 0)
Ag	16c (0 0 0)
I	32e (x x x)
	X = 0.25264
	y = 0.25264
	z = 0.25264

Defect spinel, $Fd\bar{3}m$ space group
Nearly single phase compositions : $Ag_xBi_yI_2$(x = 0.29 – 0.44, y = 0.52 – 0.57)
Impurity phase : BiI_3

Valence band level (VB) measurements by photoelectron spectroscopy

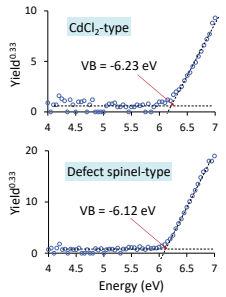

The VB levels of the defect spinel and $CdCl_2$-type compounds are located between -6.1 – -6.3 eV

VB levels of samples

Compounds		VB (eV)
Defect spinel-type	$Ag_{0.44}Bi_{0.52}I_2$	- 6.19
	$Ag_{0.35}Bi_{0.55}I_2$	- 6.12
	$Ag_{0.29}Bi_{0.57}I_2$	- 6.13
$CdCl_2$-type	$Ag_{0.65}Bi_{0.45}I_2$	- 6.26
	$Ag_{0.56}Bi_{0.48}I_2$	- 6.23

X-ray photoelectron spectra of the samples with the defect spinel and $CdCl_2$-type structures

Energy gap (Eg) measurement by UV-Vis spectroscopy

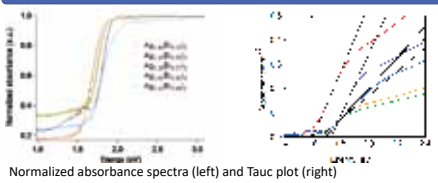
Normalized absorbance spectra (left) and Tauc plot (right)

Eg values were calculated from Tauc plot (Absorbance*hv)^2 vs. hv [1]

Eg values of the defect spinel and $CdCl_2$-type compounds were located between 1.6 – 1.8 eV

Eg values of samples

Compounds		Eg (eV)
Defect spinel	$Ag_{0.44}Bi_{0.52}I_2$	1.61
	$Ag_{0.35}Bi_{0.55}I_2$	1.68
	$Ag_{0.29}Bi_{0.57}I_2$	1.66
$CdCl_2$-type	$Ag_{0.65}Bi_{0.45}I_2$	1.70
	$Ag_{0.56}Bi_{0.48}I_2$	1.74

For both the defect spinel and $CdCl_2$-type compounds, the top of the valence bands consist of I 5*p* states, and the bottom of the conduction bands consists of Bi 6*p* and I 5*p* states. [1-2]

References
[1] *Chem.Mater.* **2015**, *27*, 7137 – 7148.
[2] *Angew.Chem.Int.Ed* . **2016**, *5*, 9586 – 9590.

Conclusions

- $Ag_xBi_yI_2$ (x = 0.20 – 1.00 , y = 0.33 – 0.60) compounds have been prepared by solid state reaction.
- Nearly single phase compounds were obtained for samples with x = 0.29 -0.44 and y = 0.52 – 0.57 compositions for the defect spinel-type structure and x = 0.56 -0.65 and y = 0.45 – 0.48 compositions for the CdI_2-type structure.
- The VB levels of defect spinel and $CdCl_2$-type compounds are between -6.1 – -6.3 eV.
- The Eg of the compounds are between 1.6 – 1.8 eV.

DFT and AFIR Study on the Mechanism and the Origin of Enantioselectivity in Iron-Catalyzed Cross-Coupling Reactions

Akhilesh K. Sharma†, W. M. C. Sameera§, Masayoshi Jin#, Laksmikanta Adak‡, Chiemi Okuzono‡, Takahiro Iwamoto‡, Masako Kato§, Keiji Morokuma†* and ○Masaharu Nakamura‡*

† FIFC, Kyoto University, § Hokkaido University, # Daiichi Sankyo Co., Ltd., ‡ IRCELS, ICR, Kyoto University, Uji

Introduction

- Use of Fe-catalyst in different reactions is increased recently due to its non-toxic nature and abundance.
- Recently, first Fe-catalyzed enantioselective cross-coupling reaction is developed. [1]
- Mechanism of Fe-catalyzed cross-coupling reaction is of recent debate, and not properly understood. [2]

Detailed Mechanism → Origin of Enantioselectivity?

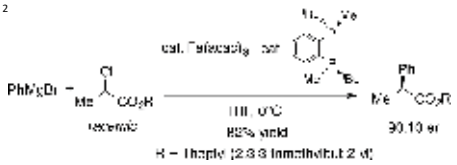

Computational Methods

- Recently developed Artificial Force Induced Reaction (AFIR) method (implemented in GRRM) is useful in finding approximate TSs without initial guess.[3]
- AFIR is very effective for finding different conformational TSs, which is necessary while dealing with stereoselective reactions.[4]

MC-AFIR : GRRM Program with Gaussian 09
ONIOM(B3LYP-D3:PM6-D3)/SDD(Fe), 3-21G(all atoms except Fe)

Optimization: Gaussian 09 RevisionD.01
PCM_{THF}/B3LYP-D3BJ/SDD(Fe,Br); 6-31+G**(O, Mg, P, Cl); 6-31G*(H, C)

Energies: PCM_{THF}/B3LYP-D3BJ/SDD(Fe, Br); cc-PVTZ (H, C, O, Mg, P, Cl)
Energies are in kcal/mol at 25°C temperature.

Proposed Mechanism

R = Theptyl, X = Ph or Cl, P^P = BenzP*

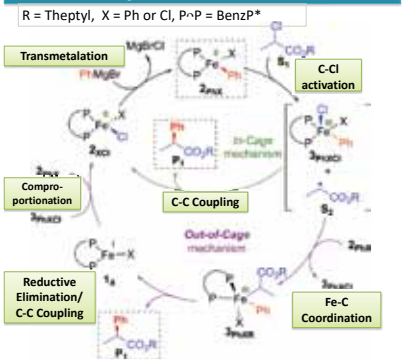

Active Species Generation

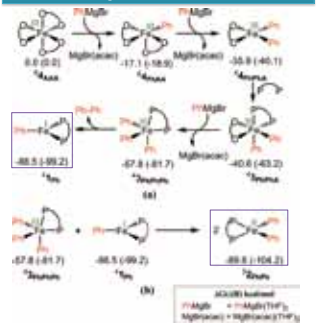

♠ Energies of Fe(I) and Fe(II) species are almost same. [5]

C-Cl Activation

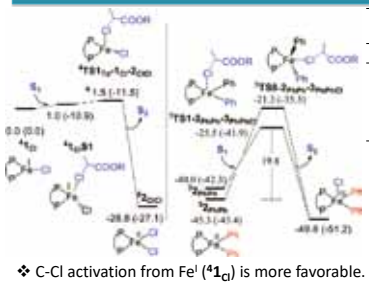

Activation Barriers (Gibbs free energy) for C-Cl activation

Fe^{II}		Fe^{I}	
$^{3}\mathbf{2}_{PhPh}$	19.8	$^{4}\mathbf{1}_{Cl}$	1.5
$^{5}\mathbf{2}_{PhCl}$	25.8	$^{4}\mathbf{1}_{Ph}$	5.0
$^{5}\mathbf{2}_{ClCl}$	38.3	Fe^{III}	
		$^{4}\mathbf{3}_{PhClCl}$	50.3

❖ C-Cl activation from Fe^{I} ($^{4}\mathbf{1}_{Cl}$) is more favorable. [5]

❖ C-Cl activation from Fe^{I} ($^{4}\mathbf{1}_{Ph}$) is less likely, as low concentration of Grignard reagent is maintained during reaction.

❖ C-Cl activation from from Fe^{II} (as proposed) will be slow due to high activation barrier.

C-C coupling

❖ Reaction of Fe^{II} species ($\mathbf{2}_{PhCl}$) with ester radical is more feasible than with Fe^{III}. [5]

❖ Reaction occurs through *inner-sphere* mechanism in quartet spin state.

❖ >50 TSs for C-Fe and TSs for C-C bond formation were studied though MC-AFIR to explore enantioselectivity.

❖ C-C bond formation step is enantioselectivity determining.

❖More deformation in **TS2** is responsible for enantioselectivity.

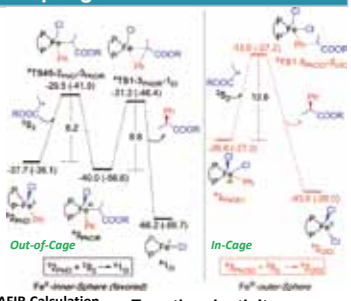

Conformations of radical and Fe^{II} used for MC-AFIR Calculation

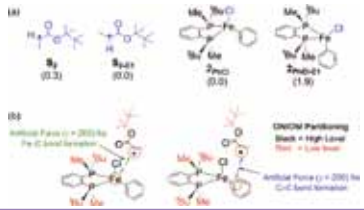

Enantioselectivity

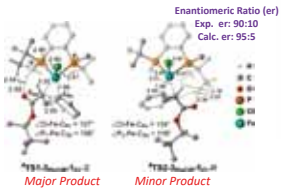

Free Energy Profile for Favorable Mechanism

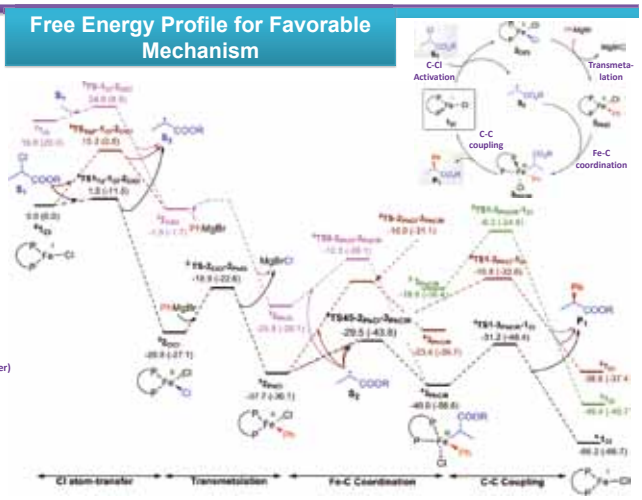

❖ Fe^{I}/Fe^{II}/Fe^{III} mechanism is found to be operating in Fe-Phosphine catalyzed C-C coupling reaction. [5]

Conclusion

- C–Cl activation occurs from iron (I) species [Fe^{I}Cl(BenzP*)] and not from iron(II) species.
- Radical species ($\mathbf{S}_2$) formed after C-Cl activation will react with Fe(II), [Fe^{II}PhCl(BenzP*)] leading to the formation of Fe(III) and followed by C-C coupling by reductive elimination in quartet spin state.
- The reaction of radical species with [$Fe^{II}Ph_2$(BenzP*)] will mainly lead to biphenyl formation, hence, slow addition of Grignard reagent is required during the reaction
- C–C bond formation is enantioselectivity determining.

References

(1) Jin, M.; Adak, L.; Nakamura, M. *J. Am. Chem. Soc.* **2015**, *137*, 7128.
(2) Bedford, R. B. *Acc. Chem. Res.* **2015**, *48*, 1485.
(3) Maeda, S.; Ohno, K.; Morokuma, K. *Phys. Chem. Chem. Phys.* **2013**, *15*, 3683.
(4) Sameera, W. M. C.; Hatanaka, M.; Kitanosono, T.; Kobayashi, S.; Morokuma, K. *J. Am. Chem. Soc.* **2015**, *137*, 11085.
(5) Sharma, A. K.; Sameera, W. M. C.; Jin, M.; Adak, L.; Okuzono, C.; Iwamoto, T.; Kato, M.; Nakamura, M.; Morokuma, K. *J. Am. Chem. Soc.* **2017**, *139*, 16117−16125.

Acknowlegment
Research Center for Computational Science and Kyoto University for Supercomputing facility.
Prof. Satoshi Maeda for the development version of the GRRM program.

Molecular Understanding of Adhesion at Silica Surface/Epoxy Resin Interface: Effects of Interfacial Water Molecules

KYUSHU UNIVERSITY

(IMCE, Kyushu University)
HIGUCHI, Chisa; TANAKA, Hiromasa; YOSHIZAWA, Kazunari

1. Fiber Reinforced Plastics/Polymer (FRP)

Epoxy resin (adhesive)
+
Glass fiber (Reinforcing material)

Property: mechanically strong, water-resistant
Examples: ships, cars, bathtubs, helmets

Mechanical properties of FRP are controlled by interfacial adhesion between epoxy resin and glass fiber.

2. Possible mechanisms of adhesive interaction [1]

- Mechanical interlocking
  Effective on porous or rough surfaces such as wood, textile, paper…
- Electronic adhesion
  Very weak interaction
- Diffusion (cohesion)
  Effective on polymers and rubbers
- Primary bond (chemical bond)
  Covalent, ionic, and metallic bonds
- Secondary bond (intermolecular interaction)
  van der Waals force, **hydrogen bond**, acid-base interaction

[1] Kinloch, A. J. *J. Mater. Sci.*, **15**, 2141 (1980).

Since the mechanism of adhesion is still unclear, molecular understanding of adhesion mechanism is demanded.
In this study, density functional theory (DFT) is applied for models of adhesion interface between glass surface and epoxy resin.

3. Models

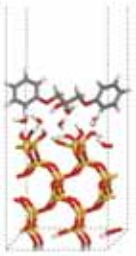

Interfacial model
(10 × 10 × 50 Å³; vacuum 40 Å)

- **Epoxy Resin** Produced by polymerization of bisphenol A

- **Water Layer**
  Without water, monolayer* (5 molecules), bilayer (10 molecules)
  *Surface concentration (monolayer) ··· 7.68 μmol H_2O/m^2 [2]
- **Glass Surface**
  α-cristobalite (0 0 1)
  Silanol groups are formed on the surface [3]

[2] K. E. Collins, V. R. de Camargo, A. B. Dimitas, D. T. C. Menezes, P. A. da Silva, C. H. Collins, *J. Colloid Interface Sci.*, **291**, 353 (2005).
[3] A. S. D'Souza, C. G. Pantano, *J. Am. Ceram. Soc.*, **82**, 1289 (1999).

4. Computational method

- **Molecular dynamics (MD)**
  Program: Forcite
  Ensemble: NVT
  Temperature: 300 K
  Time step: 1.0 fs
  Dynamics time: 100 ps
- **Density functional theory (DFT)**
  Program: CASTEP
  Method: GGA-PBE
  Ultrasoft Pseudopotential
  Cut off: 380 eV
  k-point: 0.05 $Å^{-1}$
  Dispersion correction: D2 by Grimme

5. Optimized structures

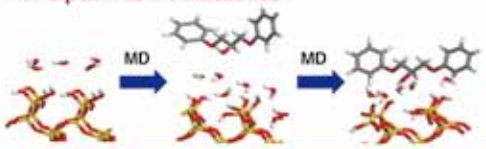

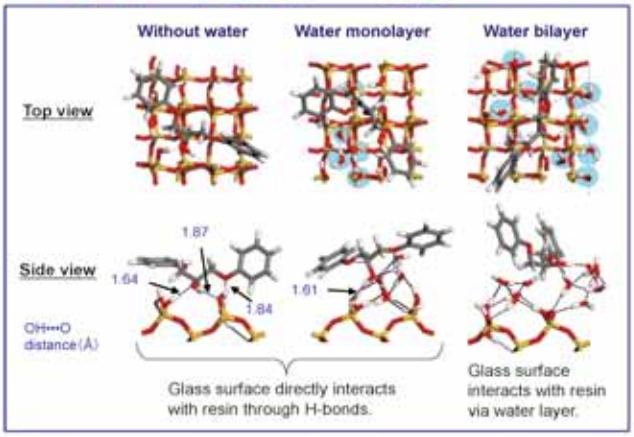

6. Adhesive force calculation

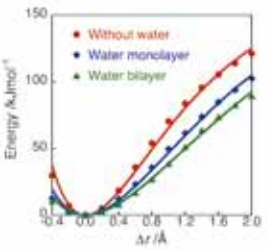

Energy-distance plots

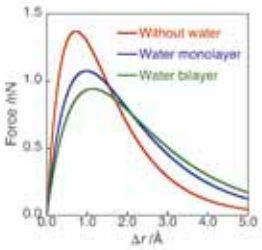

Force-distance curves

- *E*-Δ*r* plots were nicely approximated by Morse potential.
- Surface water significantly reduces adhesive force.

1. The adhesive molecule was displaced perpendicular to the surface and the energies were plotted as a function of displacement Δ*r*.
2. The energy-displacement (*E*-Δ*r*) plots were approximated by Morse potential curves.

$$E = D_e(1 - e^{-\alpha\Delta r})^2$$

3. Potential curves were differentiated to obtain force-displacement (*F*-Δ*r*) curves.

$$F = \frac{dE}{d\Delta r}$$

4. Maximum adhesive stress S_{max} was calculated from F_{max}.

T. Semoto, Y. Tsuji, K. Yoshizawa, *J. Phys. Chem. C*, **115**, 11701 (2011).
T. Semoto, Y. Tsuji, K. Yoshizawa, *Bull. Chem. Soc. Jpn.*, **85**, 672 (2012).
T. Semoto, Y. Tsuji, H. Tanaka, and K. Yoshizawa, *J. Phys. Chem. C*, **117**, 24830 (2013).

$$S_{max}\,(\text{Pa}) = \frac{F_{max}\,(\text{N})}{A_{unit}\,(\text{m}^2)} =$$

- 1.38 GPa (Without water)
- 1.08 GPa (Monolayer)
- 0.95 GPa (Bilayer)

Experimental value
17.4 MPa [4]
- Asperity
- Impurity contamination
- Internal stress
- Blister formation

S_{max}: Maximum adhesive stress
F_{max}: Maximum adhesive force
A_{unit}: Surface area per unit

[4] A. Sekuljic, A. Cunnier, *Int. J. Adhes. Adhes.*, **27**, 611 (2007).

7. Conclusions

The adhesion interface between glass surface and epoxy resin has been investigated with DFT calculations.

- Hydrogen bonds work as the primary force of adhesive interaction at the adhesion interface.
- Surface water molecules significantly reduce adhesive force.
- The calculated S_{max} would correspond to an "ideal" experimental adhesion stress in the perfect interfacial conditions.

Theoretical Study of the Influence of Water on the Adhesion Phenomena

KYUSHU UNIVERSITY

(IMCE, Kyushu University) ○Hiroyuki Murata, Hiromasa Tanaka, Kazunari Yoshizawa

1. Introduction

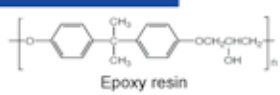

Epoxy resin

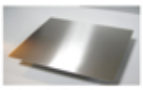

Metal aluminum

Mechanisms of adhesion

Mechanical Coupling

Electrostatic Force

Molecular Diffusion

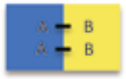

Chemical Bond

Intermolecular force

A. J. Kinloch, *J. Mater. Sci.* **15**, 1 (1980).

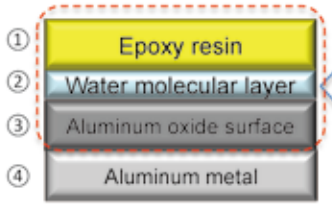

Purpose of This Research

To investigate the role of water molecular layer in adhesion by quantum chemical approach

2. Calculation Method

2. 1. Models

Adhesive molecule: epoxy resin

Adherend surface: hydroxylated alumina surface with or without adsorbed water

Atoms: 1566, 1776, 1986 /unit cell

Parameter: a = 27.9 Å, b = 25.2 Å

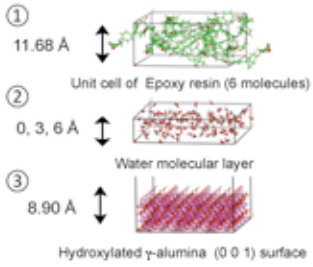

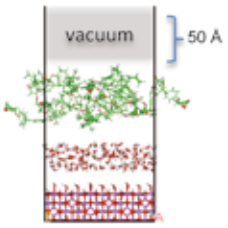

Slab Model

2. 2. Methods

Program	DFTB+ (Materials Studio 6.1)
Slater-Koster library	matsci
k-point set	1 × 1 × 1
Charge	0
Spin Multiplicity	1

2. 3. Adhesive force calculation

1. The adhesive molecules were displaced perpendicular to the surface and the energies were plotted. The energy-displacement (E-Δr) plots were approximated to potential curves.

$$E = D_e(1 - e^{-a\Delta r})^2$$

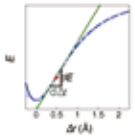

2. Potential curves were differentiated to obtain force-displacement (F-Δr) curves. F_{max} is defined as the maximum value of F.

$$F = dE/d\Delta r = 2D_e a e^{-a\Delta r}(1-e^{-a\Delta r})$$

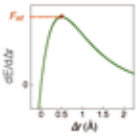

3. Adhesion stress was obtained by F/A. (A: cross-sectional area of calculation model)

3. Results

Optimized structures

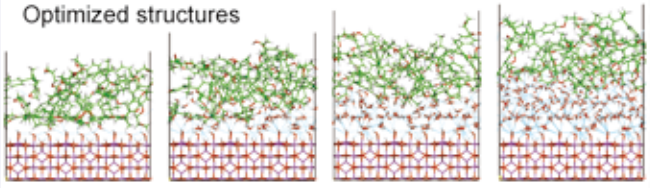

Model 1 (thickness: 0 Å) | Model 2 (thickness: 3 Å) | Model 3 (thickness: 6 Å) | Model 4 (thickness: 9 Å)

Binding energy

1. Resin/Metal (No water)
2. Resin/Water + Metal
3. Resin + Water/Metal

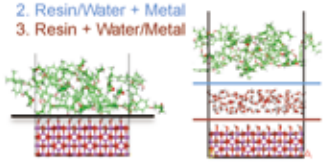

Table. Binding Energy (kcal/mol)

Model	$E_{R/A}$	$E_{R/W}$	$E_{W/M}$
1	319.8	-	-
2	-	288.6	355.3
3	-	257.5	347.1
4	-	255.4	349.7

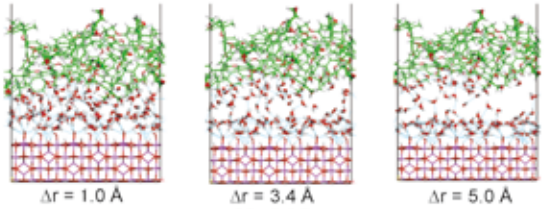

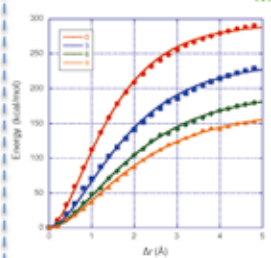

Total Energy – displacement plots

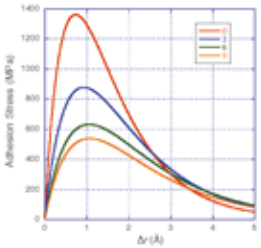

Adhesive Stress - displacement curve

4. Conclusions

1. Hydrogen bonds play an important role for the adhesion between aluminum oxide surface and epoxy resin.
2. The interaction energy between epoxy resin and water is smaller than that between epoxy resin and aluminum oxide surface.
3. Water molecules have an important influence on the adhesion between aluminum oxide surface and epoxy resin.
4. The adhesion stress of the interface between epoxy resin and alumina surface decrease as the thickness of water molecular layer increases.

Theoretical Study of Methane Activation at the Dicopper Site of pMMO

Shuhei Itoyama[1], Kazuki Doitomi[1], Yoshihito Shiota[1], Kazunari Yoshizawa[1,2]
IMCE Kyushu University[1], ESCIB Kyoto University[2]

1. Introductions

Methane Monooxygenase (MMO)

$$CH_4 + O_2 + 2e^- + 2H^+ \xrightarrow{MMO} CH_3OH + H_2O$$

- direct conversion
- physiological condition

Particulate Methane Monooxygenase (pMMO)

X-Ray crystal structure

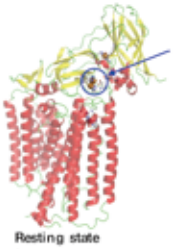

Resting state
(PDB:1YEW)
Lieberman et al. *Nature* **2005**, *434*, 177.

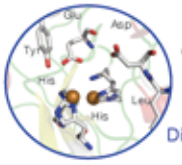

A reaction mechanism for methane activation catalyzed by pMMO

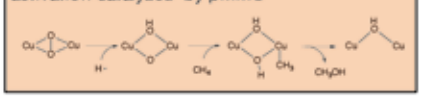

Shiota et al. *Inorg. Chem.* **2013**, *52*, 7907.

Peroxo state of other dicopper proteins

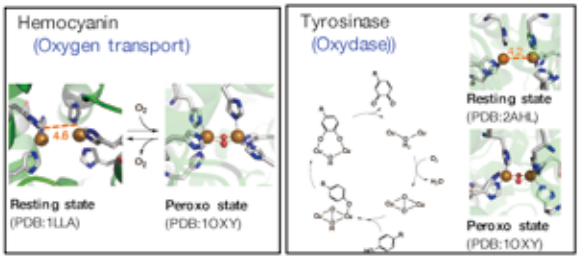

This work

- Calculate pMMO at real system by QM/MM calculation
- Propose the peroxo structure of pMMO

2. Computational Method

Computational Procedure

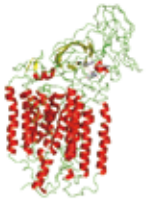

Program : Discovery Studio 3.5
Force Field : CHARMm

- pKa prediction at pH 6 (Discovery Studio and PROPKA)
- Relaxing
  Heating (50-300 K, 15 ps)
  Equilibration (300 ps, time step 1 fs, SHAKE algorithm)
- Energy minimization (CG method, 5000 steps)
- Three Cu atoms and the first coordination residues were kept fixed during minimizations and MD simulations.

QM/MM Method

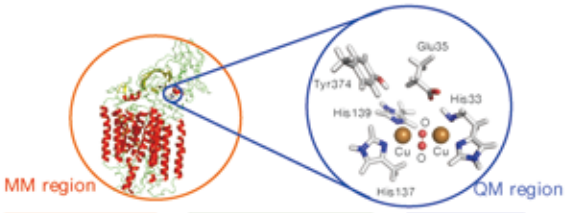

DL-POLY
CHARM force field

QM/MM interface
ChemShell
Electrostatic embedding

TURBOMOLE
B3LYP/TZVP

3. Results

The dicopper site in the resting state

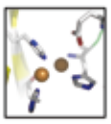

Cu-Cu
2.55 Å

QM/MM result

Cu-Cu
2.58 Å

X-ray crystal structure

Why the Cu-Cu is so near?

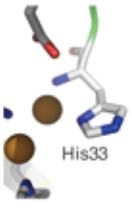

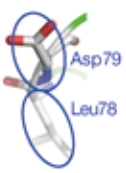

interact with His33
↓
interrupt the moving of His33
↓
enforce the Cu-Cu closely !

The dicopper site in the peroxo state

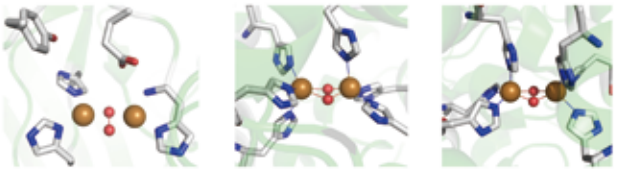

pMMO
QM/MM result

Hemocyanin
Tyrosinase
X-ray crystal structure

	pMMO	Hemocyanin	Tyrosinase
Cu-Cu (Å)	3.58	3.59	3.48
O-O (Å)	1.44	1.41	1.48
CuOOCu (˚)	149.4	156.3	145.2

similar values!

4. Conclusions

- Resting and peroxo states of pMMO were calculated by using the QM/MM method.
- The optimized structure in the resting state is consistent with X-ray crystal structures.
- Possible reason of the short Cu-Cu distance in the resting state is interaction of His33 with Leu78 and Asp79.
- The optimized structure in the peroxo state is similar to other dicopper structures (e.g. Hemocyanin and Tyrosinase).

Theoretical study on absorption wavelength control of β-carotene using solid acid

(¹IMCE, Kyushu Univ. ²Shizuoka Univ.)
○ Nobuyuki Hirosawa,¹ Yoshihito Shiota,¹ Yoshiumi Kohno,² Ryuma Asaba,² Kazunari Yoshizawa¹

1. Introduction

Phthalocyanine: Blue, Stable, Synthetic

Anthocyanin: Blue, Unstable, Natural

β-carotene (CR): Red, Stable, Natural ⇄ (H⁺ / -H⁺) Blue, Unstable, Natural

1-1. Protonation of CR

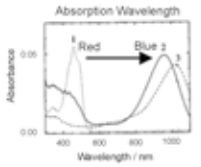

Previous work

Solvent

1 C_6H_6

2 $C_6H_6 + CF_3COOH$

3 $CH_2Cl_2 + CF_3COOH$

Konovalov, V. V.; Kispert, L. D. *J. Chem. Soc., Perkin Trans.* **1999**, *2*, 901

1-2. CR with solid acid

Experimental study

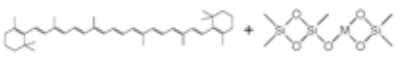

CR + M-doped mesoporous silica (M = Al^{3+}, Fe^{3+}, Ga^{3+}, B^{3+})

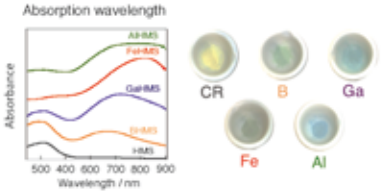

M-doped mesoporous silica indicate red-shift of absorption peak.

2. Purpose

Why do CR with solid acids indicate the red-shifted absorption spectra?

☑ Protonation of CR (3-1, 3-2)

☑ Solid acid models (3-3) (Lewis acid, Brønsted acid)

2-1. Computational Method

Program	Gaussian09
Functional	CAM-B3LYP
Basis set	6-31G*

3. Results

Optimization and TDDFT calculation of CR

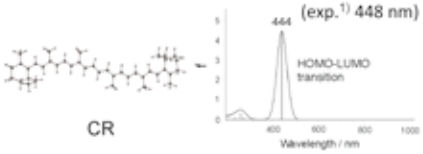

λ_{max} of CR corresponds to the HOMO - LUMO transition.

1) Craft, N. E.; Soares, J. H. *J. Agric. Food Chem.* **1992**, *40*, 431.

3-1. Protonation of CR

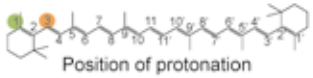

Position of protonation

Relative Energy (ΔE, kcal/mol), maximum absorption wavelength (λ_{max}, nm), Relative maximum absorption wavelength ($\Delta\lambda_{max}$, nm)

Position	ΔE (kcal/mol)	λ_{max} (nm)	$\Delta\lambda_{max}$ (nm)
CR		444	0
CR1-H⁺	0.00	709	265
CR2-H⁺	43.4	497	53
CR3-H⁺	-0.97	662	218
CR4-H⁺	35.7	462	18
CR5-H⁺	8.78	624	180
CR6-H⁺	21.2	442	-2
CR7-H⁺	8.54	566	122
CR8-H⁺	18.9	429	-15
CR9-H⁺	12.8	533	89
CR10-H⁺	14.5	450	6
CR11-H⁺	12.7	511	67

3-2. Bond alternation

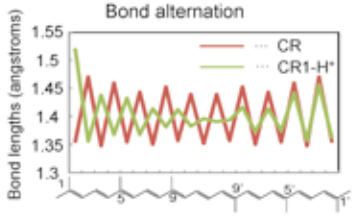

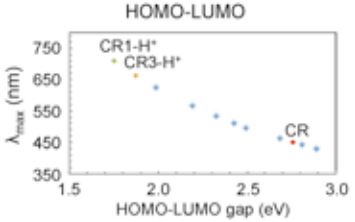

3-3. Solid acids

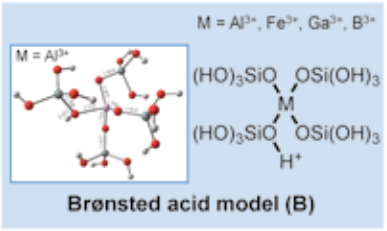

Brønsted acid model (B)

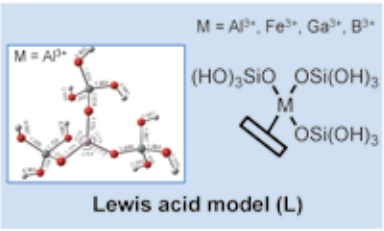

Lewis acid model (L)

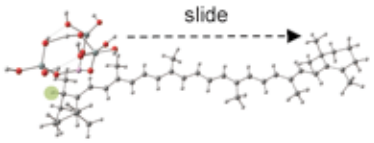

Computational search for the sliding along CR (**L + CR-H⁺**)

Calculated UV-Vis spectra (**L + CR-H⁺**)

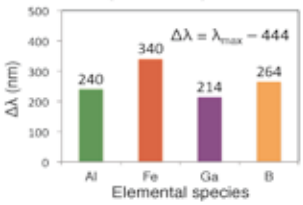

4. Conclusions

- DFT calculations show that protonation of CR is likely to occur in the 1, 3 sites of CR. The two protonated CRs show a large peak shift as well as relative energetic stability.
- The combinations of the protonated CR and Lewis acids as a model of M-doped mesoporous silica are consistent with experimental observations.

Asymmetric Synthesis of Highly Functionalized Silacyclopentanes

Kazunobu Igawa, Daisuke Yoshihiro, Akihiro Kuroo, Yusuke Abe, Katsuhiko Tomooka
IMCE, and IRCCS, Kyushu University, Japan

Background

Asymmetric Synthesis of Chiral Silicon Compound

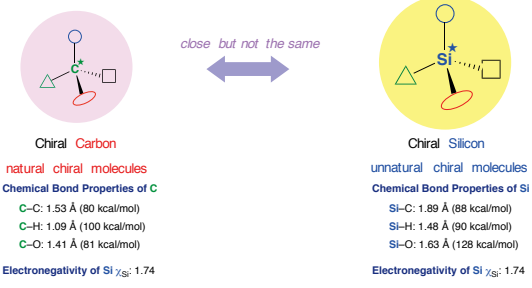

First Report of Enantio-enriched Chiral Silicon Molecule: F. S. Kipping, *J. Chem. Soc.* **1907**, 209.
Review: Brook, M. A. *Silicon in Organic, Organometallic, and Polymer Chemistry*, **2000**.

Previous Works

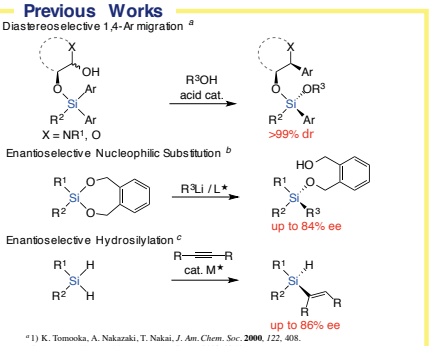

[a] 1) K. Tomooka, A. Nakazaki, T. Nakai, *J. Am. Chem. Soc.* **2000**, *122*, 408. 2) A. Nakazaki, J. Usuki, K. Tomooka, *Synlett* **2008**, 2064.
[b] K. Igawa, J. Takada, T. Shimono, K. Tomooka, *J. Am. Chem. Soc.* **2008**, *130*, 1613.
[c] K. Igawa., D. Yoshihiro, N. Ichikawa, N. Kokan, K. Tomooka, *Angew. Chem. Int. Ed.* **2012**, *51*, 12745.

This Work

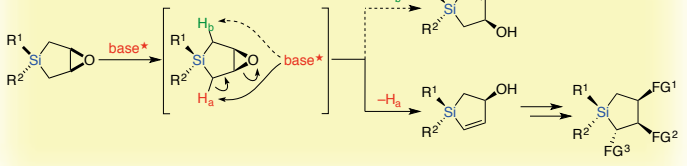

Related Report

Carbocycle System[a]

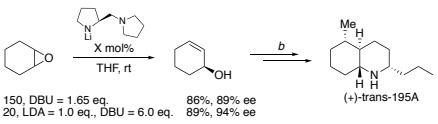

X = 150, DBU = 1.65 eq.
X = 20, LDA = 1.0 eq., DBU = 6.0 eq.
86%, 89% ee
89%, 94% ee

Silacycle System[c]

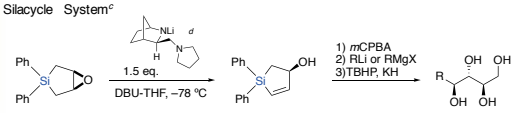

78%, 95% ee

[a] 1) M. Asami, T. Suga, K. Honda, S. Inoue, *Tetrahedron Lett.* **1997**, *38*, 6425.; 2) M. Asami, *J. Synth. Org. Chem., Jpn.* **1996**, *54*, 188. [b] N. Holub, J. Neidhöfer, S. Blechert, *Org. Lett.* **2005**, *7*, 1227. [c] D. Liu, S. A. Kozmin, *Angew. Chem. Int. Ed.* **2001**, *40*, 4757. [d] M. J. Södergren, P. G. Andersson, *J. Am. Chem. Soc.* **1998**, *120*, 10760.

Results

Preparation of Substrate

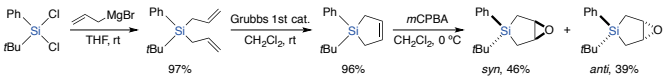

Enantioselective β-Elimination

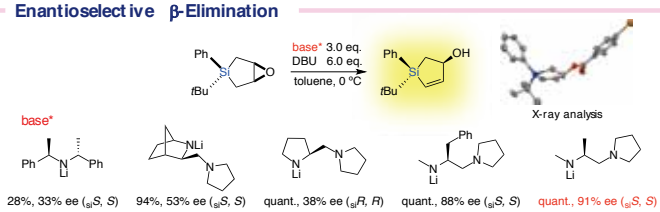

Stereoselective Transformation

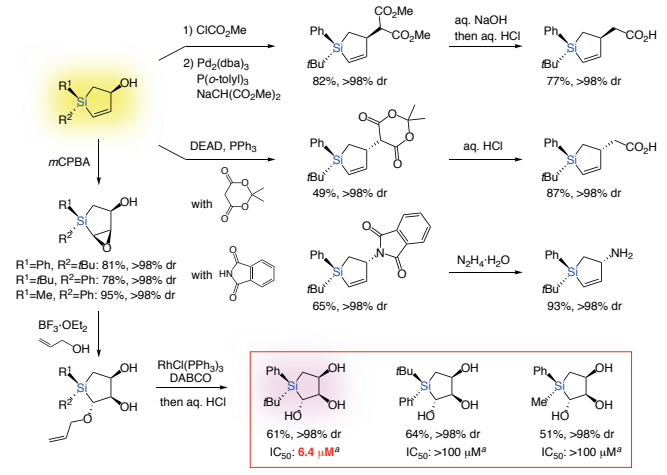

[a] Binding inhibition activity for the specific binding of 5-HT_{2B} with lysergic acid diethylamide

Scope and Limitation

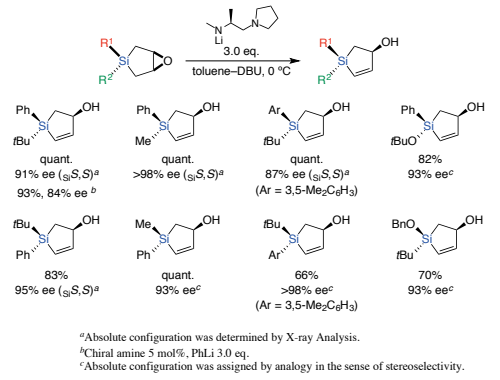

[a] Absolute configuration was determined by X-ray Analysis.
[b] Chiral amine 5 mol%, PhLi 3.0 eq.
[c] Absolute configuration was assigned by analogy in the sense of stereoselectivity.

DFT Calculation

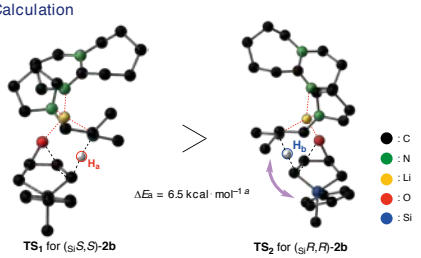

TS_1 for ($_{Si}S,S$)-**2b** > **TS_2** for ($_{Si}R,R$)-**2b**

[a] Zero-point vibrational energy calculated at B3LYP/6-311+G(d,p) level of theory.

Summary

K. Igawa, D. Yoshihiro, Y. Abe, K. Tomooka, *Angew. Chem. Int. Ed.* **2016**, *55*, 5814.
K. Igawa, A. Kuroo, D. Yoshihiro, Y. Yamanaka, K. Tomooka, *Synlett* **2017**, *28*, 2445.

Efficient Synthesis of Multi-Functionalized DACN and Its Application

Yuuya Kawasaki,[1] Shin Aoyama,[2] Takeru Kashiwagi,[1] Kazunobu Igawa[1,2] and Katsuhiko Tomooka[1,2]

[1]*Institute for Materials Chemistry and Engineering,* [2]*Department of Molecular and Material Sciences, Kyushu University*

Background

Click Chemistry[a]

"Click Chemistry: Diverse Chemical Function from a Few Good Reactions"

[a] H. C. Kolb, M. G. Finn, K. B. Sharpless, *Angew. Chem. Int. Ed.* **2001**, *40*, 2001.

wide in scope, high yield, generate only inoffensive byproducts, simple reaction condition, rapid completion, high selectivity, etc.

Huisgen Reaction [b]

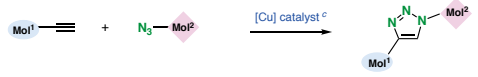

[b] Huisgen, G. Szeimies, L. Möbius, *Chem. Ber.*, **1967**, *100*, 2494.
[c] 1) C. W. R. Tornøe, C. Christensen, M. Meldal, *J. Org. Chem.* **2002**, *67*, 3057.
2) V. V. Rostovtsev, L. G. Green, V. V. Fokin, K. B. Sharpless, *Angew. Chem. Int. Ed.* **2002**, *41*, 2596.

Evolution of Click Reaction Device

1st generation: terminal alkyne

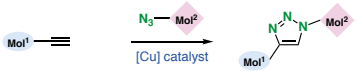

2nd generation: cyclooctyne

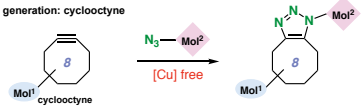

3rd generation: 4,8-diazacyclononynes (DACN)

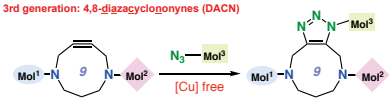

Problems

[a] R. Ni, N. Mitsuda, T. Kashiwagi, K. Igawa, K. Tomooka, *Angew. Chem. Int. Ed.* **2015**, *54*, 1190.

Result

Synthesis of DACN

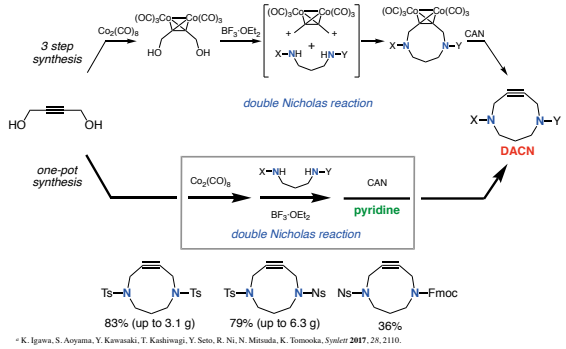

[a] K. Igawa, S. Aoyama, Y. Kawasaki, T. Kashiwagi, Y. Seto, R. Ni, N. Mitsuda, K. Tomooka, *Synlett* **2017**, *28*, 2110.

Reactivity and Stability of DACN

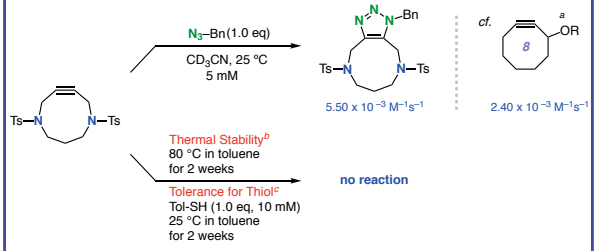

[a] N. J. Agard, J. A. Prescher, C. R. Bertozzi, *J. Am. Chem. Soc.* **2004**, *126*, 15046.
[b] H. Stöckmann, A. A. Neves, S. Stairs, H. Ireland-Zecchini, K. M. Brindle, F. J. Leeper, *Chem. Sci.* **2011**, *2*, 932.
[c] R. van Geel, G. J. M. Pruijn, F. L. van Delft, W. C. Boelens, *Bioconjugate Chem.* **2012**, *23*, 392.

Synthesis and Reaction of DACN Peptide

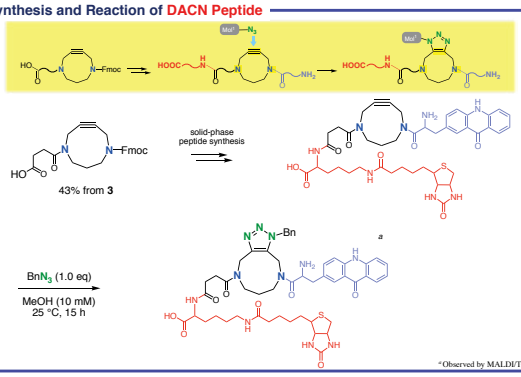

[a] Observed by MALDI/TOFMS.

Collaboration with Tanaka Group in Nagoya Univ.

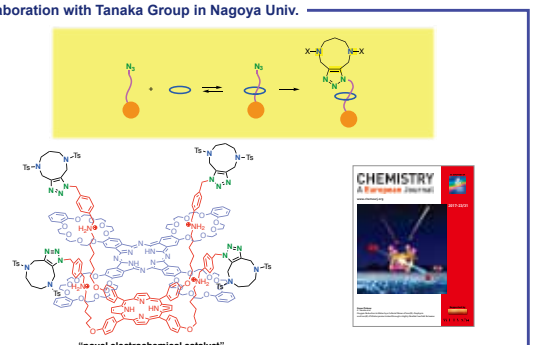

"novel electrochemical catalyst"

N. Mihara, Y. Yamada, H. Takaya, Y. Kitagawa, S. Aoyama, K. Igawa, K. Tomooka, K. Tanaka, *Chem. Eur. J.* **2017**, *23*, 7508.

Collaboration with Nagatsugi Group in Tohoku Univ.

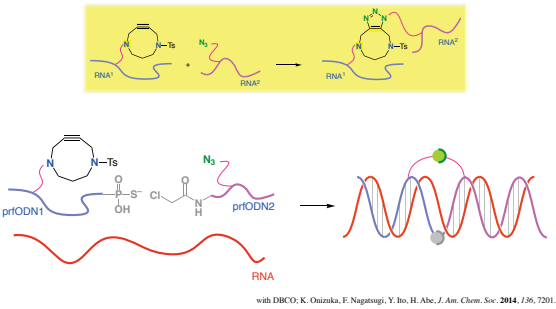

with DBCO; K. Onizuka, F. Nagatsugi, Y. Ito, H. Abe, *J. Am. Chem. Soc.* **2014**, *136*, 7201.

Summary

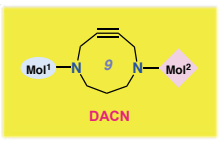

High Synthetic Efficiency
One-pot synthesis with double Nicholas approach was achieved.

High Thermal Stability
No reaction was observed at 80 °C for 2 weeks.

High Bioorthogonality
No reaction was observed with thiol at 25 °C for 2 weeks.

High Functional Diversity
A variety of functional units were introduced to endocyclic nitrogens.

Formation of Pseudo-symmetric Functional Molecules and Crystals by Using Chirality

(IMCE, Kyushu Univ.)Shinji Kanegawa and Osamu Sato
E-mail: kanegawa@cm.kyushu-u.ac.jp

Introductions

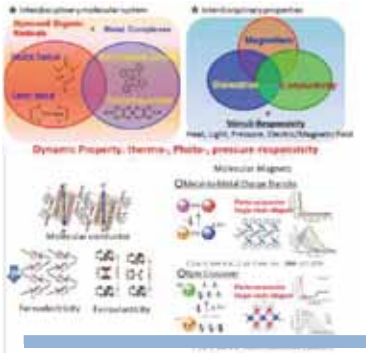

Valence Tautomerism of Homometallic [CoCo]

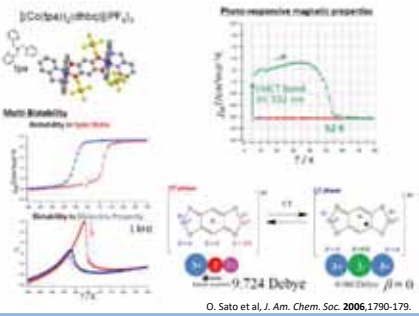

O. Sato et al, *J. Am. Chem. Soc.* **2006**,1790-179.

Electron transfer in homometallic [CoCo]

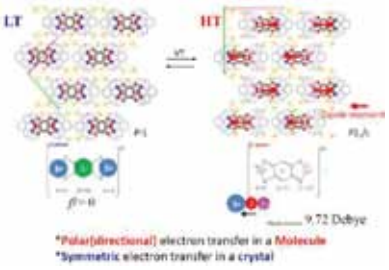

Symmetric vs. Asymmetric

Strategy

Based on [CoCo] complex; $[(Co(\textit{rac}\text{-cth}))_2(dhbq)](PF_6)_3$

Ref. A. Dei et al, Angew. Chem. Int. Ed.,2004, 43, 3136-3138.

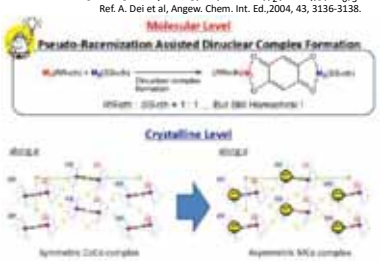

Enantiopure Monometallic Complexes

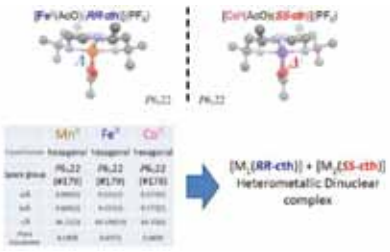

Crystal Structure of [CrCo]

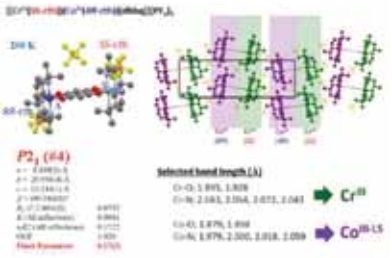

Identification of [CrCo]

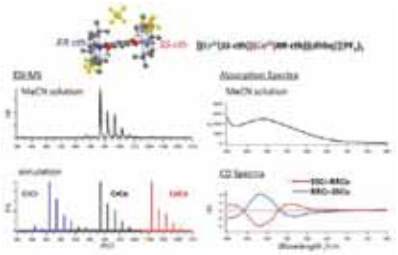

Magnetic Properties of [CrCo]

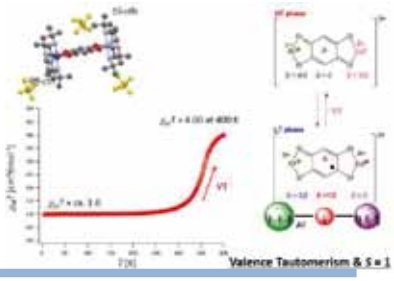

Temperature-dependent Spectra

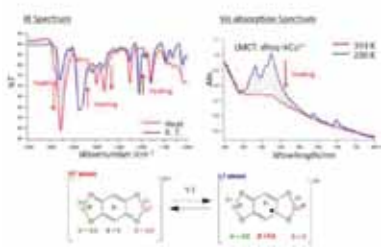

Homometallic [CoCo] vs. Heterometallic [CrCo]

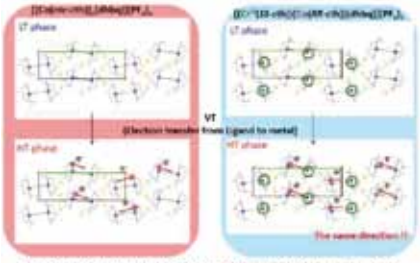

Several Heterometallic Complexes

Magnetic Properties of [CrFe]

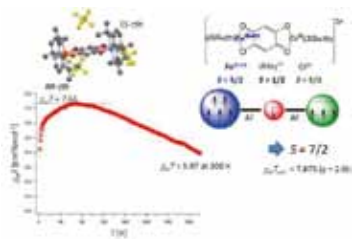

Magnetic Properties of [FeCo]

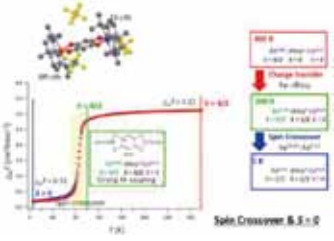

Summary

ホウ素化2-フェニルピリジン類の固相相転移とその機構解明

Solid State Phase-sransition of Borylated 2-Phenylpyridines

(九大先導研, 東工大化生研) ○吉越　裕介、國信　洋一郎、須崎　裕司、小坂田耕太郎

(Kyushu Univ.,Titech) Yusuke YOSHIGOE, Yoichiro KUNINOBU, Yuji SUZAKI, Kohtaro OSAKADA

Summary

- ホウ素化2-フェニルピリジン1の固体が、可逆的に変色する現象を見出した。
- 1の白色固体(Phase A)に光を当てるとピンク色に着色した固体になる(Phase B)。
- Phase Bの固体を加熱もしくは溶解/溶媒留去するとPhase Aにもどる。
- この現象はBN結合の結合距離の変化が原因である。

謝辞: 東大薬 花岡　健二郎准教授 (蛍光スペクトル測定)
九大先導研 出田　圭子氏 (固体NMRスペクトル測定)

Solid-state Fluorescent Spectra

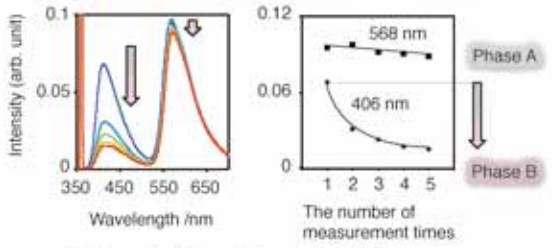

励起レーザー光(λ_{ex} = 340 nm)で転移する
→転移にともなって、蛍光 (λ_{em} = 406 nm)が減衰する

Hole orbital from NTO (S_1)　Particle orbital from NTO (S_1)

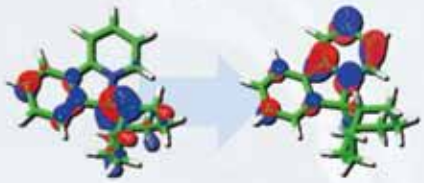

-Excitation 1-
E = 2.972 eV
λ = 418 nm
f = 0.1803

M06-2X/cc-pVDZp (*isovalue* = 0.05) (Gaussian 16, Rev. A.03)

Photo-induced Transition

Subs	State	Vessel	Treatment	After Treatment
Phase A	Solid	Quartz plate	Irrad. by Set (a)	Phase B (*ca.* 1 h)
Phase A	Solid	Glass plate	Irrad. by Set (a)	Phase B (*ca.* 3 h)
Phase A	Solid	Quartz plate	Irrad. by Set (b)	Phase B (*ca.* 6 h)
Phase A	Solid	Brown vessel	Irrad. by Set (a)	Phase A
Phase A	Solution[a]	Quartz vessel	Irrad. by Set (a)	Phase A[e]
Phase B	Solid	Quartz plate	Irrad. by Set (a)	Phase B[c]
Phase B	Solid	Glass vessel	Heating (180 °C)	Phase A (ca. 0.5 h)
Phase B	Solid	Glass vessel	Dissolved/Evap.[d]	Phase A
Phase B	Solid	Glass vessel	Exposure to solvent vapor[e]	Phase A

a. CD_2Cl_2 solution; ***b***. Determined with NMR measurement (400 MHz, r.t.); ***c***. No additional change was observed.; ***d***. Dissolved into CH_2Cl_2, then evaporated.; ***e***. CH_2Cl_2 vapor was used.

Set (a)

トルネードバルブ:
25 W, 1550 Lm,
6500 K (300-800 nm)
(日動工業(株))

Set (b)

Blue LEDテープ:
30 W, 1000 Lm,
ca. 470 nm
(akiba-LEDピカリ館)

Solid-state NMR Analysis

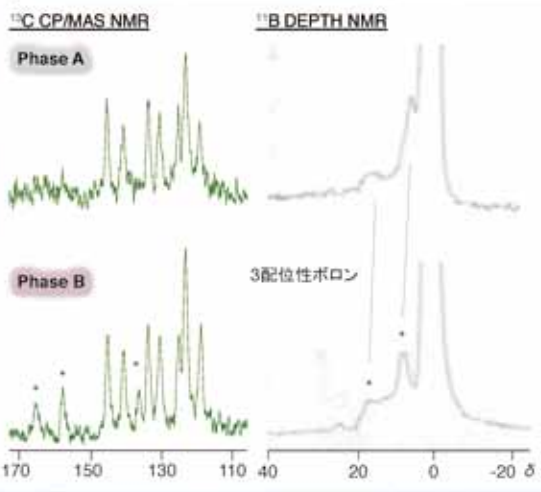

(Recorded on JEOL JMN-ECA 400)

X-ray Crystallography of Phase A

$P2_12_12_1$ (No. 19)
a = 6.939
b = 14.185
c = 14.987
$\alpha = \beta = \gamma = 90°$
Z = 4

Selected bond length (/Å) and angles (°)	
B-N	1.6590
B-C[1]	1.6234
C[2]-C[3]	1.4575
N-B-C[1]	96.127

Ref.) Sum of VWR of B and N = 3.470 Å

Packing Structure

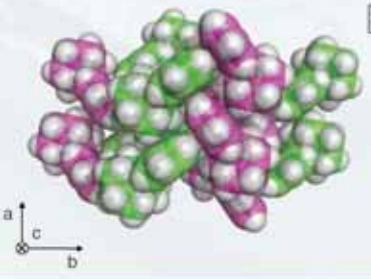

Hirsh-field Analysis

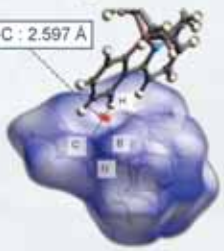

d norm. surface (*isovalue* = 0.05)

Observation of Hyperbranched Polymer/Metal Nanoparticle Composite Materials

[1]Katsumi Chikama, [1]Keisuke Kojima, [1]Yudai Morimoto,
[2]Hideo Nagashima
[1]Nissan Chemical Industries, LTD., [2]Kyushu University

Purpose

● Creation of new business using hyperbranched polymers(HBP) through collaboration with Kyushu University.

●Studies on functionalization of HBP.
●Applications of functionalized HBP to new materials.

●Elucidation of the structure of HBP and HBP/metal composites.
●Applications.

Introduction

Classification of branched polymers.
・Star polymer, Dendritic polymer, Hyperbranched polymer

Hyperbranched polymer(HBP) : Irregular branching architecture
Pseude spherical polymer with many functional groups.
Different properties from linear and crosslinked polymer.

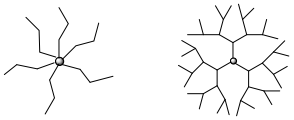

Characteristic features of our HBP
◆Nano-sized pseudo spherical structure with
・Low viscosity
・Little entanglement of polymer chains
・High dispersibility to various solvents
・High mobility in the solid matrix
◆Existence of large number of terminal functional groups, which can be chemically modified with ease.
・The functional group modification makes possible control of physical properties of HBP, e.g. compatibility and dispersibility.
・Control compatibility and solubility.
Metal- HBP composites
High dispersion stability by HBP
High catalytic reactivity of metal nanoparticles

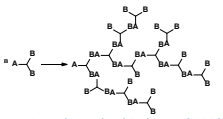

Hyperbranched Polymer(HBP)

backborn (HBP):
polystyrene, polyacrylate, etc

Visualiuzation of HBP by TEM,AFM/STM and STEM-HAADF

TEM, AFM and STM image (HBP)

TEM
: Transmission Electron Microscope
AFM
: Atomic Force Microscope
STM
: Scanning Tunneling Microscope

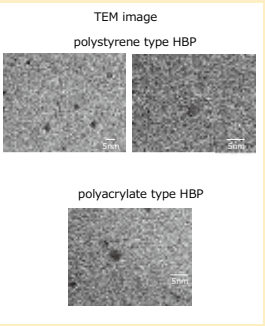

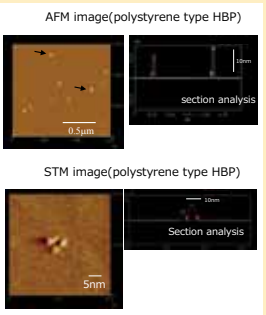

TEM image
H-8000 (HITACHI,200kV, x700000)

Samples
・polystyrene type HBP
・polyacrylate type HBP

HBP(Mw~20000):
several ~10nm(pseudo spherical shape)

AFM/STM image
nanoscope IV (Veeco Instruments)
probe: Si(AFM), W-In(STM)
mode: tapping

Sample
polystyrene type HBP

Substrate
mica

STEM-HAADF image (metal@HBP nanoparticle comosite)

STEM-HAADF
: Scanning Transmission Electron Microscope High-Angle-Annular-Dark-Field
・Heavy elements are dark in the STEM image, bright in the STEM-HAADF image
→Contrast proportional to atomic weight (Z) is obtained

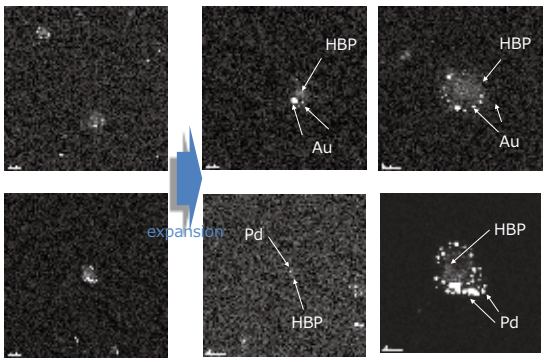

STEM-HAADF image
JEM2100F(JEOL)
200 kV(FE)

samples
Au or Pd@HBP(polystyrene type)

Application of HBP/metal composite

HBP/metal composites (metal = Pt, Ru, Pd, etc.) are applicable to catalysts for organic reactions and electroless plating.
Development of Pd@HBP ink useful for inkjet, flexo, and other printing techniques.

Chemical reaction catalyst (Hydrogeneration reaction, etc)

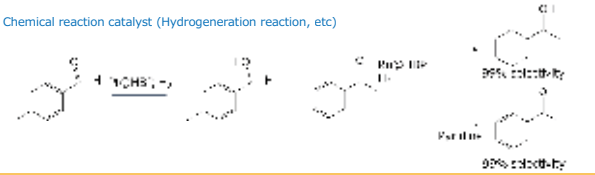

Electroless plating (Cu pattern plating)

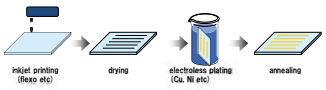

NCI process

Ink Jet printhing
(Cu plating on PI film)
L/S = 25μm/25μm

Summary

HBP is polymers with unique physical properties, of which features are different from linear polymers.
HBP well disperses various metal nanoparticles, and the composites are stable enough to industrial applications.
The resulting HBP/metal nanoparticle composite materials can be used as the catalysts for various organic reactions.
They are also applicable to the catalysts for electroless plating by using a variety of printing methods.
The electroless plating technology has a promising feature for industrial applications to flexible electronics.

日産化学工業株式会社
NISSAN CHEMICAL INDUSTRIES, LTD.

Efficient and Selective Hydrogenation of Nitroarenes using Platinum Nanoparticle Catalysts Supported by Ammonium Salts of Hyperbranched Polystyrene

Hideo Nagashima, Yuma Yamamoto, Yuki Maeda, Lei Gao, Arada Chaiyanurakkul

[1]*Institute for Materials Chemistry and Engineering ,Kyushu University, 6-1, Kasugakoen, Kasuga-shi, Fukuoka, 816-8580*

Summary: We have previously reported synthesis of ammonium salts of hyperbranched polystyrene which behave as good support of well-dispersed platinum nanoparticles, of which size is uniformly controlled by ~2 nm. By using this nanocomposite consisted of Pt@HPS-NR_3Cl as the catalysts, highly efficient hydrogenation reactions of olefins and ketones were accomplished. Further studies revealed that the same catalyst behaves as efficient catalysts of nitroarenes to aniline derivatives. The reaction was carried out under 1 atm of H_2 at room temperature (TOF = 4750 /h, stirring speed = 1500 rpm). Functional group compatible and selective preparation of hydroxylamines, which are the intermediates in the conversion of nitroarenes to anilines, were also studied.

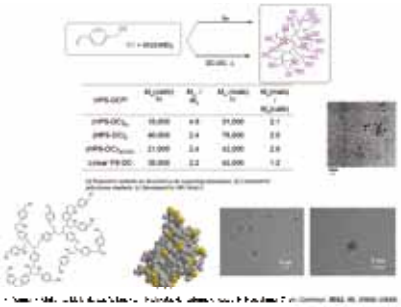

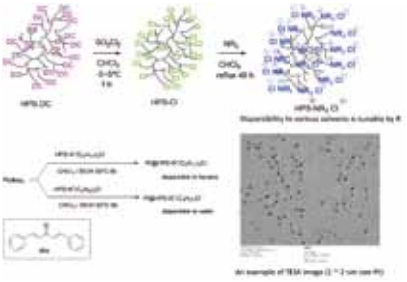

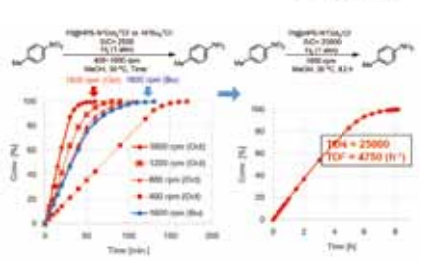

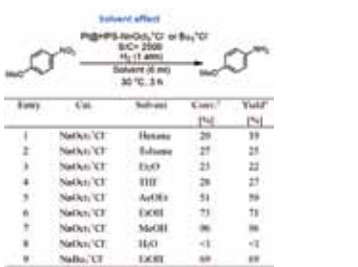

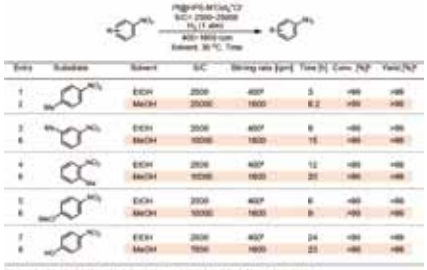

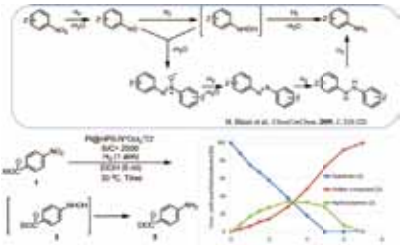

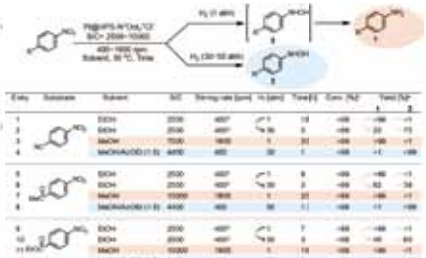

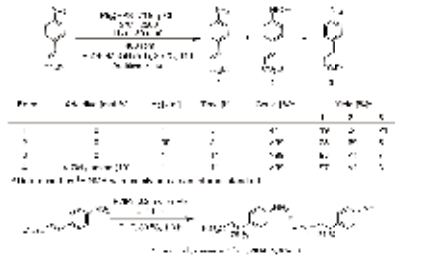

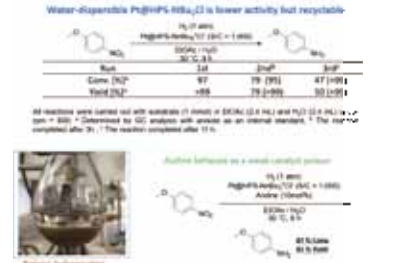

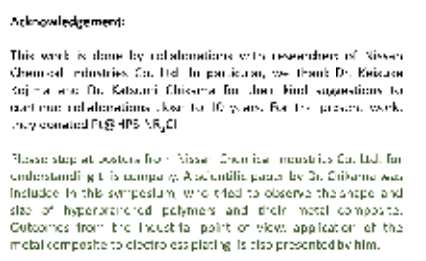

Acknowledgement:

This work is done by collaborations with researchers of Nissan Chemical Industries Co. Ltd. In particular, we thank Dr. Katsuya Sajiki and Dr. Katsuki Okuma for their kind suggestions to start our collaborations about 10 years. For the present work, they donated Pt@HPS-NR_3Cl.

Those staff at Nissan Chemical Industries Co. Ltd. for understanding this company's scientific policy by Dr. Okuma will include in this symposium, were tried to observe the shape and size of hyperbranched polymers and their metal composites. Outcomes from the industrial point of view, application of the metal composite to electroless plating is also presented by him.

Atom Transfer Radical Polymerization by Solvent-stabilized (Me_3TACN)FeX_2: A Practical Access to Reusable Iron (II) Catalysts

So-Ichiro Nakanishi,[1] Atsushi Tahara,[2] Mitsunobu Kawamura,[2] Yusuke Sunada,[2] Hideo Nagashima[1,2,3]

[1]*Graduate School of Engineering Sciences, Kyushu University, 6-1, Kasugakoen, Kasuga-shi, Fukuoka, 816-8580*
[2]*Institute for Materials Chemistry and Engineering, Kyushu University, 6-1, Kasugakoen, Kasuga-shi, Fukuoka, 816-8580*
[3]*CREST, Japan Science and Technology Agency (JST), Gobancho 7, Chiyoda-ku, Tokyo, 102-0076*

Introduction

Atom Transfer Radical Polymerization (ATRP)

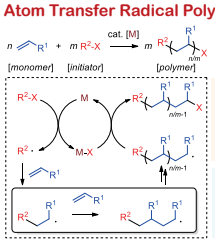

a) Matyjaszewski, K.; Xia, J. *Chem. Rev.* **2001**, *101*, 2921; b) Kamigaito, M.; Ando, T.; Sawamoto, M. *Chem. Rev.* **2001**, 3689; c) Matyjaszewski, K. Macromolecules **2012**, *45*, 4015.

Highly-controlled ATRP shows...
- Narrow Molecular Weight Distribution.
- Functionalization by changing Monomer / Initiator
- Block Copolymerization. (Late Stage Functionalization)

Problem is ...
- Control of Radical Density.
- Substrate Scope
- Efficient Removal of Metal Residue.
- Reusability of the Catalysts.

Previous Work : ATRP catalyzed by a series of (R_3TACN)FeX_2

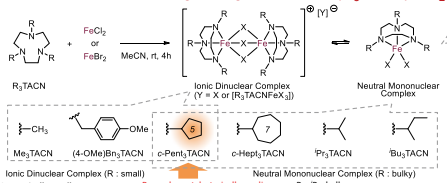

Ionic Dinuclear Complex (R : small)
<R = Me: sterically small>
- Ionic Dinuclear Complex
- × Substrate scope was limited
- × Low Reactivity (120 °C, 18h)
- ◎ Easy separation of metals by MeOH

Ionic Dinuclear Complex (R : medium)
<R = cyclopentyl: sterically medium>
- Both Ionic and neutral Complex
- ◎ Wide Substrate scope
- ◎ High reactivity & stable
- ◎ Easy separation of M by MeOH

Neutral Mononuclear Complex (R : bulky)
<R = iPr: bulky>
- Neutral Mononuclear Complex
- ◎ Wide Substrate scope
- △ High reactivity (4h) but instable
- × Impossible to separate by MeOH

<Molecular Structure of [(Cyclopentyl)$_1$TACNFeX$_2$]>

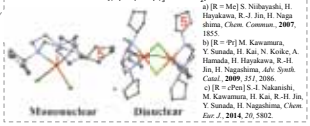

a) [R = Me] S. Niibayashi, H. Hayakawa, R.-J. Jin, H. Nagashima, *Chem. Commun.*, **2007**, 1855.
b) [R = iPr] M. Kawamura, Y. Sunada, H. Kai, N. Koike, A. Hamada, H. Hayakawa, R.-H. Jin, H. Nagashima, *Adv. Synth. Catal.*, **2009**, *351*, 2086.
c) [R = cPen] S.-I. Nakanishi, M. Kawamura, H. Kai, R.-H. Jin, Y. Sunada, H. Nagashima, *Chem. Eur. J.*, **2014**, *20*, 5802.

This Work

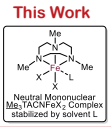

- Highly-reactive and highly-controlled ATRP iron catalysts were synthesized by using commercially-available Me_3TACN ligands.
- Substrate scope
- Reusability of catalysts
- Removal of metal residue from polymer
- *In situ* generation from FeX_2 / Me_3TACN / CNMe.

Results & Discussion (1)

Strategy : Plausible Catalytic Cycle for ATRP

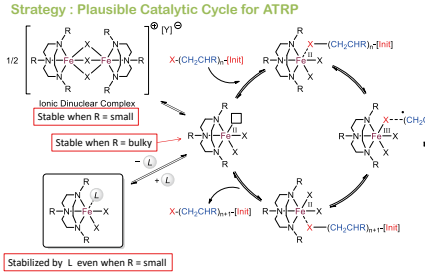

Synthesis of $Me_3TACNFeX_2L$ complexes

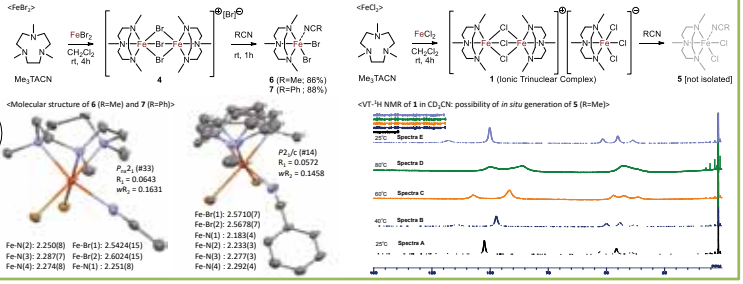

Results & Discussion (2)

[1] ATRP of Styrene catalyzed by Fe complexes

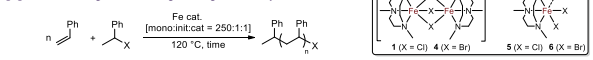

Entry	Cat.	Time (h)	Conv.(%)	M_n (exp.)	M_n (Calcd.)	M_w/M_n
1	**1**	18	>95	21,900	25,000	1.30
2	**5** (*in situ*)	8	94	23,600	23,500	1.27
3	**4**	28	93	23,900	25,000	1.25
4	**6** (*isolated*)	8	94	24,600	23,500	1.19
5	**6** (*in situ*)	8	>95	24,000	25,000	1.20
6	**7** (*isolated*)	8	>95	25,100	25,000	1.21
7	**7** (*in situ*)	8	92	24,000	23,000	1.21

In all cases, bulk polymerization experiments were performed at 120 °C with the [catalyst]/[initiator]/[monomer] ratio of 1 : 1 : 250. The initiator used was (1-chloroethyl)benzene (entries 1 and 2) or (1-bromoethyl)benzene (entries 3–5).

(a) time vs. ln([M]$_0$/[M]) plot of 1 and 5 (X=Cl) (b) time vs. ln([M]$_0$/[M]) plot of 4 and 6 (X=Br) (c) conv. vs. M_n plot / vs. M_w/M_n plot of **4** and **6**.

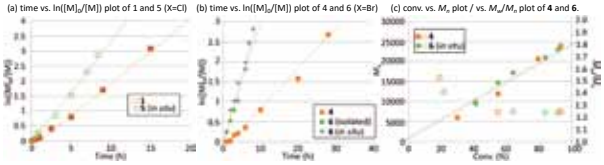

[2] ATRP of Styrene (St), Methyl methacrylate (MMA) and Butyl acrylate (BA)

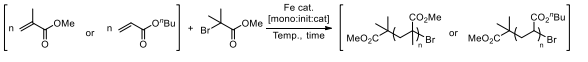

Entry	Monomer	Catalyst	Cat./init./monomer	Solvent [b]	Time (h)	Conv. (%)	M_n (exp.)	M_n (calcd.)	M_w/M_n
1	St	6 (*in situ*)	1 / 1 / 500	Toluene (1 / 1)	12	94	51,000	47,000	1.32
2		6 (*in situ*)	1 / 1 / 1,000	Toluene (1 / 1)	30	92	99,000	92,000	1.32
3		6 (*in situ*)	1 / 1 / 1,500	Toluene (1 / 1)	30	86	133,600	129,000	1.39
4		6 (*in situ*)	1 / 1 / 2,000	Toluene (1 / 1)	30	90	157,400	180,000	1.58
5		6 (*in situ*)	1 / 1 / 5,000	Toluene (1/1)	30	92	175,600	460,000	1.62
6	MMA	1	1 / 1 / 250	Bulk	5	90	30,000	22,500	1.80
7		5 (in situ)	1 / 1 / 250	Bulk	1.3	94	30,000	23,500	1.90
8		5 (in situ)	1 / 1 / 250	MeCN (1/0.2)	10	88	24,900	22,000	1.32
9		4	1 / 1 / 250	Bulk	8	90	24,900	22,500	1.65
10		6 (in situ)	1 / 1 / 250	Bulk	5	92	24,400	23,000	1.65
11		6 (in situ)	0.1 / 1 / 250	MeCN (1/0.2)	10	92	25,000	23,000	1.37
12		6 (in situ)	0.05 / 1 / 250	MeCN (1/0.2)	24	92	23,600	23,000	1.33
13		6 (in situ)	1 / 1 / 1000	Toluene (1 / 1)	30	86	89700	86000	1.38
14	BA	4	1 / 1 / 250	Bulk	20	>95	42,000	25,000	2.01
15		6 (in situ)	1 / 1 / 250	MeCN (1 / 1)	60	74	17,800	18,500	1.38
16		6 (in situ)	1 / 1 / 250	MeCN (1 / 0.3)	48	88	24,900	22,000	1.32
17		6 (in situ)	0.25 / 1 / 250	MeCN (1 / 0.3)	50	>95	24,900	25,000	1.36
18		6 (in situ)	0.125 / 1 / 250	MeCN (1 / 0.3)	120	92	27,900	23,000	1.78

[a]Polymerizations were carried out by using methyl 2-bromoisobutylate as the initiator at 90°C. [b]Figures in parenthesis are the ratio of the monomer to the solvent (v / v).

[3] Removal of Catalysts and its reusability

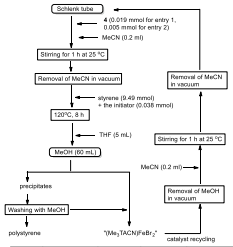

<Purification of polymer by MeOH>

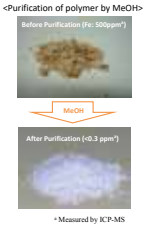

* Measured by ICP-MS

Entry	Monomer	Recycle	Time(h)	Conv.(%)	M_n(exp.)	M_n(Calcd.)	M_w/M_n
1	St[b]	1st	10	>95	22,500	25,000	1.21
2		2nd	10	92	23,200	23,000	1.26
3		3rd	10	93	26,700	23,200	1.26
4	MMA[c]	1st	8	>95	22,500	25,000	1.36
5		2nd	8	92	25,500	23,000	1.35
6		3rd	8	92	28,600	23,000	1.38
7	BA[d]	1st	50	90	23,300	22,500	1.33
8		2nd	50	>95	42,500	25,000	3.01

[a]The catalyst used was **6** (*in situ*) with the initiator (1-bromo-1-phenylethane) to monomer (styrene) ratio of 1 : 250. The reaction was performed at 120°C for 8 h. [b]The residual amount of iron species in the polystyrene was determined by ICP-MS.

[4] Block Copolymerization of St and MMA.

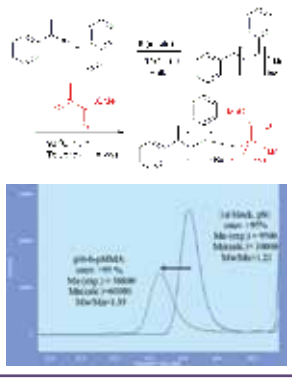

[5] ATRP of St and MMA by easy preparable $FeBr_2$ / Me_3TACN / MeCN

Entry	Monomer	Recycle	Time (h)	Conv. (%)	M_n (exp.)	M_n (Calcd.)	M_w/M_n
1	St[b]	1st	10	>95	24,500	25,000	1.24
2		2nd	10	89	20,400	23,000	1.26
3		3rd	10	89	22,700	23,200	1.24
4	MMA[c]	1st	8	>95	23,600	25,000	1.35
5		2nd	8	90	21,500	23,000	1.33
6		3rd	8	92	25,500	23,000	1.34

[a]In all cases, the ratio of catalyst/initiator/monomer was 0.25 : 1 : 250. [b]Bulk polymerization was performed at 120°C by using 1-bromo-1-phenylethane as the initiator. [c]Solution polymerization [MMA / MeCN = 1 : 0.2 (v/v)] was carried out at 90°C using methyl 2-bromoisobutylate as the initiator. [d]Solution polymerization [BA / MeCN = 1 : 0.3 (v/v)] was carried out at 90°C using methyl 2-bromoisobutylate as the initiator.

Summary

- ✓Highly-reactive and highly-controlled ATRP iron catalysts were synthesized by using commercially-available Me_3TACN ligands.
- ✓ATRP of Styrene, Methyl methacrylate and Butyl acrylate was achieved by solvent-stabilized iron complex **6**.
- ✓Reusability of catalysts
- ✓Removal of metal residue from polymer
- ✓Block copolymerization of St. and MMA was achieved
- ✓*In situ* generation from FeX_2 / Me_3TACN / CNMe.

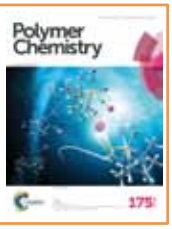

Nakanishi, S.; Kawamura, M.; Suanada, Y.; Nagashima, H. *Polymm. Chem.* **2016**, *7*, 1037-1048. [Selected as cover]

Hydrosilylation of Alkene with Hydrosiloxanes Catalyzed by Co(0) or Fe(0) Isocyanide Complexes

Atsushi SANAGAWA,[1] and Hideo NAGASHIMA*,[1,2]

[1]*Institute for Materials Chemistry and Engineering and* [2]*Graduate School of Engineering Sciences, Kyushu University, Kasuga, Fukuoka 816-8580, Japan*

ACKNOWLEDGMENTS:

This work was conducted in collaboration with Dr. Daisuke NODA and Mr. Koji SAKUTA (Shin-Etsu Chemical Co., Ltd.) and supported by CREST, JST.

Introduction

◆ Hydrosilylation of alkenes is an important reaction for...

①Synthetic intermediates

(ex)

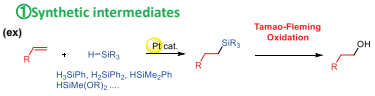

②Industrial production of organosilicon compounds

Silane coupling reagents

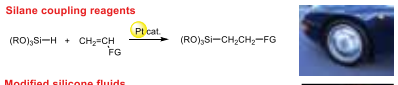

Modified silicone fluids

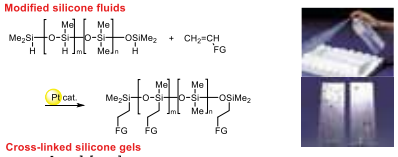

Cross-linked silicone gels

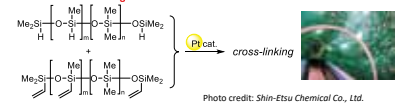

Photo credit: *Shin-Etsu Chemical Co., Ltd.*

Most commonly used catalyst

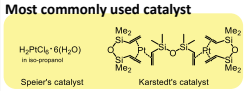

Earth-abundant metal catalyst (Fe, Co...)

◆ High catalytic activity ◆ Easy to handle

◆ High and volatile price ◆ The lack of natural resources

◆ Cobalt or iron catalysts for alkene hydrosilylation

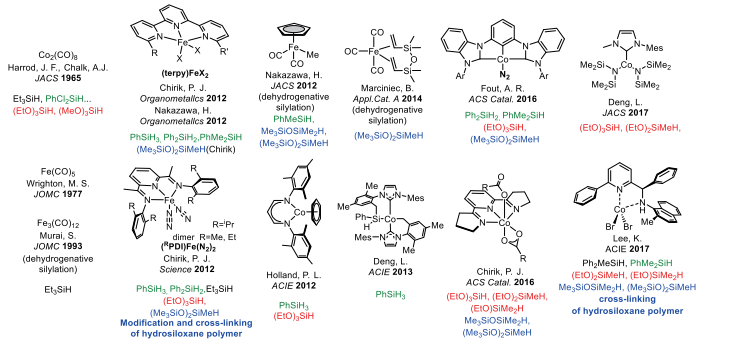

applicable to Tamao-Fleming oxidation (green), alkoxysilane (red), siloxane (blue)

◆ Previous work

Efficient and convenient catalyst systems

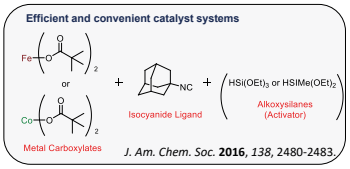

J. Am. Chem. Soc. **2016**, *138*, 2480-2483.

◆ Up to TON = 9700 (Fe), 1840 (Co)

◆ Modification and cross-linking of silicone polymers

Catalytic active species ?

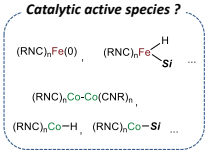

Proposed active species for hydrosilylation catalyzed by $Fe(CO)_5$ or $Co_2(CO)_8$

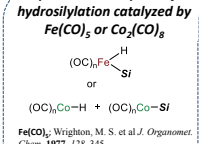

$Fe(CO)_5$: Wrighton, M. S. et al *J. Organomet. Chem.* **1977**, *128*, 345.
$Co_2(CO)_8$: Chalk, A. J.; Harrod, J. F. *J. Am. Chem. Soc.* **1967**, *89*, 1640. Wrighton, M. S. et al *Inorg. Chem.* **1980**, *19*, 3858

This Work

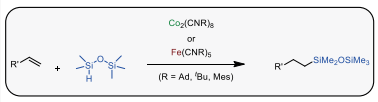

◆ Comparison with M(OPiv)$_2$/CNR systems (M = Co, Fe)

◆ Comparison with $Co_2(CO)_8$ or $Fe_n(CO)_m$

◆ Modification of silicone fluids

◆ Cross-linking of silicone polymers

◆ Synthesis of cobalt and iron isocyanide complexes

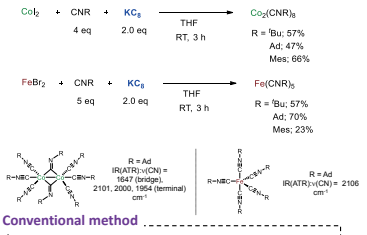

Conventional method

Reductant = Na-Hg;(Co) Woodward, P. et al. *J. Chem. Soc., Chem. Commun.* **1977**, 256. **(Fe)** G. A. Stone, et al. *J. Chem. Soc., Chem. Commun.*, **1977**, 853
K Naphthalenide: Cooper, N. J. et al *J. Am. Chem. Soc.* **1994**, *116*, 8566.

$Co_2(CO)_8$ + CNR → $Co_2(CNR)_8$; Yamamoto, Y.; Yamazaki, H. *J. Organomet. Chem.* **1977**, *137*, C31.

Na silica gel was also applicable as a reductant.

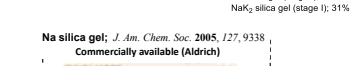

Na silica gel; *J. Am. Chem. Soc.* **2005**, *127*, 9338

Commercially available (Aldrich)

◆ Iron-catalyzed hydrosilylation of styrene with PMDS

Entry	Catalyst	Catalyst loading (mol% Fe atom)	Temp. (°C)	Conv.(%)	Yield(%)[a] a	b	c
1	$Fe(CNAd)_5$	1	80	>99	81	9	10
2	$Fe(CNAd)_5$	1	50	>99	>99(95)[b]	<1	<1
3	$Fe(CNAd)_5$	1	RT	7	7	<1	<1
4	$Fe(CNAd)_5$	0.1	50	>99	97	1	2
5	$Fe(CNMes)_5$	1	RT	9	<1	5	4
6	$Fe(CO)_5$	1	50	46	14	17	17
7	$Fe_2(CO)_9$	1	50	>99	30	38	32
8	$Fe_3(CO)_{12}$	1	50	45	13	14	14

a NMR yield. *b* Isolated yield

$Fe(OPiv)_2$/CNAd system

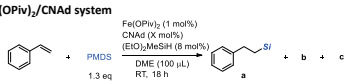

CNAd (2 mol%)	>99%	<1%	<1%
CNAd (3 mol%)	7%	<1%	<1%
CNAd (4 mol%)	4%	<1%	<1%

Catalytic activity
$Fe(CNR)_5$ < $Fe(OPiv)_2$/CNR

◆ Cobalt-catalyzed hydrosilylation of α-methylstyrene with PMDS

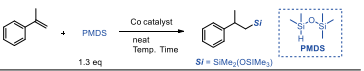

Entry	Catalyst	Catalyst loading (mol% Co atom)	Temp. (°C)	Time (h)	Conv.(%)	Yield(%)[a]
1	$Co_2(CNAd)_8$	1	RT	24	>99	>99
2	$Co_2(CNAd)_8$	0.1	80	3	>99	>99 (96)[b]
3	$Co_2(CNtBu)_8$	0.1	80	3	>99	>99
4	$Co_2(CNMes)_8$	1	RT	24	>99	>99
5	$Co_2(CNMes)_8$	0.01	RT	48	36	36
6	$Co_2(CO)_8$	1	RT	24	>99	>99
7	$Co_2(CO)_8$	0.1	80	3	88	88

a NMR yield. *b* Isolated yield

$Co(OPiv)_2$/CNAd system

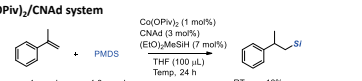

Catalytic activity
$Co_2(CNR)_8$ > $Co(OPiv)_2$/CNR

◆ Substrate scope

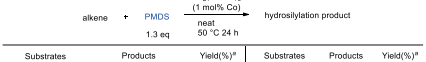

Substrates	Products	Yield(%)[a]	Substrates	Products	Yield(%)[a]
		>99 (96)			>99 (99)[b]
		>99 (97)			73[c]
		>99 (94)			>99 (83)[d]
		83 (75)			>99 (89)[d]
		94 (86)			
		99 (91)			

Si = $SiMe_2(OSiMe_3)$

a) NMR yield (Isolated yield). *b)* RT, $Co_2(CNMes)_8$ (1 mol% Co). *c)* 60 °C, $Co_2(CNAd)_8$ (1 mol% Co). *d)* RT.

◆ Modification of silicon polymers

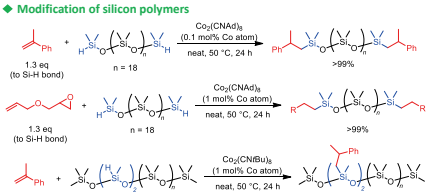

◆ Cross-linking of silicon polymers

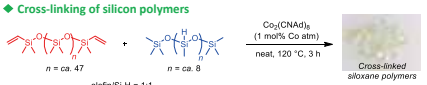

◆ Proposed reaction mechanism

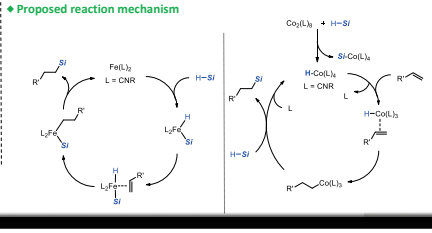

Iridium-catalyzed Syntheses of π-Conjugated Enamines bearing Acceptor Units and Their Application into Donor-Acceptor Compounds

Atsushi Tahara, Ikumi Kitahara, Hideo Nagashima

[1]*Institute for Materials Chemistry and Engineering ,Kyushu University, 6-1, Kasugakoen, Kasuga-shi, Fukuoka, 816-8580*

Introduction

●Donor-Acceptor (D-A) compounds

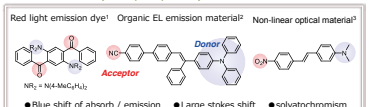

●π-Conjugated Enamines as Donors

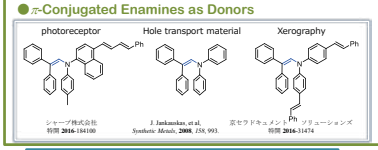

●Previous Work : Ir-catalyzed Syntheses of aldenamines

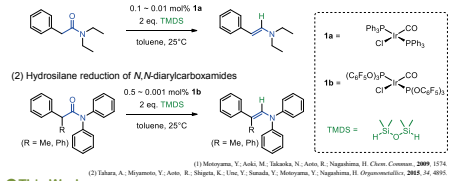

●This Work

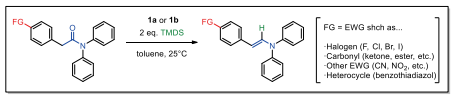

●Chemoselective Hydrosilane Reduction of Amides

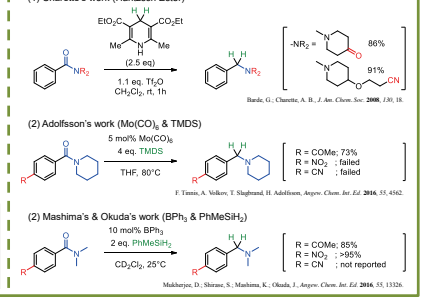

Results

●Competitive Reduction of Amides and EWGs

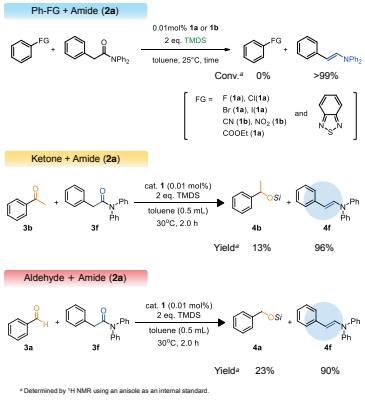

●Synthese of Amides 2 having EWG

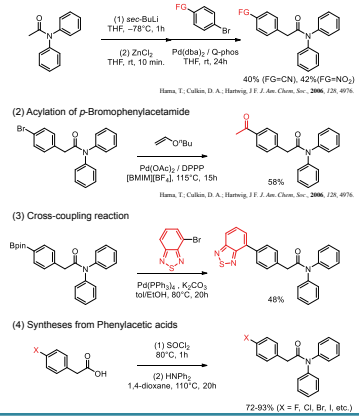

●Hydrosilane Reduction of Amides 2a-2j catalyzed by 1a or 1b

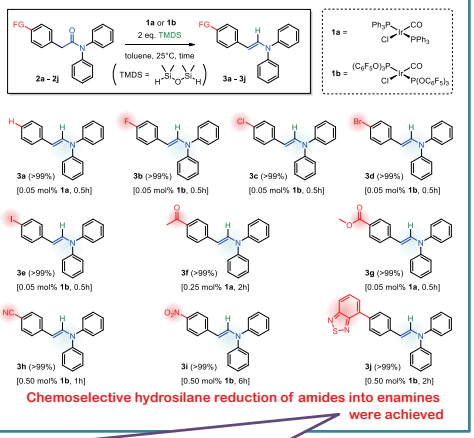

Chemoselective hydrosilane reduction of amides into enamines were achieved

Properties

●Photochemical Property of 3f (Ketone)

Solvent	λ_{abs} (nm)	ε	λ_{ex} (nm)	λ_{FL} (nm)	Φ_{FL-rel} [a]	Φ_{FL-abs} [b]
Hexane[c]	–	–	–	–	–	–
Toluene	381	25,000	390	433	0.01	0.01
THF	379	25,000	390	428,453,469	0.02	0.02
$CHCl_3$	389	32,000	390	476	0.11	< 0.01
CH_2Cl_2	386	44,000	390	483	0.01	< 0.01
DMF	388	22,000	390	481	0.03	0.06

at 1.0 × 10^{-5} M, [a]Relative to quinine sulfite in 0.5M sulfuric acid. [b]Absolute FL quantum yield

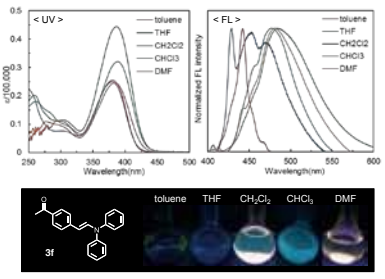

●Photochemical Property of 3i (NO_2)

Solvent	λ_{abs} (nm)	ε	λ_{ex} (nm)	λ_{FL} (nm)	Φ_{FL-rel} [a]	Φ_{FL-abs} [b]
Hexane[c]	404	26,000	405	474	0.02	0.02
Toluene	424	21,700	420	522	0.64	0.54
THF	431	30,200	430	549	0.56	0.65
$CHCl_3$	439	24,200	440	576	0.03	0.09
CH_2Cl_2	438	22,200	440	586	0.01	0.05
DMF	446	22,400	445	591	0.01	0.03

at 1.0 × 10^{-5} M, [a]Relative to quinine sulfite in 0.5M sulfuric acid. [b]Absolute FL quantum yield

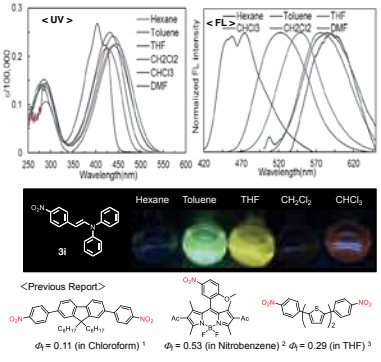

●Photochemical Property of 3j (Benzothiadiazole)

Solvent	λ_{abs} (nm)	ε	λ_{ex} (nm)	λ_{FL} (nm)	Φ_{FL-rel} [a]	Φ_{FL-abs} [b]
Hexane	419	10,000	430	500	0.96	0.37
Toluene	426	12,100	430	552	0.39	0.61
THF	425	11,600	430	589	0.04	0.26
$CHCl_3$	426	11,500	430	592	0.02	0.08
CH_2Cl_2	422	9,600	430	603	0.01	0.04
DMF	422	10,000	430	–	–	0.01

at 1.0 × 10^{-5} M, [a]Relative to quinine sulfite in 0.5M sulfuric acid. [b]Absolute FL quantum yield

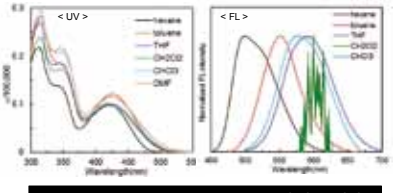

●Application (1) : Syntheses of D-A Compounds with NO_2

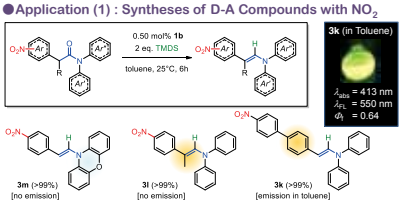

●Aplication (2) : Synthesis of D-A-D Compound

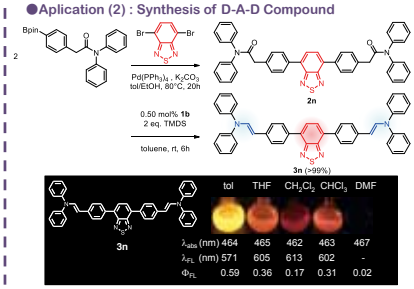

Summary

- ✓Syntheses of carboxamides which bears electron-withdrawing group.
- ✓Chemoelective hydrosilane reduction of amides were achieved to form π-conjugated enanines.
- ✓Enamines 3f, 3i, 3j showed some emission, of which quantum yield is the best compared with the reported molecules

特願2017-039057, KAKEN (17K17944)

Theoretical Studies of the Catalytic Hydrogenation of Alkenes by Disilametallacyclic Complexes bearing *cis*- and *trans*-Dicarbonyl Ligands (M = Fe, Ru, Os)

Tahara, A.;[1] Hoshi, K.;[1] Sunada, Y.;[2] Tanaka, H.;[1] Shiota, Y.;[1] Yoshizawa, K.;[1] Nagashima, H.[1]

[1]*Institute for Materials Chemistry and Engineering, Kyushu University, 6-1, Kasugakoen, Kasuga-shi, Fukuoka, 816-8580*

[2]*Institute of Industrial Science, The University of Tokyo, 4-6-1, Komaba, Meguro-ku, Tokyo, 153-8505*

Introduction

Hydrogenation of Alkenes

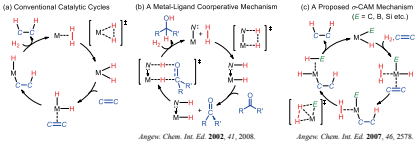

<well-defined Fe-complexes for alkene hydrogenation>

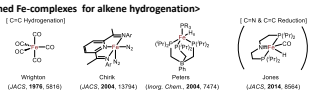

- Hard reaction condition (pressurized H_2, high temperature, irradiation) are required
- Mechanistic studies are difficult due to the high spin state of iron complexes

Syntheses of complexes 1, 2

<Fe complex>

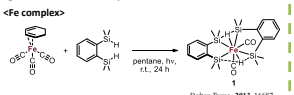

<Ru complex>

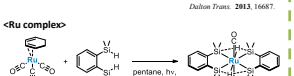

<complex 1, 2 showed catalytic activities toward...>

- Hydrosilane reduction of carbonyl compounds
- Hydrosilylation of alkenes
- Hydrogenation of alkenes (under 1atm of H_2, rt)

Hydrogenation of Alkenes catalyzed by Fe- or Ru-(CNMes)$_2$ Complex

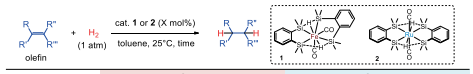

Alkenes	Cat. 1 mol%	Cat. 1 time(h)	Cat. 1 Yield(%)	Cat. 1 TON	Cat. 2 mol%	Cat. 2 time(h)	Cat. 2 Yield(%)	Cat. 2 TON
	0.25	2	>99	400	1	6	>99	100
	1	1	>99	100	5	6	>99	20
	1	2	>99	100	5	6	>99	20
	1	6	>99	20	5	6	>99	20
	5	4	>99	20	5	6	>99	20
	5	6	>99	20	5	4	>99	20
	5	6	20	4	5	6	5	1

Results (1)

<This work>

- Theoretical study for the property of complex **1**, **2** and catalytic cycles for alkene hydrogenation
- Estimation of Os analogues

<Condition of the calculation>

- For Optimization: M06 / SDD, 6-31G**
- For Energy Calculation: M06 / SDD, 6-311+G**/ PCM (toluene)

<Publications>

- For Fe:
J. Org. Chem. **2016**, *81*, 10900-10911.
- For Ru:
Bull. Chem. Soc. Jpn. **2017**, *90*, 616-623.
BCSJ award

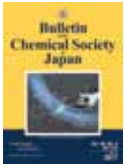

Comparison of the Structures obtained experimentally and theoretically

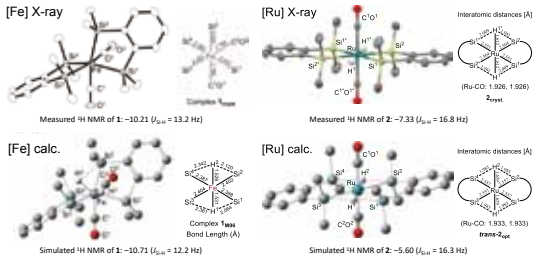

Isomerization and Ligand Exchenage

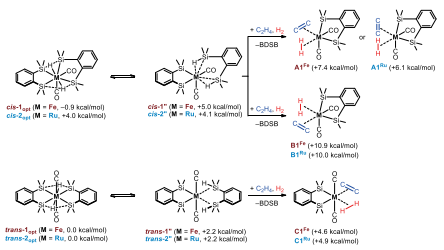

Results (2)

Suggested catalytic Cycles for Alkene Hydrogenation by 1, 2

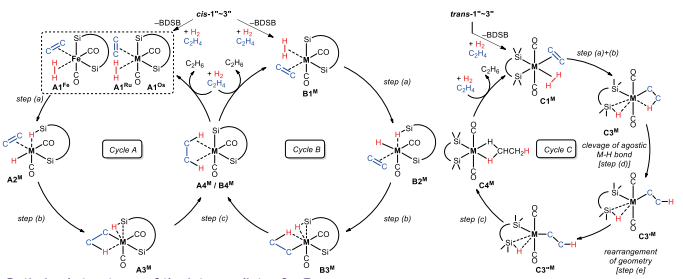

Optimized structures of the intermediates for Ru

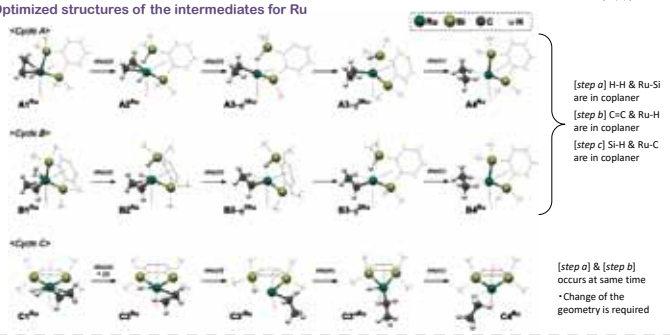

[*step a*] H-H & Ru-Si are in coplaner
[*step b*] C=C & Ru-H are in coplaner
[*step c*] Si-H & Ru-C are in coplaner

[*step a*] & [*step b*] occurs at same time
- Change of the geometry is required

Relative Energy Diagrams [Δ*G*, kcal/mol]

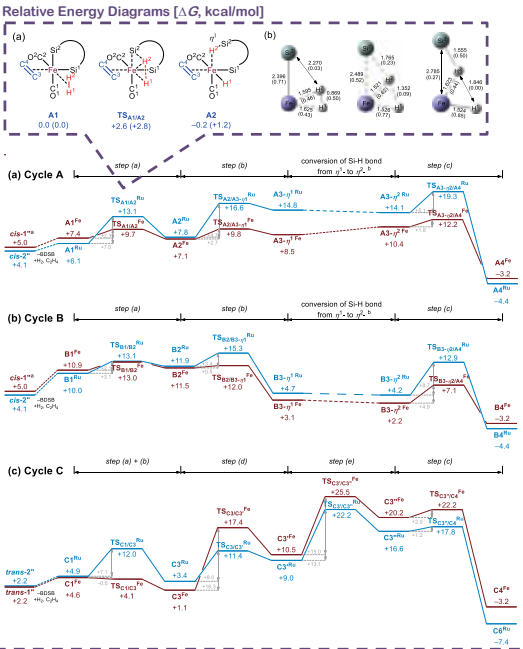

Estimation of Os analogues

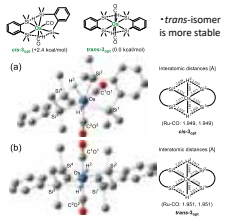

- *trans*-isomer is more stable

<Comparison of the reactivity of Fe, Ru and Os complexes toward H-H bond cleavage by Mayer bond order analyses>

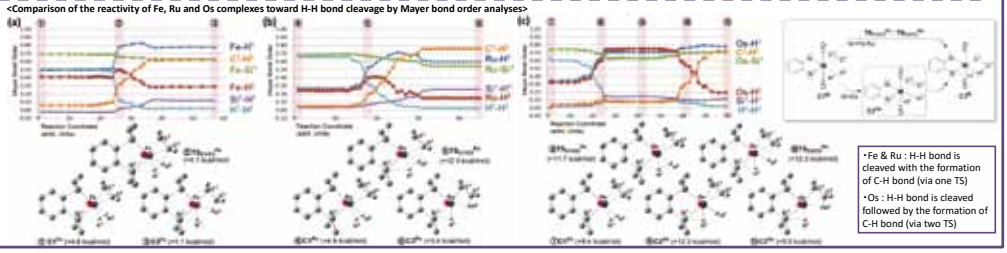

- Fe & Ru : H-H bond is cleaved with the formation of C-H bond (via one TS)
- Os : H-H bond is cleaved followed by the formation of C-H bond (via two TS)

Synthesis of Syn-Substituted Triptycenes Using Triple-Cycloadditions of Arynes to Ynolates and their Transformations

○Takayuki Iwata,[1] Tatsuro Yoshinaga,[2] Takumi Fujiwara,[2] Takuto Fukami,[2] Mitsuru Shindo[1]

[1]Institute for Materials Chemistry and Engineering, Kyushu University, [2]Interdisciplinary Graduate School of Engineering Sciences, Kyushu University

Introduction

anthracenes + benzynes —Diels-Alder reaction→ triptycene

Triptycene

D_{3h} symmetry
Rigid three-dimentional molecule
Firstly synthesized by Bartlett
Usually synthesized by DA reaction

P. D. Bartlett, *et al.*, *J. Am. Chem. Soc.* **1942**, *64*, 2649.
G. Wittig, *et al.*, *Angew. Chem.* **1956**, 68, 40.

ynolate-aryne triple cycloaddition reaction

Umezu, S.; Gomes, G. B.; Yoshinaga, T.; Sakae, M.; Matsumoto, K.; Iwata, T. Alabugin, I.; Shindo, M. *Angew. Chem. Int. Ed.*, **2017**, *56*, 1298.

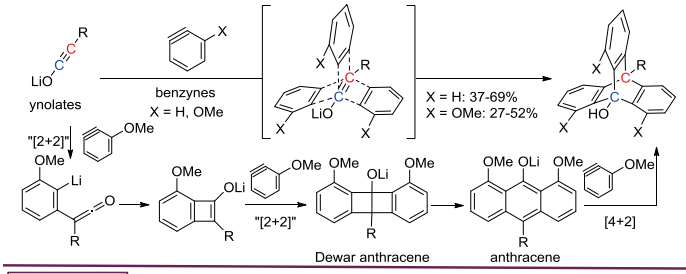

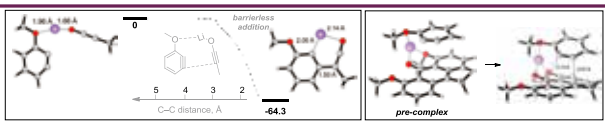

Origin of regioselectivity: negative hyperconjugation

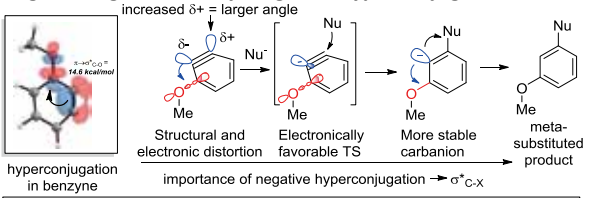

This work

- Variety of silyl-substituted triptycenes were synthesized utilizing the ynolate-aryne triple cycloaddition reaction.
- Transformations of the triptycenes were investigated.

Results

1. Synthesis and transformations of silyl triptycenes

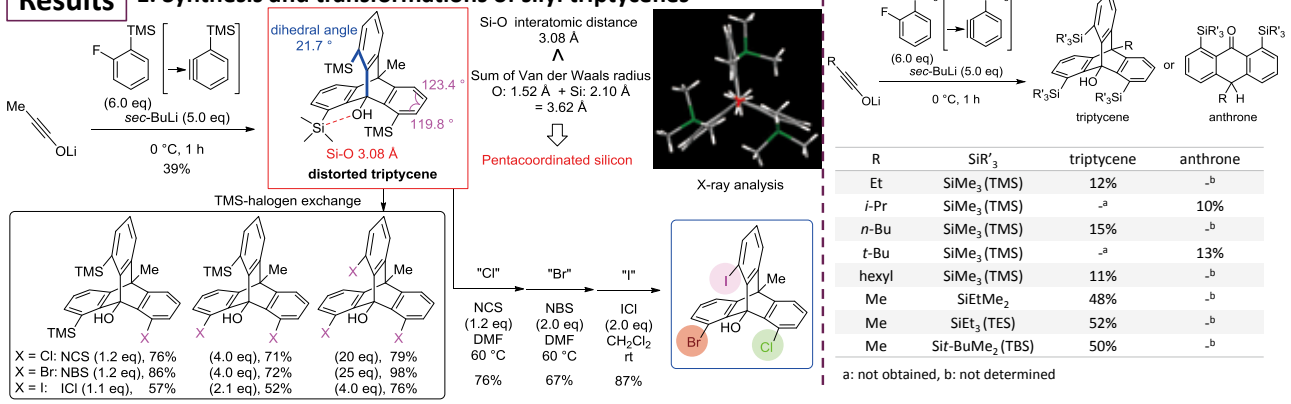

R	SiR'_3	triptycene	anthrone
Et	$SiMe_3$ (TMS)	12%	-[b]
i-Pr	$SiMe_3$ (TMS)	-[a]	10%
n-Bu	$SiMe_3$ (TMS)	15%	-[b]
t-Bu	$SiMe_3$ (TMS)	-[a]	13%
hexyl	$SiMe_3$ (TMS)	11%	-[b]
Me	$SiEtMe_2$	48%	-[b]
Me	$SiEt_3$ (TES)	52%	-[b]
Me	Si*t*-BuMe_2 (TBS)	50%	-[b]

a: not obtained, b: not determined

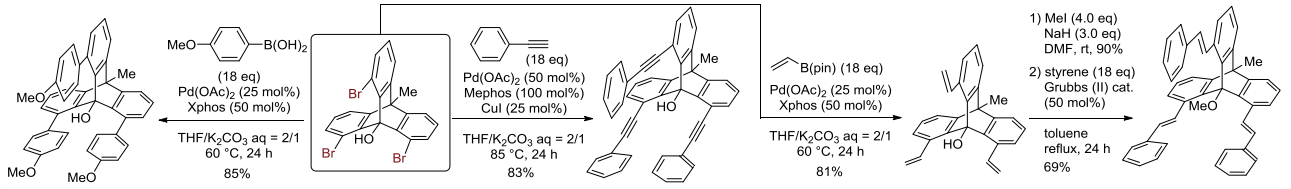

2. Generation of triptycyne (triptycene-aryne)

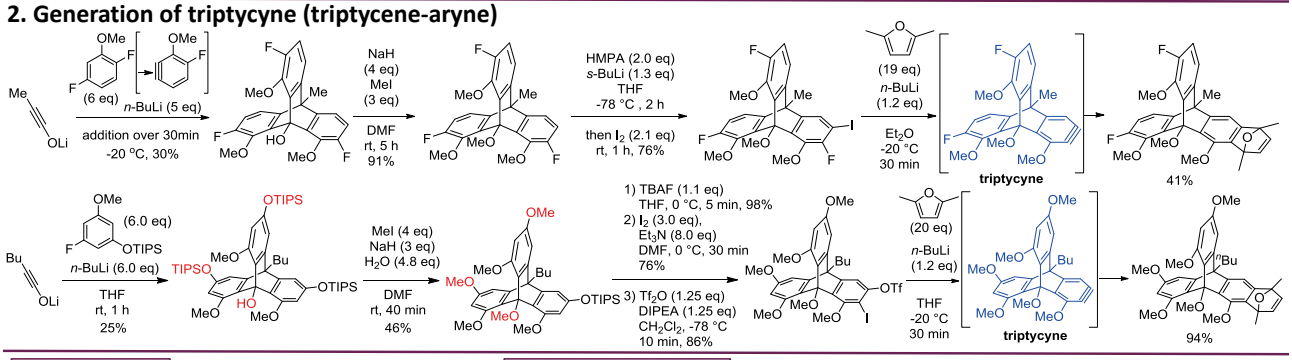

Conclusion

- Silyl-substituted triptycenes were successfully synthesized utilizing the ynolate-aryne triple cycloaddition reaction even when using steric silyl group.
- Triptycynes was also successfully generated from two types of triptycenes.

Future plan

- Triptycyne will be applied for the ynolate-aryne triple cycloaddition reaction.

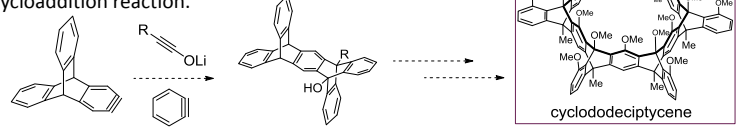

Switching Photomechanical Property by Structural Transformation

Kenta Goto and Fumito Tani

Institute for Materials Chemistry and Engineering (IMCE), Kyushu University

g2k@ms.ifoc.kyushu-u.ac.jp

Introduction

Materials that are capable of change their shape and size, or of actuation by physical stimuli are of particular importance as media for conversion energy to mechanical work. Such mechanically responsive or actuating materials are promising candidates as dynamically active elements providing a wide range of applications such as artificial muscles, actuators, and electromechanical devices. If physical stimulus is photo-irradiation, mechanical response materials are classified into three mechanisms. One is cis-trans isomerization, the others are ring opening and closure reactions, and cycloaddition reactions.[1]

We recently found the photochemical reaction of naphthalene diimides (NDI) having alkylamino side chains in the solid states.[2] Upon irradiation of light (λ = 370 nm), the compound **1** showed color change from to yellow to black (Fig. 1b). This came from the formation of radical anion of **1** as evidenced by UV-Vis-Nir spectroscopy. Furthermore, the crystal **1** showed photo-mechanical motion (Fig. 1c).

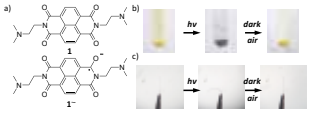

Fig.1 a) Chemical structure of **1** and **1**⁻ b) Color change of the crystal **1** upon photo-irradiation (λ = 370 nm) c) Photomechanical motion of the crystal **1**.

[1] Nath, N. K.; Panda, M. K.; Sahoo, S. C.; Naumov, P. *CrystEngComm*, **2014**, *16*, 1850-1858.
[2] Matsunaga, Y.; Goto, K.; Kubono, K.; Sako, K.; Shinmyozu, T. *Chemistry*-A European Journal, **2014**, *20*, 7309-7316.

Objective

We suggested that the photo-mechanical motion of **1** originated from the electrostatic repulsion among **1**-**1**⁻, **1**⁻-**1**⁻, and **1**-**1**⁻. When we spatially separate the donor group of NR_2 from the acceptor imide moiety by long alkyl chain, van der Waals force would be dominant or interplay with electrostatic interactions. NDI having long alkylamino chain would give an answer as to the question "how long we can separate the donor group of NR_2 from core moiety." Solution for these problems have possibilities of controlling photo-mechanical motion by chemical modification.

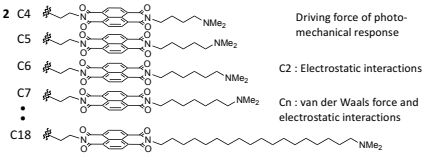

X-ray structure of 2

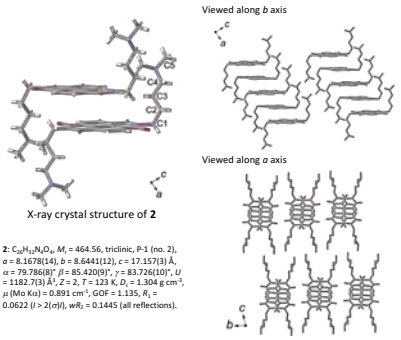

2: $C_{28}H_{32}N_4O_4$, M_r = 464.56, triclinic, P-1 (no. 2), a = 8.1678(14), b = 8.6441(12), c = 17.157(3) Å, α = 79.786(8)°, β = 85.420(9)°, γ = 83.726(10)°, U = 1182.7(3) Å³, Z = 2, T = 123 K, D_x = 1.304 g cm⁻³, μ (Mo Kα) = 0.891 cm⁻¹, GOF = 1.135, R_1 = 0.0622 ($I > 2(\sigma(I))$, wR_2 = 0.1445 (all reflections).

Thermal analysis and structural data

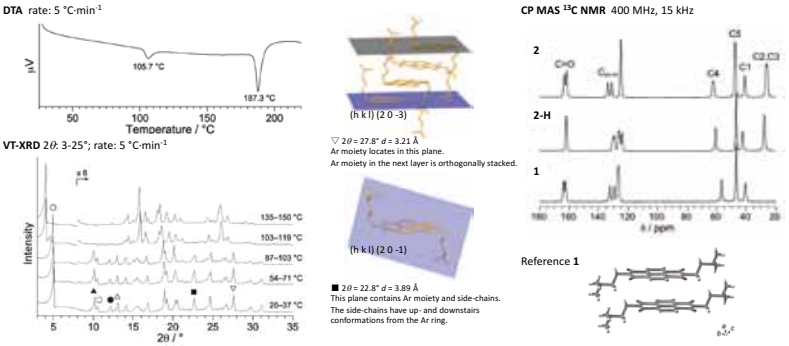

Structural transformation

Uv-Vis spectrum: thin layer 2 (○; prep. 2000 rpm, 30 sec) and heat treated 2-H (▲; 120 °C, 10 min)

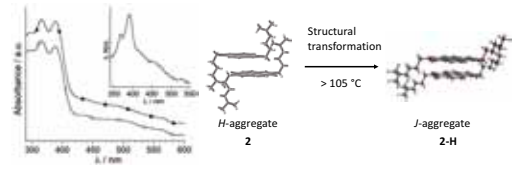

Kinetic analysis

$$B + q \xrightarrow{k_1} C \qquad C + q \xrightarrow{k_2} D \qquad \kappa = \frac{k_1}{k_2}$$

B : Radical anion dimer
C : Mixed valence species
q : quencher

Mass valance

$$[q]_0 - [q] = [C] + 2[D]$$
$$[B]_0 - [B] = [C] + [D]$$

Reaction description

$$\frac{d[B]}{dt} = -k_1[B][q]$$
$$\frac{d[C]}{dt} = k_1[B][q] - k_2[C][q]$$
$$[C] = \frac{1}{\kappa - 1}\left\{1 - \left(\frac{[B]}{[B]_0}\right)^{\kappa - 1}\right\}[B]$$

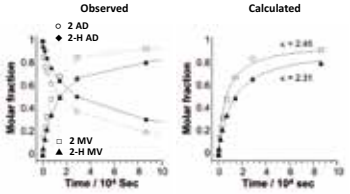

Photochemical reaction

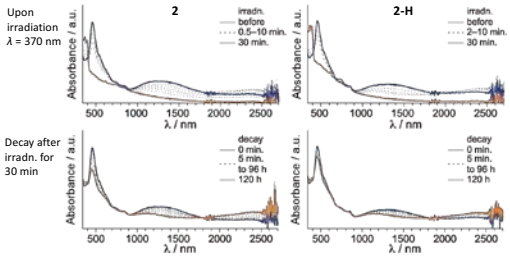

Photo-mechanical response

Conditions
Irradiation: λ_{max} = 370 nm, 30 sec, in the air

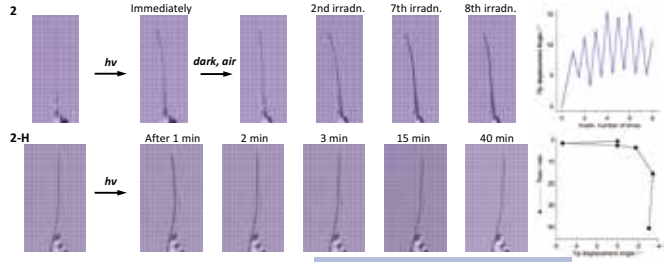

Summary

The crystals of **2** were found to have the thermal transition at 105.7 °C as observed by DTA. The crystals and thin layer of **2** were fully converted to be **2-H** by heat treatment at 120 °C for 10 min. Above the transition point, **2** was completely transformed by changing their ordered structure from *H*-aggregate to *J*-aggregate. The photochemical reaction of **2** and **2-H** showed that the decay process was different between each other. Assuming the presence of a quencher, the kinetic equation was resolved. The ratio of the reaction rate (κ) of **2-H** was smaller than that of **2**. The delay in the decay of **2-H** may reflect in photo-mechanical response. While the crystals of **2** showed immediately mechanical response, the crystals of **2-H** slowly responded bending, and sometimes swing. Using thin layered **2** and **2-H** would reveal these photo-mechanical response more clearly.

Acknowledgements

Taisuke Matsumoto (XRD, IMCE); Keiko Ideta (CP MAS NMR, IMCE); Dr. Shinji Kanegawa & Prof. Osamu Sato (IR, IMCE); Prof. Yoshihito Shiota & Prof. Kazunari Yoshizawa (Theoretical Calculation, IMCE)
This work was supported by a Grant-in-Aid for Scientific Research(C) (no. 16K05699) from the Ministry of Education, Culture, Sports, Science and Technology, Japan.

Molecularly Fingerprinted Oxide Nanowires

K. Nagashima[1], Y. He[1], A. Inoue[1], H. Yoshida[2],
G. Zhang[1], T. Takahashi[1], S. Takeda[2] and T. Yanagida[1]

[1]IMCE, Kyushu Univ. [2]ISIR, Osaka Univ.

Introduction

Breath Analysis by Molecule Recognition Electronics

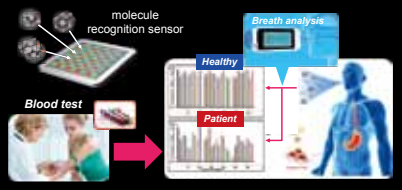

Non-invasive, Real-time, Repeatable self-diagnosis

Biomarkers in Breath

Volatile Organic Compounds (VOCs)

Over **872** species

*J. Breath Res.*8 014001 (2014)

Aldehyde・Ketone closely related to serious disease

Breath molecules vs. Health condition

Innovative technology toward early discover of serious diseases & self medication!!

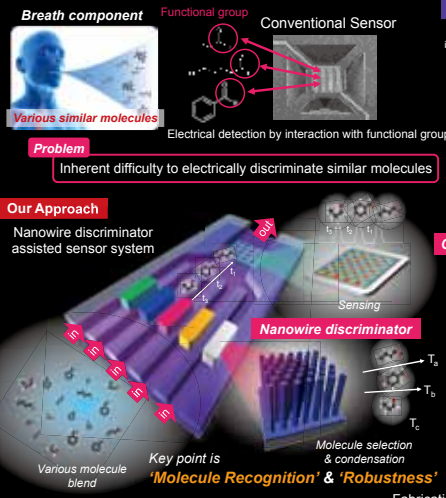

Problem

Inherent difficulty to electrically discriminate similar molecules

Our Approach

Nanowire discriminator assisted sensor system

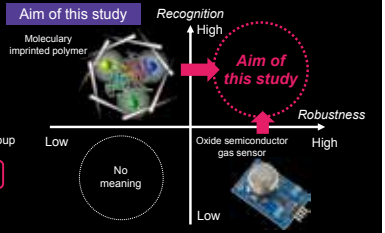

Objective *Synthesis of molecule discriminator using molecularly fingerprinted oxide nanowires*

Molecularly Fingerprinted Oxide Nanowires

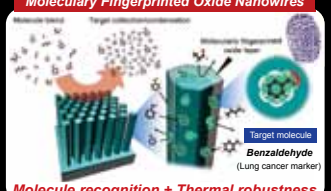

Molecule recognition + Thermal robustness

Experimental

1. Hydrothermal ZnO nanowire growth

2. Molecularly fingerprinted oxide sol-gel coating

Sol-gel mechanism: metal alkoxide reaction

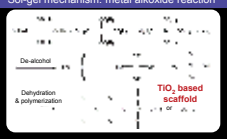

Pretreatment for molecularly fingerprinted oxide nanowires

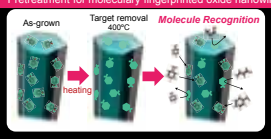

Characterization

- Field emission scanning electron microscopy (FESEM)
- Energy dispersive x-ray spectroscopy (EDS)
- Transmission electron microscopy (TEM)
- Gas chromatograph mass spectroscopy (GCMS)
- Fourier transform infrared spectroscopy (FTIR)

Fabrication of molecularly fingerprinted oxide nanowires

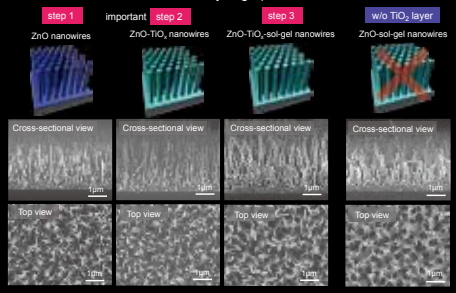

ZnO nanowires dissolve withoug TiO_2 layer by byproduct

$TiCl_4 + 2H_2O \rightarrow TiO_2 + 4HCl$ ··· ZnO dissolve

Results & Discussion

Characterization of Molecular Fingerprinted Oxide Nanowires

FESEM image

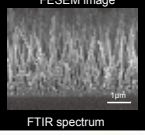

STEM image-EDS mapping

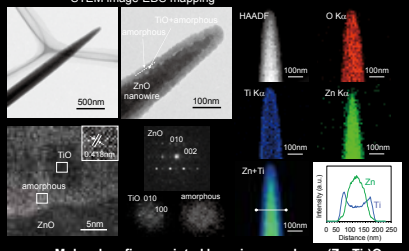

FTIR spectrum

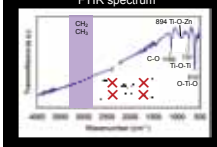

Molecularly fingerprinted layer is amorphous (Zn_xTi_y)O

Evaluation of *'Molecule collection ability'* & *'Robustness'*

Evaluation of Benzaldehyde adsorption

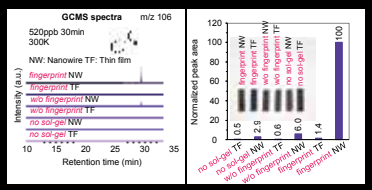

Efficient molecule collection by molecularly fingerprinted nanowires

200 times (vs. no sol-gel film)

Cycle thermal stress measurement

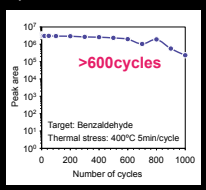

Excellent thermal robustness of molecular fingerprint

Molecularly fingerprinted oxide nanowires with 'Efficient molecule collection ability'・'High thermal robustness'

Recognition Mechanism of Molecule Fingerprint

Target molecule-fingerprint interaction

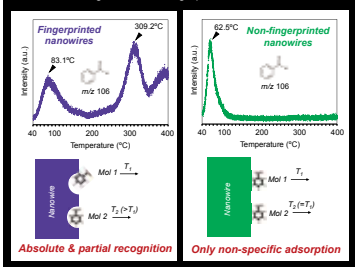

Several adsorption states

How does it recognize?

FTIR spectra for molecule adsorbed nanowires

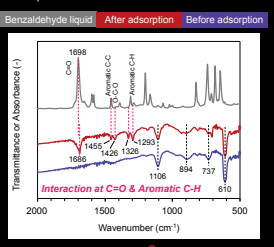

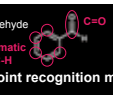

Multi-point recognition mechanism

Molecule Recognition from Molecule Blend

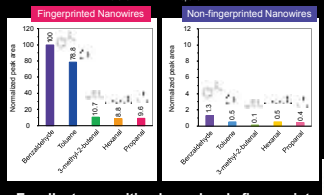

Excellent recognition by molecule fingerprint

Structural & Chemical recognition

Is it possible to discriminate from toluene?

Molecule recognition by desorption process

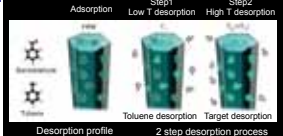

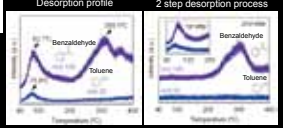

Isolation of target molecule by controlling desorption temperature

Highly reliable molecule recognition ability of molecularly fingerprinted oxide nanowires

Summary

We successfully synthesized ***'Highly discriminable'*** & ***'Thermally robust'*** molecularly fingerprinted oxide nanowires

Structural & Chemical molecule recognition / ***Thermal robustness*** **400ºC >600 cycles**

Impacts of Thermal Annealing on Electrical Properties of Hydrothermally Grown ZnO Nanowires: Nanowire Resistivity, Contact Resistance and Their Long-term Stability

九州大学 KYUSHU UNIVERSITY

Kentaro Nakamura[1], Tsunaki Takahashi[2], Hiroshi Anzai[1], Daiki Sakai[1], Masaki Kanai[2], Kazuki Nagashima[2] and Takeshi Yanagida[1,2]
1. Engineering Science, Kyushu University 2. IMCE, Kyushu University

Introduction

Metal Oxide Nanowire

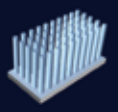

- Ferroelectricity
- Photocatalytic Activity
- Memristor etc.

Lasers

Feld-Effect Transistors

Chemical Sensors

Growth Method

- Top-down Etching
- Solid/Liquid/Gas Phase Growth Methods
- Vapor-Liquid-Solid Method
- **Hydrothermal Synthesis**

Advantage
- Simple and Low Cost
- Wafer-scale Growth

Gas Sensor

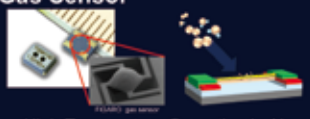

- High Temperature Operation in Air
- No Capping Layer on Sensing Channel

Degradation of Nanowire

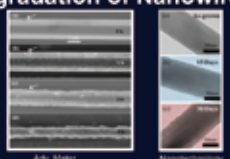

Adv. Mater. 2006, 18, 2432-2435 / Nanotechnology 2009, 20, 475702

Problem

Long-term Stability of Hydrothermal Oxide Nanowires

Approach

Thermal Annealing of Oxide Nanowires for Stable Electrical Characteristics

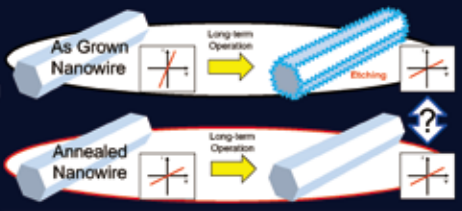

Objective

- To Investigate Impacts of Thermal Annealing on Electrical Property of ZnO Nanowires
- To Establish the Strategy Ensuring Long-term Stability

Experiments

Growth of ZnO Nanowire

Hydrothermal Synthesis

Water	
$Zn(NO_3)_2$	25mmol/L
Hexamethylenetetramine(HMTA)	25mmol/L
Polyethylenimine(PEI)	2.5mmol/L

Time : 48hours
(Exchange to New Solution in 24hours)

Length : 5~7μm
Diameter : Average 150nm

Annealing

As Grown 600 ℃, 1hour

Device

Single ZnO Nanowire
4-terminal Device

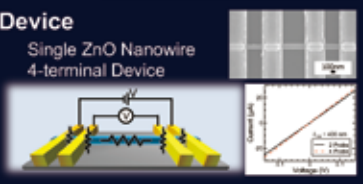

Measurements

- FE-SEM
- Photoluminescence (PL)
- X-ray Diffraction (XRD)
- 2- and 4-probe Methods

Stability Evaluation

- Nanowire Growth
- Device Fabrication

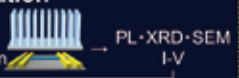

Results and Discussion

Morphology (SEM)

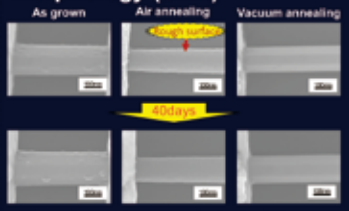

There is no clear morphological change after 40days.
Etching effect was not observed.

Crystallinity (XRD)

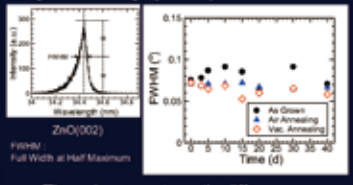

There is no systematic difference.

Optical Property (PL)

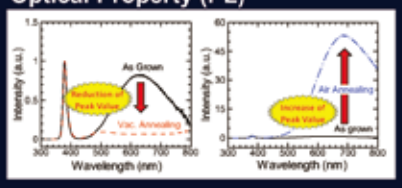

Defects in nanowires were reduced by vacuum annealing.

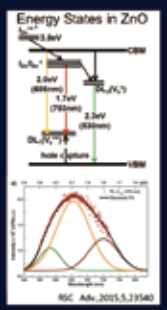

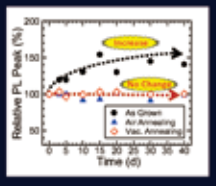

Degradation of PL characteristics was suppressed by annealing.

Electrical Characteristics

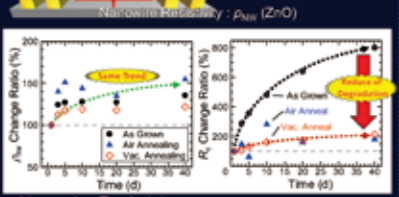

- Nanowire Resistivity : ρ_{NW}
  No Clear Impacts of Annealing
- Contact Resistance : R_c
  Great Suppression of R_c Change by Annealing

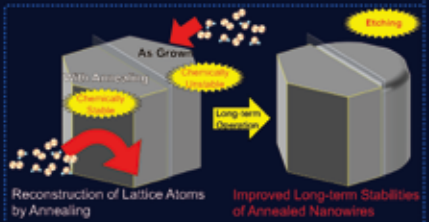

Reconstruction of Lattice Atoms by Annealing

Improved Long-term Stabilities of Annealed Nanowires

Summary

- **Long-term stability of PL and electrical characteristics of ZnO nanowires was improved by thermal annealing.**
- **Chemical stability of ZnO nanowires is considered to be enhanced by atomic reconstruction during thermal annealing.**

Future Plan

Physical/chemical origin of the degradation will be clarified through experiments which are stability evaluations under controlled atmosphere and/or by TEM.

Effect of Tungsten Doping on Hydrothermal ZnO Nanowire growth

[1]Interdiciplinary Graduate School of Engineering Sciences
[2]Institute for Materials Chemistry and Engineering

○Hiroki Yamashita[1], Kazuki Nagashima[1,2], Daiki Sakai[1], Tsunaki Takahashi[2], Zhang Guozhu[2], Masaki Kanai[2] and Takeshi Yanagida[1,2]

Introduction

Metal oxide Nanowire

Nanowire has a lot of application to several scene

Hydrothermal synthesis

Water soluble Regent + Water → Heat, High pressure

There are various advantages to grow Nanowire

Impurity doping

Impurity, Substitute

Possibility of changing characteristics

Reaction by hydrothermal synthesis method uses chemical reaction

$Zn(NH_3)_4^{2+}$

+ Tungsten species

We don't know how chemical species relate to nanowire growth reaction

What's "Flux-window principle"?

Pursuing Nanowire's critical nucleation conc.(rapid grown process) by changing the size (c-plane) and diameter (m-plane) of Nanowire as main constituent elements (Zn^{2+}) conc.

Crystal growth can be considered that correspond to each crystal plane c-plane・m-plane

Objective

Clarification of growth mechanism in liquid phase

Experiment

SiO_2, Si, Sputtering, SiO_2/Si(100) substrate

ZnO seed layer(50nm), Ti

Nanowire growth

W doped Nanowire

Ionic distribution Visual MINTEQ3.1

Structural validation FE-SEM

Doping validation EDS

Sputtering condition

RF sputter
Target1 : Ti
Target2 : ZnO
RF Power : 100/50(W)
Position : 90/70(cm)
Base pressure : 5.0×10^{-4}(Pa)
Used pressure : 0.3(Pa)
Rotation : 1
Time : Ti-1min, ZnO-30min

The scheme of reaction

$$HMTA + 6H_2O \leftrightarrow 4NH_3 + 6HCHO$$
$$NH_3 + H_2O \leftrightarrow NH_4^+ + OH^-$$
$$Zn^{2+} + 4NH_3 \leftrightarrow [Zn(NH_3)_4]^{2+}$$
$$Zn^{2+} + 2OH^- \leftrightarrow Zn(OH)_2$$
$$Zn(OH)_2 \leftrightarrow ZnO + H_2O$$

Hydrothermal synthesis

PEI (Poly ethylene imine) : 0～1mM
HMTA (Hexamethylene tetramine) :25mM
$Na_2WO_4 \cdot 2H_2O$: 0～12.5mM (0～1%)
$Zn(NO_3)_2 \cdot 6H_2O$:0～25mM
Reaction time : 5hours
Reaction temp. : 95℃

Validation items

・Structural validation as W addition
・Ionic distribute calculation as under reaction pH condition
・Crystal growth validation as each PEI & Zn conc. changing

Result & Discussion

W ration change effect

Side view, Top view

As the amount of W increases, the length is shorter and the diameter is larger

Scenario

1. The addition of W changed the pH & affected the reactive chemical species
2. c-plane was capped by W, and m-plane growth of Zn was promoted
3. W covers the m-plane, which attracts Zn to promote m-plane growth

Ionic distribution

W:0% pH6.7 → W:1% pH6.7

pH value was not changed between W contained and not contained

There is almost no influence on Zn-derived chemical species distribution by addition of W

PEI effect

PEI is well known as capping agent of m-plane

A little add: c-plane grown promotion

Excessive add: Crystal grows suppression

ZnO, W 1%

White precipitation

W 20%

EDS measurement

Zn & W interaction is probably strong

Increasing the conc. of PEI returned to Nanowire shape even if W was added

Zn critical nucleation conc. measurement

Nucleation conc. is same with W & without W

W add sample occurs at the lower conc. side

Scenario 2 isn't clear

It is considered to be Scenario 3 from this result

model

1. WO_4^{2-} ion is captured by PEI
2. This complex approach to ZnO m-plane
3. WO_4^{2-} ion insert to Zn^{2+} site
4. And, ZnO m-plane growth is enhance

Summary We could successful to clarify the growth mechanism.

Next plan We'll measure EDS of W amount changing condition (a little addition)

IRCCS 統合物質創製化学研究推進機構

阿波賀邦夫　**エネルギー・資源研究プラットホーム**
〒464-8602　名古屋市千種区不老町 名古屋大学大学院理学研究科
TEL 052-789-2291　FAX 052-789-5947

中野　環　**新反応・新触媒研究プラットホーム**
〒001-0021　北海道札幌市北区北 21 条西 10 丁目 北海道大学触媒科学研究所
TEL 011-706-9155　FAX 011-706-9156

島川祐一　**マテリアル研究プラットホーム**
〒611-0011　京都府宇治市五ヶ庄 京都大学化学研究所附属元素科学国際研究センター
TEL 0774-38-3110　FAX 0774-38-3118

吉澤一成　**ケムバイオ研究プラットホーム**
〒819-0395　福岡市西区元岡 744 九州大学先導物質化学研究所
TEL 092-802-2529　FAX 092-802-2528

機構事務室
〒464-8602　名古屋市千種区不老町 名古屋大学物質科学国際研究センター
TEL 052-789-5907　FAX 052-789-5900


IRCCS, Integrated Research Consortium on Chemical Sciences